

สารต้านมะเร็งและสารต้านจุลชีพจากไม้แดง *Xylia xylocarpa*

และแอ้ม *Coscinium fenestratum*

และการศึกษาความสัมพันธ์ของโครงสร้างและฤทธิ์



นายวีรชัย พงษ์กิตติพันธ์

จุฬาลงกรณ์มหาวิทยาลัย

CHULALONGKORN UNIVERSITY

บทคัดย่อและแฟ้มข้อมูลฉบับเต็มของวิทยานิพนธ์ตั้งแต่ปีการศึกษา 2554 ที่ให้บริการในคลังปัญญาจุฬาฯ (CUIR)

เป็นแฟ้มข้อมูลของนิสิตเจ้าของวิทยานิพนธ์ ที่ส่งผ่านทางบัณฑิตวิทยาลัย

The abstract and full text of theses from the academic year 2011 in Chulalongkorn University Intellectual Repository (CUIR)

are the thesis authors' files submitted through the University Graduate School.

วิทยานิพนธ์นี้เป็นส่วนหนึ่งของการศึกษาตามหลักสูตรปริญญาวิทยาศาสตรดุษฎีบัณฑิต

สาขาวิชาเคมี ภาควิชาเคมี

คณะวิทยาศาสตร์ จุฬาลงกรณ์มหาวิทยาลัย

ปีการศึกษา 2557

ลิขสิทธิ์ของจุฬาลงกรณ์มหาวิทยาลัย

ANTICANCER AND ANTIMICROBIAL COMPOUNDS  
FROM *Xylia xylocarpa* AND *Coscinium fenestratum*  
AND STRUCTURE-ACTIVITY RELATIONSHIP STUDIES

Mr. Veerachai Pongkittiphan



A Dissertation Submitted in Partial Fulfillment of the Requirements  
for the Degree of Doctor of Philosophy Program in Chemistry  
Department of Chemistry  
Faculty of Science  
Chulalongkorn University  
Academic Year 2014  
Copyright of Chulalongkorn University

Thesis Title                                 ANTICANCER AND ANTIMICROBIAL COMPOUNDS  
  FROM *Xylia xylocarpa* AND *Coscinium*  
  *fenestratum* AND STRUCTURE-ACTIVITY  
  RELATIONSHIP STUDIES

By   Mr. Veerachai Pongkittiphan

Field of Study                                 Chemistry

Thesis Advisor                                 Assistant Professor Warinthorn Chavasiri, Ph.D.

---

Accepted by the Faculty of Science, Chulalongkorn University in Partial  
Fulfillment of the Requirements for the Doctoral Degree

.....Dean of the Faculty of Science  
(Professor Supot Hannongbua, Dr.rer.nat.)

THESIS COMMITTEE

.....Chairman  
(Assistant Professor Preecha Lertpratchya, Ph.D.)

.....Thesis Advisor  
(Assistant Professor Warinthorn Chavasiri, Ph.D.)

.....Examiner  
(Associate Professor Nongnuj Muangsin, Ph.D.)

.....Examiner  
(Assistant Professor Khanitha Pudhom, Ph.D.)

.....Examiner  
(Supakarn Chamni, Ph.D.)

.....External Examiner  
(Assistant Professor Veena Nukoolkarn, Ph.D.)

วีรชัย พงษ์กิตติพันธ์ : สารต้านมะเร็งและสารต้านจุลชีพจากไม้แดง *Xylia xylocarpa* และแฉ้ม *Coscinium fenestratum* และการศึกษาความสัมพันธ์ของโครงสร้างและฤทธิ์ (ANTICANCER AND ANTIMICROBIAL COMPOUNDS FROM *Xylia xylocarpa* AND *Coscinium fenestratum* AND STRUCTURE-ACTIVITY RELATIONSHIP STUDIES) อ.ที่ปรึกษาวิทยานิพนธ์หลัก: ผศ. ดร.วรินทร์ ชวนศิริ, 184 หน้า.

Sandaracopimaradiene-3 $\beta$ ,18-diol (D1), sandaracopimaradien-3-one (D2) sandaracopimaradien-3 $\beta$ -ol (D3) และ sandaracopimaric acid (D4) แยกได้จากสิ่งสกัดไดคลอโรมีเทนของแก่นไม้ *Xylia xylocarpa* (Roxb.) Taub. ได้เลือก D1 เป็นสารต้นแบบสำหรับการศึกษาความสัมพันธ์ทางโครงสร้างและฤทธิ์ เพื่อสังเคราะห์อนุพันธ์ D7, D8, D15, D18 และ D19 ซึ่งให้ผลการต้านแบคทีเรียได้ปานกลางถึงดี กับ *Staphylococcus aureus*, *Propionibacterium acnes*, *Streptococcus mutans*, *Streptococcus sobrinus*, และ *Salmonella typhi* D7 และ D19 แสดงค่า MIC ต่ำมากที่ 31.2–62.5  $\mu\text{M}$  ในการยับยั้งเชื้อ *S. aureus*, *S. mutans*, *S. sobrinus*, และ *S. typhi* เฉพาะ D7 ที่แสดงค่า MBC ที่ 62.5  $\mu\text{M}$  เพื่อฆ่าเชื้อ *S. sobrinus* นอกจากนี้ได้สังเคราะห์ C2 ผ่านปฏิกิริยา cyclopropanation จาก D1 ร่วมกับ alkynyl diazoacetate L3 ในการทดสอบความเป็นพิษต่อเซลล์ของ D1-D3 และอนุพันธ์ต่างๆ (D7, D8, D15, D18, D19 และ C2) ต่อการต้าน HepG2 (เซลล์มะเร็งตับ) ด้วยการทดสอบ MTS พบว่า D7, D15 และ D18 ให้ผลที่ดีด้วยค่า  $\text{IC}_{50}$  3.45 $\pm$ 0.47, 1.00 $\pm$ 0.47 และ 0.99 $\pm$ 0.08  $\mu\text{M}$  ตามลำดับ

Berberine chloride (B1) แยกได้จากเถาของ *Coscinium fenestratum* (Goetgh.) Colebr. และเลือกใช้เป็นสารต้นแบบเพื่อสังเคราะห์อนุพันธ์แปดชนิด B2-B9 เพื่อศึกษาความสัมพันธ์ทางโครงสร้างและฤทธิ์ สำหรับฤทธิ์ต้านเชื้อแบคทีเรีย เฉพาะ B3 แสดงผลดีที่สุดในการต้านเชื้อ *Xanthomonas oryzae* pv. *oryzae* และ pv. *oryzicola* ในส่วนการทดสอบการต้านสารอนุมูลอิสระด้วยวิธี DPPH พบว่าเฉพาะ B9, B8 และ B7 ให้ผลที่ดี ( $\text{IC}_{50}$  = 10.72  $\pm$  1.76, 55.24  $\pm$  2.24 และ 87.35  $\pm$  6.65  $\mu\text{M}$ , ตามลำดับ) และการทดสอบความเป็นพิษต่อเซลล์มะเร็งเนื้อเยื่ออ่อน (HT1080) ด้วยวิธี MTT ในระยะเวลา 7 วันพบว่าค่า  $\text{IC}_{50}$  เรียงลำดับได้ดังนี้ B1 < B9 < B7 (0.44  $\pm$  0.03, 2.88  $\pm$  0.23, และ 6.05  $\pm$  0.64  $\mu\text{M}$ , ตามลำดับ) สำหรับ B7 และ B9 แสดงผลที่ใกล้เคียงกันของระดับ CAT และผลที่เพิ่มขึ้นของระดับ SOD อย่างมีนัยสำคัญในปริมาณสารที่ต่างกันเมื่อเทียบกับ B1 ที่เวลาการทดลอง 7 วัน ด้วยวิธีปฏิกิริยาลูกโซ่พอลิเมอไรเซชันแบบย้อนกลับ (RT-PCR) พบว่าอนุพันธ์ที่ประกอบด้วยหมู่ฟีนอลิก (B7-B9) ให้ผลที่ดีต่อการต้านสารอนุมูลอิสระโดยตรงดีกว่า B1 ในระบบที่ปราศจากเซลล์ แต่สำหรับระบบภายในเซลล์นั้น B1 ให้ผลที่ดีกว่าอนุพันธ์ (B7-B9) ต่อการทดสอบความเป็นพิษต่อเซลล์ ในขณะที่ B7 และ B9 แสดงผลที่ดีกว่าในการเพิ่มระดับการแสดงของยีน SOD

ภาควิชา เคมี  
สาขาวิชา เคมี  
ปีการศึกษา 2557

ลายมือชื่อนิสิต .....

ลายมือชื่อ อ.ที่ปรึกษาหลัก .....

# # 5273856523 : MAJOR CHEMISTRY

KEYWORDS: XYLIA XYLOCARPA / ANTIBACTERIA / ANTIFUNGI / ANTICANCER / COSCINIUM FENESTRATUM / BERBERINE / DITERPENOID / HUMAN FIBROSARCOMA CELLS (HT1080) / ANTIOXIDANT ACTIVITY

VEERACHAI PONGKITTIPHAN: ANTICANCER AND ANTIMICROBIAL COMPOUNDS FROM *Xylia xylocarpa* AND *Coscinium fenestratum* AND STRUCTURE-ACTIVITY RELATIONSHIP STUDIES. ADVISOR: ASST. PROF. WARINTHORN CHAVASIRI, Ph.D., 184 pp.

Sandaracopimaradiene-3 $\beta$ ,18-diol (D1), sandaracopimaradien-3-one (D2) sandaracopimaradien-3 $\beta$ -ol (D3) and sandaracopimaric acid (D4) were isolated from the dichloromethane extract of the heartwoods of *Xylia xylocarpa* (Roxb.) Taub. D1 was selected as a model for SAR study. Five derivatives: D7, D8, D15, D18 and D19 were synthesized and displayed moderate to good antibacterial activity against *Staphylococcus aureus*, *Propionibacterium acnes*, *Streptococcus mutans*, *Streptococcus sobrinus*, and *Salmonella typhi*. D7 and D19 revealed the best MIC as 31.2–62.5  $\mu\text{M}$  to inhibit *S. aureus*, *S. mutans*, *S. sobrinus*, and *S. typhi*. Only D7 showed MBC at 62.5  $\mu\text{M}$  to kill *S. sobrinus*. C2 was synthesized via cyclopropanation of D1 with alkynyl diazoacetate L3. The cytotoxicity of D1-D3 and their derivatives (D7, D8, D15, D18, D19 and C2) against HepG2 (liver hepatocellular carcinoma) by MTS assay displayed that D7, D15 and D18 expressed good activity with  $\text{IC}_{50}$  3.45 $\pm$ 0.47, 1.00 $\pm$ 0.47 and 0.99 $\pm$ 0.08  $\mu\text{M}$ , respectively.

Berberine chloride (B1), isolated from the vines of *Coscinium fenestratum* (Goetgh.) Colebr., was used as a lead structure to synthesize eight derivatives B2-B9 for SAR study. Only B3 exhibited the highest antibacterial activity against *Xanthomonas oryzae* pv. *oryzae* and pv. *oryzicola*. B9, B8, and B7 showed good antioxidant activity ( $\text{IC}_{50}$  = 10.72  $\pm$  1.76, 55.24  $\pm$  2.24, and 87.35  $\pm$  6.65  $\mu\text{M}$ , respectively) via DPPH assay. For cytotoxicity assay against human fibrosarcoma cells (HT1080) using MTT reagent, the sequence of  $\text{IC}_{50}$  at 7-day treatment stated that B1 < B9 < B7 (0.44  $\pm$  0.03, 2.88  $\pm$  0.23, and 6.05  $\pm$  0.64  $\mu\text{M}$ , respectively). B7 and B9 showed approximately the same level of CAT expression and significantly up-regulation of SOD expression in a dose-dependent manner compared to B1 treatment for 7-day exposure using reverse transcription-polymerase chain reaction (RT-PCR) assay. These findings displayed better direct-antioxidant activity of the derivatives containing phenolic groups (B7-B9) than B1 in a cell-free system. For cell-based system, B1 was able to express better cytotoxic activity than its derivatives (B7-B9), whereas B7 and B9 showed better up-regulation of SOD gene expression.

Department: Chemistry

Student's Signature .....

Field of Study: Chemistry

Advisor's Signature .....

Academic Year: 2014

## ACKNOWLEDGEMENTS

The author wishes to express his highest appreciation to his advisor and collaborator, Assist. Prof. Dr. Warinthorn Chavasiri and Prof. Dr. Daniel Romo for his valuable instruction, very kind assistance generous guidance and encouragement throughout the course of this research. Moreover sincere thanks are extended to Natural Products Research Unit (NPRU), Department of Chemistry, Faculty of Science, Chulalongkorn University, and Romo group, Department of Chemistry, Texas A&M University at College Station for the support of chemical and laboratory facilities. The Chulalongkorn University Dutsadi Phiphat Scholarship from Chulalongkorn University is also acknowledged for financial support.

The greatest thanks are also extended to Assist. Prof. Dr. Preecha Lertpratchya, Assoc. Prof. Dr. Nongnuj Muangsin, Assist. Prof. Dr. Khanitha Pudhom, Assist. Prof. Dr. Veena Nukoolkarn and Dr. Supakarn Chamni for their suggestion, comments, correction and helps as thesis examiners.

The author acknowledged Prof. Dr. Ratna Ray from Edward A. Doisy Research Center, Saint Louis University for anticancer assay of diterpenoid compound and Dr. Morgan Jouanneau from Romo Group, Texas A&M University for his technical support. In addition, the author would also like to express special thanks to Assist. Prof. Dr. Roongtawan Supabphol from Department of Physiology, Faculty of Medicine, Srinakharinwirot University for advice, assistance and opinions during the antioxidant research, and also Ms. Waraporn Yahayo for her technical support.

Further acknowledgment is extended to his friend not only in Thailand but also in College Station for friendship and helps throughout the entire of study. Especially, the author is very appreciate to his family members for their love, assistance, understanding, encouragement, and social support throughout his entire education. Without them, the author would never have been able to achieve this goal.

## CONTENTS

	Page
THAI ABSTRACT .....	iv
ENGLISH ABSTRACT .....	v
ACKNOWLEDGEMENTS .....	vi
CONTENTS .....	vii
LIST OF TABLES .....	xii
LIST OF FIGURES .....	xiii
LIST OF SCHEMES .....	xx
LIST OF ABBREVIATIONS .....	xxv
CHAPTER I INTRODUCTION.....	1
CHAPTER II DITERPENOIDS AND THEIR DERIVATIVES FROM <i>Xylia xylocarpa</i> (Roxb.) Taub. AND SAR STUDIES.....	3
I. Introduction.....	3
2.1 Botanical Characteristics of <i>X. xylocarpa</i> .....	3
2.2 Diterpenoids and Chemical Constituent of <i>Xylia sp.</i> .....	4
2.3 Literature Reviews of Diterpenoids and Biological Activities .....	6
2.3.1 Antibacterial Activity .....	6
2.3.2 Antiplasmodial Activity.....	8
2.3.3 Allelopathic Activity .....	8
2.3.4 Antifungal Activity.....	8
2.3.5 Anti-HIV Activity.....	9
2.3.6 Cytotoxicity .....	9
2.4 Literature Reviews of SAR Study of Diterpenoids .....	11
2.4.1 Antibacterial Activity .....	11

	Page
2.4.2 Anti-Inflammatory.....	12
2.4.3 COX-2 Inhibitory Activity .....	12
2.4.4 Cytotoxicity .....	12
2.5 Beta-Lactone Containing Natural Products and Biological Relevance.....	14
2.6 Literature Reviews of Methodology for Beta-Lactone Synthesis.....	15
2.6.1 The Lactonization Process.....	15
2.6.2 Nucleophile-Catalyzed Aldol Lactonization Process (NCAL).....	16
2.6.3 Intermolecular Lewis Acid Catalyzed [2+2] Cycloaddition .....	18
2.6.4 Intermolecular Lewis Base Catalyzed [2+2] Cycloaddition .....	19
2.7 Strategy for Simultaneous Arming and Structure Activity Relationship (SAR) Information of Natural Products .....	20
2.8 Literature Reviews of Strategy for Simultaneous Arming and Structure- Activity Relationship (SAR) Information of Natural Products .....	22
2.9 Objective of This Research .....	25
II. Experimental.....	25
2.10 General Information.....	25
2.11 Extraction and Isolation of Diterpenoids from the Heartwoods of <i>X.</i> <i>xylocarpa</i> .....	26
2.12 Conversion of Non-Covalent Inhibitors to Covalent through Introduction of Beta-Lactones .....	30
2.13 Derivatization of Sandaracopimaradiene-3 $\beta$ ,18-diol (D1) by Simultaneous- Arming .....	38
2.14 Antibacterial Activity Test.....	46



	Page
2.14.1 Preliminary Screening Test of Antibacterial Activity by Diffusion	
Method .....	46
2.14.2 Antibacterial Activity Method Test for MIC and MBC.....	47
2.14.3 Preliminary Screening Test of Antifungal Assay .....	48
2.15 Cytotoxicity (MTS assay) .....	49
2.15.1 Cell Culture .....	49
2.15.2 Preliminary Screening Test of Cytotoxicity by MTS Assay .....	49
III. Results and Discussion.....	50
2.16 Extraction and Isolation of Diterpenoids from the Heartwoods of <i>X.</i> <i>xylocarpa</i> .....	50
2.17 Conversion of Non-Covalent Inhibitors to Covalent through Introduction of Beta-Lactones.....	55
2.17.1 Andrenosterone.....	55
2.17.2 Cholic acid .....	56
2.17.3 Andrographolide .....	57
2.17.4 Sandaracopimaradiene-3 $\beta$ , 18-diol.....	58
2.18 Derivatization of Sandaracopimaradiene-3 $\beta$ ,18-diol (D1) by Simultaneous- Arming .....	70
2.18.1 Synthesis of Alkynyl Diazo Acetate L3.....	71
2.18.2 O-H Insertion of Sandaracopimaradiene-3 $\beta$ ,18-diol (D1).....	73
2.18.3 Synthesis of ( <i>R</i> )-1,1,1-Trichloro-4-(hex-5-yn-1-ylamino)-4-oxobutan-2- yl sulfamate.....	74
2.18.4 C-H Amination of Sandaracopimaradiene-3 $\beta$ ,18-diol (D1).....	76
2.18.5 Cyclopropanation of Sandaracopimaradiene-3 $\beta$ ,18-diol (D1) .....	77

	Page
2.19 Biological Activity of Diterpenoids and Their Derivatives.....	80
2.19.1 Antibacterial Activity.....	80
2.19.2 Antifungal Activity.....	83
2.19.3 Cytotoxic Activity.....	84
CHAPTER III BERBERINE AND ITS DERIVATIVES FROM <i>Coscinium fenestratum</i>	
(Goetgh.) Colebr. AND SAR STUDIES .....	87
I. Introduction.....	87
3.1 Biological Activities of Berberine.....	87
3.1.1 Antibacterial Activity.....	87
3.1.2 Antifungal Activity.....	88
3.1.3 Anti-Inflammatory.....	88
3.1.4 Anticancer Activity.....	89
3.2 Literature Review of Berberine and its Derivatives for SAR Study.....	89
3.2.1 Antimicrobial Activity.....	89
3.2.2 Antifungal Activity.....	91
3.2.3 Antiprotozoal Activity.....	92
3.2.4 Anticancer Activity.....	93
3.3 Reactive Oxygen Species and Enzymatic Antioxidants .....	96
3.4 The Literature Reviews of Berberine for Antioxidant Activity.....	98
3.5 The Human Fibrosarcoma Cells (HT1080).....	99
3.6 Objective of This Research .....	100
II. Experimental.....	101
3.7 General Information .....	101

	Page
3.8 Extraction of Berberine (B1) from <i>C. fenestratum</i> .....	101
3.9 Synthesis of Berberine Derivatives B2-B9.....	102
3.10 Preliminary Screening Test of Antibacterial Activity by Diffusion Method (B1-B9).....	107
3.11 Antioxidant Activity (DPPH assay).....	107
3.12 General Procedure of Cytotoxicity on HT1080 Cell Lines.....	108
3.12.1 Dulbecco's Modified Eagle Medium (DMEM).....	108
3.12.2 Phosphate Buffered Saline (PBS Buffer).....	108
3.12.3 0.02% EDTA solution.....	108
3.12.4 0.1% Trypsin.....	109
3.13 Cell Cultures.....	109
3.14 Cytotoxic Assay.....	109
3.15 RNA Extraction and Reverse Transcriptase PCR.....	110
3.16 Statistical Analysis.....	111
III. Results and Discussion.....	111
3.17 Extraction of Berberine Chloride (B1) from <i>C. fenestratum</i> .....	111
3.18 Synthesis of Berberine Derivative B2-B9.....	112
3.19 The Preliminary Results of Antibacterial Activity of Berberine and Its Derivatives B2-B9.....	120
3.20 The Antioxidant Activity of Berberine (B1) and Its Derivatives B2-B9.....	121
3.21 The Results of Cytotoxicity of Compounds B1 and B7-B9.....	123
3.22 Antioxidant Gene Expression of Compounds B1 and B7-B9 on HT1080.....	125
CHAPTER IV CONCLUSION.....	127
REFERENCES.....	131

	Page
APPENDIX.....	146
VITA.....	184



## LIST OF TABLES

Tables	Pages
2.1 $^1\text{H}$ and $^{13}\text{C}$ NMR chemical shift assignments of compound <b>D1</b> .....	28
2.2 $^1\text{H}$ and $^{13}\text{C}$ NMR chemical shift assignment and 2D correlation of hydroxy acid derivative <b>D18</b> .....	65
2.3 $^1\text{H}$ and $^{13}\text{C}$ NMR chemical shift assignment and 2D correlation of beta-lactone derivative <b>D19</b> .....	68
2.4 Preliminary antibacterial activity of compounds <b>D1-D3, D7, D8, D15, D18</b> and <b>D19</b> at 1,000 $\mu\text{M}$ by disc diffusion method .....	81
2.5 MIC and MBC of compounds <b>D1, D3, D7, D8,</b> and <b>D19</b> .....	82
3.1 List of primers used for PCR amplification .....	111
3.2 Antibacterial activity of berberine chloride ( <b>B1</b> ) and its derivatives <b>B2-B9</b> .....	120
A1 Crystal data and structure refinement for sandaracopimaradiene- $3\beta,18$ -diol ( <b>D1</b> ) .....	147

## LIST OF FIGURES

Figures	Pages
1.1 The structure of sandaracopimaric acid .....	1
2.1 Diterpenoids from the light petroleum extract of the heartwoods of <i>X. dolabriformis</i> .....	5
2.2 The structure of dolabriproanthocyanidin .....	5
2.3 The structure of <i>trans</i> -5-hydroxy pipercolic acid.....	6
2.4 The structures of diterpenoids from the dichloromethane extract of the heartwoods of <i>X. xylocarpa</i> .....	6
2.5 The structure of ferruginol acid.....	7
2.6 The structures of <i>ent</i> -15-pimarene-8 $\beta$ ,19-diol and <i>ent</i> -8(14),15-pimaradien-3 $\beta$ -acetoxy .....	7
2.7 The structure of pedinophyllol A.....	8
2.8 The structures of gemmacolide V and Y.....	9
2.9 The structures of eurifoloids E, F and M .....	9
2.10 The structures of compounds <b>13-15</b> .....	10
2.11 The structures of compounds <b>16-18</b> .....	10
2.12 The structures of fokihodgins I and J .....	10
2.13 The structures of hawaiiolides A-D.....	11
2.14 The structures of acanthoic acid and their derivatives <b>19-21</b> .....	12
2.15 Abietane-type diterpenoids from <i>Perovskia abrotanoides</i> and abietane-type analogues <b>22-23</b> .....	13
2.16 The structures of sphaeropsidin A-C, hawaiiolides D and derivatives <b>24-25</b> .....	13
2.17 Beta-lactone containing natural products.....	14

Figures	Pages
2.18 The acylation of bioactive beta-lactone compounds .....	15
2.19 The structures of TMSQn and TMSQd .....	20
2.20 The mechanism of the Wynberg Lewis base catalyzed [2+2] cycloaddition .....	20
2.21 The heartwoods of <i>X. xylocarpa</i> .....	27
2.22 Antibacterial activity method (resazurin assay).....	48
2.23 The structures of four <i>ent</i> -pimarane diterpenoids <b>D1-D4</b> .....	50
2.24 The perspective ORTEP plot of sandaracopimaradiene-3 $\beta$ ,18-diol ( <b>D1</b> ).....	52
2.25 The structures of andrenosterone, cholic acid, andrographolide and compound <b>D1</b> .....	55
2.26 Selectivity of cyclopropanation, C-H amination and O-H insertion in compound <b>D1</b> .....	71
2.27 Mass spectrum of C-H amination reaction by LCMS.....	77
2.28 The exact mass of C-H amination product <b>P1</b> and aziridinated product <b>P2</b> .....	77
2.29 LCMS Data of cyclopropanation derivative <b>C2</b> (Purity 95%).....	79
2.30 Preliminary antibacterial activity of compounds <b>D1-D3, D7, D8, D15, D18</b> and <b>D19</b> at 1.0 mM by disc diffusion method .....	80
2.31 Effects of CH <sub>2</sub> Cl <sub>2</sub> and EtOAc extracts on the mycelia growth of phytopathogenic fungi on PDA: concentration of testing sample at 10 mg/mL and metalaxyl at 10 mg/mL.....	83
2.32 Inhibitory effects of compounds <b>D1, D2</b> and <b>D4</b> on the mycelial growth of <i>P. Parasittica</i> on a solid culture medium (concentration of testing sample at 1.0 mM and metalaxyl at 10 ppm).....	84
2.33 Preliminary cytotoxicity of compounds <b>D1-3, 7, 8, 15, 18, 19</b> and <b>C2</b> at 5.0 $\mu$ M against HepG2 by MTS assay (treated cells for 24 h) .....	85
3.1 The structures of canadine, beta-hydrastine and canadaline.....	87

Figures	Pages
3.2 The structures of palmatine and jatrorrhizine.....	88
3.3 The structures of compounds <b>H1</b> , <b>INF55</b> and arylmethyl ether hybrid derivatives.....	90
3.4 The structures of compound <b>H2</b> and berberine triazoles.....	91
3.5 The structure of 5,6-didehydro-8,8-diethyl-13-oxodihydroberberine chloride ...	93
3.6 The structures of lincangene, thaicanine and their 8-hydroxy-7,8-dihydro-derivatives.....	94
3.7 The structures of 13- <i>n</i> -hexyl and 13- <i>n</i> -octyl derivatives of berberine and palmatine.....	95
3.8 The role of antioxidant enzymes in the combat of oxidative stress .....	97
3.9 The structures of berberrubine and coptisine .....	99
3.10 The Human Fibrosarcoma Cells (HT1080).....	100
3.11 The vines of <i>Coscinium fenestratum</i> .....	102
3.12 The structure of berberine chloride ( <b>B1</b> ).....	102
3.13 The structure of berberine chloride ( <b>B1</b> ).....	112
3.14 The IC <sub>50</sub> of compounds <b>B5</b> , <b>B7</b> , <b>B8</b> , <b>B9</b> and BHT .....	122
3.15 The effect of compounds <b>B1</b> and <b>B7-B9</b> on % proliferation of HT1080 for 1, 4 and 7 days.....	124
3.16 The effect of compounds <b>B1</b> and <b>B7-B9</b> on the expression levels of SOD and CAT.....	126
4.1 The structures of four known diterpenoids ( <b>D1-D4</b> ) and six derivatives ( <b>D7</b> , <b>D8</b> , <b>D15</b> , <b>D18</b> , <b>D19</b> and <b>C2</b> ).....	128
4.2 The structures of berberine chloride ( <b>B1</b> ) and eight derivatives ( <b>B2-B9</b> ).....	130
A1 The <sup>1</sup> H NMR spectrum of sandaracopimaradiene-3 $\beta$ ,18-diol ( <b>D1</b> ) (CDCl <sub>3</sub> ).....	148



Figures	Pages
A2 The <sup>13</sup> C NMR spectrum of sandaracopimaradiene-3 $\beta$ ,18-diol ( <b>D1</b> ) (CDCl <sub>3</sub> ) .....	148
A3 The <sup>1</sup> H NMR spectrum of sandaracopimaradien-3-one ( <b>D2</b> ) (CDCl <sub>3</sub> ) .....	149
A4 The <sup>13</sup> C NMR spectrum of sandaracopimaradien-3-one ( <b>D2</b> ) (CDCl <sub>3</sub> ) .....	149
A5 The <sup>1</sup> H NMR spectrum of sandaracopimaradien-3 $\beta$ -ol ( <b>D3</b> ) (CDCl <sub>3</sub> ).....	150
A6 The <sup>13</sup> C NMR spectrum of sandaracopimaradien-3 $\beta$ -ol ( <b>D3</b> ) (CDCl <sub>3</sub> ) .....	150
A7 The <sup>1</sup> H NMR spectrum of sandaracopimaric acid ( <b>D4</b> ) (CDCl <sub>3</sub> ).....	151
A8 The <sup>13</sup> C NMR spectrum of sandaracopimaric acid ( <b>D4</b> ) (CDCl <sub>3</sub> ).....	151
A9 The <sup>1</sup> H NMR spectrum of triketochoLANic acid ( <b>A5</b> ) (CD <sub>3</sub> OD).....	152
A10 The <sup>13</sup> C NMR spectrum of triketochoLANic acid ( <b>A5</b> ) (CD <sub>3</sub> OD) .....	152
A11 The <sup>1</sup> H NMR spectrum of 19-dehydroandrographolide ( <b>A10</b> ) (CDCl <sub>3</sub> ).....	153
A12 The <sup>1</sup> H NMR spectrum of sandaracopimaradien-3 $\beta$ ,18-olal ( <b>D7</b> ) (CDCl <sub>3</sub> ).....	153
A13 The <sup>13</sup> C NMR spectrum of sandaracopimaradien-3 $\beta$ ,18-olal ( <b>D7</b> ) (CDCl <sub>3</sub> ).....	154
A14 The <sup>1</sup> H NMR spectrum of 3 $\beta$ -hydroxysandaracopimaric acid ( <b>D8</b> ) (CDCl <sub>3</sub> ) .....	154
A15 The <sup>13</sup> C NMR spectrum of 3 $\beta$ -hydroxysandaracopimaric acid ( <b>D8</b> ) (CD <sub>3</sub> OD) .....	155
A16 The <sup>1</sup> H NMR spectrum of ester derivative <b>D12</b> (CDCl <sub>3</sub> ).....	155
A17 The <sup>1</sup> H NMR spectrum of diterpenoid derivative <b>D13</b> (CDCl <sub>3</sub> ) .....	156
A18 The <sup>1</sup> H NMR spectrum of keto acid derivative <b>D15</b> (CDCl <sub>3</sub> ) .....	156
A19 The <sup>13</sup> C NMR spectrum of keto acid derivative <b>D15</b> (CDCl <sub>3</sub> ) .....	157
A20 The <sup>1</sup> H NMR spectrum of keto derivative <b>D16</b> (CDCl <sub>3</sub> ) .....	157
A21 The <sup>13</sup> C NMR spectrum of keto derivative <b>D16</b> (CDCl <sub>3</sub> ).....	158
A22 The <sup>1</sup> H NMR spectrum of hydroxy acid derivative <b>D18</b> (CDCl <sub>3</sub> ).....	158
A23 The <sup>13</sup> C NMR spectrum of hydroxy acid derivative <b>D18</b> (CDCl <sub>3</sub> ).....	159
A24 The HSQC spectrum of hydroxy acid derivative <b>D18</b> (CDCl <sub>3</sub> ) .....	159

Figures	Pages
A25 The HMBC spectrum of hydroxy acid derivative <b>D18</b> (CDCl <sub>3</sub> ).....	160
A26 The COSY spectrum of hydroxy acid derivative <b>D18</b> (CDCl <sub>3</sub> ).....	160
A27 The <sup>1</sup> H NMR spectrum of beta-lactone derivative <b>D19</b> (CDCl <sub>3</sub> ).....	161
A28 The <sup>13</sup> C NMR spectrum of beta-lactone derivative <b>D19</b> (CDCl <sub>3</sub> ).....	161
A29 The <sup>13</sup> C NMR (DEPT 135°) spectrum of beta-lactone derivative <b>D19</b> (CDCl <sub>3</sub> ) ....	162
A30 The COSY spectrum of beta-lactone derivative <b>D19</b> (CDCl <sub>3</sub> ).....	162
A31 The NOSEY spectrum of beta-lactone derivative <b>D19</b> (CDCl <sub>3</sub> ).....	163
A32 The HSQC spectrum of beta-lactone derivative <b>D19</b> (CDCl <sub>3</sub> ) .....	163
A33 The HMBC spectrum of beta-lactone derivative <b>D19</b> (CDCl <sub>3</sub> ).....	164
A34 The <sup>1</sup> H NMR spectrum of 6-(trimethylsilyl)-hex-5-yn-1-ol ( <b>L1</b> ) (CDCl <sub>3</sub> ).....	164
A35 The <sup>13</sup> C NMR spectrum of 6-(trimethylsilyl)-hex-5-yn-1-ol ( <b>L1</b> ) .....	165
A36 The <sup>1</sup> H NMR spectrum of 6-(trimethylsilyl)hex-5-yn-1-yl 2-cyanoacetate ( <b>L2</b> ) (CDCl <sub>3</sub> ).....	165
A37 The <sup>13</sup> C NMR spectrum of 6-(trimethylsilyl)hex-5-yn-1-yl 2-cyanoacetate ( <b>L2</b> ) (CDCl <sub>3</sub> ).....	166
A38 The <sup>1</sup> H NMR spectrum of imidazole-1-sulfonyl azide hydrochloride ( <b>I1</b> ) (D <sub>2</sub> O)	166
A39 The <sup>13</sup> C NMR spectrum of imidazole-1-sulfonyl azide hydrochloride ( <b>I1</b> ) (D <sub>2</sub> O)	167
A40 The <sup>1</sup> H NMR spectrum of 6-(trimethylsilyl)hex-5-yn-1-yl 2-cyano-2- diazooacetate ( <b>L3</b> ) (CDCl <sub>3</sub> ).....	167
A41 The <sup>13</sup> C NMR spectrum of 6-(trimethylsilyl)hex-5-yn-1-yl 2-cyano-2- diazooacetate ( <b>L3</b> ) (CDCl <sub>3</sub> ).....	168
A42 The <sup>1</sup> H NMR spectrum of mixture diastereomer <b>1</b> ( <b>O1</b> ) (CDCl <sub>3</sub> ).....	168
A43 The <sup>1</sup> H NMR spectrum of mixture diastereomer <b>2</b> ( <b>O1</b> ) (CDCl <sub>3</sub> ).....	169

Figures	Pages
<b>A44</b> The $^1\text{H}$ NMR spectrum of ( <i>R</i> )-4,4,4-trichloro- <i>N</i> -(hex-5-yn-1-yl)-3-hydroxybutanamide ( <b>L4</b> ) ( $\text{CDCl}_3$ ).....	169
<b>A45</b> The $^{13}\text{C}$ NMR spectrum of ( <i>R</i> )-4,4,4-trichloro- <i>N</i> -(hex-5-yn-1-yl)-3-hydroxybutanamide ( <b>L4</b> ) ( $\text{CDCl}_3$ ).....	170
<b>A46</b> The $^1\text{H}$ NMR spectrum of ( <i>R</i> )-1,1,1-trichloro-4-(hex-5-yn-1-ylamino)-4-oxobutan-2-yl sulfamate ( <b>L5</b> ) ( $\text{CDCl}_3$ ).....	170
<b>A47</b> The $^{13}\text{C}$ NMR spectrum of ( <i>R</i> )-1,1,1-trichloro-4-(hex-5-yn-1-ylamino)-4-oxobutan-2-yl sulfamate ( <b>L5</b> ) ( $\text{CDCl}_3$ ).....	171
<b>A48</b> The $^1\text{H}$ NMR spectrum of Di-OTMS-sandaracopimaradiene ( <b>D20</b> ) ( $\text{CDCl}_3$ ).....	171
<b>A49</b> The $^{13}\text{C}$ NMR spectrum of Di-OTMS-sandaracopimaradiene ( <b>D20</b> ) ( $\text{CDCl}_3$ ).....	172
<b>A50</b> The $^1\text{H}$ NMR spectrum of Di-OTMS-sandaracopimaradiene <b>C1</b> with dr = 6:1:4:1 ( $\text{CDCl}_3$ ).....	172
<b>A51</b> The $^{13}\text{C}$ NMR spectrum of Di-OTMS-sandaracopimaradiene <b>C1</b> with dr = 6:1:4:1 ( $\text{CDCl}_3$ ).....	173
<b>A52</b> The $^1\text{H}$ NMR spectrum of cyclopanation derivative <b>C2</b> with dr = 6:1:4:1 ( $\text{CDCl}_3$ ).....	173
<b>A53</b> The $^{13}\text{H}$ NMR spectrum of cyclopanation derivative <b>C2</b> with dr = 6:1:4:1 ( $\text{CDCl}_3$ ).....	174
<b>A54</b> The $^1\text{H}$ NMR spectrum of berberine chloride ( <b>B1</b> ) ( $\text{CD}_3\text{OD}$ ).....	174
<b>A55</b> The $^{13}\text{C}$ NMR spectrum of berberine chloride ( <b>B1</b> ) ( $\text{CD}_3\text{OD}$ ).....	175
<b>A56</b> The $^1\text{H}$ NMR spectrum of acetonyl-berberine ( <b>B2</b> ) ( $\text{CDCl}_3$ ).....	175
<b>A57</b> The $^{13}\text{C}$ NMR spectrum of acetonyl-berberine ( <b>B2</b> ) ( $\text{CDCl}_3$ ).....	176
<b>A58</b> The $^1\text{H}$ NMR spectrum of 13-benzyl-berberine ( <b>B3</b> ) ( $\text{CDCl}_3$ ).....	176
<b>A59</b> The $^{13}\text{C}$ NMR spectrum of 13-benzyl-berberine ( <b>B3</b> ) ( $\text{CDCl}_3$ ).....	177

Figures	Pages
A60 The $^1\text{H}$ NMR spectrum of 8-cyano-13, 14-dehydrocanadiene ( <b>B4</b> ) ( $\text{CDCl}_3$ ) .....	177
A61 The $^{13}\text{C}$ NMR spectrum of 8-cyano-13, 14-dehydrocanadiene ( <b>B4</b> ) ( $\text{CDCl}_3$ ) .....	178
A62 The $^1\text{H}$ NMR spectrum of canadine ( <b>B5</b> ) ( $\text{CDCl}_3$ ).....	178
A63 The $^{13}\text{C}$ NMR spectrum of canadine ( <b>B5</b> ) ( $\text{CDCl}_3$ ).....	179
A64 The $^1\text{H}$ NMR spectrum of 8-phenyl-13, 14-dehydrocanadiene ( <b>B6</b> ) ( $\text{CDCl}_3$ ).....	179
A65 The $^{13}\text{C}$ NMR spectrum of 8-phenyl-13, 14-dehydrocanadiene ( <b>B6</b> ) ( $\text{CDCl}_3$ ).....	180
A66 The $^1\text{H}$ NMR spectrum of berberrubine ( <b>B7</b> ) ( $\text{CDCl}_3$ ).....	180
A67 The $^{13}\text{C}$ NMR spectrum of berberrubine ( <b>B7</b> ) ( $\text{CDCl}_3$ ).....	181
A68 The $^1\text{H}$ NMR spectrum of berberrubine HCl ( <b>B8</b> ) ( $\text{DMSO}-d_6$ ).....	181
A69 The $^{13}\text{C}$ NMR spectrum of berberrubine HCl ( <b>B8</b> ) ( $\text{DMSO}-d_6$ ).....	182
A70 The $^1\text{H}$ NMR spectrum of 2,3,9,10- <i>tetra</i> -hydroxyberberine chloride ( <b>B9</b> ) ( $\text{CD}_3\text{OD}$ ).....	182
A71 The $^{13}\text{C}$ NMR spectrum of 2,3,9,10- <i>tetra</i> -hydroxyberberine chloride ( <b>B9</b> ) ( $\text{CD}_3\text{OD}$ ).....	183

## LIST OF SCHEMES

Schemes	Pages
1.1 The general preparation of berberine derivatives.....	2
2.1 The lactonization step to synthesize beta-lactone in belactosin C.....	16
2.2 The synthesis of (+)-vittatalactone <i>via</i> lactonization.....	16
2.3 Proposed mechanistic pathway of the NCAL process.....	17
2.4 The asymmetric NCAL process using ( <i>S</i> )-HBTM as a catalyst.....	17
2.5 The NCAL process to synthesized bicyclic beta-lactone in ( $\pm$ )-spongiolactone .....	18
2.6 Beta-lactone synthesis <i>via</i> asymmetric [2+2] cycloaddition of TMS-ketene and aldehydes .....	18
2.7 The beta-lactone synthesis using quinidine or quinine as catalyst.....	19
2.8 Generalized two-step derivatization/conjugation strategy for simultaneous arming and structure activity studies of natural products for use in chemical genetics employing substrate or substrate/reagent control, a type of “double diastereodifferentiation”. FG = Functional group.....	21
2.9 Two-step O-H insertion/Sharpless Huisgen cycloaddition sequence for simultaneous arming and SAR studies of natural products .....	22
2.10 Two-step iodination/metal-mediated coupling reactions sequence for simultaneous arming and SAR studies of arene-containing natural products.....	23
2.11 Simultaneous arming and SAR studies of alkene-containing natural products by cyclopropanation.....	24
2.12 C–H Amination or aziridination-conjugation sequence for simultaneous arming and SAR studies of natural products.....	24
2.13 The oxidation of andrenosterone ( <b>A1</b> ) to keto acid derivative ( <b>A2</b> ).....	31

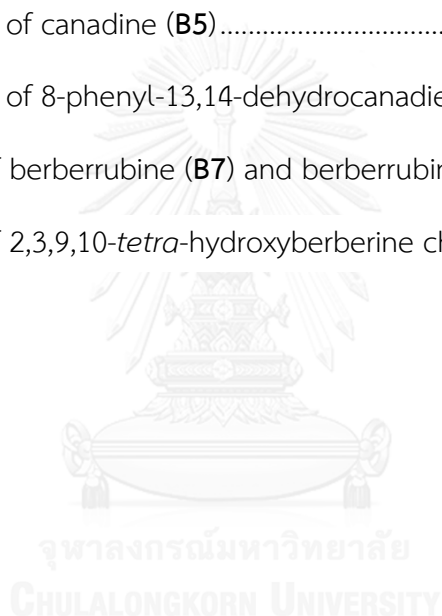
Schemes	Pages
2.14 The synthesis of triketocholanic acid (A5).....	31
2.15 The synthesis of 19-dehydroandrographolide (A10).....	32
2.16 The synthesis of sandaracopimaradien-3 $\beta$ ,18-olal (D7).....	33
2.17 The synthesis of 3 $\beta$ -hydroxysandaracopimaric acid (D8).....	34
2.18 The synthesis of ester derivative D12.....	34
2.19 The hydrolysis of mixture D12 to D13.....	35
2.20 The synthesis of derivatives D15 and D16.....	36
2.21 The synthesis of hydroxy acid derivative D18.....	37
2.22 The synthesis of beta-lactone derivative D19.....	38
2.23 The synthesis of 6-(trimethylsilyl)-hex-5-yn-1-ol (L1).....	39
2.24 The synthesis of 6-(trimethylsilyl)hex-5-yn-1-yl 2-cyanoacetate (L2).....	39
2.25 The synthesis of imidazole-1-sulfonyl azide hydrochloride (I1).....	40
2.26 The synthesis of 6-(trimethylsilyl)hex-5-yn-1-yl 2-cyano-2-diazoacetate (L3)....	40
2.27 The synthesis of O-H insertion derivative (O1).....	41
2.28 The synthesis of ( <i>R</i> )-4,4,4-trichloro- <i>N</i> -(hex-5-yn-1-yl)-3-hydroxybutanamide (L4).....	42
2.29 The synthesis of ( <i>R</i> )-1,1,1-trichloro-4-(hex-5-yn-1-ylamino)-4-oxobutan-2-yl sulfamate (L5).....	43
2.30 C-H Amination of sandaracopimaradiene-3 $\beta$ ,18-diol.....	44
2.31 The synthesis of di-OTMS-sandaracopimara-3 $\beta$ ,18-diene (D20).....	44
2.32 Cyclopropanation of sandaracopimara-3 $\beta$ ,18-diene (C1).....	45
2.33 The synthesis of cyclopropanation derivative C2.....	46
2.34 Reduction of resazurin (blue) to resorufin (pink).....	48
2.35 Reduction of MTS to formazen.....	50

Schemes	Pages
2.36 Proposed conversion of andrenosterone ( <b>A1</b> ) to beta-lactone derivative <b>A3</b> ....	55
2.37 The synthesis of 1,5-keto acid derivative <b>A2</b> .....	56
2.38 Proposed conversion of cholic acid ( <b>A4</b> ) to beta-lactone derivative <b>A6</b> .....	56
2.39 The forward synthesis of triketocholanic ( <b>A5</b> ).....	57
2.40 The NCAL process of triketocholanic ( <b>A5</b> ) .....	57
2.41 Proposed conversion of andrographolide ( <b>A7</b> ) to beta-lactone derivative <b>A9</b> ..	57
2.42 The TEMPO oxidation of andrographolide ( <b>A7</b> ) to give 19-dehydroandrographolide ( <b>A10</b> ) .....	58
2.43 The first route to synthesize beta-lactone derivative <b>D6</b> .....	59
2.44 The TEMPO oxidation of <b>D1</b> to prepare sandaracopimaradiene-3 $\beta$ ,18-olal ( <b>D7</b> ) .....	59
2.45 The synthesis of 3 $\beta$ -hydroxysandaracopimaric acid ( <b>D8</b> ) from <b>D7</b> .....	60
2.46 Mitsunobu cyclization of 3 $\beta$ -hydroxysandaracopimaric acid ( <b>D8</b> ).....	60
2.47 The proposed synthesis of beta-lactone derivative <b>D6</b> .....	61
2.48 Mitsunobu reaction of sandaracopimaradiene-3 $\beta$ ,18-diol ( <b>D1</b> ).....	61
2.49 Hydrolysis of mixture <b>D12</b> to <b>D13</b> .....	62
2.50 The third route to synthesize of beta-lactone derivative <b>D6</b> .....	62
2.51 Jones oxidation of sandaracopimaradiene-3 $\beta$ ,18-diol ( <b>D1</b> ) .....	63
2.52 Proposed mechanism for the formation of compounds <b>D15</b> and <b>D16</b> from <b>D1</b> .....	64
2.53 Reduction of keto acid derivative <b>D15</b> to hydroxy acid derivative <b>D18</b> .....	64
2.54 The synthesis of beta-lactone derivative <b>D19</b> <i>via</i> NCAL process.....	67
2.55 The formation of the acylammonium transition state for high diastereoselectivity .....	70

Schemes	Pages
2.56 The synthesis of 6-(trimethylsilyl)-hex-5-yn-1-ol ( <b>L1</b> ) .....	71
2.57 The synthesis of 6-(trimethylsilyl)-hex-5-yn-1-yl 2-cyanoacetate ( <b>L2</b> ) .....	72
2.58 The synthesis of imidazole-1-sulfonyl azide hydrochloride ( <b>I1</b> ).....	72
2.59 The synthesis of 6-(trimethylsilyl)-hex-5-yn-1-yl 2-cyano-2- diazoacetate ( <b>L3</b> ) ..	73
2.60 O-H insertion of sandaracopimaradiene-3 $\beta$ ,18-diol ( <b>D1</b> ).....	73
2.61 The preparation of ( <i>R</i> )-4,4,4-trichloro- <i>N</i> -(hex-5-yn-1-yl)-3-hydroxybutanamide ( <b>L4</b> ).....	75
2.62 The synthesis of ( <i>R</i> )-1,1,1-trichloro-4-(hex-5-yn-1-ylamino)-4-oxobutan-2-yl sulfamate ( <b>L5</b> ) .....	76
2.63 C-H Amination of sandaracopimaradiene-3 $\beta$ ,18-diol ( <b>D1</b> ) with compound <b>L5</b> ...	76
2.64 The synthesis of di-OTMS-sandaracopimara-3 $\beta$ ,18-diene ( <b>D20</b> ) .....	77
2.65 Cyclopropanation reaction of di-OTMS-sandaracopimara-3 $\beta$ , 18-diene ( <b>D20</b> ) ....	79
2.66 Desilylation of compound <b>C1</b> .....	79
3.1 The synthesis of 8-alkyl-, 8-phenyl-substituted and 12-bromo-derivatives from berberine.....	90
3.2 The preparation of 13-(substituted benzyl) of berberine and berberrubine derivatives .....	92
3.3 The structures of synthesized berberine derivatives .....	93
3.4 The synthesis of 9- <i>O</i> -alkyl- and 9- <i>O</i> -terpenyl- substituted berberine .....	95
3.5 The synthesis of acetyl-berberine ( <b>B2</b> ) .....	103
3.6 The synthesis of 13-benzyl-berberine ( <b>B3</b> ) .....	103
3.7 The synthesis of 8-cyano-13, 14-dehydrocanadiene ( <b>B4</b> ).....	104
3.8 The synthesis of canadine ( <b>B5</b> ).....	104
3.9 The synthesis of 8-phenyl-13, 14-dehydrocanadiene ( <b>B6</b> ) .....	105



Schemes	Pages
3.10 The synthesis of berberrubine ( <b>B7</b> ) and Berberrubine chloride ( <b>B8</b> ).....	106
3.11 The synthesis of 2,3,9,10- <i>tetra</i> -hydroxyberberine chloride ( <b>B9</b> ) .....	106
3.12 Reduction of MTT to formazen .....	110
3.13 The synthesis of acetonyl-berberine ( <b>B2</b> ) .....	113
3.14 The synthesis of 13-benzyl-berberine ( <b>B3</b> ) .....	114
3.15 The preparation of 8-cyano-13,14-dehydrocanadiene ( <b>B4</b> ).....	115
3.16 The preparation of canadine ( <b>B5</b> ).....	116
3.17 The preparation of 8-phenyl-13,14-dehydrocanadiene ( <b>B6</b> ).....	117
3.18 The synthesis of berberrubine ( <b>B7</b> ) and berberrubine chloride ( <b>B8</b> ).....	118
3.19 The synthesis of 2,3,9,10- <i>tetra</i> -hydroxyberberine chloride ( <b>B9</b> ) .....	119



## LIST OF ABBREVIATIONS

Å	angstroms
AlCl <sub>3</sub>	aluminum chloride
aq.	aqueous
BHT	3,5-di- <i>tert</i> -butyl-4-hydroxytoluene
Bn	benzyl
Bu	<i>n</i> -butyl
bs	broad singlet (NMR)
calcd	calculated
conc.	concentrated
CH <sub>2</sub> Cl <sub>2</sub>	dichloromethane
d	doublet (NMR)
DCC	1,3-dicyclohexylcarbodiimide
dd	doublet of doublets (NMR)
ddd	doublet of doublet of doublets (NMR)
DIPEA	<i>N,N</i> -diisopropylethylamine
DMA	<i>N,N</i> -dimethylacetamide
DMAP	4-( <i>N,N</i> -dimethylamino)pyridine
DMF	<i>N,N</i> -dimethylformamide
DMSO	dimethylsulfoxide
DPPH	2,2-diphenyl-1-picrylhydrazyl
dt	doublet of triplets (NMR)
EC <sub>50</sub>	effective concentration 50 %
equiv.	equivalent (s)
Et	ethyl
EtOAc	ethyl acetate

EtOH	ethanol
g	gram (s)
h	hour (s)
HepG2	liver hepatocellular carcinoma
HT1080	human fibrosarcoma cell
Hz	hertz
IC <sub>50</sub>	inhibition concentration 50 %
IR	infrared
<i>J</i>	coupling constant (NMR)
m	multiplet (NMR)
MBC	minimum bactericidal concentration
Me	methyl
MeOH	methanol
MIC	minimal inhibitory concentration
μg	microgram (s)
μM	micromolar (s)
M	molar (s)
mg	milligram (s)
min	minute (s)
mL	milliliter (s)
mmol	millimole (s)
MTT	3-(4,5-dimethylthiazol-2-yl)-2,5-diphenyltetrazolium bromide
MTS	3-(4,5-dimethylthiazol-2-yl)-5-(3-carboxymethoxyphenyl)-2-(4-sulfophenyl)-2H-tetrazolium
N	normal
Na <sub>2</sub> CO <sub>3</sub>	sodium carbonate
NaClO <sub>2</sub>	sodium chlorite

nm	nanometer (s)
NMR	nuclear magnetic resonance
°C	degree of Celsius
Ph	phenyl
ppm	part per million
<i>p</i> -TsCl	4-toluenesulfonyl chloride
q	quartet (NMR)
quant	quantitative
$R_f$	retardation factor
rt	room temperature
s	singlet (NMR)
t	triplet (NMR)
<i>t</i>	tert
TBAF	tetrabutylammonium fluoride
TBAI	tetrabutylammonium iodide
td	triplet of doublets (NMR)
THF	tetrahydrofuran
TLC	thin layer chromatograph
UV	ultraviolet
%	percent
$\alpha$	alpha
$\beta$	beta
$\gamma$	gamma
$\delta$	chemical shift

## CHAPTER I

### INTRODUCTION

Diterpenoids, the secondary metabolites of natural products, had a diverse structure. Most diterpenoids were isolated from plant sources and displayed a wide variety of biological activities including antimicrobial [1, 2], anti-HIV [3], anti-inflammatory [4] and anticancer [5]. Moreover, the structural activity relationship (SAR) of diterpenoids and their derivatives gave a rich of data to improve and synthesize new desired compounds [6].

*Xylia xylocarpa* (Roxb.) Taub. (synonym: *Xylia dolabriformis*), Thai hardwoods which are normally used for building construction, constituted several *ent*-pimarane diterpenoids [7]. These diterpenoids exhibited interesting biological activities including antimicrobial [8, 9] and cytotoxicity [10]. In addition, the dichloromethane extract of the hardwoods contained several *ent*-pimarane diterpenoids and sandaracopimaric acid (Figure 1.1) exhibited the highest antifeedant activity against *Spodoptera litura* ( $ED_{50} = 2.75 \times 10^{-7}$  mol/cm<sup>2</sup>). Moreover, all isolated compounds had potent feeding inhibitory against termites and showed negative tests for phytotoxicity against lettuce seedlings [11, 12]. The structure activity relationship study of diterpenoids provide the informative data of a role of functional group and structural skeleton towards activity including antibacterial [13], cyclooxygenase 2 (COX-2) inhibition [14], cytotoxicity [15] and antifouling [16].

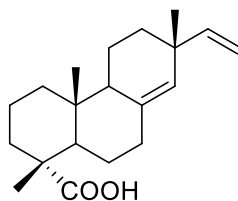
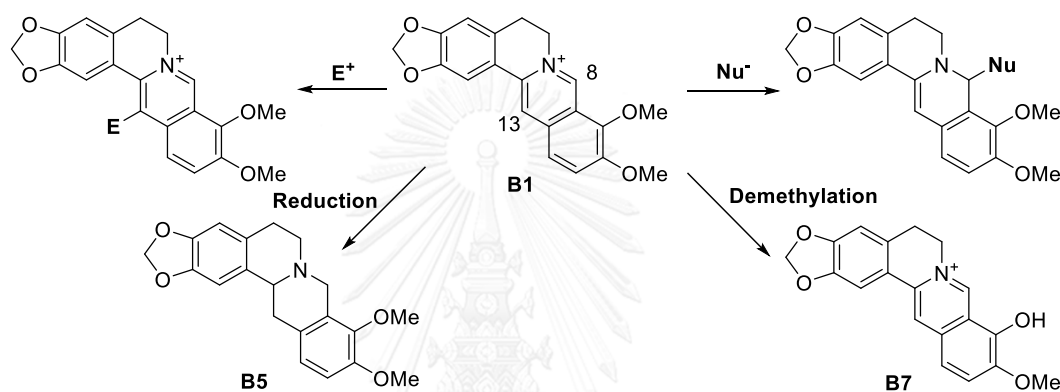


**Figure 1.1** The structure of sandaracopimaric acid

Berberine chloride (**B1**), an isoquinoline alkaloid, was found as a major constituent in *Coscinium fenestratum* (Goetgh.) Colebr. [17]. This compound exhibited a wide variety of biological activities including anti-inflammatory [18], antibacteria [19], antifeedant [20], antifungi [21], anticancer [22] and maintenance of insulin level [23]. In general, berberine can be converted to several derivatives for SAR studies [21] by electrophilic addition to C-13 position, nucleophilic addition to C-8 position, reduction to canadine (**B5**), or demethylation to berberrubine (**B7**) (Scheme 1.1) [24-26].



**Scheme 1.1** The general preparation of berberine derivatives

Recently, berberine has been modified to several advanced structural derivatives and could improve their biological activities toward antibacterial [26], antifungal [27] or anticancer activity [28]. Moreover, this compound was explored for the mechanistic pathway in gene not only *in vitro* but also *in vivo* including cyclophosphamide (CP)-induced hepatotoxicity [29], the axonal transport impairment induced by Calyculin A in N2a cells [30], or antifungal activity to inhibit the growth of *Cryptococcus neoformans* by regulating gene expression [31].

As mentioned above, the researcher aims to isolate diterpenoids from the heartwoods of *X. xylocarpa* and berberine chloride from the vines of *C. fenestratum*. These derivatives were then synthesized and tested for biological activities and to investigate the SAR studies.

CHAPTER II  
DITERPENOIDS AND THEIR DERIVATIVES  
FROM *Xylia xylocarpa* (Roxb.) Taub. AND SAR STUDIES

## I. Introduction

### 2.1 Botanical Characteristics of *X. xylocarpa*

*Xylia* belongs to Leguminosae-Mimosoideae family. There are 12 different species in this genus mainly in Tropical Africa and Madagascar. Only one species is found in Asia and this genus can be separated into 2 varieties [32].

#### 1. *kerrii*:

Botanical name: *Xylia xylocarpa* (Roxb.) Taub. var. *kerri* (Craib&Hutch) I.C. Nielsen

Synonym: *Xylia kerrii* Craib & Hutch

Distribution: Burma, Laos, Cambodia, Vietnam, Thailand

#### 2. *xylocarpa*:

Botanical name: *Xylia xylocarpa* (Roxb.) Taub.

Synonym: *Xylia dolabriformis* Benth.

Distribution: India and Burma

Anthers and leaflets of these 2 varieties are different. The leaflets of *kerrii* type is puberulous to densely velutinous but *xylocarpa* type is glabrous to faintly puberulous beneath. The anthers of *kerrii* is glandular but *xylocarpa* is glandular. This plant namely Daeng is general name or other names are Phan, Kwai, Jalan, Khom, Takhom and others [33]. This plant grows in dry deciduous dipterocarp forests, mixed

deciduous forest, dry evergreen forest, and deciduous forest. The botanical characteristics can be classified:

**Tree:** deciduous tree to 30 m with slender drooping branches and straight trunk.

**Bark:** heartwood reddish brown, thin, red-brown or creamy brown, inner bark pink, peeling in round flakes.

**Leaves:** bipinnate with a single pair of side stalks, 10 - 30 cm, each with 3 - 7 pairs of opposite leaflets, top ones largest, 4 - 15 x 2.5 - 6 cm, narrowly ovate or elliptic with slightly pointed tips. Young leaves delicate pink, appearing in March to April just after the flowers. Leaflet stalks 0.2 - 0.3 cm, main stalk 3 - 8 cm, all joints with rounded glands. Young shoots densely covered with yellowish hairs, mature leaves smooth above, normally with minute pale brown hairs below.

**Flowers:** pale yellow, in dense spherical heads, 1.5 - 2 cm, and solitary or in very short, unbranched clusters in axils of fallen leaves. Head stalks 3.5 - 5 cm, individual flowers without stalks, 5 petals, 3.5 - 4.5 mm, slightly fused at base, hairy outside. 10 - 12 free stamens, 5 - 12 mm, much longer than petals, 5 stamens longer than other, anthers without glands.

**Seed:** 6 - 10 flat in a fruit, dark brown seed 2 x 1.2 cm.

**Fruit:** 10 - 15 x 5 - 6 cm, thick & woody, slightly curved, tapering at base, pale creamy brown, splitting suddenly into 2 parts which curl backwards, remaining on the tree for a long time.

## 2.2 Diterpenoids and Chemical Constituent of *Xylia* sp.

There are a few researches on the chemical constituents for var. *xylocarpa* since Laidlaw and Morgan reported in 1963 [7]. The light petroleum extract of the heartwoods of *X. dolabriformis* composed of six diterpenoids including manoyl oxide (8 $\alpha$ , 13R-epoxy-14-labdaen-3-ol) (**1**), 3-oxomanyl oxide (8 $\alpha$ , 13R-epoxy-14-labdaen-



3one) (2), 8(14),15-isopimaradiene (3), 8(14),15-isopimaradiene-3-one (4), 8(14),15-isopimaradiene-3 $\beta$ -ol (5), and 8(14),15-isopimaradiene-3,18-diol (6) [7]. The structures of these compounds were displayed below in Figure 2.1.

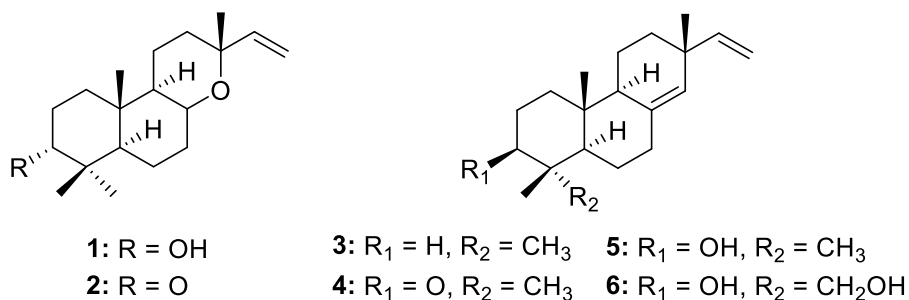


**Figure 2.1** Diterpenoids from the light petroleum extract of the heartwoods of *X. dolabriformis*

In 1976, Kumar *et al.* reported that dolabripuroanthocyanidin was isolated from the stem barks of *X. dolabriformis* (Figure 2.2) [34].

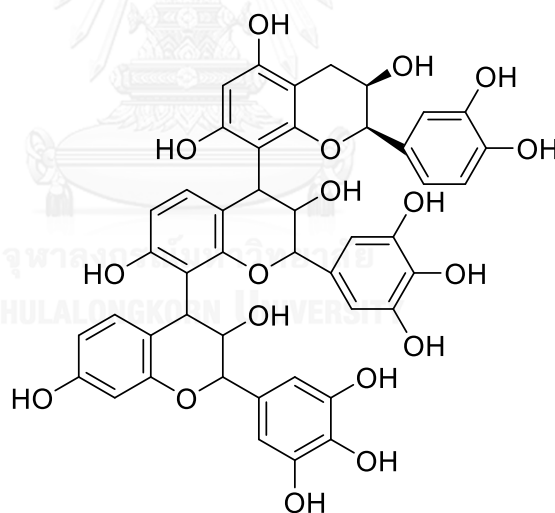


**Figure 2.2** The structure of dolabripuroanthocyanidin

In 1979, Mester *et al.* isolated *trans*-5-hydroxy pipecolic acid (Figure 2.3), which revealed a good inhibitor of platelet aggregation induced by serotonin from the leaves of *X. dolabriformis* [35].

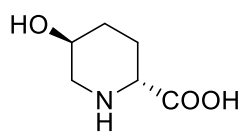


**Figure 2.3** The structure of *trans*-5-hydroxy pipercolic acid

In 2003, Sittiwong investigated the chemical constituents of the dichloromethane extract of *X. xylocarpa*, local Thai hardwood (Iron wood). A wide variety of diterpenoids **7-12** (Figure 2.4) was identified. Sandaracopimaric acid (**9**) showed the highest antifeedant activity against *S. litura* ( $ED_{50} = 2.75 \times 10^{-7}$  mol/cm<sup>2</sup>). Moreover, all isolated compounds had potent feeding inhibitory against termites and showed negative tests for phytotoxicity against lettuce seedlings [11].

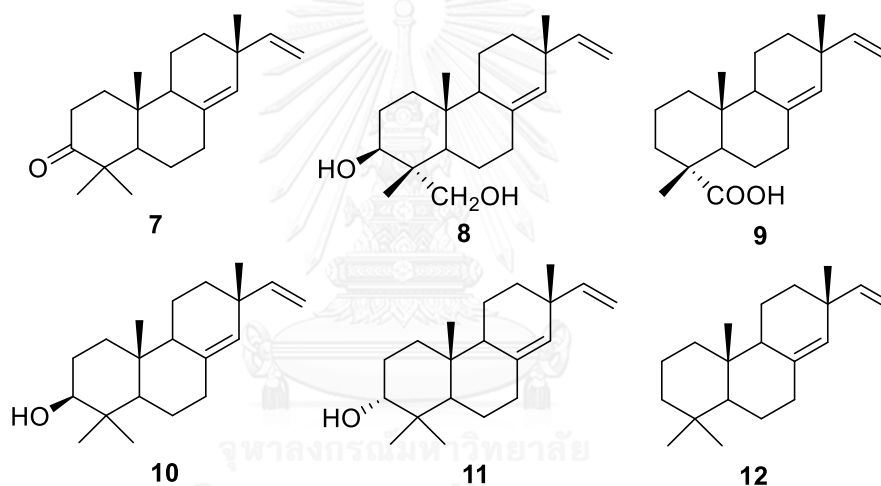


**Figure 2.4** The structures of diterpenoids from the dichloromethane extract of the heartwoods of *X. xylocarpa*

## 2.3 Literature Reviews of Diterpenoids and Biological Activities

### 2.3.1 Antibacterial Activity

In 2008, Li *et al.* disclosed that the ethanolic extract of the stembarks of *Cryptomeria japonica* displayed good antibacterial activity against *Enterococcus faecalis*, *Staphylococcus aureus*, *Staphylococcus epidermidis* and Methicillin-resistant *Staphylococcus aureus* (MRSA). Seven diterpenoids (ferruginol, isopimaric acid, iguestol, isopimarol, phyllocladan-16 $\alpha$ -ol, sandaracopimarinol and sugiol) and two

steroids ( $\beta$ -sitosterol and  $\beta$ -sitostenone) were isolated. Ferruginol acid (Figure 2.5) possessed the strongest antibacterial activity against all bacteria with MIC ranging from 6.3 to 12.5  $\mu\text{g}/\text{mL}$  [1].

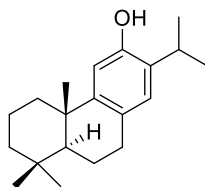


**Figure 2.5** The structure of ferruginol acid

In 2009, Porto *et al.* reported that the dichloromethane extract from the roots of *Viguiera arenaria* was significantly active only against Gram-positive bacteria. The major isolated diterpenes, *ent*-pimara-8(14),15-dien-19-oic acid (**9**), *ent*-8(14),15-pimaradien-3 $\beta$ -ol (**10**), *ent*-15-pimarene-8 $\beta$ ,19-diol, and *ent*-8(14),15-pimaradien-3 $\beta$ -acetoxo (Figure 2.6) exhibited highest antibacterial activity (MIC < 10  $\mu\text{g}/\text{mL}$ ) [2].

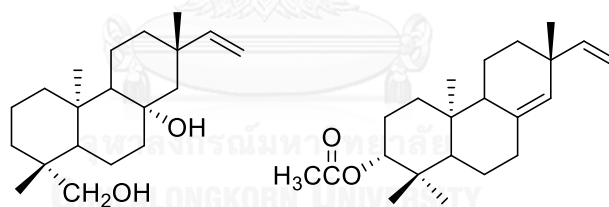


**Figure 2.6** The structures of *ent*-15-pimarene-8 $\beta$ ,19-diol and *ent*-8(14),15-pimaradien-3 $\beta$ -acetoxo

In 2013, Porto *et al.* studied the antimicrobial activity of five pimarane-type diterpenes from fungal biotransformation against several nosocomial multidrug-resistant bacteria. *ent*-8(14),15-Pimaradien-3 $\beta$ -ol (**10**) displayed the most active compound with MIC 8.0 and 25.0  $\mu\text{g}/\text{mL}$  against *S. aureus* and *E. faecalis*, respectively. This compound revealed antibacterial activity that exerted time-kill assays against *S. aureus* (HCRP180) within 24 h at all evaluated concentrations (8, 16, and 24  $\mu\text{g}/\text{mL}$ ). The result of combination was able to rapidly reduce the number of viable strains of

*S. aureus* within the first 6 h, when this metabolite was associated with vancomycin at their MIC values [8].

### 2.3.2 Antiplasmodial Activity

In 2004, Asili *et al.* reported that six labdanes and four isopimarane diterpenoids were isolated from *Platycladus orientalis*. These compounds were tested for their *in vitro* antiplasmodial activity against *Plasmodium falciparum* strain 3D7 and for their ability to induce changes of erythrocyte shape. All tested compounds exhibited weak activity ( $IC_{50} > 25 \mu M$ ) [4].

### 2.3.3 Allelopathic Activity

In 2013, Liu *et al.* isolated ten highly oxygenated *ent*-pimarane-type diterpenoids, pedinophyllols A–J from the Chinese liverwort *Pedinophyllum interruptum*. Allelopathic testing displayed that these diterpenoids inhibited the germination of *Arabidopsis thaliana* seeds. Pedinophyllol A (Figure 2.7) significantly retarded *Arabidopsis* seed germination with  $IC_{50}$  7.8  $\mu g/mL$  [6].

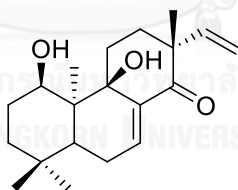
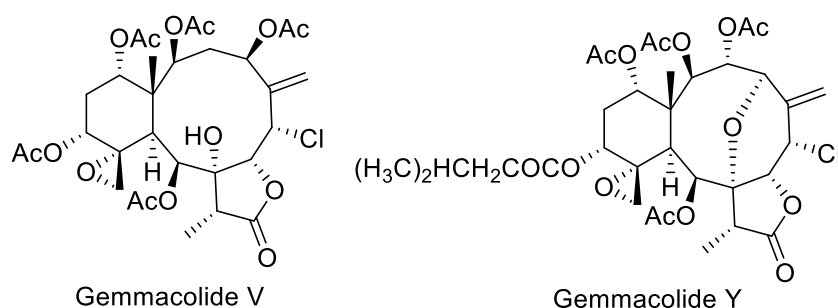


Figure 2.7 The structure of pedinophyllol A

### 2.3.4 Antifungal Activity

In 2012, Li and co-workers isolated six briarane diterpenoids: gemmacolides T–Y together with three known compounds: juncenolide J, praelolide, and junceollolide C from the South China Sea gorgonian *Dichotella gemmacea*. These compounds revealed weak antimicrobial activity against fungi, *Microbotryum violaceum* and *Septoria tritici*, and the bacterium *Escherichia coli*. Moreover, gemmacolides V and Y (Figure 2.8) displayed potent growth inhibition towards tumor

cell lines of A549 and MG63, being stronger than adriamycin as the positive control [36].



**Figure 2.8** The structures of gemmacolide V and Y

### 2.3.5 Anti-HIV Activity

In 2014, Zhao and co-workers discovered eighteen diterpenoids: eurifoloids A–R including ingenane, abietane, isopimarane, and *ent*-atisane types from *Euphorbia nerifolia*. Eurifoloid M disclosed a rare class of *ent*-atisane-type norditerpenoid. Eurifoloids E and F (Figure 2.9) exhibited significant anti-HIV activity with  $EC_{50}$   $3.58 \pm 0.31$  (SI = 8.6) and  $7.40 \pm 0.94$   $\mu$ M (SI = 10.3), respectively [3].

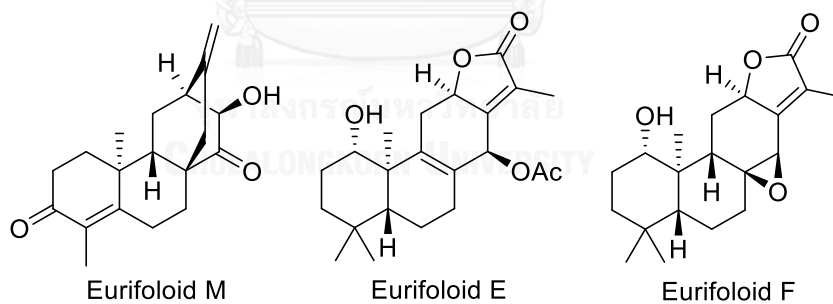


**Figure 2.9** The structures of eurifoloids E, F and M

### 2.3.6 Cytotoxicity

In 2004, Barrero *et al.* isolated eight abietane diterpenoids from the leaves of *Juniperus thurifera* var. *africana* and *Juniperus phoenicea*, grown in Morocco. These compounds were tested with cytotoxicity against five cell lines including A-549 (human lung carcinoma), H-116 (human colon carcinoma), PSN1 (human pancreatic adenocarcinoma), T98G (human caucasian glioblastoma), and SKBR3 (human breast

carcinoma). Compounds **13-15** (Figure 2.10) showed an inhibitory activity against H-116 with  $IC_{50}$  2.5  $\mu\text{g/mL}$  [37].

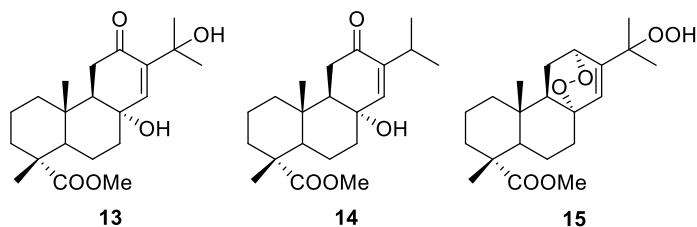


**Figure 2.10** The structures of compounds **13-15**

In 2010, Zhao *et al.* isolated isopimarane and aromatic diterpenoids from *Trogopterus xanthipes*. All isolated diterpenoids were evaluated *in vitro* for cytotoxic activity against six human tumor cell lines: HL-60, K562, U937, HepG2, MCF-7, and SGC7901. Only compounds **16-18** (Figure 2.11) exhibited moderate cytotoxic activity with  $IC_{50}$  in range of 19.7-35.0  $\mu\text{M}$ , whereas most compounds showed no significant activity [15].

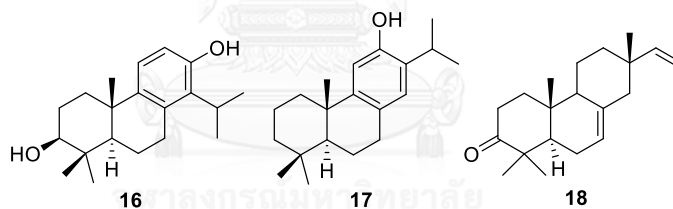


**Figure 2.11** The structures of compounds **16-18**

In 2013, Wu *et al.* isolated isopimarane diterpenoids, fokihodgins A-E, four labdane diterpenoids, fokihodgins F-I and one icetexane diterpenoid, fokihodgin J (Figure 2.12) from *Fokienia hodginsii*. Only fokihodgin I showed moderate cytotoxicity against HL-60 and SMMC-7721 cell lines with  $IC_{50}$  9.10 and 7.50  $\mu\text{M}$ , respectively [5].

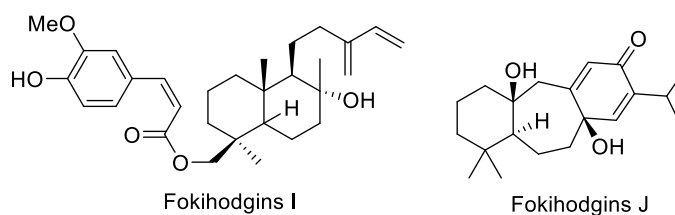


**Figure 2.12** The structures of fokihodgins I and J

In 2014, Chen and co-workers isolated hawaiiinolides A–D (Figure 2.13), which are three cleistanthanes (A, C, and D) and one cassane (B) type of diterpene lactone, from the extract of *Paraconiothyrium hawaiiense*, a fungus entomogenous to the *Septobasidium*-infected insect *Diaspidiotus sp.* Hawaiiinolides A demonstrated significant cytotoxicity against a small panel of five human tumor cell lines including A549, T24, HeLa, HCT116, and MCF-7 with  $IC_{50}$  in range of 2.84 – 7.48  $\mu\text{M}$  [12].

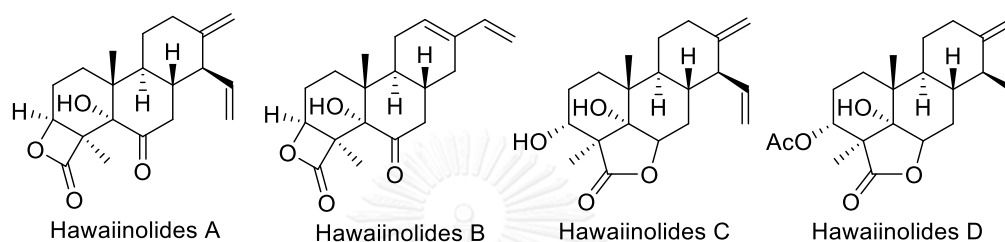


**Figure 2.13** The structures of hawaiiinolides A–D

## 2.4 Literature Reviews of SAR Study of Diterpenoids

### 2.4.1 Antibacterial Activity

In 2008, Urzúa and co-workers analyzed antibacterial activities of fifteen terpenoids and suggested two structural requirements for antibacterial activity of these and related compounds including hydrophobic moiety, consisting of a substituted decalin skeleton, and a hydrophilic region possessing one hydrogen-bond-donor group. These requirements are responsible for an optimal insertion of these and related compounds into cell membranes by the results of docking some of these compounds into a model phospholipid bilayer [13].

In 2011, Carvalho *et al.* isolated six pimarane-type diterpenes from *Viguiera arenaria* and two synthesized derivatives. All compounds were tested *in vitro* against a panel of representative microorganisms responsible for dental root canal infections. *ent*-Pimara-8(14),15-dien-19-oic acid and *ent*-8(14), its sodium salt, and 15-pimaradien-3 $\beta$ -ol displayed the highest activity, with MIC ranging from 1 to 10  $\mu\text{g}/\text{mL}$  [38].

### 2.4.2 Anti-Inflammatory

In 2004, Suh and co-workers synthesized novel derivatives from acanthoic acid analogues for anti-inflammatory to inhibit edema formation. The analogues **19-21** (Figure 2.14) exhibited highly potent NO inhibitory activities than acanthoic acid analog with  $IC_{50}$  1.2, 8.8, and 2.3  $\mu M$ , respectively [39].

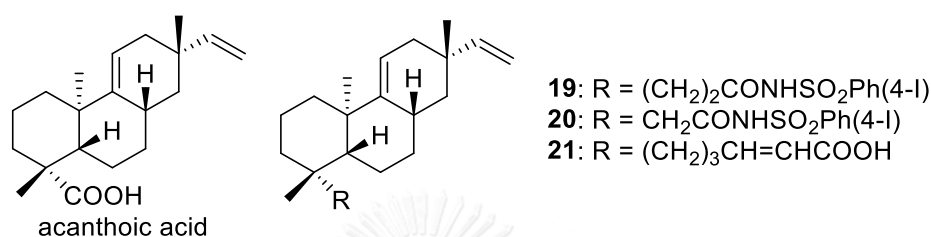


**Figure 2.14** The structures of acanthoic acid and their derivatives **19-21**

### 2.4.3 COX-2 Inhibitory Activity

In 2001, Suh *et al.* reported the SAR study and molecular modeling of a novel pimarane COX-2 inhibitor. For SAR study of acanthoic acid, the modification of the carboxyl group or extension of linker between C-4 and the carboxyl group displayed significant enhancement of COX-2 inhibitory activity and selectivity [14].

### 2.4.4 Cytotoxicity

In 2006, Aoyagi *et al.* isolated seven known abietane diterpenoids and 11-*O*- and 12-*O*-acetyl carnosic acids (Figure 2.15) from the methanol extract of *Perovskia abrotanoides* (Labiatae). The cytotoxic activity of these compounds and semisynthetic analogues of the presently isolated abietane diterpenoids were studied using P388 murine leukemia cells. From the SAR study, abietane-type analogues **22** and **23**, having both 20-ester group and *o*-quinone or *o*-quinone equivalent structure in the C-ring, revealed the most cytotoxic activity with  $IC_{50}$  0.27 and 0.22  $\mu g/mL$ , respectively [10].



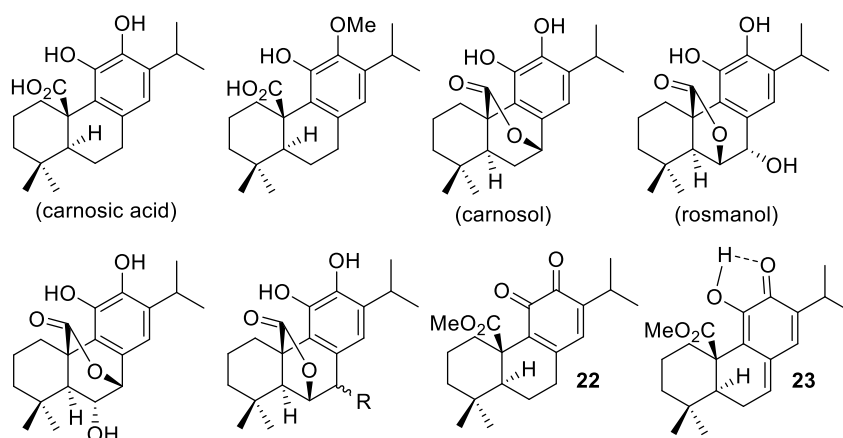


**Figure 2.15** Abietane-type diterpenoids from *Perovskia abrotanoides* and abietane-type analogues **22-23**

In 2012, Lallemand and co-workers isolated three fungal phytotoxins: sphaeropsidins A, B and C as unrearranged pimarane diterpenes produced by *Diplodia cupressi*. Moreover, ten derivatives were synthesized to evaluate their *in vitro* anticancer activities. Sphaeropsidin A and two derivatives **24** and **25** (Figure 2.16) exhibited 50% growth-inhibitory concentration at the low micromolar range for all cell lines. Structure activity relationship showed that the phytopathogenic and antimicrobial activities were paralleled. However, the vinyl group at C-13 did not seem to be required for their antipathogenic activity [40].

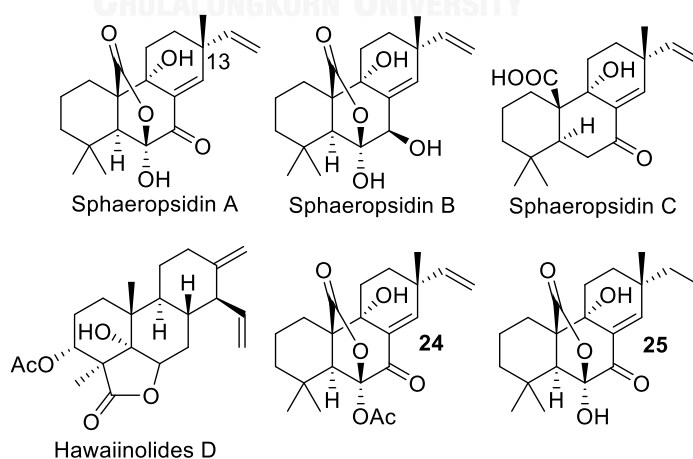


**Figure 2.16** The structures of sphaeropsidin A-C, hawaiiinolides D and derivatives **24-25**

## 2.5 Beta-Lactone Containing Natural Products and Biological Relevance

Beta-lactone ring is a cyclic ester with three carbon atoms namely oxetan-2-one or 2-oxetanone. There are several beta-lactone containing natural products, which were isolated from nature and have a wide variety of biological activities (Figure 2.17) [12, 41-43].

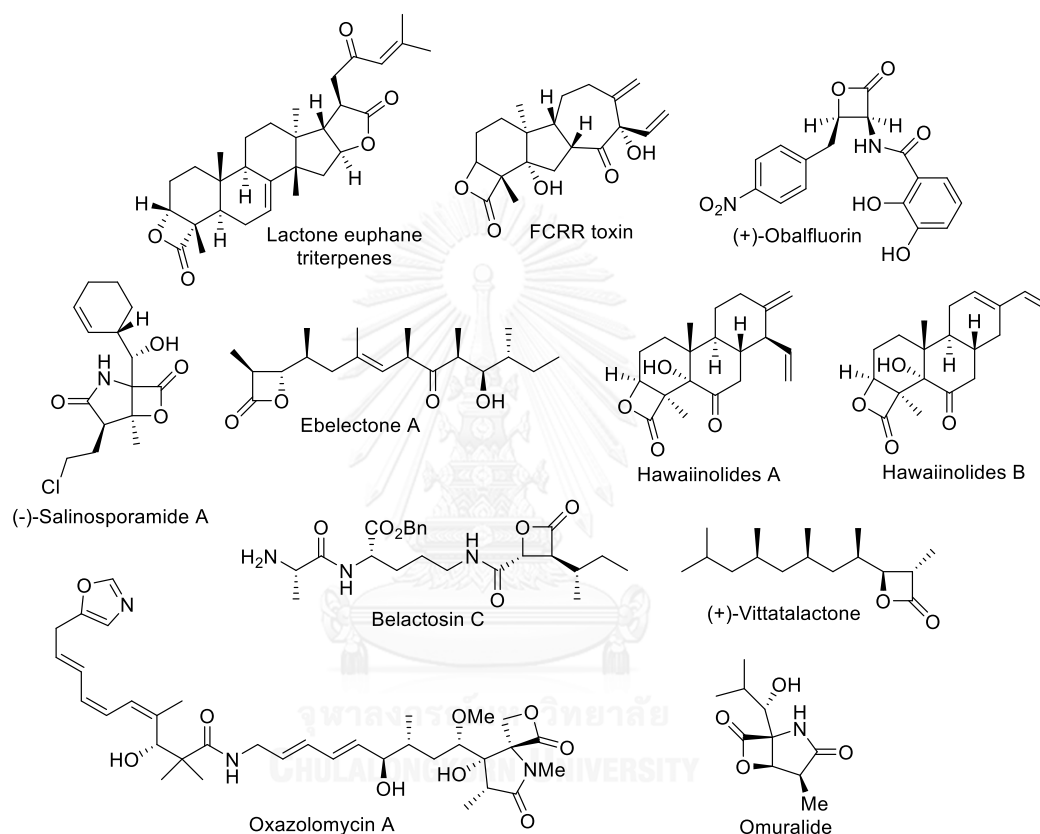


**Figure 2.17** Beta-lactone containing natural products

The simple beta-lactones have also taken on the important role as a sporicide, providing protection from vegetative bacteria and pathogenic fungi [44]. Several derivatives of *trans*- $\beta$ -lactones including the belactosins [45], ebelactones [46], panlicin [47], and tetrahydrolipstatin [48], have often been considered pivotal structural motifs functioning as pancreatic lipase inhibitors [49]. Moreover, irreversible acylation by the serine protease<sup>90</sup> of the aforementioned natural products permit the absorption of fat.

The acylation (Figure 2.18) *via* the hydroxyl or thiol group of cysteine, serine or threonine amino acids in enzyme active sites illustrated facilitating selective and irreversible inhibition under mildly acidic media [50].

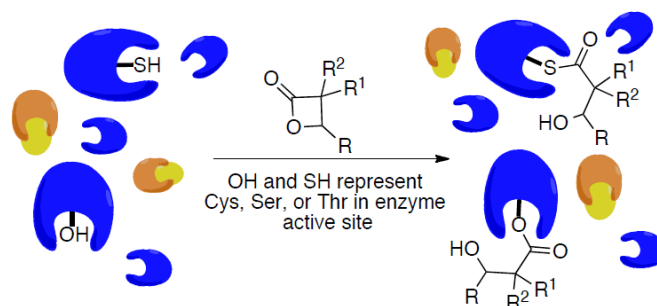


**Figure 2.18** The acylation of bioactive beta-lactone compounds

Covalent reactions with active sites of enzymes permit beta-lactone containing natural products to have promising and varied biological activities [51]. Ebelectone A has become an interesting antimicrobial agent because of irreversible acylation of the beta-lactone with Ser143 in the active site of homoserine transacetylase (HTA). The beta-lactone moieties of omuralide and salinosporamide A displayed an important feature in retaining bioactivity for selective inhibition of the 20S proteasome [52].

## 2.6 Literature Reviews of Methodology for Beta-Lactone Synthesis

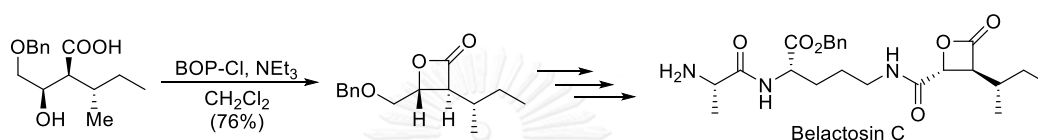
There are several methodologies for beta-lactone synthesis including lactonization process from 1,2-hydroxy acids [53], nucleophile-catalyzed aldol lactonization (NCAL) process from 1,5- or 1,6-keto acids [54], intermolecular Lewis acid catalyzed [2+2] cycloaddition from ketenes and aldehydes [55] or Lewis base catalyzed [2+2] cycloaddition [56]. The most diagnostic feature that has aided in the characterization of beta-lactone is the intense IR absorption at  $\nu = 1840\text{-}1810\text{ cm}^{-1}$ , attributed to the carbonyl stretching [57].

### 2.6.1 The Lactonization Process

In 1988, Vederas and co-workers synthesized optically pure (2*S*)- $\alpha$ -amino acids in good isolated yield *via* *N*-(*tert*-butoxycarbonyl)-L-serine  $\beta$ -lactone and

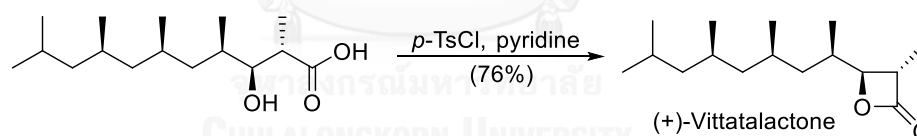
trifluoroacetic acid. This beta-lactone could be prepared by Mitsunobu cyclization using PPh<sub>3</sub>, DEAD and the corresponding *N*-protected serine derivative to produce 3-amino-2-oxetanone [58].

In 2007, Kumaraswamy and Markondaiah disclosed the highly concise stereoselective total synthesis of belactosin C. In the during step of total synthesis, the lactonization of 1,2-hydroxy acid was occurred using BOP-Cl with Et<sub>3</sub>N in CH<sub>2</sub>Cl<sub>2</sub> 23 °C for 1 h to provide beta-lactone desired product in good yield (Scheme 2.1) [53].



**Scheme 2.1** The lactonization step to synthesize beta-lactone in belactosin C

In 2010, Schmidt *et al.* developed the asymmetric total synthesis of vittatalactone, and 10- norvittatalactone. In the key step of beta-lactone synthesis, 3-hydroxy-2,4,6,8,10-pentamethylundecanoic acid was reacted with *p*-TsCl in the presence of pyridine at rt to give (+)-vittatalactone in good yield (Scheme 2.2) [59].

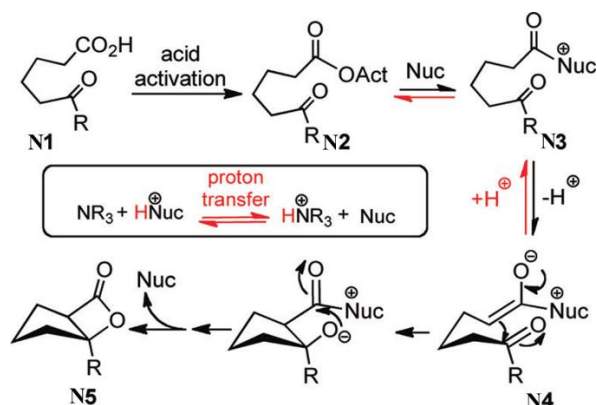


**Scheme 2.2** The synthesis of (+)-vittatalactone *via* lactonization

## 2.6.2 Nucleophile-Catalyzed Aldol Lactonization Process (NCAL)

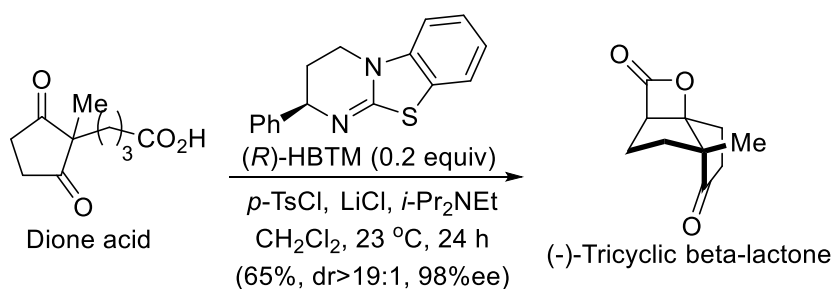
In 2012, Liu and co-workers improved the NCAL process, which has shortened reaction time for the construction of bicyclic beta-lactone from 1,5-keto acid in high yield. Commercially available reagents: *p*-TsCl as activator and DMAP as nucleophilic promoter (Lewis base) were used in this reaction. The mechanistic pathway for the NCAL process (Scheme 2.3) involved an acyl ammonium specie **N3** and followed by deprotonation to form an ammonium enolate **N4**. An aldol process following lactonization provides the beta-lactone product **N5**. Moreover,  $\beta$ -

substituents of substrates with respect to the carboxylic acid, displayed excellent levels of diastereoselectivity during the *bis*-cyclization event [54].



**Scheme 2.3** Proposed mechanistic pathway of the NCAL process

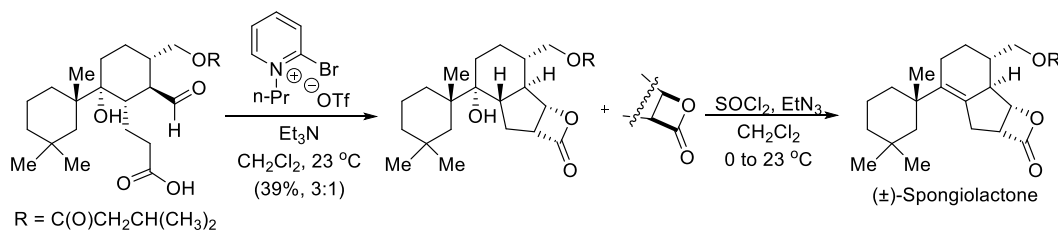
In the same year, Leverett *et al.* disclosed the optimization of the NCAL process with dione acid to prepare tricyclic beta-lactone for total synthesis of (-)-curcumanolide A and (-)-curcumalactone. Several catalysts were selected for asymmetric NCAL process including (-)-tetramisole, (*S*)-BTM, (*S*)-HBTM, (*S*, *R*)-naphth/Me HBTM. The reaction (Scheme 2.4) using (*S*)-HBTM as a catalyst gave excellent yields and enantioselectivities of tricyclic  $\beta$ -lactone in combination with *p*-TsCl as activating agent and LiCl as Lewis acid. Furthermore, this condition can be applied up to gram scale [60].



**Scheme 2.4** The asymmetric NCAL process using (*S*)-HBTM as a catalyst

In 2014, Harvey and co-workers synthesized ( $\pm$ )-spongiolactone from 1,3-cyclohexanedione in eleven steps. In the step of installed the anticipated beta-lactone pharmacophore of the natural product (Scheme 2.5), a diastereoselective,

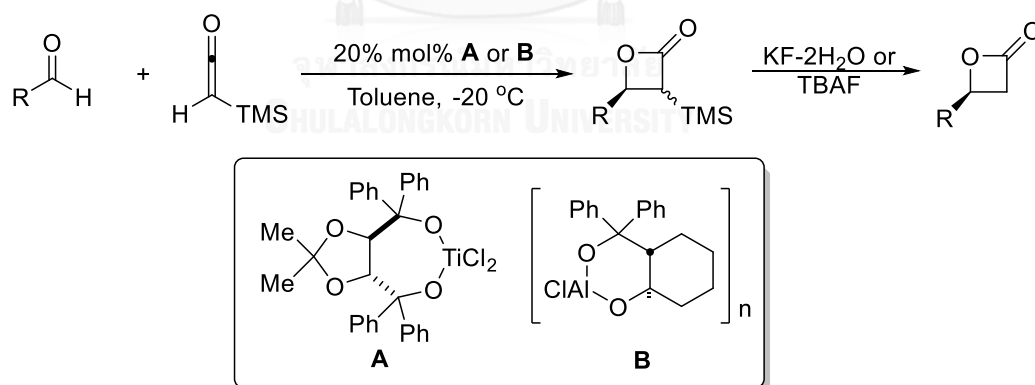
NCAL was processed with an advanced keto acid intermediate using modified Mukaiyama's reagent, 2-bromo-*N*-*n*-propyl-pyridinium-1,1,1-trifluoromethanesulfonate and triethylamine provided desired tricyclic beta-lactone with its separable diastereomer [61].



**Scheme 2.5** The NCAL process to synthesized bicyclic beta-lactone in  
(±)-spongiolactone

### 2.6.3 Intermolecular Lewis Acid Catalyzed [2+2] Cycloaddition

In 1998, Romo and co-workers found that varieties of titanium **A** and aluminum **B** complexes catalyzed the addition of preformed TMS-ketene to aldehydes for asymmetric [2+2] cycloaddition (Scheme 2.6). This condition provided optically active beta-lactone with moderate to good enantioselection [62].



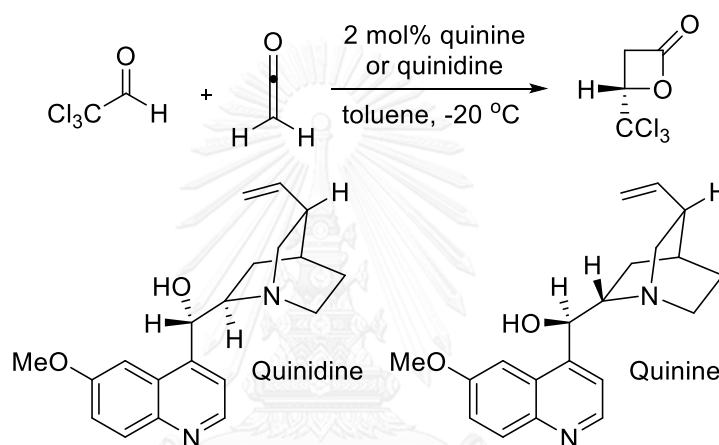
**Scheme 2.6** Beta-lactone synthesis *via* asymmetric [2+2] cycloaddition of  
TMS-ketene and aldehydes

In 2003, Orr and Calter reported that the utility of ketenes or *in situ* generated ketenes with aldehydes was the forefront for synthesizing enantiomerically

pure beta-lactone *via* [2+2] cycloadditions by Lewis acid-controlled addition or nucleophile-catalyzed addition [63].

#### 2.6.4 Intermolecular Lewis Base Catalyzed [2+2] Cycloaddition

In the early 1980s, Wynberg *et al.* reported the first catalytic, asymmetric approach to beta-lactone. Quinidine or quinine catalyzed the addition of ketene to chloral at  $-20\text{ }^{\circ}\text{C}$  in toluene to furnish (*S*)-4-trichloromethyl-2-oxetanone with optically pure (Scheme 2.7) [56].



**Scheme 2.7** The beta-lactone synthesis using quinidine or quinine as catalyst

The general mechanism for the Wynberg Lewis base catalyzed [2+2] employed a chiral tertiary amine nucleophile ( $\text{*NR}_3$ , including TMSQ*d* or TMSQ*n*) (Figure 2.19) adding to the electrophilic ketene creating an ammonium enolate intermediate (Figure 2.20). Intermolecular aldol with an activated, non-enolizable aldehyde and ensuing beta-lactonization regenerated the catalyst and delivered the optically active beta-lactone. The Lewis base catalyzed variant involved a stepwise mechanism and could generally be coined as a nucleophile catalyzed aldol-lactonization (NCAL) process (Figure 2.20) [64].

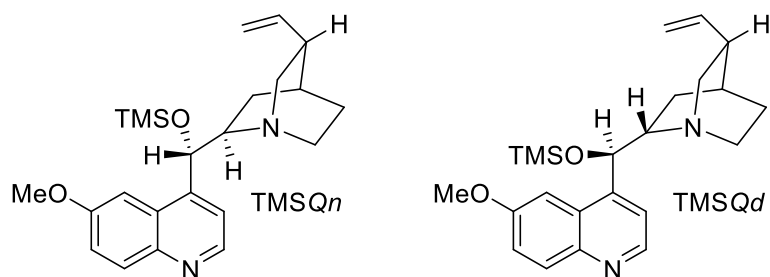


Figure 2.19 The structures of TMSQn and TMSQd

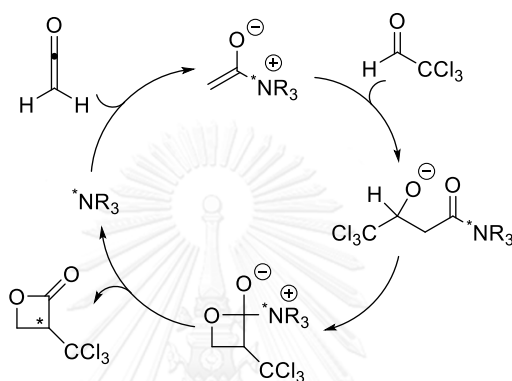
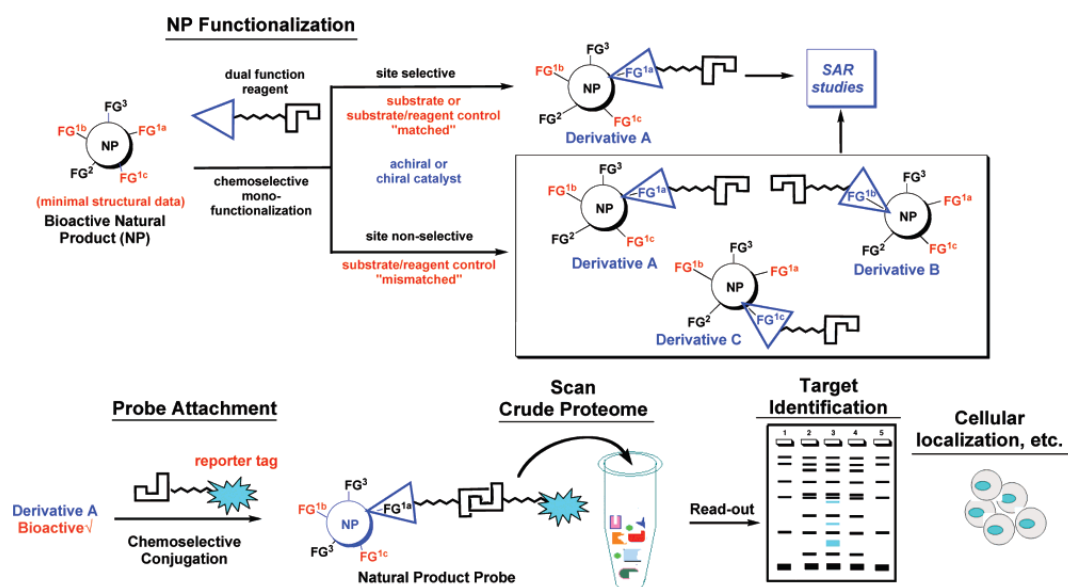


Figure 2.20 The mechanism of the Wynberg Lewis base catalyzed [2+2] cycloaddition

## 2.7 Strategy for Simultaneous Arming and Structure Activity Relationship (SAR) Information of Natural Products

Natural products are tools for basic cellular studies and lead for identifying medically relevant protein targets, whereas their uses for these studies are often hindered by limited quantities and a lack of selectivity and mild monofunctionalization reactions. The selective methods developed (Scheme 2.8) could simultaneously equip the natural product with a reactive functional group for subsequent conjugation to reporter tags such as FK506-biotin. These obtained important information of SAR, which need knowledge of functional groups present in the natural products, could significantly decrease the time between bioactive natural products isolation and target identification [65].





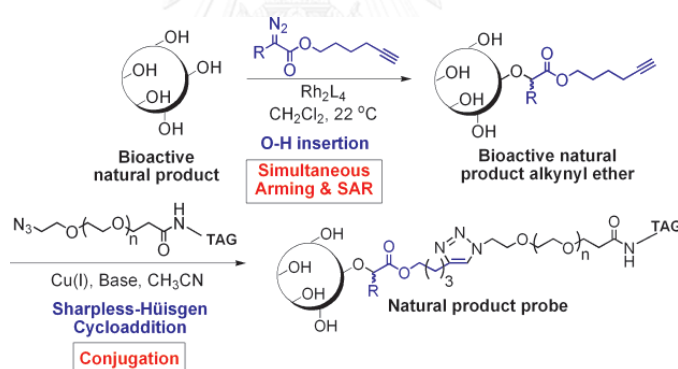
**Scheme 2.8** Generalized two-step derivatization/conjugation strategy for simultaneous arming and structure activity studies of natural products for use in chemical genetics employing substrate or substrate/reagent control, a type of “double diastereodifferentiation”. FG = Functional group.

As for the strategy in this research, bioactive natural products would be synthesized with dual function reagent that provide non-selective or selective products. There are several methods based on functional groups in natural products including O-H insertion reactions of alcohol-containing natural products with rhodium carbenoids derived from alkynyl diazo acetates and a subsequent Sharpless-Huisgen [3+2] cycloaddition reaction [65], iodination with *N*-iodosuccinimide catalyzed in combination with  $\text{In}(\text{OTf})_3$  of arene-containing natural products [66], C-H amination with alkynyl sulfamate and  $\text{Rh}(\text{II})$  as a catalyst of C-H allylic-containing natural products [67], or cyclopropanations with an alkynyl diazo ester and  $\text{Rh}(\text{II})$  as a catalyst of alkene-containing natural products and then be assayed for bioactivity to provide SAR data [68]. The functionalized natural products having biological activity were selected for the synthesis of a variety of probes such as biotin, fluorophore, radiolabel *etc.* and

subsequent scanning of select proteomes for binding proteins *via* affinity experiments, activity-based profiling, and cellular localization studies [65, 69].

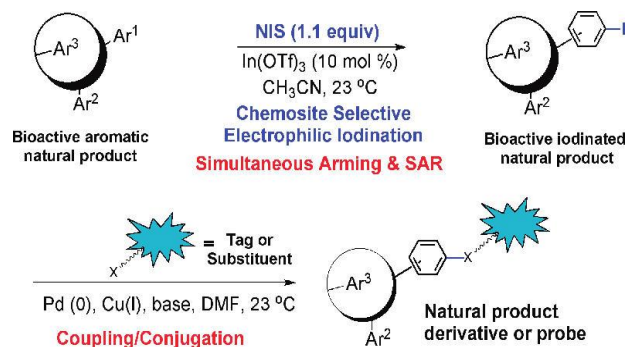
## 2.8 Literature Reviews of Strategy for Simultaneous Arming and Structure-Activity Relationship (SAR) Information of Natural Products

In 2007, Peddibhotla reported a strategy (Scheme 2.9) that enabled simultaneous arming and SAR studies of alcohol-containing natural products by O-H insertion reactions having selectivity with rhodium carbenoids derived from alkynyl diazo acetates. A subsequent Sharpless-Huisgen [3+2] cycloaddition reaction with the appended alkyne allows for attachment of a variety of reporter tags to provide a novel FK506-biotin conjugate. This novel probe enabled pull-down of the entire “immunosuppressive complex” including FKBP12, calcineurins A and B, and calmodulin [65].



**Scheme 2.9** Two-step O-H insertion/Sharpless Huisgen cycloaddition sequence for simultaneous arming and SAR studies of natural products

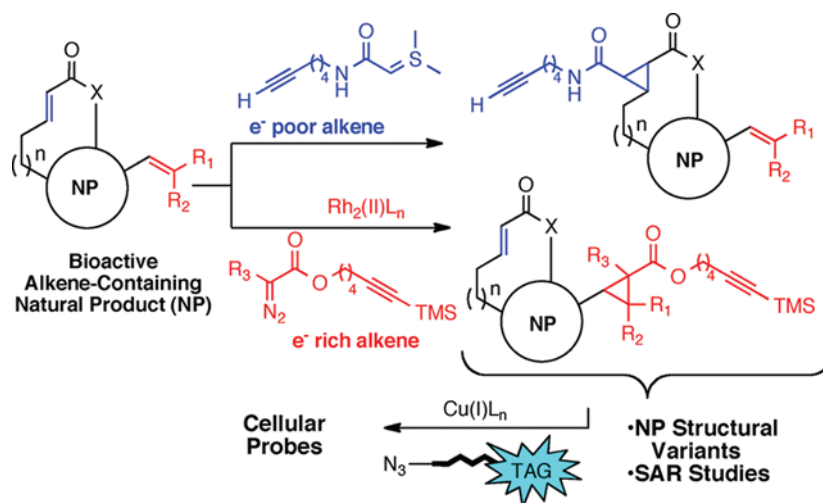
In 2010, Zhou and co-workers described a versatile and mild conditions for arene-containing natural products derivatization. This strategy (Scheme 2.10) can be amenable to small scale by using iodination with *N*-iodosuccinimide catalyzed in combination with In(OTf)<sub>3</sub> at ambient temperature, and also conjugation with reporters such as biotin *via* subsequent metal-mediated coupling reactions [66].



**Scheme 2.10** Two-step iodination/metal-mediated coupling reactions sequence for simultaneous arming and SAR studies of arene-containing natural products

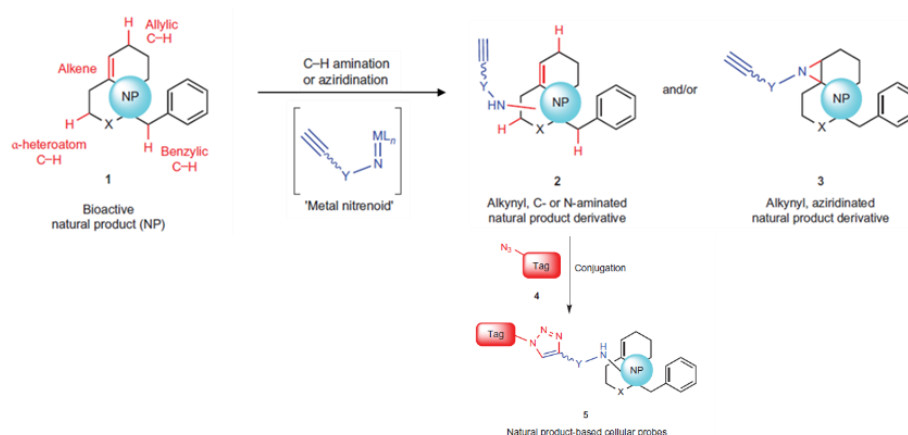
In 2011, Chamni *et al.* reported novel diazo reagents for simultaneous arming and SAR studies of alcohol-containing natural products with a small steric footprint ( $\alpha$ -trifluoroethyl (HTFB) substituted reagent). The Rh(II)-catalyzed O-H insertion reaction of many natural products, including the potent translation inhibitor lactimidomycin was investigated. Useful reactivity and both chemo- and region-selectivities were observed. Different binding to the known protein targets of both FK506 and fumagillol was demonstrated, thus validating the advantage of the smaller steric footprint of  $\alpha$ -trifluoroethyl derivatives. A *p*-azidophenyl diazo reagent would be useful for photo affinity labeling of low affinity small molecule protein receptors [69].

In 2012, Robles and co-workers disclosed simultaneous arming and SAR studies of alkene-containing natural products by cyclopropanations under mild conditions (Scheme 2.11). An alkynyl diazo ester with Rh(II) as a catalyst was employed for cyclopropanations of electron-rich olefins whereas an alkynyl sulfonium ylide was used for electron-poor olefins. This method enabled simultaneous natural product derivatization *via* alkyne attachment for SAR studies and arming for subsequent conjugation with reporter tags including biotin, fluorophores, photoaffinity labels for studies the mechanism such as cellular target identification and proteome profiling experiments [68].



**Scheme 2.11** Simultaneous arming and SAR studies of alkene-containing natural products by cyclopropanation

In 2013, Li and co-workers described the use of rhodium (II)-catalyzed C–H amination reactions to carry out simultaneous SAR studies and arming (alkynylation) of natural products at ‘unfunctionalized’ positions (Scheme 2.12). Olefins in the natural products undergo aziridination while allylic and benzylic C–H bonds undergo amination. Moreover, tertiary amine-containing natural products are converted to amidines *via* a C–H amination-oxidation sequence or to hydrazine sulfamate zwitterions by an unusual *N*-amination. These alkynylated derivatives are converted into cellular probes that can be used for mechanism-of-action studies [67].



**Scheme 2.12** C–H Amination or aziridination-conjugation sequence for simultaneous arming and SAR studies of natural products.

## 2.9 Objective of This Research

For these aforementioned reasons, a variety of diterpenoid had several biological activities. The strategy for simultaneous arming can be applied to synthesize diterpenoid derivatives, which connected with a variety of reporter tags for bioactivity mechanism to obtain important information of SAR. Moreover, a wide variety biological activities of beta-lactone-containing natural products were found. Furthermore, the efficient methods were modified for beta-lactone synthesis including NCAL process and lactonization. This led to the conversion of diterpenoids *via* a few steps of reactions to create keto acid or hydroxy acid, and followed by NCAL process or lactonization to provide beta-lactone containing derivatives. Consequently, this beta-lactone can improve non-covalent to covalent interaction for SAR study. Therefore, the objective of this research could be summarized as follows:

1. The isolation of diterpenoids from the dichloromethane extract of the heartwoods of *X. xylocarpa*
2. The derivatization of these diterpenoids for SAR study towards antibacterial, antifungal and cytotoxic activities
3. The conversion of natural products such as andrenosterone, cholic acid, andrographolide, and sandaracopimaradiene-3 $\beta$ ,18-diol to beta-lactone-containing derivatives
4. The simultaneous arming and SAR studies of diterpenoids

## II. Experimental

### 2.10 General Information

All reactions were completed under nitrogen atmosphere in oven-dried glassware unless indicated otherwise. Tetrahydrofuran, dichloromethane, methanol

were dried by passage through alumina or activated molecular sieves (MBraun solvent purification system). Benzene was dried over activated molecular sieves (4 Å). Triethylamine, Hünig's base, diisopropyl amine and trimethylsilyl chloride were distilled from calcium hydride. Cerium chloride heptahydrate was flame-dried under high vacuum. Commercially available reagents were used as received from Sigma-Aldrich.  $^1\text{H}$  NMR spectra were measured at 500, 400 or 300 MHz and chemical shifts were reported as  $\delta$  values in ppm relative to  $\text{CDCl}_3$  (7.26 ppm,) or  $\text{CD}_3\text{OD}$  (4.78 and 3.31 ppm), coupling constants ( $J$ ) were reported in Hertz (Hz), and multiplicity follows normal convention: s, singlet; d, doublet; t, triplet; q, quartet; dd, doublet of doublets; ddd, doublet of doublet of doublets; dt, doublet of triplets; m, multiplet; bs, broad singlet.  $^{13}\text{C}$  NMR spectra were measured at 125, 100 or 75 MHz with  $\text{CDCl}_3$  (77.2 ppm) or  $\text{CD}_3\text{OD}$  (49.2 ppm) as the internal standard. Flash column chromatography was performed using 60 Å silica gel (Silicycle, 230-400 mesh). Mass spectra (ESI) were obtained at the Center for Chemical Characterization and Analysis (Texas A&M University). Thin layer chromatography was performed using glass-backed 60 Å silica gel F-254 (Silicycle, 250  $\mu\text{m}$  thickness). Developed plates were visualized by potassium permanganate stain followed by heating. Infrared spectra were obtained on a FT-IR spectrometer as a thin film on NaCl plate. X-ray data was collected and processed by the X-ray Diffraction Laboratory at Texas A&M University.

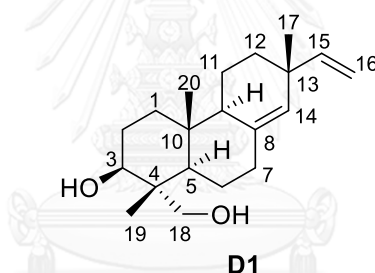
### **2.11 Extraction and Isolation of Diterpenoids from the Heartwoods of *X. xylocarpa***

The heartwoods of *X. xylocarpa* (Figure 2.21), purchased from Chaokrompoe store in June 2010, were ground to small pieces and soaked with dichloromethane for 5 days (3 times). The residue was extracted again with ethyl acetate to obtain the dichloromethane and ethyl acetate extracts in 4.47 and 3.80%, respectively. The dichloromethane extract (112.0 g) was separated by column chromatography (gradient

SiO<sub>2</sub>, 0 → 100% EtOAc/hexane) to furnish diterpenoids: sandaracopimaradiene-3 $\beta$ ,18-diol (**D1**) (0.39 g, 0.35% yield), sandaracopimaradien-3-one (**D2**) (5.29 g, 4.72% yield), sandaracopimaradien-3 $\beta$  ol (**D3**) (3.64 g, 3.25% yield), and sandaracopimaric acid (**D4**) (0.21 g, 0.19%).



Figure 2.21 The heartwoods of *X. xylocarpa*



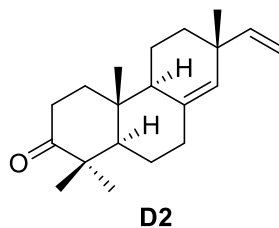
**Sandaracopimaradiene-3 $\beta$ ,18-diol (D1):** colorless crystal (0.39 g, 0.35% yield).

TLC (EtOAc:hexane, 1:1 v/v):  $R_f$  = 0.24; <sup>1</sup>H NMR (500 MHz, CDCl<sub>3</sub>):  $\delta$  5.78 (dd,  $J$  = 17.4, 10.6 Hz, 1H), 5.24 (s, 1H), 4.93 (d,  $J$  = 17.6 Hz, 1H), 4.92 (dd,  $J$  = 10.6, 1.2 Hz, 1H), 3.73 (d,  $J$  = 10.3 Hz, 1H), 3.66 (dd,  $J$  = 11.1, 4.7 Hz, 1H), 3.44 (d,  $J$  = 10.3 Hz, 1H), 2.26 (dt,  $J$  = 14.2, 3.3 Hz, 1H), 2.04 (m, 1H), 1.77 (dt,  $J$  = 13.1, 3.5 Hz, 1H), 1.70 (m, 1H), 1.66 (m, 2H), 1.58 (m, 2H), 1.48 (m, 1H), 1.42 (m, 2H), 1.37 (dd,  $J$  = 12.3, 3.7 Hz, 1H), 1.25 (dd,  $J$  = 13.1, 4.4 Hz, 1H), 1.17 (ddd,  $J$  = 15.0, 11.6, 5.7 Hz, 1H), 1.05 (s, 3H), 0.95 (s, 3H), 0.86 (s, 3H); <sup>13</sup>C NMR (125 MHz, CDCl<sub>3</sub>):  $\delta$  148.9, 136.2, 129.0, 110.1, 77.2, 72.3, 50.3, 48.6, 42.1, 37.9, 37.4, 36.9, 35.5, 34.4, 27.2, 25.9, 22.4, 18.7, 15.5, 11.4. IR (thin film): 3346, 2938, 2827 cm<sup>-1</sup>; HRMS (ESI+)  $m/z$  calcd. for [M+Li]<sup>+</sup>: 311.2562; found 311.2563 (C<sub>20</sub>H<sub>32</sub>O<sub>2</sub>, MW = 304.4740) [11].

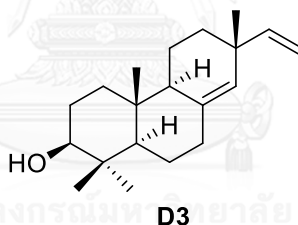
**Table 2.1**  $^1\text{H}$  and  $^{13}\text{C}$  NMR chemical shift assignments of compound **D1**

Position		Chemical shift (ppm)	
		$^{13}\text{C}$	$^1\text{H}$
1	CH <sub>2</sub>	36.9	1.77 (dt, $J = 13.1, 3.5$ Hz), 1.25 (dd, $J = 13.1, 4.4$ Hz)
2	CH <sub>2</sub>	27.2	1.66 (m)
3	CHOH	77.2	3.73 (d, $J = 10.3$ Hz)
4	C	37.4	
5	CH	48.6	1.17 (ddd, $J = 15.0, 11.6, 5.7$ Hz)
6	CH <sub>2</sub>	22.4	1.42 (m)
7	CH <sub>2</sub>	34.4	2.26 (dt, $J = 14.2, 3.3$ Hz), 2.04 (m)
8	C	136.2	
9	CH	50.3	1.70 (m)
10	C	37.9	
11	CH <sub>2</sub>	18.7	1.58 (m)
12	CH <sub>2</sub>	35.5	1.48 (m), 1.37 (dd, $J = 12.3, 3.7$ Hz)
13	C	42.1	
14	CH	129.0	5.24 (s)
15	CH	148.9	5.78 (dd, $J = 17.4, 10.6$ Hz)
16	CH <sub>2</sub>	110.1	4.93 (d, $J = 17.6$ Hz), 4.92 (dd, $J = 10.6, 1.2$ Hz)
17	CH <sub>3</sub>	25.9	0.86 (s)
18	CH <sub>2</sub> OH	72.3	3.66 (dd, $J = 11.1, 4.7$ Hz), 3.44 (d, $J = 10.3$ Hz)
19	CH <sub>3</sub>	11.4	1.05 (s)
20	CH <sub>3</sub>	15.5	0.95 (s)

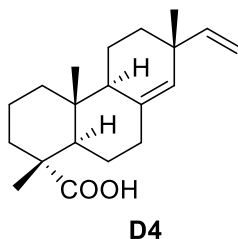




**Sandaracopimaradien-3-one (D2):** colorless crystal (5.29 g, 4.72% yield). TLC (EtOAc:hexane, 1:5 v/v):  $R_f = 0.58$ ;  $^1\text{H NMR}$  (500 MHz,  $\text{CDCl}_3$ ):  $\delta$  5.78 (dd,  $J = 17.5, 10.6$  Hz, 1H), 5.30 (s, 1H), 4.94 (dd,  $J = 17.4, 1.7$  Hz, 1H) 4.91 (dd,  $J = 10.5, 1.7$  Hz, 1H), 2.67 (td,  $J = 14.5, 5.8$  Hz, 1H), 2.33 (dd,  $J = 15.0, 3.4$  Hz, 1H), 2.15-1.99 (m, 2H), 1.77 (t,  $J = 7.7$  Hz, 1H), 1.71-1.62 (m, 1H), 1.62-1.53 (m, 3H), 1.53-1.45 (m, 4H), 1.40 (m, 1H), 1.11 (s, 3H), 1.08 (s, 6H), 1.02 (s, 3H);  $^{13}\text{C NMR}$  (125 MHz,  $\text{CDCl}_3$ ):  $\delta$  217.1, 148.6, 135.8, 129.6, 110.4, 55.3, 49.5, 47.8, 38.0, 37.7, 37.5, 35.6, 34.8, 34.3, 26.1, 25.8, 23.2, 22.3, 18.9, 14.7. IR (thin film): 2938, 1706  $\text{cm}^{-1}$ ; HRMS (ESI+)  $m/z$  calcd. for  $[\text{M}+\text{Li}]^+$ : 293.2457; found 293.2466 ( $\text{C}_{20}\text{H}_{30}\text{O}$ , MW = 286.4590) [11].



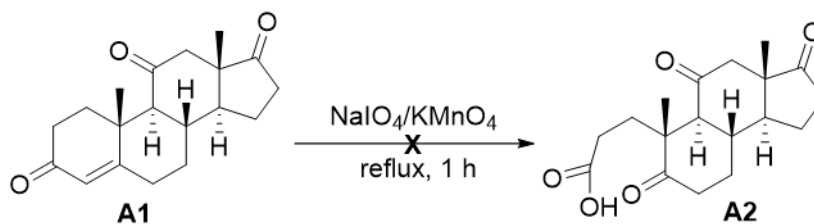
**Sandaracopimaradien-3 $\beta$ -ol (D3):** colorless crystal (3.64 g, 3.25% yield). TLC (EtOAc:hexane, 1:4 v/v):  $R_f = 0.76$ ;  $^1\text{H NMR}$  (500 MHz,  $\text{CDCl}_3$ ):  $\delta$  5.79 (dd,  $J = 17.5, 10.1$  Hz, 1H), 5.23 (s, 1H), 4.92 (dd,  $J = 11.3, 1.5$  Hz, 1H), 4.87 (dd,  $J = 4.4, 1.5$  Hz, 1H), 3.27 (dt,  $J = 13.8, 5.5$  Hz, 1H), 2.27 (ddd,  $J = 14.2, 4.5, 2.2$  Hz, 1H), 2.10 (m, 1H), 1.75 (dt,  $J = 12.9, 3.5$  Hz, 1H), 1.68 (m, 1H), 1.66 – 1.60 (m, 2H), 1.58 (m, 2H), 1.51 – 1.40 (m, 2H), 1.41 – 1.32 (m, 2H), 1.30 (m, 1H), 1.18 (dt,  $J = 9.9, 5.0$  Hz, 1H), 1.04 (s, 3H), 0.99 (s, 3H), 0.81 (s, 3H), 0.80 (s, 3H).  $^{13}\text{C NMR}$  (125 MHz,  $\text{CDCl}_3$ ):  $\delta$  148.9, 136.6, 128.8, 110.1, 79.1, 54.1, 50.3, 39.0, 38.1, 37.4, 37.2, 35.8, 34.5, 28.5, 27.6, 26.0, 22.2, 18.7, 15.7, 15.0. IR (thin film): 3286, 2940, 2869  $\text{cm}^{-1}$  [11].



**Sandaracopimaric acid (D4):** white solid (0.21 g, 0.19% yield). TLC (EtOAc:hexane, 1:4 v/v):  $R_f = 0.70$ ;  $^1\text{H}$  NMR (400 MHz,  $\text{CDCl}_3$ ):  $\delta$  5.77 (dd,  $J = 17.4, 10.6$  Hz, 1H), 5.22 (s, 1H), 4.91 (dd,  $J = 12.7, 1.4$  Hz, 1H), 4.88 (dd,  $J = 5.8, 1.4$  Hz, 1H), 2.22 (dd,  $J = 14.2, 2.8$  Hz, 1H), 2.12 (td,  $J = 13.5, 5.2$  Hz, 1H), 1.92 (dd,  $J = 12.4, 2.3$  Hz, 1H), 1.86 – 1.70 (m, 4H), 1.59 (m, 4H), 1.54 – 1.42 (m, 3H), 1.38 (dd,  $J = 12.1, 3.6$  Hz, 1H), 1.32 – 1.22 (m, 1H), 1.20 (s, 3H), 1.03 (s, 3H), 0.83 (s, 3H).  $^{13}\text{C}$  NMR (100 MHz,  $\text{CDCl}_3$ ):  $\delta$  185.3, 148.9, 136.6, 129.1, 110.1, 50.6, 48.8, 47.3, 38.3, 37.7, 37.4, 37.1, 35.5, 34.4, 26.0, 24.9, 18.6, 18.1, 16.8, 15.2 [11].

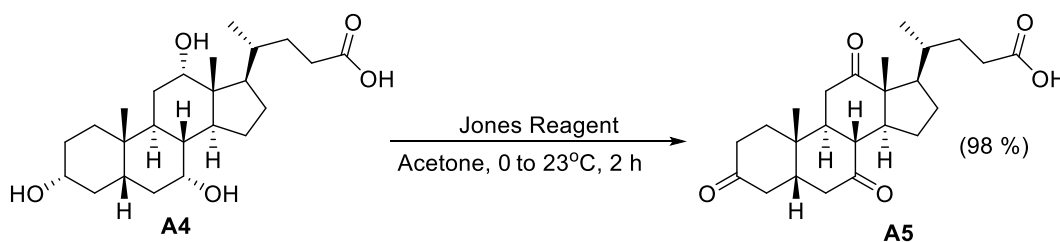
## 2.12 Conversion of Non-Covalent Inhibitors to Covalent through Introduction of Beta-Lactones

**Oxidation of andrenosterone (A1) to keto acid derivative (A2):** To solution of andrenosterone (300 mg, 1.0 mmol) in isopropanol (15 mL) was added a solution of  $\text{Na}_2\text{CO}_3$  (160 mg in 1 mL of water). The mixture was brought to reflux and a solution of  $\text{NaIO}_4$  (1.54 g, 7.18 mmol) and  $\text{KMnO}_4$  (10 mg, 0.06 mmol) in warm water (10 mL at 75 °C) was added gradually for 1 h while reflux temperature was maintained. The reaction was cooled to 23 °C and after 15 min, the solid was removed by filtration. The solid was washed with water and combined filtrates were concentrated under low pressure to remove isopropanol. The aqueous phase residue was cooled and acidified with conc. HCl, and then extracted with  $\text{CH}_2\text{Cl}_2$ , washed with water and dried over anhydrous  $\text{Na}_2\text{SO}_4$ . However, none of the desired product (A2) was obtained in this condition (Scheme 2.13) [70, 71].



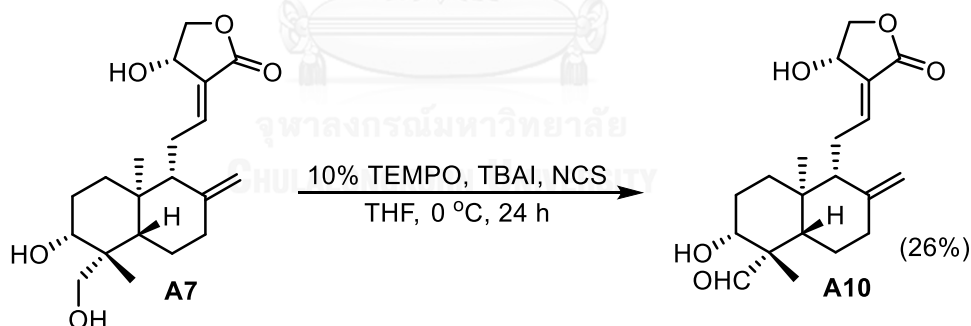
**Scheme 2.13** The oxidation of andrenosterone (A1) to keto acid derivative (A2)

**Triketocholanic acid (A5):** Cholic acid (A4) (418.3 mg, 1.024 mmol) was dissolved in acetone (60 mL) and cooled to 0 °C. 2.5 mL of Jones reagent (CrO<sub>3</sub> 13.4 g, water 40 mL and conc. H<sub>2</sub>SO<sub>4</sub> 12 mL) was added dropwise until the orange color persisted. The reaction was allowed to warm up to 23 °C and stirred for 2 h. The reaction was quenched by adding isopropanol until the deep-green color persist and extracted with EtOAc (50 mL x 2). The organic layer was washed with brine (50 mL), dried over anhydrous Na<sub>2</sub>SO<sub>4</sub>, filtered and concentrated *in vacuo*. The residue was purified by flash column chromatography (gradient SiO<sub>2</sub>, 50 → 100% EtOAc/hexane) to give triketocholanic acid (387.5 mg, 98%) as white solid (Scheme 2.14). TLC (EtOAc 100%): R<sub>f</sub> = 0.58; <sup>1</sup>H NMR (500 MHz, CD<sub>3</sub>OD): δ 3.08 (m, 2H), 2.98 (t, *J* = 12.7, 1H), 2.87 (t, *J* = 12.7 Hz, 1H), 2.49 (m, 1H), 2.44-2.32 (m, 2H), 2.26 (dd, *J* = 18.3, 10.3, Hz, 4H), 2.19-2.08, (m, 4H), 2.08-1.97 (m, 4H), 1.94 (dd, *J* = 13.2, 1.8 Hz, 1H), 1.91-1.79 (2H), 1.74 (m, 1H), 1.63 (m, 1H), 1.45 (s, 3H), 1.37 (d, *J* = 8.1 Hz, 3H), 1.14 (s, 3H); <sup>13</sup>C NMR (125 MHz, CD<sub>3</sub>OD): δ 213.8, 211.1, 210.2, 176.6, 56.86, 52.1, 48.5, 46.7, 45.7, 45.4, 44.5, 42.3, 38.3, 35.9, 35.8, 35.5, 34.7, 30.9, 30.5, 27.3, 24.6, 20.5, 17.7, 10.8; HRMS (ESI-) *m/z* calcd. for [M-H]<sup>-</sup>: 401.2406; found 401.2274 (C<sub>24</sub>H<sub>34</sub>O<sub>5</sub>, MW = 402.2406) [72, 73].



**Scheme 2.14** The synthesis of triketocholanic acid (A5)

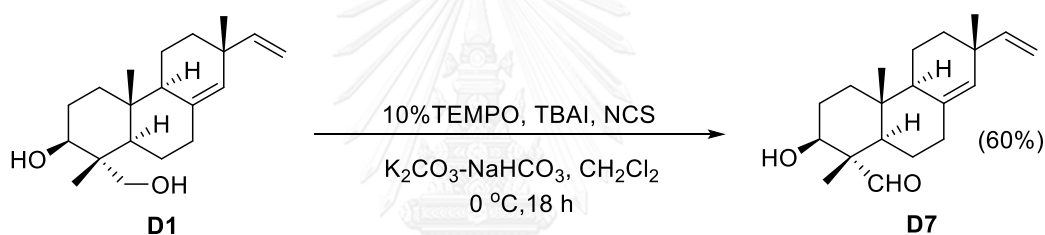
**19-Dehydroandrographolide (A10):** To a solution of andrographolide (**A7**) (55.0 mg, 0.16 mmol) in EtOAc (1 mL) were added 10% TEMPO (7.0 mg, 0.016 mmol),  $K_2CO_3$ - $NaHCO_3$  buffer (1 mL), TBAI (12.0 mg, 0.016 mmol) and NCS (36.0 mg, 0.24 mmol) and was cooled to 0 °C. The reaction mixture was then stirred vigorously for 9 h. The organic layer was separated and the aqueous layer was extracted with EtOAc (5 mL x 2). The combined organic layer was washed with brine (10 mL x 2), dried over anhydrous  $Na_2SO_4$ . The crude reaction was purified by flash column chromatography (gradient  $SiO_2$ , 40  $\rightarrow$  100% EtOAc/hexane) to give the desired aldehyde product (7.0 mg, 26% yield) as white solid and recovered andrographolide (44.0 mg) (Scheme 2.15). TLC (EtOAc 100%):  $R_f$  = 0.48;  $^1H$  NMR (500 MHz,  $CDCl_3$ ):  $\delta$  9.77 (s, 1H), 6.96 (t,  $J$  = 6.1 Hz, 1H), 5.05 (s, 1H), 4.96 (s, 1H), 4.64 (s, 1H), 4.47 (dd,  $J$  = 10.5, 6.1 Hz, 1H), 4.26 (dd,  $J$  = 10.5, 2.0 Hz, 1H), 3.25 (m, 1H), 2.77 (s, 1H), 2.51 (m, 3H), 2.03-1.80 (m, 6H), 1.68 (m, 1H), 1.41 (dd,  $J$  = 13.1, 2.6 Hz, 1H), 1.31 (s, 3H), 0.69 (s, 3H); HRMS (ESI+)  $m/z$  calcd. for  $[M+Li]^+$ : 355.1913; found 355.1995 ( $C_{20}H_{28}O_5$ , MW = 348.1937) [74, 75].



**Scheme 2.15** The synthesis of 19-dehydroandrographolide (**A10**)

**Sandaracopimaradien-3 $\beta$ ,18-olal (D7):** To a solution of sandaracopimaradiene-3 $\beta$ ,18-diol (**D1**) (304 mg, 1.0 mmol) in  $CH_2Cl_2$  (10 mL), were added TEMPO (16 mg, 0.10 mmol), buffer  $K_2CO_3$ - $NaHCO_3$  (10 mL), TBAI (39.4 mg, 0.10 mmol) and NCS (200 mg, 1.5 mmol) at 0 °C. The reaction mixture was then stirred vigorously for 9 h at the same temperature. The organic layer was separated and the aqueous layer was extracted with  $CH_2Cl_2$  (10 mL x 2). Combined organic layers were

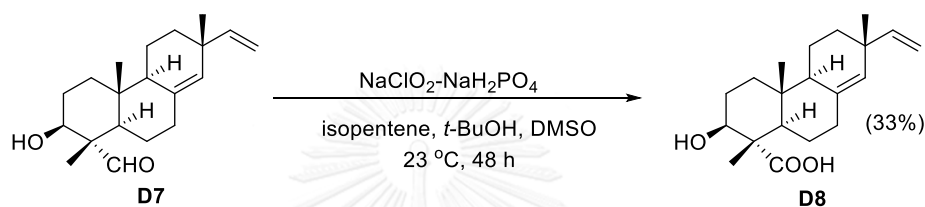
washed with brine (15 mL x 2), dried over anhydrous Na<sub>2</sub>SO<sub>4</sub> and concentrated under reduced pressure. The residue was purified by flash column chromatography (gradient SiO<sub>2</sub>, 0 → 15% EtOAc/hexane) providing sandaracopimaradiene-3 $\beta$ ,18-olal (**D7**) (181 mg, 60% yield) as colorless crystal (Scheme 2.16). TLC (EtOAc:hexane, 1:1 v/v): R<sub>f</sub> = 0.63; <sup>1</sup>H NMR (300 MHz, CDCl<sub>3</sub>):  $\delta$  9.43 (s, 1H), 5.79 (dd, *J* = 17.4, 10.6, 1H), 5.28 (s, 1H), 4.96 (dd, *J* = 6.8, 1.4 Hz, 1H), 4.90 (s, 1H), 3.82 (dd, *J* = 11.5, 4.2 Hz, 1H), 2.28 (ddd, *J* = 14.0, 4.4, 2.1 Hz, 1H), 2.03 (m, 1H), 1.78 (m, 1H), 1.71 (m, 1H), 1.64 (m, 2H), 1.58 (m, 2H), 1.48 (m, 2H), 1.42 (m, 2H), 1.32 (m, 1H), 1.21 (m, 1H), 1.13 (m, 3H), 1.07 (s, 3H), 0.88 (s, 3H); <sup>13</sup>C NMR (75 MHz, CDCl<sub>3</sub>):  $\delta$  206.9, 148.5, 135.6, 129.7, 110.4, 72.1, 55.3, 50.1, 46.8, 37.4, 37.1, 36.8, 35.2, 34.2, 26.5, 26.0, 24.0, 18.7, 15.3, 9.2 [74, 75].



**Scheme 2.16** The synthesis of sandaracopimaradien-3 $\beta$ ,18-olal (**D7**)

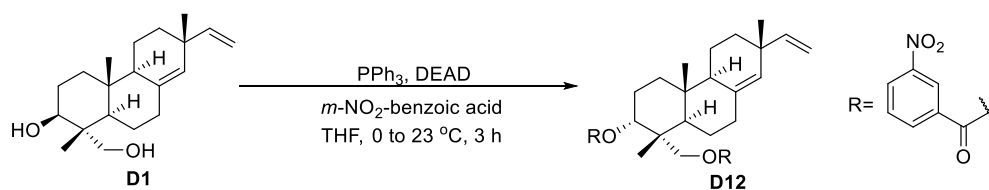
**3 $\beta$ -Hydroxysandaracopimaric acid (**D8**):** To a solution of sandaracopimaradien-3 $\beta$ ,18-olal (**D7**) (50 mg, 0.165 mmol) in DMSO (0.4 mL) were added isopentene (0.7 mL), *t*-BuOH (4.0 mL) and freshly-prepared NaClO<sub>2</sub>-NaH<sub>2</sub>PO<sub>4</sub> buffer 1.32 mL (NaClO<sub>2</sub> 0.226 g and NaH<sub>2</sub>PO<sub>4</sub> 0.272 g in water 8 mL) dropwise at 0 °C. After 0.5 h, the reaction mixture was allowed to warm up to 23 °C and stirred for 48 h. The reaction mixture was then diluted in EtOAc (5 mL). The organic layer was separated and aqueous layer was extracted with EtOAc (15 mL x 2). Organic layers were combined, washed with brine (15 mL x 2), and dried over anhydrous Na<sub>2</sub>SO<sub>4</sub>. Residue was purified by flash column chromatography (gradient SiO<sub>2</sub>, 20 → 50% EtOAc/hexane) to provide 3 $\beta$ -hydroxysandaracopimaric acid (17.7 mg, 33% yield) as white solid (Scheme 2.17). TLC (EtOAc:hexane, 1:2 v/v): R<sub>f</sub> = 0.31; <sup>1</sup>H NMR (500 MHz, CDCl<sub>3</sub>):  $\delta$  5.76 (dd, *J* = 17.4, 10.6 Hz, 1H), 5.25 (s, 1H), 4.90 (dd, *J* = 6.8, 1.4 Hz, 1H), 4.89

(s, 1H), 4.04 (dd,  $J = 11.9, 4.1$  Hz, 1H), 2.25 (ddd,  $J = 14.4, 4.5, 1.8$  Hz, 1H), 2.10 (td,  $J = 13.3, 5.4$  Hz, 1H), 1.78 (m, 1H), 1.71 (m, 1H), 1.64 (m, 2H), 1.58 (m, 2H), 1.48 (m, 2H), 1.42 (m, 2H), 1.32 (m, 1H), 1.21 (m, 1H), 1.19 (m, 3H), 1.04 (s, 3H), 0.84 (s, 3H);  $^{13}\text{C}$  NMR (125 MHz,  $\text{CD}_3\text{OD}$ ):  $\delta$  179.9, 148.4, 136.2, 128.9, 109.4, 74.9, 53.3, 50.4, 50.0, 37.2, 37.1, 36.9, 35.1, 34.2, 26.5, 25.1, 24.1, 18.4, 14.3, 10.4. IR (thin film): 3630, 2936, 1654, 1542  $\text{cm}^{-1}$ ; HRMS (ESI-)  $m/z$  calcd. for  $[\text{M}-\text{H}]^-$ : 317.3410; found 317.2098 ( $\text{C}_{20}\text{H}_{30}\text{O}_3$ , MW = 318.4570) [76, 77].



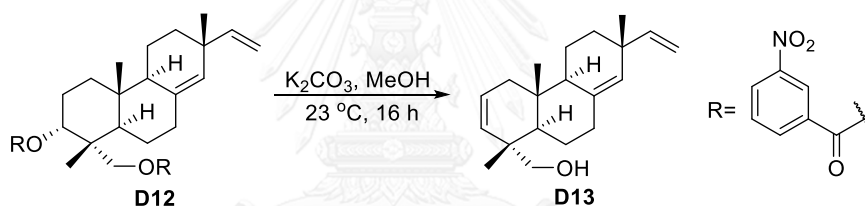
**Scheme 2.17** The synthesis of  $3\beta$ -hydroxysandaracopimaric acid (**D8**)

**Ester derivative (D12):** Sandaracopimaradiene- $3\beta,18$ -diol (**D1**) (51 mg, 0.168 mmol) and *m*-nitrobenzoic acid (84 mg, 0.503 mmol) were added into benzene (1 mL) and dried under high vacuum. The mixture was added with dried THF (1 mL) and stirred at 0 °C for 10 min. The DEAD solution (40% in toluene, 0.80 mL, 0.5780 mmol) in THF (1 mL) was added *via* syringe pump for 1 h and then the reaction was warmed up to 23 °C and further stirred for 2 h. The crude reaction was purified by flash column chromatography (gradient  $\text{SiO}_2$ , 10  $\rightarrow$  60% EtOAc/hexane) to afford the ester derivative **D12** (19.4 mg) as colorless oil (Scheme 2.18). TLC (EtOAc:hexane, 1:1 v/v):  $R_f = 0.70$ ;  $^1\text{H}$  NMR (300 MHz,  $\text{CDCl}_3$ ) found the signal of *m*-nitrobenzoyl at  $\delta$  8.99 (s), 8.50 (m), 7.75 (m), vinyl protons of diterpenoid at  $\delta$  5.77 (dd,  $J = 16.6, 10.4$  Hz, 1H), 5.31 (s, 1H), 4.94 (m, 2H) and 3 methyl groups at  $\delta$  1.14 (s, 3H), 1.07 (s, 3H), 0.92 (s, 3H) [78].



**Scheme 2.18** The synthesis of ester derivative **D12**

**Hydrolysis of D12:** Compound **D12** (19.4 mg) was reacted with  $K_2CO_3$  (20 mg, 1.541 mmol) in MeOH (1 mL) at 23 °C for 16 h. The residue was diluted with water (5 mL) and extracted with EtOAc (5 mL x 2). The organic phase was evaporated and then purified by preparative TLC (EtOAc:hexane, 1:1 v/v) to give product **D13** as colorless oil (5 mg) (Scheme 2.19). TLC (EtOAc:hexane, 1:1 v/v):  $R_f = 0.65$ .  $^1H$  NMR (500 MHz,  $CDCl_3$ ):  $\delta$  5.91 (ddd,  $J = 10.0, 6.5, 1.9$  Hz, 1H), 5.78 (dd,  $J = 17.8, 10.2$  Hz, 1H), 5.30 (dd,  $J = 10.1, 2.9$  Hz, 1H), 5.25 (s, 1H), 4.93 (dd,  $J = 5.2, 1.6$  Hz, 1H), 4.90 (q,  $J = 1.6$  Hz, 1H), 3.36 (d,  $J = 10.5$  Hz, 1H), 3.12 (d,  $J = 10.6$  Hz, 1H), 2.30 (dd,  $J = 4.4, 2.4$  Hz, 1H), 2.27 (dd,  $J = 4.4, 2.4$  Hz, 1H), 2.16 – 2.04 (m, 2H), 1.88 (dd,  $J = 12.7, 3.2$  Hz, 1H), 1.82 (dd,  $J = 15.9, 9.1$  Hz, 2H), 1.65 – 1.59 (m, 2H), 1.51 – 1.37 (m, 3H), 1.06 (s, 3H), 0.86 (s, 3H), 0.85 (s, 3H) [58].

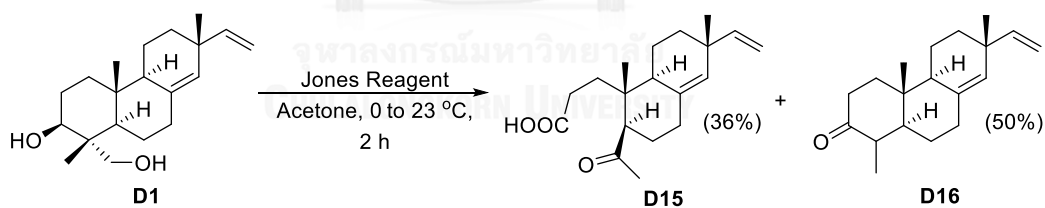


**Scheme 2.19** The hydrolysis of **D12** to **D13**

**Keto acid derivative D15:** Sandaracopimaradiene-3 $\beta$ ,18-diol (**D1**) (306 mg, 1.006 mmol) was dissolved in acetone (60 mL) and cooled to 0 °C. 2.5 mL of Jones reagent ( $CrO_3$  13.4 g, water 40 mL and conc.  $H_2SO_4$  12 mL) was added dropwise until the orange color persisted. The reaction was allowed to warm up to 23 °C and stirred for 2 h. The reaction was quenched by adding isopropanol until the deep-green color persisted and extracted with EtOAc (50 mL x 2). The organic layer was washed with brine (50 mL), dried over anhydrous  $Na_2SO_4$ , filtered and concentrated *in vacuo*. The residue was purified by flash column chromatography (gradient  $SiO_2$ , 20  $\rightarrow$  80% EtOAc/hexane) to give keto acid product **D15** (116 mg, 36% yield) as colorless oil (Scheme 2.20) [72, 73]. TLC (EtOAc:hexane, 1:1 v/v):  $R_f = 0.31$ ;  $^1H$  NMR (500 MHz,  $CDCl_3$ ):  $\delta$  5.77 (dd,  $J = 17.9, 10.1$  Hz, 1H), 5.32 (s, 1H), 4.93 (s, 1H), 4.90 (dd,  $J = 4.6, 0.6$  Hz, 1H),

2.60 (dd,  $J = 12.5, 3.3$  Hz, 1H), 2.52 (m, 1H), 2.36 (m, 1H), 2.30 (m, 1H), 2.19 (s, 3H), 2.05 (m, 1H), 1.92 (t,  $J = 7.5$  Hz, 1H), 1.82 (m, 2H), 1.68 (m, 2H), 1.59 (m, 2H), 1.49 (m, 1H), 1.40 (m, 1H), 1.06 (s, 3H), 0.99 (s, 3H);  $^{13}\text{C}$  NMR (125 MHz,  $\text{CDCl}_3$ ):  $\delta$  211.7, 179.7, 148.2, 134.8, 130.5, 110.6, 56.4, 42.0, 39.9, 37.4, 34.5, 34.2, 32.0, 31.6, 28.4, 26.1, 25.3, 18.3, 17.3. IR (thin film): 3429, 1707  $\text{cm}^{-1}$ ; HRMS (ESI-)  $m/z$  calcd. for  $[\text{M}-\text{H}]^-$ : 303.1940; found 303.1976 ( $\text{C}_{19}\text{H}_{28}\text{O}_3$ , MW = 304.4300).

**Keto derivative D16:** Colorless oil (137 mg, 50% yield) (Scheme 2.20). TLC (EtOAc:hexane, 2:4 v/v):  $R_f = 0.81$ ;  $^1\text{H}$  NMR (300 MHz,  $\text{CDCl}_3$ ):  $\delta$  5.75 (dd,  $J = 17.4, 10.6$  Hz, 1H), 5.28 (s, 1H), 4.91 (dd,  $J = 9.8, 1.5$  Hz, 1H), 4.86 (dd,  $J = 3.0, 1.5$  Hz, 1H), 2.42 (m, 1H), 2.34 (m, 1H), 2.28 (m, 1H), 2.21 (m, 1H), 2.12 – 1.99 (m, 2H), 1.80 – 1.62 (m, 4H), 1.54 (m, 2H), 1.47 – 1.33 (m, 3H), 1.32 – 1.26 (m, 1H), 1.08 (s, 3H), 0.98 (d,  $J = 6.5$  Hz, 3H) 0.97 (s, 3H);  $^{13}\text{C}$  NMR (75 MHz,  $\text{CDCl}_3$ ):  $\delta$  213.2, 148.6, 135.6, 129.6, 110.4, 53.5, 47.8, 45.2, 38.8, 38.0, 37.9, 37.5, 35.0, 34.4, 26.5, 25.9, 19.3, 13.8, 11.6. IR (thin film): 2948, 2867, 1711  $\text{cm}^{-1}$ ; HRMS (ESI+)  $m/z$  calcd. for  $[\text{M}+\text{Li}]^+$ : 279.2300; found 279.2292 ( $\text{C}_{19}\text{H}_{28}\text{O}$ , MW = 272.4320).

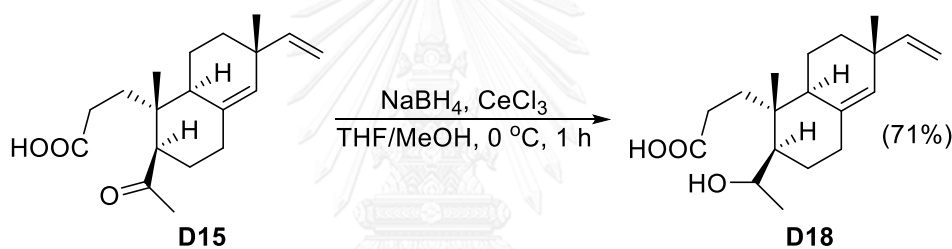


**Scheme 2.20** The synthesis of derivatives **D15** and **D16**

**Hydroxy acid derivative D18:** Keto acid derivative **D15** (143 mg, 0.471 mmol) was dissolved in THF (6 mL) and MeOH (4 mL).  $\text{CeCl}_3 \cdot 7\text{H}_2\text{O}$  was added and the solution was stirred for 5 min at 0  $^\circ\text{C}$ .  $\text{NaBH}_4$  (170 mg, 4.494 mmol) was added portionwise and the reaction was stirred for 1 h at 0  $^\circ\text{C}$ . A 10% aqueous solution of HCl (10 mL) was added and diluted with EtOAc (15 mL), and then extracted with water (20 mL x2) and dried over anhydrous  $\text{Na}_2\text{SO}_4$ . The crude reaction was purified by flash column



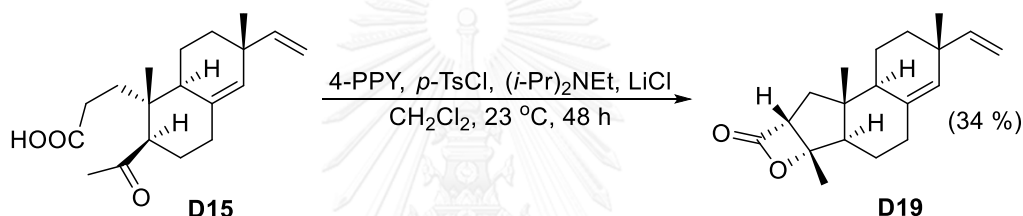
chromatography (gradient SiO<sub>2</sub>, 20 → 70% EtOAc/hexane) to give hydroxy acid **D18** (103 mg, 71% yield) as colorless oil (Scheme 2.21). TLC (EtOAc:hexane, 1:2 v/v with 1% acetic acid): R<sub>f</sub> = 0.37; <sup>1</sup>H NMR (500 MHz, CDCl<sub>3</sub>): δ 5.80 (dd, *J* = 17.5, 10.6 Hz, 1H), 5.29 (s, 1H), 4.93 (dd, 17.5, *J* = 1.5 Hz, 1H), 4.88 (s, 1H), 4.18 (q, *J* = 6.4 Hz, 1H), 2.30 (dt, *J* = 8.2, 3.4 Hz, 1H), 2.17 (m, 2H), 2.00 (m, 1H), 1.95 (m, 1H), 1.85 (m, 2H), 1.65 (m, 2H), 1.62 (m, 1H), 1.58 (m, 2H), 1.38 (m, 1H), 1.20 (d, *J* = 6.4 Hz, 3H), 1.06 (s, 3H), 0.97 (s, 3H); <sup>13</sup>C NMR (75 MHz, CDCl<sub>3</sub>): δ 179.7, 148.6, 136.2, 129.4, 110.4, 65.7, 48.2, 42.0, 40.2, 37.3, 35.2, 34.3, 30.7, 27.9, 26.1, 24.1, 20.1, 18.9, 17.9; IR (thin film): 3431, 2967, 1707 cm<sup>-1</sup>; HRMS (ESI-) *m/z* calcd. for [M-H]<sup>-</sup>: 305.2004; found 305.2105 (C<sub>19</sub>H<sub>30</sub>O<sub>3</sub>, MW = 306.4460) [79].



**Scheme 2.21** The synthesis of hydroxy acid derivative **D18**

**Beta-lactone derivative D19:** To an oven-dried round-bottomed flask (5 mL) equipped with a magnetic stir bar was added keto acid **D15** (23.3 mg, 0.0765 mmol) and was azeotropically dried in benzene (0.5 mL) under high vacuum. To a separate oven-dried round-bottomed flask (10 mL) equipped with a magnetic stir bar were added solid with LiCl (3.2 mg, 0.076 mmol), *p*-TsCl (18.2 mg, 0.096 mmol) and 4-PPY (13.3 mg, 0.076 mmol). The flask contents were azeotropically dried with benzene (0.5 mL) under high vacuum and then dissolved in CH<sub>2</sub>Cl<sub>2</sub> (2 mL). To stirred homogenous solution was added (*i*-Pr)<sub>2</sub>NEt (0.06 mL, 0.306 mmol) *via* syringe and followed by a solution of keto acid **D15** in CH<sub>2</sub>Cl<sub>2</sub> (1 mL) dropwise and then stirred for 48 h. The crude reaction was purified by flash column chromatography (gradient SiO<sub>2</sub>, 20 → 50% EtOAc/hexane) to give beta-lactone product **D19** (7.3 mg, 34% yield) as colorless

oil with diastereomeric ratios (dr) = 14:1 which was determined by  $^1\text{H}$  NMR at  $\delta_{\text{H}} = 4.19$ : 4.13. (Scheme 2.22). TLC (EtOAc:hexane, 1:1 v/v):  $R_f = 0.81$ ;  $^1\text{H}$  NMR (300 MHz,  $\text{CDCl}_3$ ):  $\delta$  5.74 (m, 1H), 5.31 (s), 4.93 (s, 1H), 4.88 (dd,  $J = 7.3, 1.5$  Hz, 1H), 3.59 (dd,  $J = 9.8, 7.5$  Hz, 1H), 2.30 (ddd,  $J = 14.6, 4.9, 2.0$  Hz, 1H), 2.11 (m, 1H), 2.08 (dd,  $J = 13.2, 3.3$  Hz, 1H), 1.99 (m, 2H), 1.83 (m, 2H), 1.81 (m, 2H), 1.62 (t, 2H), 1.58 (s, 3H), 1.43 (m, 2H), 1.04 (s, 3H), 0.72 (s, 3H);  $^{13}\text{C}$  NMR (125 MHz,  $\text{CDCl}_3$ ):  $\delta$  172.6, 147.9, 134.9, 130.6, 110.8, 87.5, 58.6, 56.5, 52.0, 47.8, 37.7, 37.3, 34.5, 33.9, 26.5, 21.7, 20.4, 20.2, 15.2; IR (thin film): 2926, 2868, 1816  $\text{cm}^{-1}$ ; HRMS (ESI+)  $m/z$  calcd. for  $[\text{M}+\text{Li}]^+$ : 293.1936; found 293.2095 ( $\text{C}_{19}\text{H}_{26}\text{O}_2$ , Mw = 286.4150) [54, 60].

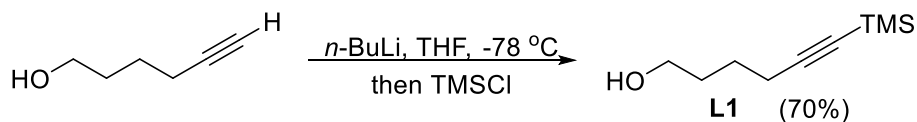


**Scheme 2.22** The synthesis of beta-lactone derivative **D19**

### 2.13 Derivatization of Sandaracopimaradiene-3 $\beta$ ,18-diol (D1) by Simultaneous-Arming

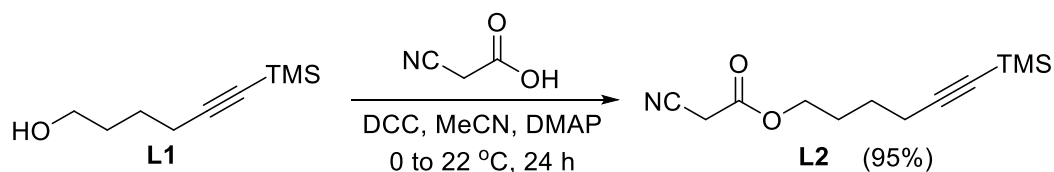
**6-(Trimethylsilyl)-hex-5-yn-1-ol (L1):** 5-Hexyn-1-ol (1.0 g, 10.19 mmol) was dissolved in THF (20 mL), and then the solution was cooled to  $-78\text{ }^\circ\text{C}$ .  $n\text{-BuLi}$  (8.97 mL, 2.5 M in hexane, 22.42 mmol) was then added slowly dropwise *via* syringe. The reaction mixture was stirred for 1 h at  $-78\text{ }^\circ\text{C}$  and then  $\text{TMSCl}$  (3.88 mL, 30.57 mmol) was added. The mixture was allowed to warm up to  $23\text{ }^\circ\text{C}$  over 1 h and then further stirred for 1 h. The reaction mixture was diluted with  $\text{Et}_2\text{O}$  (15 mL) and then quenched with saturated  $\text{NH}_4\text{Cl}$  (15 mL). The organic fraction was washed with 2 N  $\text{HCl}$  (2 x 25 mL) and water (25 mL), dried over anhydrous  $\text{Na}_2\text{SO}_4$ . The residue was purified by flash column chromatography (gradient  $\text{SiO}_2$ , 0  $\rightarrow$  20% EtOAc/hexane) to provide the desired product (1.289 g, 70% yield) as colorless oil (Scheme 2.23). TLC (EtOAc:hexane, 4:1 v/v):  $R_f = 0.39$ ;  $^1\text{H}$  NMR (300 MHz,  $\text{CDCl}_3$ ):  $\delta$  3.67 (t,  $J = 6.2$  Hz, 2H), 2.26 (t,  $J = 7.1$  Hz,

2H), 1.63 (m, 4H), 0.14 (s, 9H)  $^{13}\text{C}$  NMR (75 MHz,  $\text{CDCl}_3$ ):  $\delta$  107.1, 84.7, 62.3, 31.7, 24.8, 19.6, 0.12 [68].



**Scheme 2.23** The synthesis of 6-(trimethylsilyl)hex-5-yn-1-ol (L1)

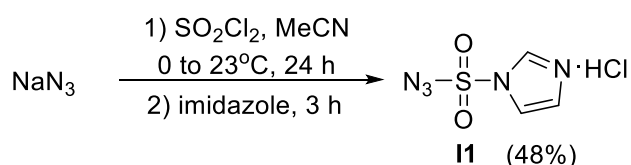
**6-(Trimethylsilyl)hex-5-yn-1-yl 2-cyanoacetate (L2):** Cyanoacetic acid (1.040 g, 11.55 mmol) was dissolved in MeCN (40 mL) and cooled to 0 °C. The reaction mixture was stirred at 0 °C for 10 min and then DCC (2.390 g, 11.55 mmol) in combination with 10% DMAP (120.2 mg, 0.77 mmol) were added. 6-(Trimethylsilyl)hex-5-yn-1-ol (L1) (1.310 g, 7.70 mmol) was added dropwise and then the mixture was stirred at 23 °C for 24 h. The mixture was diluted with  $\text{Et}_2\text{O}$  and extracted with water and then dried over anhydrous  $\text{Na}_2\text{SO}_4$ . The residue was purified by flash column chromatography (gradient  $\text{SiO}_2$ , 0  $\rightarrow$  20% EtOAc/hexane) to give desired product (1.733 g, 95% yield) as pale yellow oil (Scheme 2.24). TLC (EtOAc:hexane, 3:1 v/v):  $R_f$  = 0.50;  $^1\text{H}$  NMR (300 MHz,  $\text{CDCl}_3$ ):  $\delta$  4.24 (t,  $J$  = 6.5 Hz, 2H), 3.46 (s, 2H), 2.28 (t,  $J$  = 6.9 Hz, 2H), 1.81 (m, 2H), 1.60 (m, 2H), 0.14 (s, 9H);  $^{13}\text{C}$  NMR (75 MHz,  $\text{CDCl}_3$ ):  $\delta$  162.9, 113.1, 106.3, 85.2, 66.4, 27.3, 24.7, 24.6 19.3, 0.05 [68].



**Scheme 2.24** The synthesis of 6-(trimethylsilyl)hex-5-yn-1-yl 2-cyanoacetate (L2)

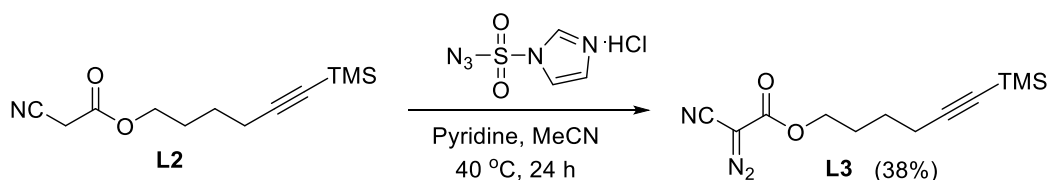
**Imidazole-1-sulfonyl azide hydrochloride (I1):** Sulfuryl chloride (8.05 mL, 100 mmol) was added dropwise to an ice-cooled suspension of  $\text{NaN}_3$  (6.5 g, 100 mmol) in MeCN (100 mL) and the mixture stirred overnight at 23 °C. Imidazole (13.10 g, 190 mmol) was added portion-wise to the ice cooled mixture and the resulting slurry stirred for 3 h at 23 °C. The mixtures was diluted in EtOAc, washed with water then saturated

aqueous  $\text{NaHCO}_3$  dried over  $\text{Na}_2\text{SO}_4$  and filtrate. A solution of 5%  $\text{HCl}/\text{EtOH}$  was added dropwise to the filtrate with stirring. The mixture chilled in an ice-bath, filtered and the filter product was washed with  $\text{EtOAc}$  to give white crystal needle (10.16 g, 48% yield) (Scheme 2.25).  $^1\text{H}$  NMR (300 MHz,  $\text{D}_2\text{O}$ ):  $\delta$  9.22 (bs, 1H), 7.89 (dd,  $J = 2.1, 1.6$  Hz, 1H), 7.47 (dd,  $J = 2.1, 1.2$  Hz, 1H);  $^{13}\text{C}$  NMR (75 MHz,  $\text{D}_2\text{O}$ ):  $\delta$  137.7, 123.8, 119.9 [80].



**Scheme 2.25** The synthesis of imidazole-1-sulfonyl azide hydrochloride (**11**)

**6-(Trimethylsilyl)hex-5-yn-1-yl 2-cyano-2-diazoacetate (L3):** The 6-(trimethylsilyl)hex-5-yn-1-yl 2-cyanoacetate (**L2**) (1.458 g, 6.32 mmol) and imidazole-1-sulfonyl azide hydrochloride (**11**) (2.000 g, 9.48 mmol) were dissolved in  $\text{MeCN}$  (30 mL) and then pyridine (2.55 mL, 31.60 mmol) was added. The mixture was stirred at  $40^\circ\text{C}$  for 24 h and then was cooled to rt and diluted with  $\text{EtOAc}$  (75 mL), washed with 1N  $\text{HCl}$  (2 x 75mL) and  $\text{H}_2\text{O}$  (75 mL). The organic layer was dried over  $\text{Na}_2\text{SO}_4$ , filtered and concentrated under reduced pressure. The residue was purified by flash column chromatography (gradient  $\text{SiO}_2$ , 0  $\rightarrow$  10%  $\text{EtOAc}/\text{hexane}$ ) to give the desired product (627.8 mg, 38% yield) as pale yellow oil (Scheme 2.26). TLC ( $\text{EtOAc}:\text{hexane}$ , 1:2 v/v):  $R_f = 0.73$ ;  $^1\text{H}$  NMR (300 MHz,  $\text{CDCl}_3$ ):  $\delta$  4.31 (t,  $J = 6.5$  Hz, 2H), 2.28 (t,  $J = 6.9$  Hz, 2H), 1.82 (m, 2H), 1.59 (m, 2H), 0.15 (s, 9H);  $^{13}\text{C}$  NMR (75 MHz,  $\text{CDCl}_3$ ):  $\delta$  161.2, 107.7, 106.2, 85.3, 66.8, 27.6, 24.7, 19.3, 0.07 [68].

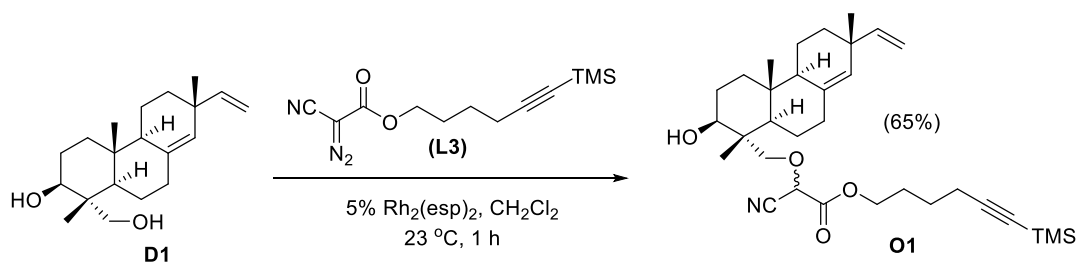


**Scheme 2.26** The synthesis of 6-(trimethylsilyl)hex-5-yn-1-yl 2-cyano-2-diazoacetate (**L3**)

**OH-insertion derivative (O1):** Sandaracopimaradiene-3 $\beta$ ,18-diol (**D1**) (10.0 mg, 0.033 mmol) and 5% Rh<sub>2</sub>(esp)<sub>2</sub>, Bis-(rhodium ( $\alpha,\alpha,\alpha',\alpha'$ -tetra-methyl-1,3-benzenedipropionic acid)) (165  $\mu$ L (7.7 mg/mL of stock solution in CH<sub>2</sub>Cl<sub>2</sub>), 0.00165 mmol), were added into flame-dried vial and dissolved with dried CH<sub>2</sub>Cl<sub>2</sub> (1.0 mL) of under N<sub>2</sub> atmosphere. A solution of diazoacetate (**L3**) (13.0 mg, 0.05 mmol) in dry CH<sub>2</sub>Cl<sub>2</sub> (1.0 mL) was added *via* syringe pump (flow rate 2.0 mL/h) over 1 h at 23 °C. The residue was purified by preparative TLC (20% EtOAc/hexane) to give mixtures of diastereomers (10 mg, 65% yield) as colorless oil (Scheme 2.27). The mixture of diastereomers was purified by preparative TLC (20% EtOAc/hexane) to obtain two mixtures of diastereomer with dr = 1:4 [65, 69].

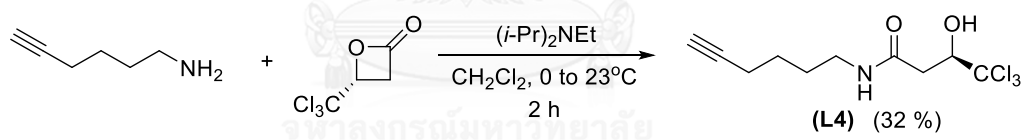
**Mixtures of diastereomer (1):** colorless oil (2.4 mg). TLC (EtOAc:hexane, 4:1 v/v): R<sub>f</sub> = 0.38. <sup>1</sup>H NMR (300 MHz, CDCl<sub>3</sub>):  $\delta$  5.80 (dd, *J* = 17.4, 10.1 Hz), 5.27 (s), 5.05 – 4.81 (m), 4.36 (dt, *J* = 12.0, 5.4 Hz), 3.79 (dd, *J* = 11.5, 4.2 Hz), 3.71 – 3.52 (m), 3.42 (t, *J* = 11.5 Hz), 2.32 (t, *J* = 6.9 Hz), 2.08 (dd, *J* = 22.7, 14.8 Hz), 1.96 – 1.78 (m), 1.75 – 1.43 (m), 1.45 – 1.33 (m), 1.07 (s), 0.89 (s), 0.80 (d, *J* = 5.3 Hz), 0.18 (s).

**Mixtures of diastereomer (2):** colorless oil (8.0 mg). TLC (EtOAc:hexane, 4:1 v/v): R<sub>f</sub> = 0.31. <sup>1</sup>H NMR (300 MHz, CDCl<sub>3</sub>):  $\delta$  5.79 (dd, *J* = 17.4, 10.6 Hz), 5.27 (s), 5.04 – 4.73 (m), 4.46 – 4.29 (m), 3.79 (ddd, *J* = 11.3, 4.6, 2.2 Hz), 3.58 (ddd, *J* = 21.9, 11.0, 6.1 Hz), 2.32 (tt, *J* = 7.9, 3.9 Hz), 2.17 – 1.97 (m), 1.96 – 1.78 (m), 1.78 – 1.56 (m), 1.46 (dd, *J* = 10.6, 5.2 Hz), 1.28 (s), 1.07 (s), 0.87 (s), 0.18 (d, *J* = 0.5 Hz).



**Scheme 2.27** The synthesis of O-H insertion derivative (**O1**)

**(R)-4,4,4-Trichloro-N-(hex-5-yn-1-yl)-3-hydroxybutanamide (L4):** EtN(*i*-Pr)<sub>2</sub> (2.60 mL, 7.09 mmol) was added to a solution of (*R*)-(-)-3-hydroxy-4,4,4-trichlorobutyric  $\beta$ -lactone (1.788 g, 10.6 mmol) in CH<sub>2</sub>Cl<sub>2</sub> (25 mL) and cooled to 0 °C. A solution of hex-5-yn-1-amine (689.0 mg, 7.09 mmol), was synthesized according to the previous procedure, in CH<sub>2</sub>Cl<sub>2</sub> (10 mL) was added dropwise into the above solution at 0 °C. The reaction mixture was stirred at 0 °C for 1 h, and then kept warm up to rt for 1 h. After the reaction was completed, the solvent was removed by evaporator and the residue was purified by flash column chromatography (gradient SiO<sub>2</sub>, 20 → 40% EtOAc/hexane) to give the desired product (631 mg, 32% yield) as colorless oil (Scheme 2.28). TLC (EtOAc:hexane, 1:1 v/v): R<sub>f</sub> = 0.36; <sup>1</sup>H NMR (500 MHz, CDCl<sub>3</sub>)  $\delta$  6.01 (bs, 1H), 5.02 (s, 1H), 4.59 (d, *J* = 9.2 Hz, 1H), 3.32 (dd, *J* = 12.9, 6.9 Hz, 2H), 2.94 (dd, *J* = 14.9, 2.4 Hz, 1H), 2.59 (dd, *J* = 15.0, 9.3 Hz, 1H), 2.24 (td, *J* = 6.8, 2.6 Hz, 2H), 1.98 (t, *J* = 2.6 Hz, 1H) 1.65-1.56 (m, 4H). <sup>13</sup>C NMR (125 MHz, CDCl<sub>3</sub>):  $\delta$  170.0, 102.4, 83.9, 79.7, 68.9, 39.2, 37.9, 28.4, 25.6, 18.1 [67].

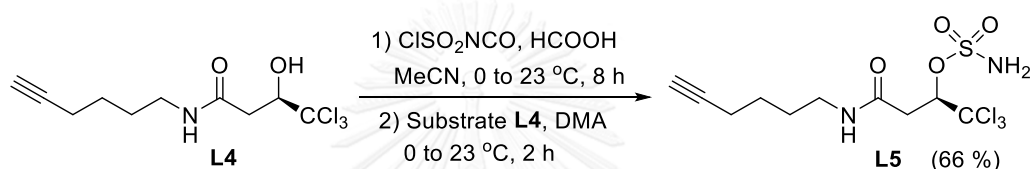


**Scheme 2.28** The synthesis of (*R*)-4,4,4-trichloro-*N*-(hex-5-yn-1-yl)-3-hydroxybutanamide (**L4**)

**(R)-1,1,1-Trichloro-4-(hex-5-yn-1-ylamino)-4-oxobutan-2-yl sulfamate (L5):**

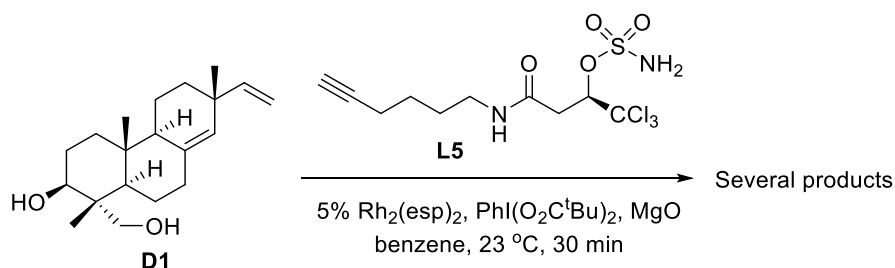
A solution of HCO<sub>2</sub>H (0.15 mL, 3.65 mmol) in MeCN (1.5 mL) was added to a solution of chlorosulfonyl isocyanate (ClSO<sub>2</sub>NCO) (0.7 mL, 3.65 mmol) in MeCN (2.5 mL) at 0 °C over 10 min and the mixture was stirred at ambient temperature for 8 h. A solution of alcohol substrate **L4** (520 mg, 1.82 mmol) in dimethylacetamide (DMA, 3 mL) was then added to the reaction mixture at 0 °C and the resulting solution was stirred at 23 °C for 2 h. Upon completion of the reaction, it was quenched with water (20 mL) and extracted with Et<sub>2</sub>O (50 mL). The separated aqueous layer was extracted with Et<sub>2</sub>O

(15 x 2) and the combined organic layer was washed with water (20 x 5), dried over anhydrous  $\text{Na}_2\text{SO}_4$ , and concentrated. The residue was purified by flash column chromatography (gradient  $\text{SiO}_2$ , 20  $\rightarrow$  40% EtOAc/hexane) to give sulfamate product **L5** (440 mg, 66.4% yield) as white solid (Scheme 2.29). TLC (EtOAc:hexane, 1:1 v/v):  $R_f$  = 0.12;  $^1\text{H}$  NMR (500 MHz,  $\text{CDCl}_3$ )  $\delta$  6.07 (bs, 1H), 5.52 (dd,  $J$  = 6.8, 2.0 Hz, 1H), 3.33 (dd,  $J$  = 6.2, 2.7 Hz, 2H), 3.19 (dd,  $J$  = 16.5, 1.8 Hz, 1H), 2.95 (dd,  $J$  = 16.5, 8.7 Hz, 1H), 2.24 (dt,  $J$  = 6.8, 2.2 Hz, 2H), 2.00 (t,  $J$  = 2.4 Hz, 1H), 1.67 (m, 2H), 1.65 (m, 2H);  $^{13}\text{C}$  NMR (125 MHz,  $\text{CDCl}_3$ ):  $\delta$  168.9, 98.4, 85.8, 83.9, 69.1, 39.6, 38.0, 28.3, 25.5, 18.0 [67].



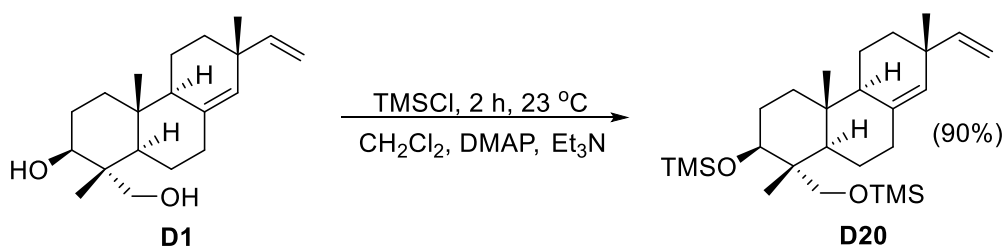
**Scheme 2.29** The synthesis of (*R*)-1,1,1-trichloro-4-(hex-5-yn-1-ylamino)-4-oxobutan-2-yl sulfamate (**L5**)

**C-H Amination of sandaracopimaradiene-3 $\beta$ ,18-diol:** Sandaracopimaradiene-3 $\beta$ ,18-diol (**D1**) (15.2 mg, 0.05 mmol) and sulfamate (**L5**) (36.4 mg, 0.10 mmol) were mixed in a small vial and dried under high vacuum for 10 min before being purged with  $\text{N}_2$  atmosphere.  $\text{Rh}_2(\text{esp})_2$  and  $\text{MgO}$  (10 mg, 0.25 mmol) were mixed for stock solution in benzene and 0.4 mL of such suspension (2.0 mg, 0.0025 mmol) was added into the reaction mixture and then stirred at rt under  $\text{N}_2$  atmosphere for 10 min.  $\text{PhI}(\text{O}_2\text{C}^t\text{Bu})_2$  (81.2 mg, 0.20 mmol) was then added in one portion and the reaction mixture was vigorously stirred at 23  $^\circ\text{C}$  for 30 min (Scheme 2.30). Several products were detected on TLC, the observed molecular ion of (ACPI+) 666.2, should be the desired product, from LCMS [67].



**Scheme 2.30** C-H Amination of sandaracopimaradiene-3 $\beta$ ,18-diol

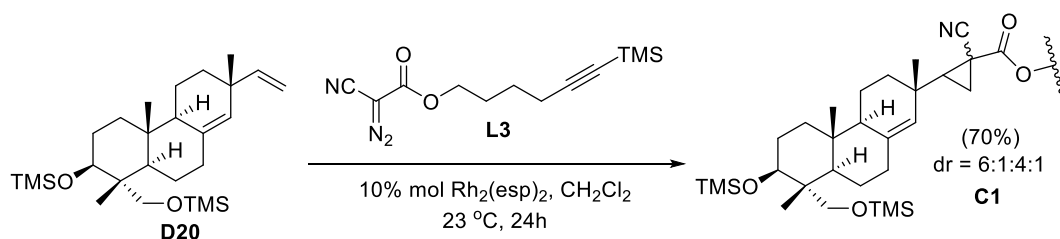
**Di-OTMS-sandaracopimara-3 $\beta$ ,18-diene (D20):** Sandaracopimaradiene-3 $\beta$ ,18-diol (**D1**) (51 mg, 0.167 mmol) was dissolved in dry CH<sub>2</sub>Cl<sub>2</sub> (10 mL) and then DMAP (4.0 mg, 0.033 mmol) was added followed by Et<sub>3</sub>N (0.10 mL, 0.657 mmol) and TMSCl (85  $\mu$ L, 0.675 mmol). The reaction mixture was stirred for 2 h at 23 °C and subsequently quenched with a pH 7 NaH<sub>2</sub>PO<sub>4</sub>/Na<sub>2</sub>HPO<sub>4</sub> buffer solution (1 mL). The organic layer was dried over anhydrous Na<sub>2</sub>SO<sub>4</sub>, filtered and concentrated under reduced pressure. The residue was filtered through a short plug of silica gel and eluted with 10% EtOAc/hexane to afford the desired product **D20** (65 mg, 87% yield) as colorless oil (Scheme 2.31). TLC (EtOAc:hexane, 4:2 v/v): R<sub>f</sub> = 0.84; <sup>1</sup>H NMR (300 MHz, CDCl<sub>3</sub>):  $\delta$  5.77 (dd, *J* = 17.5, 10.6 Hz, 1H), 5.22 (s, 1H), 4.92 (dd, *J* = 12.4, 1.5 Hz, 1H), 4.87 (dd, *J* = 5.6, 1.5 Hz, 1H), 3.73 (dd, *J* = 11.2, 4.8 Hz, 1H), 3.19 (dd, *J* = 37.1, 9.9 Hz, 2H), 2.24 (ddd, *J* = 14.0, 4.3, 2.1 Hz, 1H), 2.03 (td, *J* = 13.3, 5.7 Hz, 1H), 1.78 (m, 1H), 1.71 (m, 1H), 1.64 (m, 2H), 1.58 (m, 2H), 1.48 (m, 2H), 1.42 (m, 2H), 1.21 (m, 1H), 1.13 (m, 1H), 1.01 (s, 3H), 0.82 (s, 3H), 0.63 (s, 3H), 0.09 (s, 9H), 0.08 (s, 9H); <sup>13</sup>C NMR (75 MHz, CDCl<sub>3</sub>):  $\delta$  149.0, 137.1, 128.6, 110.0, 71.9, 63.7, 50.3, 44.9, 43.1, 37.7, 37.4, 36.9, 35.7, 34.6, 27.5, 26.0, 21.8, 18.8, 15.6, 12.8, 0.41, -0.50 [68].



**Scheme 2.31** The synthesis of di-OTMS-sandaracopimara-3 $\beta$ ,18-diene (**D20**)



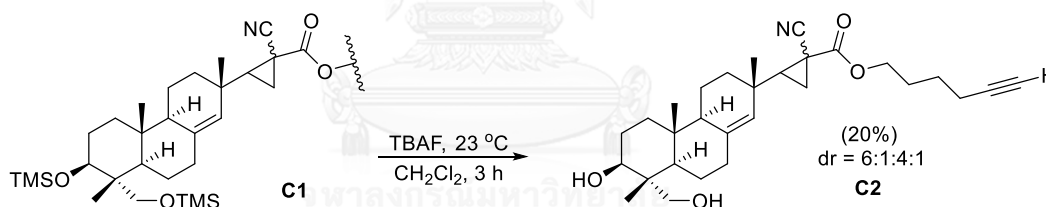
**Cyclopropanation of sandaracopimara-3 $\beta$ ,18-diene (C1):** Di-OTMS-sandaracopimara-3 $\beta$ ,18-diene (**D20**) (77 mg, 0.172 mmol) and Rh<sub>2</sub>(esp)<sub>2</sub> (13.0 mg, 0.0172 mmol) were mixed with benzene (1.0 mL) in a small vial and dried under high vacuum. The mixture was dissolved in dry CH<sub>2</sub>Cl<sub>2</sub> (1.0 mL) and stirred under N<sub>2</sub> atmosphere at 23 °C. A solution of diazoacetate (**L3**) (135.7 mg, 0.515 mmol) in dry CH<sub>2</sub>Cl<sub>2</sub> (3.0 mL) was added *via* syringe pump over 4 h at 23 °C. The reaction mixture was concentrated under reduced pressure and was purified by flash column chromatography (gradient SiO<sub>2</sub>, 0 → 15% EtOAc/hexane) to give desired product **C1** (76.5 mg, 70% yield, dr = 6:1:4:1 which was determined by <sup>1</sup>H NMR at  $\delta_{\text{H}}$  = 5.39 : 5.26 : 5.12 : 4.94) as colorless oil (Scheme 2.32). TLC (EtOAc:hexane, 5:1 v/v): R<sub>f</sub> = 0.68; <sup>1</sup>H NMR (300 MHz, CDCl<sub>3</sub>):  $\delta$  5.39 (s), 5.26 (s), 5.12 (s), 4.94 (s), 4.23 (td, *J* = 6.4, 2.1 Hz), 3.74 (dd, *J* = 11.1, 4.8 Hz), 3.27 (dd, *J* = 9.9, 2.4 Hz), 3.14 (d, *J* = 9.8 Hz), 2.31 (dd, *J* = 7.7, 6.2 Hz), 2.14 – 1.23 (m), 1.19 (s), 1.15 (s), 1.10 – 1.05 (m), 1.00 (s), 0.99 – 0.97 (m), 0.91 (s), 0.87 – 0.83 (m), 0.82 (s), 0.64 (d, *J* = 2.1 Hz), 0.18 (s), 0.17 (s), 0.11 (d, *J* = 1.0 Hz), 0.10 (s), 0.10 (s), 0.09 (s); <sup>13</sup>C NMR (75 MHz, CDCl<sub>3</sub>):  $\delta$  168.6, 168.5, 165.9, 164.9, 164.6, 140.5, 139.8, 138.8, 138.2, 126.7, 125.4, 124.9, 124.0, 120.1, 120.1, 117.7, 117.1, 106.4, 85.1, 85.1, 71.8, 71.8, 66.2, 66.2, 63.7, 50.6, 49.8, 44.8, 44.6, 43.3, 43.1, 43.1, 43.0, 37.9, 37.4, 36.7, 36.7, 35.6, 35.3, 35.2, 34.6, 33.8, 33.3, 31.6, 27.5, 27.4, 24.8, 22.6, 19.4, 16.7, 15.6, 15.5, 15.4, 14.1, 12.7, 11.4, 0.42, 0.42, 0.14, -0.49, -0.51 [68].



**Scheme 2.32** Cyclopropanation of sandaracopimara-3 $\beta$ ,18-diene (**C1**)

**Cyclopropanation derivative C2:** compound **C1** (77 mg, 0.112 mmol) was dissolved in CH<sub>2</sub>Cl<sub>2</sub> (10 mL) and then TBAF (1 M in THF, 1.10 mL, 1.1189 mmol) was added. The reaction was stirred for 1 h at 23 °C. The reaction mixture was filtered

through a short plug of silica gel to remove TBAF and then purified by preparative TLC (50% EtOAc/hexane) to provide the desired product **C2** (10.6 mg, 20% yield) as colorless oil with diastereomeric ratios (dr) = 6:1:4:1 which was determined by  $^1\text{H}$  NMR at  $\delta_{\text{H}}$  = 5.36: 5.26:5.05:4.94 and recovery compound **C1** (49.5 mg, 65% recovery yield) (Scheme 2.33). TLC (EtOAc:hexane, 1:1 v/v):  $R_f$  = 0.39;  $^1\text{H}$  NMR (500 MHz,  $\text{CDCl}_3$ ):  $\delta$  5.36 (s), 5.26 (s), 5.05 (s), 4.94 (s), 4.20 (tt,  $J$  = 6.4, 3.2 Hz), 4.10 (ddd,  $J$  = 17.6, 9.3, 4.9 Hz), 3.67 (ddd,  $J$  = 11.5, 6.7, 4.6 Hz), 3.39 (t,  $J$  = 12.1 Hz), 2.60 – 2.45 (m), 2.32 – 2.16 (m), 2.11 – 1.89 (m), 1.89 – 1.21 (m), 1.16 (s), 1.12 (s), 1.04 (s), 0.96 – 0.88 (m), 0.82 (s), 0.79 (s), 0.78 (s);  $^{13}\text{C}$  NMR (125 MHz,  $\text{CDCl}_3$ ):  $\delta$  168.4, 140.1, 138.9, 137.4, 125.9, 124.0, 117.6, 116.8, 83.6, 72.0, 68.8, 66.2, 66.2, 53.3, 50.7, 49.8, 48.3, 48.1, 43.2, 42.9, 42.1, 38.0, 37.5, 36.8, 35.4, 35.0, 34.7, 33.7, 33.3, 27.3, 27.0, 25.1, 24.6, 22.2, 20.6, 18.5, 18.0, 16.8, 15.7, 15.4, 13.9, 11.4. HRMS (ESI+)  $m/z$  calcd. for  $[\text{M}+\text{H}]^+$ : 468.3036; found 468.3108 ( $\text{C}_{29}\text{H}_{41}\text{NO}_4$ , MW = 467.6500) [68].



**Scheme 2.33** The synthesis of cyclopentanone derivative **C2**

## 2.14 Antibacterial Activity Test

### 2.14.1 Preliminary Screening Test of Antibacterial Activity by Diffusion Method

Five bacteria: *Propionibacterium acne*, *Staphylococcus aureus*, *Streptococcus sobrinus*, *Streptococcus mutans* and *Salmonella typhi* were given from Laboratory of Forest Products Chemistry, Faculty of Forestry, Mulawarman University, East Kalimantan, Indonesia. All compounds at the concentration of 1,000  $\mu\text{M}$  in 10% DMSO were tested for antibacterial activity against pathogens. Agar diffusion method was carried out as described from previous work with some modifications [81]. Nutrient

broth was inoculated with the tested organisms and incubated at 37 °C for 24 h. The testing used a cell suspension of about  $1.5 \times 10^8$  CFU/mL obtained from a McFarland turbidity standard No. 0.5. The agar was allowed to set and harden and the required number of wells is cut using a sterile cork borer ensuring proper distribution of wells. The bacterial inoculum was uniformly spread using sterile cotton swab on a sterile petri dish nutrient agar. The tested compound (50  $\mu$ L) was put into the well and 10% DMSO was used as a negative control. The plates were incubated at 37 °C for 24 h. Antimicrobial activity was evaluated by measuring the diameter of the inhibition zone around the disc.

#### 2.14.2 Antibacterial Activity Method Test for MIC and MBC

The method was carried out as described from previous work with some modifications [82]. The stock solution 2,000  $\mu$ M of compounds possessing good activity on preliminary screening test and 500  $\mu$ M of chloramphenicol were prepared in 10% (v/v) DMSO/sterile water. The tested compound 100  $\mu$ L was pipetted into the first row of 96 wells microplate and all other wells was added 50  $\mu$ L of nutrient broth. Serial dilutions were performed *via* a multichannel pipette and the last row were discarded 50  $\mu$ L of solution. Finally, bacterial suspension 10  $\mu$ L ( $1.5 \times 10^8$  CFU/mL obtained from a McFarland turbidity standard No. 0.5) was added by pipette to each well. Each plate had a set of controls that were a column with chloramphenicol as positive control, a column with all solutions except the test compound as negative control and a column with all solutions except the bacterial solution adding 10  $\mu$ L of nutrient broth instead. All plates were prepared in triplicate and closed with cover, and then placed for incubation at 37 °C for 18 to 24 h. Resazurin solution, 260 mg tablet was dissolved in 40 mL of sterile water, 50  $\mu$ L was added to each well to give blue color, and then left for 30 min before observed the result. Any wells changed to pink or colorless were recorded as a negative and the MIC was the lowest concentration of wells which still

had blue color. All blue color solution wells were taken by a sterile lop to put into the new wells which had 150  $\mu\text{L}$  of nutrient broth and then placed for incubation at 37 °C for 18 to 24 h. Resazurin solution 50  $\mu\text{L}$  was added to each well to give blue color (Scheme 2.34) and the MBC was the lowest concentration of wells that still had blue color after 30 min (Figure 2.22).

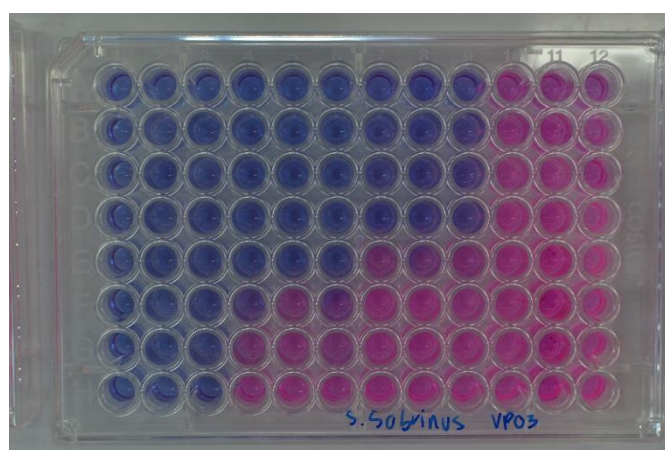
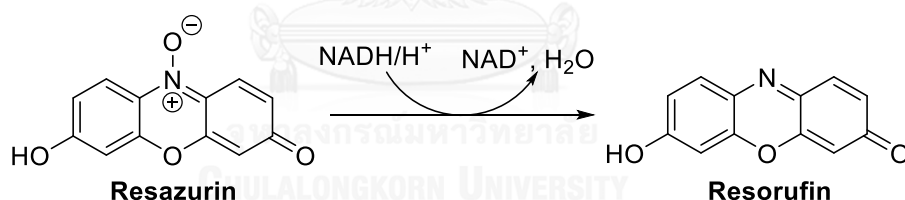


Figure 2.22 Antibacterial activity method (resazurin assay)



Scheme 2.34 Reduction of resazurin (blue) to resorufin (pink)

### 2.14.3 Preliminary Screening Test of Antifungal Assay

Dichloromethane extract, ethyl acetate extract, sandaracopimaradiene-3 $\beta$ ,18-diol (**D1**), sandaracopimaradien-3-one (**D2**), and sandaracopimaric acid (**D4**) were preliminary tested for antifungal activity by agar medium assay *via* adding to PDA at the final concentration of extract at 10 mg/mL and compound at 10 mM [83]. The control plates contained only PDA. A 8 mm diameter disc of pure culture of phytopathogenic fungi: *Alternaria porri*, *Collectotrichum gloeosporioides*, *Fusarium oxysporum* and *Phytophthora parasitica* was aseptically transferred to the center of

the petri plate. The plates were incubated at rt. Radial measurements of growth were taken when fungi reached the edge of the control plates, colony diameter was measured in centimeter and converted for percent inhibition.

$$\% \text{ Inhibition} = [(C - T) \times 100]/C$$

C = colony diameter of control plate (cm)

T = Colony diameter of treatment (cm)

## 2.15 Cytotoxicity (MTS assay)

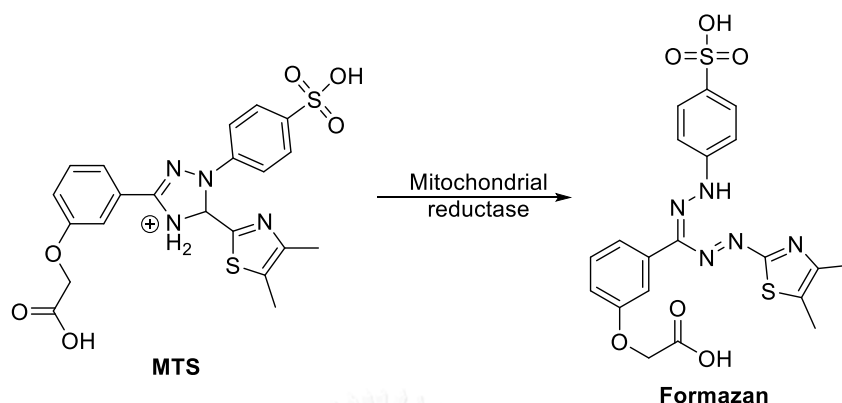
### 2.15.1 Cell Culture

Cultivation of the cell line HepG2 has previously been described [84, 85]. Briefly, HepG2 cells were maintained in T-flasks and incubated at 37 °C in a 98% humid atmosphere of 5% CO<sub>2</sub>/95% air (standard conditions). The culture medium consisted of DMEM supplemented by 10% FCS, gentamicin (50 μg/mL), and *p*-hydroxybenzoic acid n-butyl ester (0.2 μg/mL). Cells of passage number 5 and 21 were used. HepG2 cells were detached from the flasks by trypsin-EDTA treatment.

### 2.15.2 Preliminary Screening Test of Cytotoxicity by MTS Assay

The MTS assay was initiated as follows: HepG2 cells originating from a maintenance culture at the logarithmic phase of growth were seeded in a 96-well culture plate using  $2 \times 10^4$  cells/well (n = 4) in 100 μL culture medium. In the same plate, wells without cells (n = 4) were supplied with 100 μL culture medium. The solution of tested compounds 50 μL were added into wells with several dilution concentrations. The plate was incubated for 24 h under standard conditions. After incubation, the culture medium was removed by inverting the plate and gently tapping on the bottom of the plate. Subsequently, optimization of the MTS assay (Scheme 2.35) or a cellular sensitivity test was carried out. Generally, after addition of 50 μL MTS reagent (240 μg/mL) to each well, the plate was protected against light and further incubated under standard conditions. The stated concentrations of the MTS reagents

are final concentrations. The OD values were recorded at the absorbance maximum of 490 nm using a micro plate reader [84, 85].



Scheme 2.35 Reduction of MTS to formazan

### III. Results and Discussion

#### 2.16 Extraction and Isolation of Diterpenoids from the Heartwoods of *X. xylocarpa*

The heartwoods of *X. xylocarpa* were extracted with  $\text{CH}_2\text{Cl}_2$  for 5 days (3 times) and then the residue was reextracted with EtOAc to obtain the  $\text{CH}_2\text{Cl}_2$  and EtOAc extracts in 4.47 and 3.80%, respectively. The  $\text{CH}_2\text{Cl}_2$  extract (112.0 g) was purified by column chromatography (gradient  $\text{SiO}_2$ , 0  $\rightarrow$  100% EtOAc/hexane) to give four known *ent*-pimarane diterpenoids: sandaracopimaradiene-3 $\beta$ ,18-diol (**D1**) (0.393 g, 0.35% yield), sandaracopimaradien-3-one (**D2**) (5.290 g, 4.72% yield), sandaracopimaradien-3 $\beta$ -ol (**D3**) (3.640 g, 3.25% yield) and sandaracopimaric acid (**D4**) (0.210 g, 0.19%) (Figure 2.23). The structures of all diterpenoids were elucidated by  $^1\text{H}$  and  $^{13}\text{C}$  NMR, X-ray diffraction analysis or high resolution mass spectrometry.

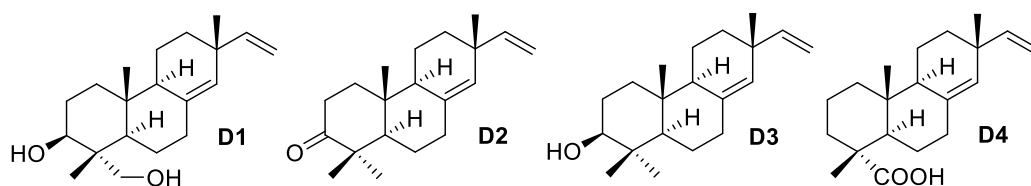
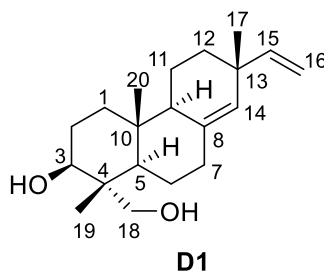


Figure 2.23 The structures of four *ent*-pimarane diterpenoids **D1-D4**



Sandaracopimaradiene-3 $\beta$ ,18-diol (**D1**) as colorless crystal and its molecular ion of  $[M-Li]^+$  311.2563 was in good agreement with the molecular formula  $C_{20}H_{32}O_2$  (MW = 304.4740). The  $^1H$  NMR spectrum of **D1** (Figure A1) showed a doublet of doublets signal of vinyl proton (H-15) at  $\delta_H$  5.78 ( $J = 17.4, 10.6$  Hz) and a singlet signal of vinyl proton (H-14) at  $\delta_H$  5.24. Two signals of vinyl protons (H-16) were detected at  $\delta_H$  4.93 ( $J = 17.6$  Hz) as a doublet and  $\delta_H$  4.92 ( $J = 10.6, 1.2$  Hz) as a doublet of doublets. The doublet signal of proton (H-3) was found at  $\delta_H$  3.73 ( $J = 10.3$  Hz) and two signals of methylene protons (H-18) were observed at  $\delta_H$  3.66 as a doublet of doublets ( $J = 11.1, 4.7$  Hz) and  $\delta_H$  3.44 as a doublet ( $J = 10.3$  Hz). Two signals of methylene protons (H-7) were observed at  $\delta_H$  2.26 ( $J = 14.2, 3.3$  Hz) as doublet of triplets and  $\delta_H$  2.04 as multiplet. Three methyl groups displayed singlet signals at  $\delta_H$  1.05 (H-19), 0.95 (H-20) and 0.86 (H-17). Five methylene signals (H-1, 2, 6, 11 and 12) and two CH (H-5 and 9) signals were observed in ranged  $\delta_H$  1.77-1.17.

The  $^{13}C$  NMR spectrum (Figure A2) displayed resonances for all twenty carbons belonging to sandaracopimaradiene-3 $\beta$ ,18-diol (**D1**). Four olefinic carbons were observed at  $\delta_C$  148.9 (C-15), 136.2 (C-8), 129.0 (C-14) and 110.1 (C-16) and two oxygenated carbons were found at  $\delta_C$  77.2 (C-3) and 72.3 (C-18). Three methyl carbons were found at  $\delta_C$  25.9 (C-17), 15.5 (C-20) and 11.4 (C-19). Moreover, six methylene carbons were detected at  $\delta_C$  36.9 (C-1), 27.2 (C-2), 34.4 (C-7), 22.4 (C-6), 35.5 (C-12) and 18.7 (C-11). Two tertiary carbons at  $\delta_C$  50.3 (C-9), 48.6 (C-5) and three quaternary carbons at  $\delta_C$ , 42.1 (C-13), 37.9 (C-10) and 37.4 (C-4) were observed. All aforementioned data were well matched with the skeleton of *ent*-pimarane type of diterpenoids [11].

The sandaracopimaradiene-3 $\beta$ ,18-diol (**D1**) was assigned *via* single-crystal X-ray diffraction analysis using Cu K $\alpha$  radiation (Table A1) and the perspective ORTEP plot is presented in Figure 2.24. The absolute configuration established by X-ray giving 3*S*, 4*R*, 5*R*, 9*S*, 10*R*, 13*R*.

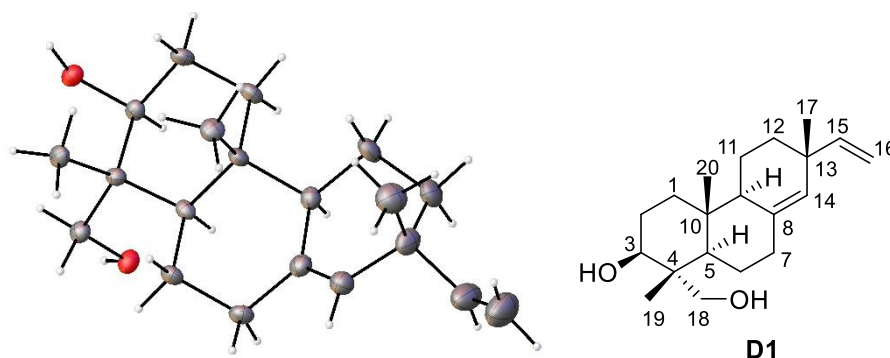
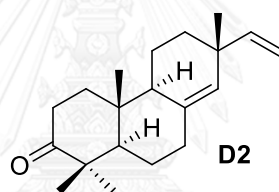


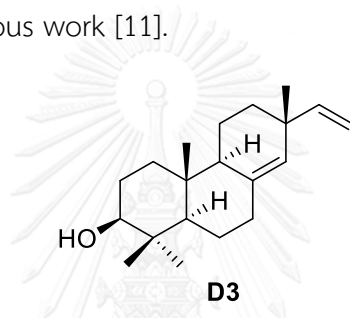
**Figure 2.24** The perspective ORTEP plot of sandaracopimaradiene-3 $\beta$ ,18-diol (**D1**)



Sandaracopimaradiene-3-one (**D2**) as colorless crystal and its molecular ion of  $[M-Li]^+$  293.2466 was agreement with the molecular formula  $C_{20}H_{30}O$  (MW = 286.4590). The  $^1H$  NMR spectrum of **D2** (Figure A3) displayed a doublet of doublets signal of vinyl proton (H-15) at  $\delta_H$  5.78 ( $J = 17.5, 10.6$  Hz) and a singlet signal of vinyl proton (H-14) at  $\delta_H$  5.30. Two signals of vinyl protons (H-16) were observed at  $\delta_H$  4.94 ( $J = 17.4, 1.7$  Hz) as a doublet of doublets and  $\delta_H$  4.91 ( $J = 10.5, 1.7$  Hz) as a doublet of doublets. Two signals of methylene proton (H-2) were observed at  $\delta_H$  2.67 ( $J = 14.5, 5.8$  Hz) as triplet of doublets and  $\delta_H$  2.33 ( $J = 15.0, 3.4$  Hz) as doublet of doublets. Four methyl groups showed singlet signals at  $\delta_H$  1.11 (H-18), 1.08 (H-18 and H-17) and 0.86 (H-19). Five methylene signals (H-1, 6, 7, 12 and 11) and two CH signals (H-5 and H-9) were observed in range of  $\delta_H$  2.15-1.40.



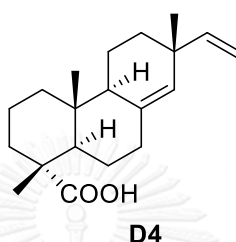
The  $^{13}\text{C}$  NMR spectrum of **D2** (Figure A4) displayed twenty carbon signals. The carbonyl carbon at  $\delta_{\text{C}}$  217.1 and four olefinic carbons were observed at  $\delta_{\text{C}}$  148.6 (C-15), 135.8 (C-8), 129.6 (C-14) and 110.4 (C-16). Four methyl carbons were detected at  $\delta_{\text{C}}$  26.1 (C-17), 25.8 (C-19), 22.3 (C-18) and 14.7 (C-20). Six methylene carbons were observed at  $\delta_{\text{C}}$  37.7 (C-4), 35.6 (C-7), 34.8 (C-2) 34.3 (C-12), 23.2 (C-6) and 18.9 (C-11). Two tertiary carbons were visualized at  $\delta_{\text{C}}$  55.3 (C-5) and 49.5 (C-9), and three quaternary carbons were found at  $\delta_{\text{C}}$  47.8 (C-4), 38.0 (C-10) and 37.5 (C-13). As above data, the structure of sandaracopimaradien-3-one (**D2**) could be deduced based on the comparison with previous work [11].



Sandaracopimaradien-3 $\beta$ -ol (**D3**) was colorless crystal. The  $^1\text{H}$  NMR spectrum (Figure A5) showed a doublet of doublets signal of vinyl proton (H-15) at  $\delta_{\text{H}}$  5.79 ( $J = 17.5, 10.1$  Hz) and a singlet signal of vinyl proton (H-14) at  $\delta_{\text{H}}$  5.23. Two signals of vinyl protons (H-16) were observed at  $\delta_{\text{H}}$  4.92 ( $J = 11.3, 1.5$  Hz) as a doublet of doublets and  $\delta_{\text{H}}$  4.87 ( $J = 4.4, 1.5$  Hz) as a doublet of doublets. The doublet of triplets signal of proton (H-3) was found at  $\delta_{\text{H}}$  3.27 ( $J = 13.8, 5.5$  Hz). Two signals of methylene protons (H-7) were observed at  $\delta_{\text{H}}$  2.27 ( $J = 14.2, 3.3$  Hz) as doublet of doublet of doublets and  $\delta_{\text{H}}$  2.10 as multiplet. Four methylene groups showed singlet signals at  $\delta_{\text{H}}$  1.04 (H-17), 0.99 (H-19), 0.81 (H-18) and 0.80 (H-20). Five methyl signals (H-1, 2, 6, 11 and 12) and two CH signals (H-5 and 9) were observed in range of  $\delta_{\text{H}}$  1.75-1.18.

The  $^{13}\text{C}$  NMR spectrum (Figure A6) showed resonances for all twenty carbons belonging to sandaracopimaradien-3 $\beta$ -ol (**D3**). Four olefinic carbons were detected at  $\delta_{\text{C}}$  148.9 (C-15), 136.6 (C-8), 128.8 (C-14) and 110.1 (C-16) and one oxygenated carbon

at  $\delta_c$  79.21 (C-3). Four methyl carbons were observed at  $\delta_c$  26.0 (C-17), 15.0 (C-20), 28.5 (C-19) and 15.7 (C-18). Moreover, six methylene carbons were detected at  $\delta_c$  37.2 (C-1), 27.6 (C-2), 35.8 (C-7), 22.2 (C-6), 34.5 (C-12) and 18.7 (C-11). Two tertiary carbons at  $\delta_c$  50.3 (C-9) and 54.1 (C-5) and three quaternary carbons at  $\delta_c$ , 37.4 (C-13), 38.1 (C-10) and 39.0 (C-4) were also observed. All aforementioned data were well matched with the skeleton of *ent*-pimarane type of diterpenoids to previous work [11].



Sandaracopimaric acid (**D4**) was obtained as white solid. Its  $^1\text{H}$  NMR spectrum (Figure A7) showed a doublet of doublets signal of vinyl proton (H-15) at  $\delta_H$  5.77 ( $J = 17.4, 10.6$  Hz) and a singlet signal of vinyl proton (H-14) at  $\delta_H$  5.22. Two signals of vinyl proton (H-16) could be visualized at  $\delta_H$  4.91 ( $J = 12.7, 1.4$  Hz) as a doublet of doublets and  $\delta_H$  4.88 ( $J = 5.8, 1.4$  Hz) as a doublet of doublets. Two signals of methylene protons (H-7) were observed at  $\delta_H$  2.22 ( $J = 14.2, 2.8$  Hz) as doublet of doublets and  $\delta_H$  2.12 ( $J = 13.5, 5.2$  Hz) as triplet of doublets. Three methyl groups displayed singlet signals at  $\delta_H$  1.20 (H-19), 1.03 (H-17) and 0.83 (H-20). Five methylene signals (H-1, 2, 6, 11 and 12) and two CH signals (H-5 and H-9) were observed in range of  $\delta_H$  1.92-1.22.

The  $^{13}\text{C}$  NMR spectrum (Figure A8) displayed resonances for all twenty carbons belonging to sandaracopimaric acid (**D4**). The carboxyl group was observed at  $\delta_c$  185.3 and four olefinic carbons were observed at  $\delta_c$  148.9 (C-15), 136.6 (C-8), 129.1 (C-14) and 110.1 (C-16). Three methyl carbons were found at  $\delta_c$  26.0 (C-17), 15.2 (C-20) and 16.8 (C-19). Furthermore, six methylene carbons were presented at  $\delta_c$  38.3 (C-1), 18.1 (C-2), 35.5 (C-7), 24.9 (C-6), 34.4 (C-12) and 18.76 (C-11). Two tertiary carbons at  $\delta_c$  50.6

(C-9) and 48.8 (C-5) and three quaternary carbons at  $\delta_c$ , 37.4 (C-13), 37.7 (C-10) and 47.3 (C-4) were also observed. All data were well matched with the skeleton of *ent*-pimarane type of diterpenoids to previous work [11].

## 2.17 Conversion of Non-Covalent Inhibitors to Covalent through Introduction of Beta-Lactones

Four natural products including andrenosterone, cholic acid, andrographolide and sandaracopimaradiene-3 $\beta$ ,18-diol (**D1**) (Figure 2.25) were selected as a lead structure to synthesize their beta-lactone derivatives. These compounds were converted to 1,5- or 1,6-keto acid or 1,2-hydroxy acid using general reaction in a few steps, and then followed by NCAL process or lactonization to form beta-lactone.

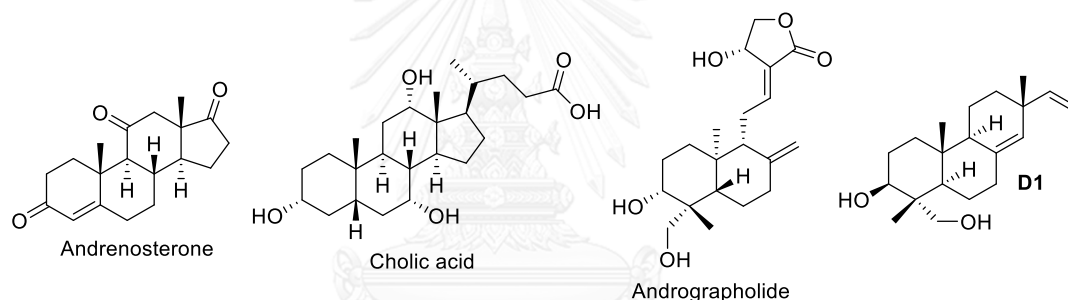
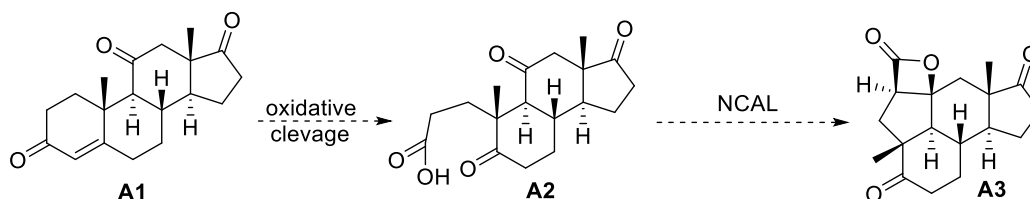


**Figure 2.25** The structures of andrenosterone, cholic acid, andrographolide and compound **D1**

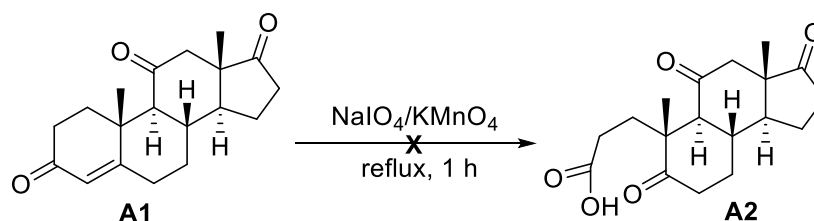
### 2.17.1 Andrenosterone

The beta-lactone derivative **A3** could be synthesized from andrenosterone (**A1**) by oxidative cleavage to provide 1,5-keto acid derivative **A2** and followed by NCAL process to give the desired product (Scheme 2.36).



**Scheme 2.36** Proposed conversion of andrenosterone (**A1**) to beta-lactone derivative **A3**

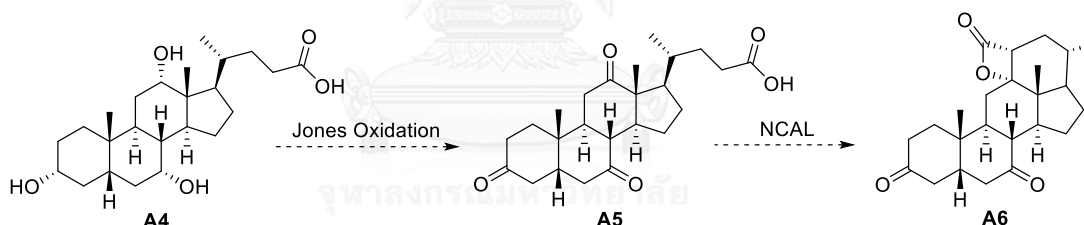
Andrenosterone was reacted with  $\text{NaIO}_4$  and  $\text{KMnO}_4$  under reflux condition for 1 h to prepare 1,5-keto acid derivative **A2** (Scheme 2.37), unfortunately this reaction did not provide a desired product **A2** because of the decomposition of product under this condition [70, 71]



**Scheme 2.37** The synthesis of 1,5-keto acid derivative **A2**

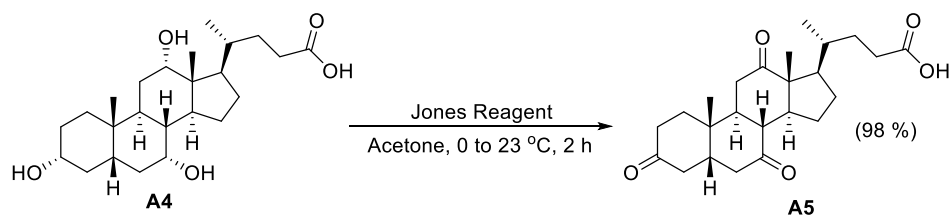
### 2.17.2 Cholic acid

Cholic acid (**A4**) could be converted to beta-lactone derivative **A6** using Jones oxidation to synthesize triketocholanic (**A5**) and then using NCAL process for beta lactone synthesis to provide the desired product (Scheme 2.38).



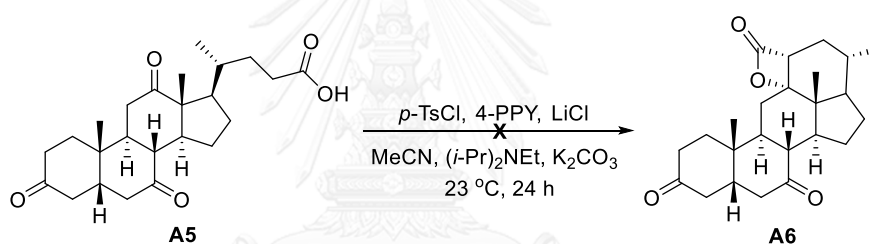
**Scheme 2.38** Proposed conversion of cholic acid (**A4**) to beta-lactone derivative **A6**

Jones oxidation of cholic acid (**A4**) with chromic acid in acetone at 0 to 22 °C for 2 h provided triketocholanic (**A5**) as white solid in 98% yield (Scheme 2.39). The HRMS found the molecular ion at 401.2274  $[\text{Mw-H}]^-$  ( $\text{C}_{24}\text{H}_{34}\text{O}_5$ ; MW = 402.5310). The  $^1\text{H}$  NMR spectrum of the desired product (**A5**) was not observed three oxygenated protons ( $\text{CHOH}$ ) of **A4** at  $\delta_{\text{H}}$  3.97, 3.81 and 3.39 (Figure A9) and its  $^{13}\text{C}$  NMR spectrum found the signals of three carbonyl groups at  $\delta_{\text{C}}$  213.8, 211.1 and 210.2 (Figure A10)



**Scheme 2.39** The forward synthesis of triketocholanic (**A5**)

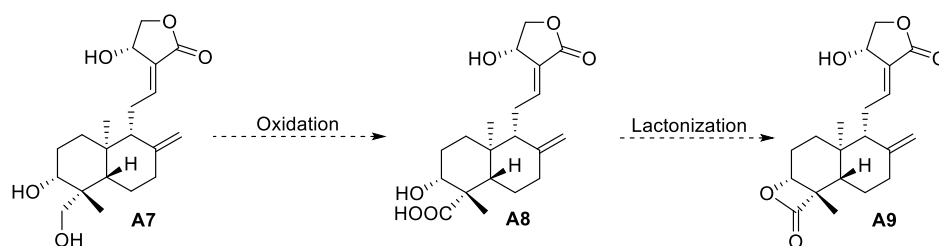
Triketocholanic (**A5**) was then reacted with *p*-TsCl, DMAP, (*i*-Pr)<sub>2</sub>NEt, LiCl and K<sub>2</sub>CO<sub>3</sub> in MeCN at 22 °C for 24 h to prepare beta-lactone derivative **A6** (Scheme 2.40). However, the crude reaction showed no sign of beta-lactone signal at ~1800 cm<sup>-1</sup> by FT-IR. Only starting material was found on TLC. The main reason of this reaction was not occurred because the desired product (**A6**) had a high ring strain and steric of cyclic structure in molecule to form the beta-lactone ring.



**Scheme 2.40** The NCAL process of triketocholanic (**A5**)

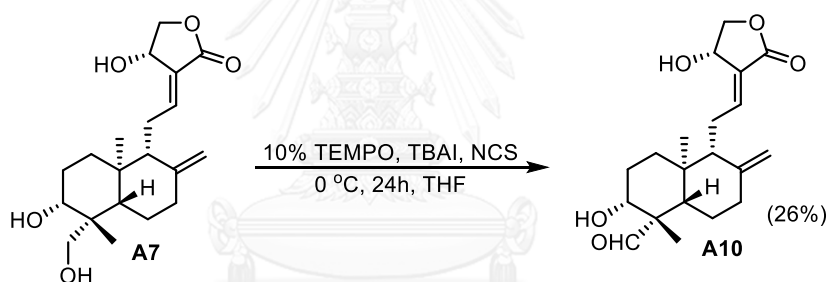
### 2.17.3 Andrographolide

Andrographolide (**A7**) was planned to convert to beta-lactone derivative **A9** by selective oxidation at primary alcohol to give 1,2-hydroxy acid derivative **A8** and then followed by lactonization to form the desired product beta-lactone **A9** (Scheme 2.41).



**Scheme 2.41** Proposed conversion of andrographolide (**A7**) to beta-lactone derivative **A9**

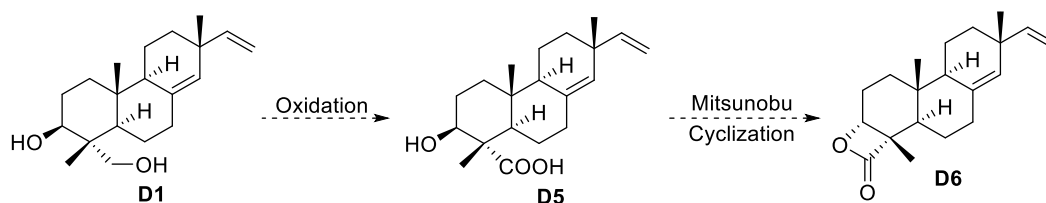
According to the reaction proceeded, the primary hydroxyl group of andrographolide (**A7**) was oxidized by TEMPO oxidation using 10% TEMPO, TBAI and NCS in THF at 0 °C for 24 h to yield 19-dehydroandrographolide (**A10**), not **A8** as expected. Compound **A10** was obtained as white solid in 26% yield with the recovered andrographolide (44.0 mg) (Scheme 2.42). The  $^1\text{H}$  NMR spectrum of **A10** showed the singlet signal of aldehyde functional group at  $\delta_{\text{H}}$  9.77 (Figure A11) and its molecular ion of  $[\text{M-Li}]^+$  355.1995 was in good agreement with the molecular formula  $\text{C}_{20}\text{H}_{28}\text{O}_5$  (MW = 348.4390) [75]. Since the lack of substrate **A7**, the reaction was not carried on. However, for further study 19-dehydroandrographolide (**A10**) should be oxidized to 1,2-hydroxy acid derivative **A8** and using lactonization to synthesize beta-lactone desired product **A9**.



**Scheme 2.42** The TEMPO oxidation of andrographolide (**A7**) to give 19-dehydroandrographolide (**A10**)

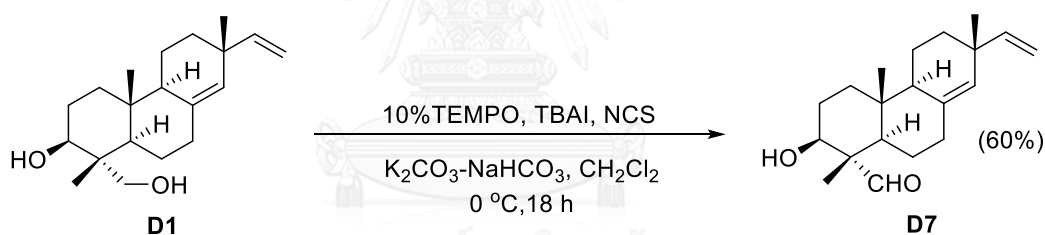
#### 2.17.4 Sandaracopimaradiene-3 $\beta$ , 18-diol

In the first route, the primary alcohol at C-18 of sandaracopimaradiene-3 $\beta$ ,18-diol (**D1**) was oxidized to carboxyl group to give 3 $\beta$ -hydroxysandaracopimaric acid (**D5**) and then followed by Mitsunobu cyclization for lactonization to prepare beta-lactone derivative **D6** (Scheme 2.43).



**Scheme 2.43** The first route to synthesize beta-lactone derivative **D6**

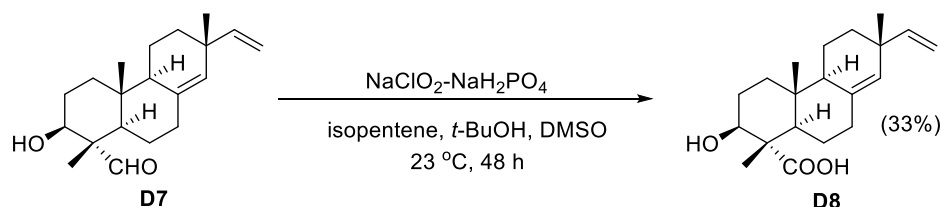
Sandaracopimaradiene-3 $\beta$ ,18-diol (**D1**) was subjected to TEMPO oxidation using 10% TEMPO, TBAI, and NCS, in CH<sub>2</sub>Cl<sub>2</sub> with K<sub>2</sub>CO<sub>3</sub>-NaHCO<sub>3</sub> buffer at 0 °C for 18 h to give sandaracopimaradiene-3 $\beta$ ,18-olal (**D7**) in 60% yield as colorless crystal (Scheme 2.44). The <sup>1</sup>H NMR spectrum (Figure A12) showed the formyl group at C-18 as a singlet signal at  $\delta_{\text{H}}$  9.43. Nonetheless, two signals of methylene protons (H-18) at  $\delta_{\text{H}}$  3.66 and 3.44 were not observed. The <sup>13</sup>C NMR spectrum (Figure A13) displayed the formyl carbon at  $\delta_{\text{C}}$  206.9 without the signal belonging to the oxygenated carbon at  $\delta_{\text{C}}$  72.3 (C-18). The oxygenated proton (H-3) and carbon (C-3) signals were instead observed at  $\delta_{\text{H}}$  3.82 as a doublet of doublets ( $J = 11.5, 4.2$  Hz) and  $\delta_{\text{C}}$  72.1, respectively. The *ent*-pimarane skeleton was observed from <sup>1</sup>H and <sup>13</sup>C NMR spectra (Figures A12 and A13) [86].



**Scheme 2.44** The TEMPO oxidation of **D1** to prepare sandaracopimaradiene-3 $\beta$ ,18-olal (**D7**)

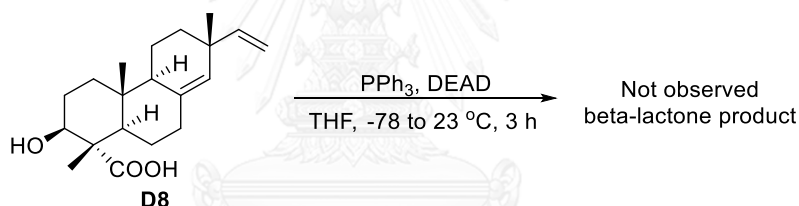
3 $\beta$ -Hydroxysandaracopimaric acid (**D8**) was synthesized from sandaracopimaradiene-3 $\beta$ ,18-olal (**D7**) by selective oxidation at formyl group using NaClO<sub>2</sub>-NaH<sub>2</sub>PO<sub>4</sub>, isopentene, *t*-BuOH in DMSO at 23 °C for 48 h to obtain the desired product as white solid in 33% yield (Scheme 2.45). Its molecular ion of [M-H]<sup>-</sup> 317.2098 was in good agreement with the molecular formula C<sub>20</sub>H<sub>30</sub>O<sub>3</sub> (MW = 318.4570). The <sup>13</sup>C NMR spectrum (Figure A15) exhibited the carboxyl carbon at  $\delta_{\text{C}}$  179.9 and the oxygenated proton (H-3) and carbon (C-3) signals were observed at  $\delta_{\text{H}}$  4.04 as a doublet

of doublets ( $J = 11.9, 4.1$  Hz) and  $\delta_C$  74.9, respectively. The *ent*-pimarane skeleton was observed from  $^1\text{H}$  and  $^{13}\text{C}$  NMR spectra (Figures A14 and A15) [76, 77].



**Scheme 2.45** The synthesis of  $3\beta$ -hydroxysandaracopimaric acid (**D8**) from **D7**

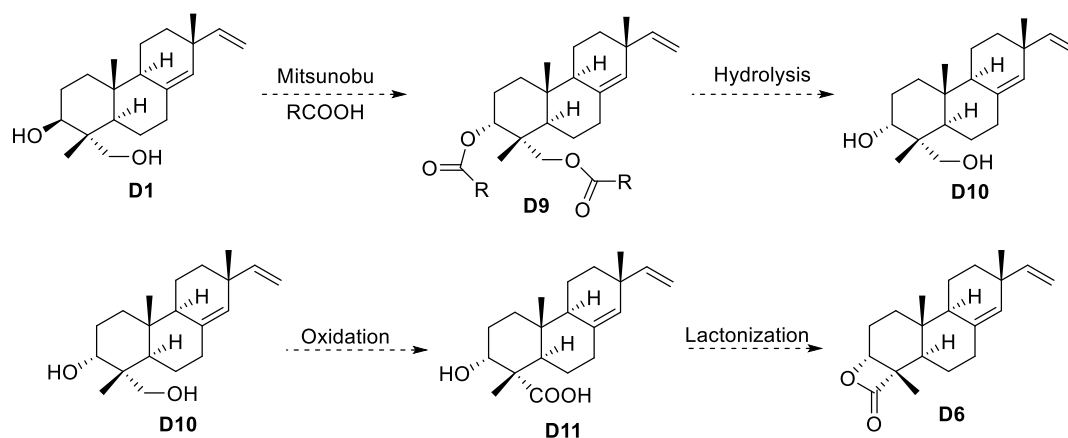
$3\beta$ -Hydroxysandaracopimaric acid (**D8**) was reacted with  $\text{PPh}_3$  (13.0 mg, 0.0471 mmol), DEAD (40% in toluene, 0.2 mL, 0.471 mmol) in THF (0.5 mL) at  $-78$   $^\circ\text{C}$  for 25 min and warmed up to  $23$   $^\circ\text{C}$  for 2.5 h to prepare beta-lactone derivative **D6** via Mitsunobu cyclization (Scheme 2.46). However, the IR spectrum of the crude reaction did not show the signal of beta-lactone at  $\sim 1800$   $\text{cm}^{-1}$ .



**Scheme 2.46** Mitsunobu cyclization of  $3\beta$ -hydroxysandaracopimaric acid (**D8**)

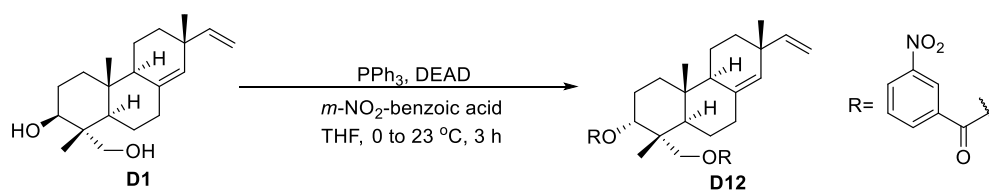
The route of synthesis was changed to the second route (Scheme 2.47) that the stereochemistry of the hydroxyl group at C-3 of sandaracopimaradiene- $3\beta,18$ -diol (**D1**) was converted from  $\beta$ - to  $\alpha$ -configuration via Mitsunobu reaction by reacting with carboxylic acid to give ester derivative **D9**, and then followed by hydrolysis to give sandaracopimaradiene- $3\alpha,18$ -diol (**D10**). In the lactonization step, this compound was oxidized to  $3\alpha$ -hydroxysandaracopimaric acid (**D11**) and was synthesized to beta-lactone derivative **D6**.





**Scheme 2.47** The proposed synthesis of beta-lactone derivative **D6**

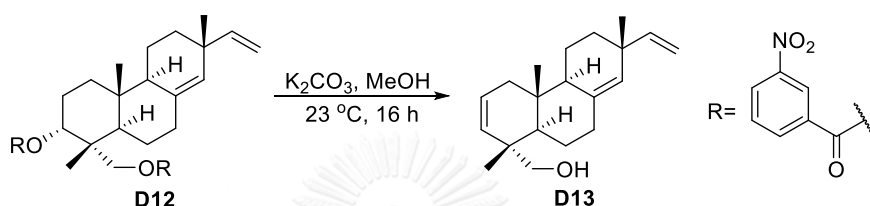
Thus, sandaracopimaradiene-3β,18-diol (**D1**) was reacted with PPh<sub>3</sub>, DEAD and *m*-nitrobenzoic acid in THF (1 mL) at 0 to 23 °C for 16 h (Scheme 2.48) to provide the desired product **D12** (19.4 mg). The <sup>1</sup>H NMR spectrum (Figure A16) displayed the signals of *m*-nitrobenzoyl moiety at δ<sub>H</sub> 8.99 as singlet, 8.50 as multiplet, and 7.75 as triplet. The vinyl proton signal (H-15) was observed at δ<sub>H</sub> 5.77 as doublet of doublets (*J* = 16.6, 10.4 Hz) and two vinyl proton signals (H-16) were found at δ<sub>H</sub> 4.94 as multiplet. The vinyl proton (H-14) was detected at δ<sub>H</sub> 5.31 and three methyl proton signals were found at δ<sub>H</sub> 1.14 (H-19), 1.07 (H-20) and 0.92 (H-17).



**Scheme 2.48** Mitsunobu reaction of sandaracopimaradiene-3β,18-diol (**D1**)

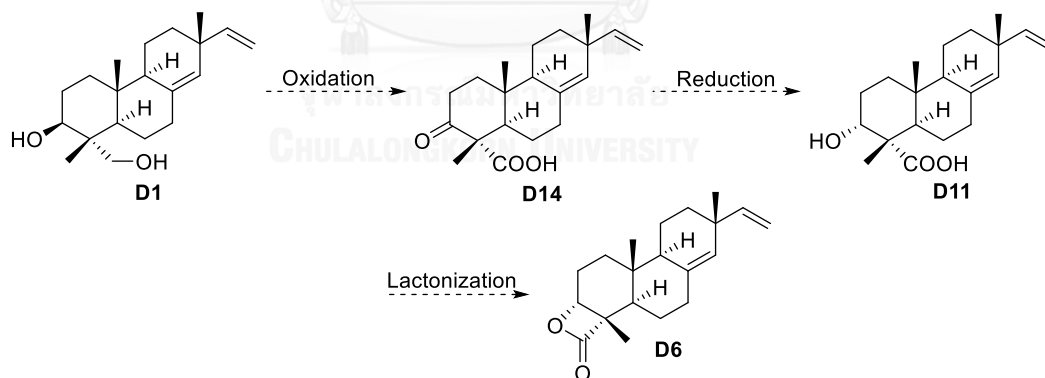
The ester derivative **D12** was subjected to hydrolysis with K<sub>2</sub>CO<sub>3</sub> in MeOH at 23 °C for 16 h (Scheme 2.49). However, this reaction provided undesired derivative product **D13** by elimination of hydroxyl group at C-3. The <sup>1</sup>H NMR spectrum (Figure A17) revealed two olefinic proton signals (H-3) at δ<sub>H</sub> 5.91 as doublet of doublet of doublets (*J* = 10.0, 6.5, 1.9 Hz) and 5.30 (H-2) as doublet of doublets (*J* = 10.1, 2.9

Hz). The methylene proton signals (H-18) were found at  $\delta_{\text{H}}$  3.36 as doublet ( $J = 10.5$  Hz) and 3.12 as doublet ( $J = 10.6$  Hz). The vinyl proton signal (H-14) was observed at  $\delta_{\text{H}}$  5.25 as singlet and two signals of vinyl proton (H-16) were detected at  $\delta_{\text{H}}$  4.93 ( $J = 5.2, 1.6$  Hz) as a doublet of doublets and  $\delta_{\text{H}}$  4.90 as doublet of doublets ( $J = 10.6, 1.2$  Hz). The vinyl proton (H-15) displayed  $\delta_{\text{H}}$  5.78 as a doublet of doublets ( $J = 17.8, 10.2$  Hz). Three methyl groups were found at  $\delta_{\text{H}}$  1.06 (H-19), 0.86 (H-17) and 0.85 (H-20).



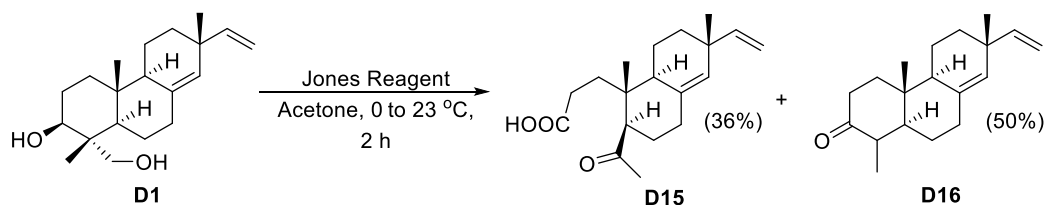
**Scheme 2.49** Hydrolysis of mixture **D12** to **D13**

In the third route, sandaracopimaradiene-3 $\beta$ ,18-diol (**D1**) was oxidized to keto acid derivative **D14** via Jones oxidation and then performed selective reduction by converting the carbonyl to  $\alpha$ -hydroxyl to obtain 3 $\alpha$ -hydroxysandaracopimaric acid (**D11**) which was then synthesized to beta-lactone **D6** by lactonization (Scheme 2.50).



**Scheme 2.50** The third route to synthesize of beta-lactone **D6**

Sandaracopimaradiene-3 $\beta$ ,18-diol (**D1**) was reacted with Jones reagent in acetone at 0 to 23 °C for 2 h. However, this reaction did not provide the desired product. The reaction gave instead two new unexpected products: compound **D15** which lost tricyclic ring system and the keto derivative **D16** having nineteen carbon atoms in 36 and 50% yield, respectively (Scheme 2.51).



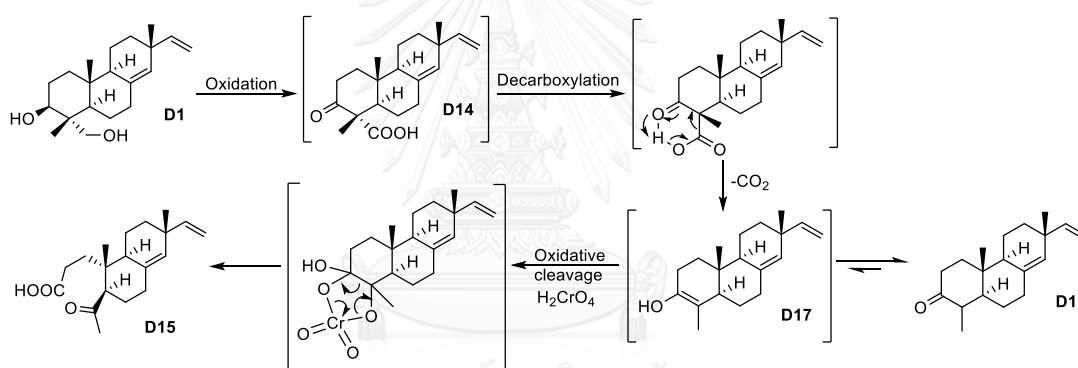
**Scheme 2.51** Jones oxidation of sandaracopimaradiene-3 $\beta$ ,18-diol (**D1**)

Keto acid **D15** as colorless oil and its molecular ion of  $[M-H]^-$  303.1967 was in good agreement with the molecular formula  $C_{19}H_{28}O_3$  (MW = 304.4300). The  $^1H$  NMR spectrum (Figure A18) displayed vinyl proton signal (H-14) at  $\delta_H$  5.32 as singlet and two vinyl proton signals (H-16) at  $\delta_H$  4.93 as singlet and 4.90 as doublet of doublets ( $J = 4.6, 0.6$  Hz). The vinyl proton signal (H-15) was observed at  $\delta_H$  5.77 as doublet of doublets ( $J = 17.9, 10.1$  Hz). The methyl proton signal, connected to the carbonyl group ( $CH_3CO-$ ), was detected at  $\delta_H$  2.19 as singlet. Two methyl proton signals were observed at  $\delta_H$  1.06 (H-17) and 0.99 (H-19) as singlet. The  $^{13}C$  NMR spectrum (Figure A19) exhibited the carboxyl signal at  $\delta_C$  179.7 and the carbonyl signal at  $\delta_C$  211.7. Four vinyl carbon signals were observed at  $\delta_C$  148.2 (C-15), 134.8 (C-8), 130.5 (C-14) and 110.6 (C-16). The signals assigned for two quaternary carbons were visualized at  $\delta_C$  37.4 (C-13) and 42.0 (C-10). Nonetheless, no signal for C-4 was detected. The methyl carbon signal, connected to carbonyl group ( $CH_3CO-$ ) at  $\delta_C$  56.4 and two methyl carbon signals at  $\delta_C$  26.1 (C-17) and 17.3 (C-20) were observed.

Keto derivative **D16** as colorless oil and its molecular ion of  $[M-Li]^+$  279.2292 was in good agreement with the molecular formula  $C_{19}H_{28}O$  (MW = 272.4320). The  $^1H$  NMR spectrum (Figure A20) exhibited the vinyl proton signal (H-14) at  $\delta_H$  5.28 as singlet and two vinyl proton signals (H-16) at  $\delta_H$  4.91 as doublet of doublets ( $J = 9.8, 1.5$  Hz) and 4.86 as doublet of doublets ( $J = 3.0, 1.5$  Hz). The vinyl proton signal (H-15) was observed at  $\delta_H$  5.75 as doublet of doublets ( $J = 17.4, 10.6$  Hz). The methyl proton signal (H-19) was detected at  $\delta_H$  0.98 as doublet ( $J = 6.5$  Hz) and two methyl proton signals were observed at  $\delta_H$  1.08 (H-17) and 0.97 (H-19) as singlet. The  $^{13}C$  NMR

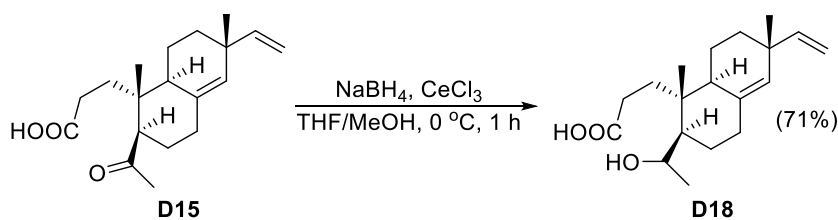
spectrum (Figure A21) showed the carbonyl signal at  $\delta_c$  213.2. Four vinyl carbon signals were observed at  $\delta_c$  148.6 (C-15), 135.6 (C-8), 129.6 (C-14) and 110.4 (C-16). Three quaternary carbons revealed the signals at  $\delta_c$  38.8 (C-13), 37.9 (C-10) and 37.5 (C-4), whereas three methyl carbons were detected at  $\delta_c$  25.9 (C-17), 13.8 (C-20) and 11.6 (C-18).

The proposed mechanism (Scheme 2.52) for the formation of compounds **D15** and **D16** started with the oxidation of compound **D1** into keto acid derivative **D14** and followed by decarboxylation to form enol intermediate **D17** which either gave compound **D15** by oxidative cleavage or compound **D16** by tautomerization.



**Scheme 2.52** Proposed mechanism for the formation of compounds **D15** and **D16** from **D1**

In addition, hydroxy acid derivative **D18** was synthesized from keto acid derivative **D15** by reduction of carbonyl group with  $NaBH_4/CeCl_3$  in THF/MeOH at  $0\text{ }^\circ\text{C}$  for 1 h in 71% yield (Scheme 2.53).

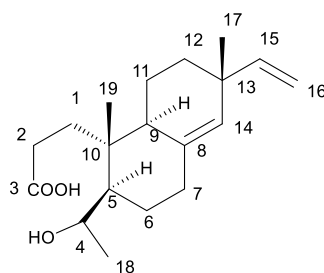


**Scheme 2.53** Reduction of keto acid derivative **D15** to hydroxy acid derivative **D18**

Hydroxy acid derivative **D18** as colorless oil with diastereomeric ratios (dr) = 14:1 was determined by  $^1\text{H}$  NMR at  $\delta_{\text{H}} = 4.19: 4.13$  and its molecular ion of  $[\text{M}-\text{H}]^-$  305.2105 were in good agreement with the molecular formula  $\text{C}_{19}\text{H}_{30}\text{O}_3$  (MW = 306.4460). The  $^1\text{H}$  NMR spectrum (Figure A22) exhibited vinyl proton signal (H-14) at  $\delta_{\text{H}}$  5.29 as singlet and two vinyl proton signals (H-16) at  $\delta_{\text{H}}$  4.93 as doublet of doublets ( $J = 17.5, 1.5$  Hz) and 4.88 as singlet. The vinyl proton signal (H-15) was observed at  $\delta_{\text{H}}$  5.80 as doublet of doublets ( $J = 17.5, 10.6$  Hz). The methyl proton signal ( $\text{CH}_3\text{CHOH}$ , H-18) was found at  $\delta_{\text{H}}$  1.20 as doublet ( $J = 6.4$  Hz), while two methyl proton signals were observed at  $\delta_{\text{H}}$  1.06 (H-17) and 0.97 (H-19) as singlet. The oxygenated proton signal (H-4) was detected at  $\delta_{\text{H}}$  4.18 as quartet ( $J = 6.4$  Hz).

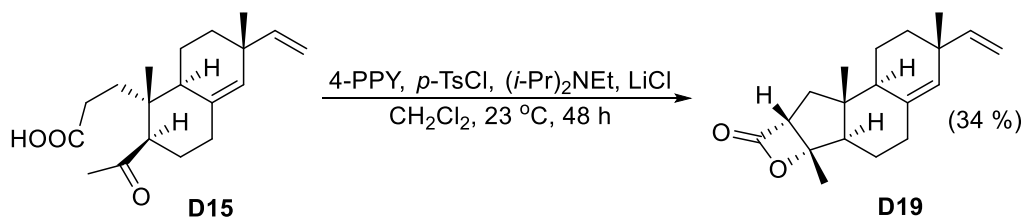
The  $^{13}\text{C}$  NMR spectrum (Figure A23) displayed the carboxyl signal at  $\delta_{\text{C}}$  179.7 and oxygenated carbon signal (C-4) at  $\delta_{\text{C}}$  65.7. Four vinyl carbon signals were observed at  $\delta_{\text{C}}$  148.6 (C-15), 136.2 (C-8), 129.4 (C-14) and 110.4 (C-16), whereas two quaternary carbons revealed the signals at  $\delta_{\text{C}}$  37.3 (C-13) and 40.2 (C-10). Three methyl carbon signals were observed at  $\delta_{\text{C}}$  26.1 (C-17), 24.1 (C-18) and 17.3 (C-19). The assignment of other carbons and protons of hydroxy acid derivative **D18** is displayed in Table 2.2. The 2D correlation was confirmed by COSY, HSQC and HMBC (Figures A24-A26).

**Table 2.2**  $^1\text{H}$  and  $^{13}\text{C}$  NMR chemical shift assignment and 2D correlation of hydroxy acid derivative **D18**



Position	DEPT	Chemical shift (ppm)		HMBC
		<sup>13</sup> C	HSQC	
1	CH <sub>2</sub>	30.7	1.85 (m)	C1, C5, C9, C10, C19
2	CH <sub>2</sub>	20.1	1.58 (m)	C9, C10, C12, C13
3	COOH	179.7		
4	CHOH	65.7	4.18 (q, <i>J</i> = 6.4 Hz, 1H)	C2, C5, C8, C10, C18
5	CH	48.2	1.38 (m)	
6	CH <sub>2</sub>	27.9	2.17 (m)	C5, C7
7	CH <sub>2</sub>	35.2	2.30 (dt, <i>J</i> = 8.2, 3.4 Hz), 2.00 (m)	C5, C6, C8, C14
8	C	136.2		
9	CH	42.0	1.95 (m)	C8, C10, C11, C14, C19
10	C	40.2		
11	CH <sub>2</sub>	18.9	1.65 (m)	C9, C12
12	CH <sub>2</sub>	34.3	1.62 (m), 1.38 (m)	C2, C11, C14, C15, C17
13	C	37.3		
14	CH	129.4	5.29 (s)	C7, C9, C12, C13, C15
15	CH	148.6	5.80 (dd, <i>J</i> = 17.5, 10.6 Hz)	C12, C13, C14, C17
16	CH <sub>2</sub>	110.4	4.93 (dd, <i>J</i> = 17.5, 1.5 Hz, 1H), 4.88 (s, 1H)	C13, C15
17	CH <sub>3</sub>	26.1	1.06 (s)	C12, C13, C14, C15
18	CH <sub>3</sub>	24.1	1.20 (d, <i>J</i> = 6.4 Hz)	C4, C5, C10, C19
19	CH <sub>3</sub>	17.9	0.97 (s)	C1, C5, C6, C9, C10

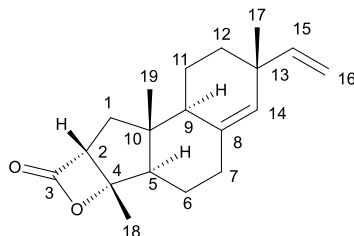
Compound **D15** with 1,5-keto acid functional group, could be converted to bicyclic beta-lactone *via* NCAL process. Thus keto acid derivative **D15** was reacted with *p*-TsCl, 4-PPY, (*i*-Pr)<sub>2</sub>NEt and LiCl under N<sub>2</sub> atmosphere in CH<sub>2</sub>Cl<sub>2</sub> at 23 °C for 48 h to give beta-lactone derivative **D19** in 34% yield as colorless oil (Scheme 2.54).



**Scheme 2.54** The synthesis of beta-lactone derivative **D19** *via* NCAL process

The mass spectrometric analysis of beta-lactone derivative **D19** presented molecular ion of [M-Li]<sup>+</sup> 293.2095 which was in good agreement with the molecular formula C<sub>19</sub>H<sub>26</sub>O<sub>2</sub> (MW = 286.4150). The IR spectrum displayed beta-lactone signal at 1,816 cm<sup>-1</sup>. The <sup>1</sup>H NMR spectrum (Figure A27) exhibited the vinyl proton signal (H-14) at δ<sub>H</sub> 5.31 as singlet and two vinyl proton signals (H-16) at δ<sub>H</sub> 4.93 as a quartet (*J* = 1.4 Hz) and 4.90 as a doublet of doublets (*J* = 9.3, 1.4 Hz). The vinyl proton signal (H-15) was observed at δ<sub>H</sub> 5.75 as doublet of doublets (*J* = 17.2, 10.8 Hz). The methyl group proton signal (H-18) was found at δ<sub>H</sub> 1.59 as a singlet. Two methyl proton signals were observed at δ<sub>H</sub> 1.05 (H-17) and 0.74 (H-19) as a singlet. The assignment of other carbons and protons of beta-lactone derivative **D19** is displayed in Table 2.3. The 2D correlation was confirmed by COSY, HSQC and HMBC (Figures A30, A32-A33). From 2D-NOSEY of this compound **D19** (Figure A31), the proton H-2 displayed the correlation between proton H-18 and H-17. Moreover, the proton H-17 showed the correlation with proton H-19, H-18 and H-2. From this result, the absolute structure was confirmed.

**Table 2.3**  $^1\text{H}$  and  $^{13}\text{C}$  NMR chemical shift assignment and 2D correlation of beta-lactone derivative **D19**

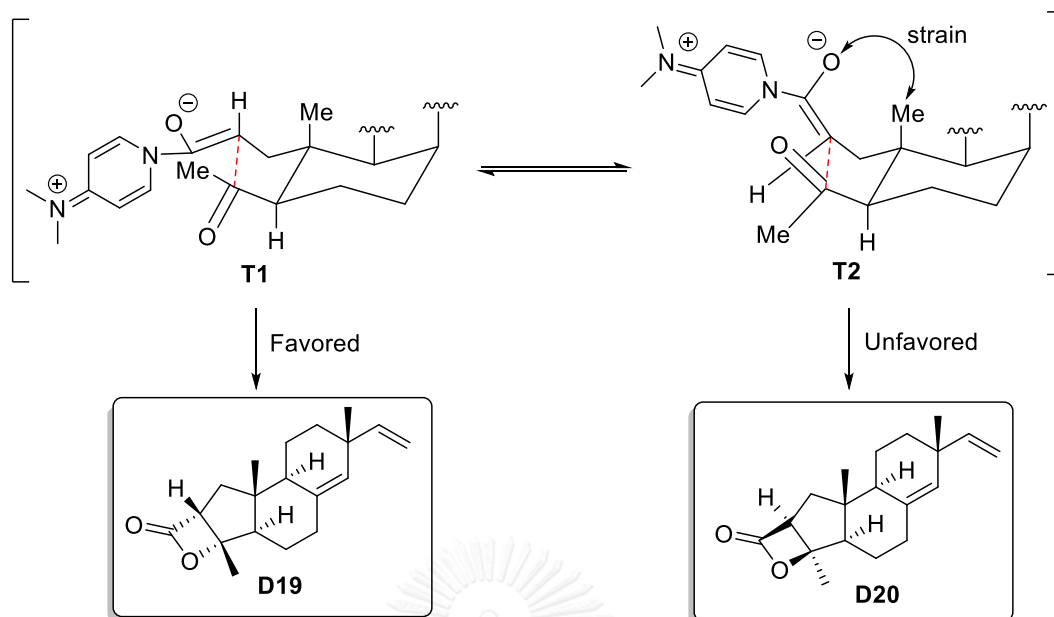


Position	DEPT	Chemical shift (ppm)		HMBC	2D-NOSEY
		$^{13}\text{C}$	HSQC		
1	CH <sub>2</sub>	37.3	1.96 (dd, $J = 12.8, 9.9$ Hz), 1.81 (dd, $J = 12.8, 7.4$ Hz)	C2, C4, C5	
2	CH	58.7	3.60 (dd, $J = 9.9, 7.4$ Hz)	C1	H17, H18, H19
3	COO	172.2			
4	C	87.5			
5	CH	56.5	2.15 (m)	C4, C6, C8	
6	CH <sub>2</sub>	21.8	1.78 (m)	C9, C10, C11	
7	CH <sub>2</sub>	34.6	2.30 (ddd, $J = 14.5, 4.6, 1.8$ Hz), 2.11 (m)	C9, C5, C8, C14	H14
8	C	134.9			
9	CH	47.8	2.06 (m)	C8, C10, C11, C19	
10	C	52.1			
11	CH <sub>2</sub>	20.2	1.68-1.61 (m)	C9, C12, C14, C19	
12	CH <sub>2</sub>	33.9	1.58-1.49 (m)	C8, C9, C11, C13	



13	C	37.8			
14	CH	130.6	5.31 (s)	C7, C9, C13	H7, H17
15	CH	147.9	5.75 (dd, $J = 17.2, 10.8$ Hz)	C16	H17
16	CH <sub>2</sub>	110.8	4.93 (q, $J = 1.4$ Hz), 4.90 (dd, $J = 9.3, 1.4$ Hz)	C13, C15, C17	H17
17	CH <sub>3</sub>	26.5	1.05 (s)	C12, C13, C14, C15	H2, H7, H14, H15, H16, H18, H19
18	CH <sub>3</sub>	20.4	1.59 (s)	C2, C4, C5,	H2, H17, H19
19	CH <sub>3</sub>	15.2	0.74 (s)	C1, C5, C9, C10	H2, H17, H18

The high diastereoselectivity was observed from the proposed transition-state arrangements for the NCAL process. Following the formation of the acylammonium species could exist in two possible transition-state arrangements **T1** and **T2** (Scheme 2.55). The higher energy arrangement **T2** was a further unfavorable transition-state in this conformation because of steric interactions in transition-state. The arrangement **T1** led to the conformation being the lower energy pathway and the formation of the desired product **D19** [54].



**Scheme 2.55** The formation of the acylammonium transition state for high diastereoselectivity

### 2.18 Derivatization of Sandaracopimaradiene-3 $\beta$ ,18-diol (**D1**) by Simultaneous-Arming

In previous researches, methods for simultaneous arming and SAR studies of natural products were reported by Romo group including Rh(II)-catalyzed for O-H insertions of alcohol-containing natural products, cyclopropanations of alkene-containing natural products, C-H amination of allylic and benzylic-containing natural products and In(OTf)<sub>3</sub>-catalyzed for iodination of arene-containing natural products. These natural product-based cellular probes can rapidly be synthesized *via* “Click Chemistry” including biotin, fluorophore, and photoaffinity natural product conjugates for the study of biological processes and the discovery of protein targets for therapeutic intervention.

Compound **D1** contained an electron-rich olefins at C15-C16 that could be connected to alkynyl diazo acetates **L3** *via* cyclopropanation. Thus, the O-H insertion of primary alcohol at C-18 could react with compound **L3**. Moreover, allylic proton at C-7 could be reacted with alkynyl sulfamate **L5** by C-H amination (Figure 2.26).

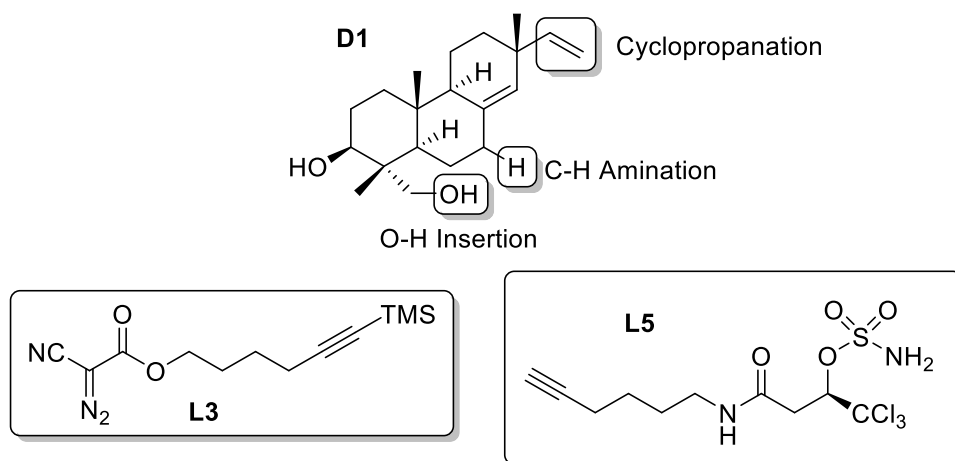
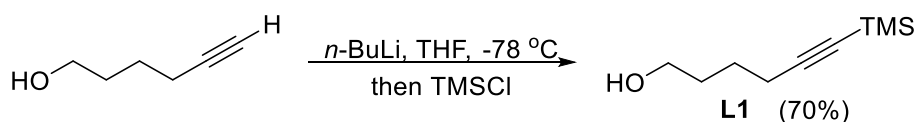


**Figure 2.26** Selectivity of cyclopropanation, C-H amination and O-H insertion in compound **D1**

### 2.18.1 Synthesis of Alkynyl Diazo Acetate **L3**

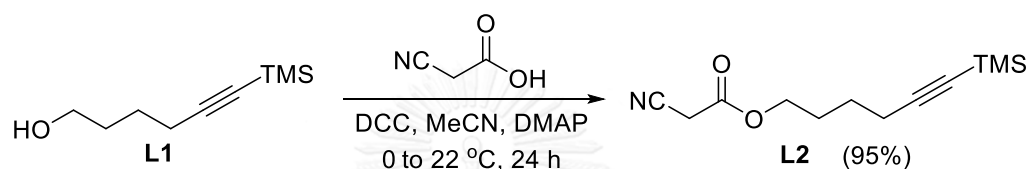
Alkynyl diazo acetate **L3** could be synthesized from commercially available substrate with the procedure described previously [68]. 5-Hex-yn-1-ol was reacted with TMSCl and *n*-BuLi in THF at  $-78\text{ }^{\circ}\text{C}$  to rt to give 6-(trimethylsilyl)-hex-5-yn-1-ol (**L1**) in 70% yield (Scheme 2.56). The  $^1\text{H}$  NMR spectrum (Figure A34) of this desired product **L1** showed TMS proton signal at  $\delta_{\text{H}}$  0.14 as singlet and four methylene proton signals were observed at  $\delta_{\text{H}}$  3.67 (t,  $J = 6.2$  Hz, 2H), 2.26 (t,  $J = 7.1$  Hz, 2H) and 1.63 (m, 4H). The  $^{13}\text{C}$  NMR spectrum (Figure A35) displayed the alkyne carbon signals at  $\delta_{\text{C}}$  107.1 and 84.7. TMS carbon signal was found at  $\delta_{\text{C}}$  0.12 and four methylene carbon signals were displayed at  $\delta_{\text{C}}$  62.3, 31.7, 24.8 and 19.6.



**Scheme 2.56** The synthesis of 6-(trimethylsilyl)-hex-5-yn-1-ol (**L1**)

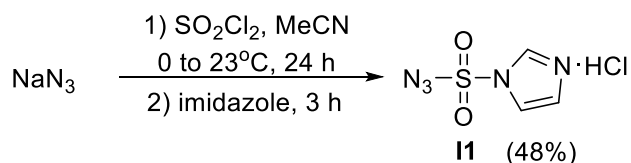
6-(Trimethylsilyl)-hex-5-yn-1-yl 2-cyanoacetate (**L2**) was prepared *via* DCC coupling with cyanoacetic acid in MeCN and 10% DMAP at 0 to  $22\text{ }^{\circ}\text{C}$  for 24 h to obtain the desired product in 95% yield as pale yellow oil (Scheme 2.57). The  $^1\text{H}$  NMR spectrum (Figure A36) exhibited the TMS proton signal at  $\delta_{\text{H}}$  0.14 as singlet and four

methylene proton signals at  $\delta_{\text{H}}$  4.24 (t,  $J = 6.5$  Hz, 2H), 2.28 (t,  $J = 6.9$  Hz, 2H), 1.81 (m, 2H) and 1.60 (m, 2H). The methylene proton signal which connected to cyano group was detected at  $\delta_{\text{H}}$  3.46 (s, 2H). The  $^{13}\text{C}$  NMR spectrum (Figure A37) displayed the alkyne carbon signals at  $\delta_{\text{C}}$  106.3 and 85.2. TMS carbon signal was found at  $\delta_{\text{C}}$  0.05 and five methylene carbon signals were displayed at  $\delta_{\text{C}}$  66.4, 27.3, 24.7, 24.6 and 19.3. The carbonyl ester signal was detected at  $\delta_{\text{C}}$  162.9, while cyano group was found at  $\delta_{\text{C}}$  113.1 [68].



**Scheme 2.57** The synthesis of 6-(trimethylsilyl)-hex-5-yn-1-yl 2-cyanoacetate (**L2**)

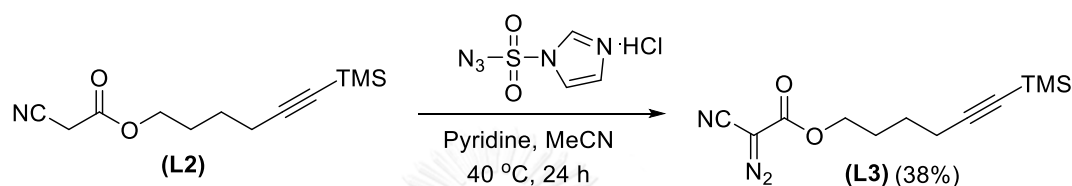
Imidazole-1-sulfonyl azide hydrochloride (**I1**) was synthesized (Scheme 2.58) as an azide reagent for the synthesis of 6-(trimethylsilyl)-hex-5-yn-1-yl 2-cyano-2-diazoacetate (**L3**). Compound **I1** could be prepared from sodium azide *via* reacted with sulfonyl chloride in MeCN at 0 to 23 °C for 24 h. Imidazole was added and further stirred for 3 h to provide the desired product in 48% yield as white crystal needle. The  $^1\text{H}$  NMR spectrum (Figure A38) displayed three proton signals of imidazole ring at  $\delta_{\text{H}}$  9.22 as a broad singlet, 7.89 as a doublet of doublets ( $J = 2.1, 1.6$  Hz) and 7.47 as a doublet of doublets ( $J = 2.1, 1.2$  Hz). The  $^{13}\text{C}$  NMR spectrum (Figure A39) revealed three carbon signals of imidazole ring at  $\delta_{\text{C}}$  137.7, 123.8 and 119.9 [80].



**Scheme 2.58** The synthesis of imidazole-1-sulfonyl azide hydrochloride (**I1**)

6-(Trimethylsilyl)-hex-5-yn-1-yl 2-cyanoacetate (**L2**) was reacted with imidazole-1-sulfonyl azide hydrochloride (**I1**) and pyridine in MeCN at 40 °C for 24 h to receive 6-(trimethylsilyl)hex-5-yn-1-yl 2-cyano-2-diazoacetate (**L3**) in 38% yield as pale

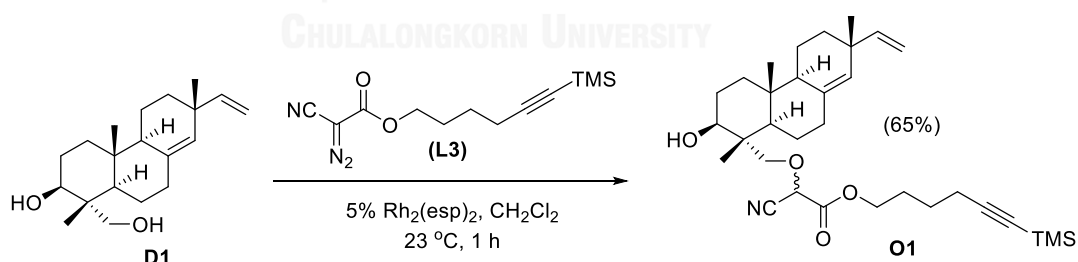
yellow oil (Scheme 2.59). The  $^1\text{H}$  NMR spectrum (Figure A40) of compound **L3** exhibited TMS proton signal at  $\delta_{\text{H}}$  0.15 as singlet and four methylene proton signals at  $\delta_{\text{H}}$  4.31 (t,  $J = 6.5$  Hz), 2.28 (t,  $J = 6.9$  Hz), 1.82 (m) and 1.59 (m). The  $^{13}\text{C}$  NMR spectrum (Figure A41) displayed the alkyne carbon signals at  $\delta_{\text{C}}$  107.7 and 85.3. TMS carbon signal was detected at  $\delta_{\text{C}}$  0.07 and four methylene carbon signals were displayed at  $\delta_{\text{C}}$  66.8, 27.6, 24.7 and 19.3. The diazo carbon signal was found at  $\delta_{\text{C}}$  106.2 [68].



**Scheme 2.59** The synthesis of 6-(trimethylsilyl)-hex-5-yn-1-yl 2-cyano-2-diazoacetate (**L3**)

### 2.18.2 O-H Insertion of Sandaracopimaradiene-3 $\beta$ ,18-diol (**D1**)

Sandaracopimaradiene-3 $\beta$ ,18-diol (**D1**) could undergo O-H insertion with alkynyl diazoacetate **L3** in combination with  $\text{Rh}_2(\text{esp})_2$  as a catalyst in  $\text{CH}_2\text{Cl}_2$  at 23 °C for 1 h with high chemoselectivity at primary alcohol (C-18) to give the mixture of diastereomeric products **O1** in 65% yield (Scheme 2.60).



**Scheme 2.60** O-H insertion of sandaracopimaradiene-3 $\beta$ ,18-diol (**D1**)

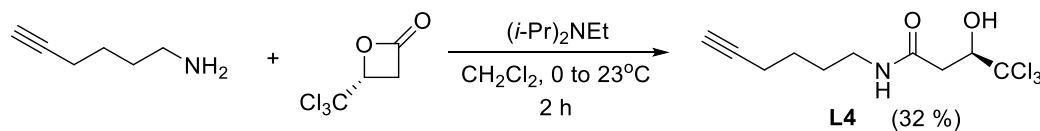
The separation of diastereomers **O1** was carried on by preparative TLC giving two mixtures of diastereomer with dr = 1:4, mixtures of diastereomers **1** (2.4 mg) and **2** (8.0 mg). The  $^1\text{H}$  NMR spectrum of the mixture of diastereomers **1** (Figure A42) exhibited the olefinic proton (H-15) signal at  $\delta_{\text{H}}$  5.80 as doublet of doublets ( $J = 17.4$ , 10.1 Hz) and the olefinic proton (H-14) signal at  $\delta_{\text{H}}$  5.27 as singlet. The olefinic proton

(H-16) was detected at  $\delta_{\text{H}}$  5.05 – 4.81 as multiplet. The TMS group signal was visualized at  $\delta_{\text{H}}$  0.18 as singlet. The  $^1\text{H}$  NMR spectrum of the mixture of diastereomers **2** (Figure A43) showed the olefinic proton (H-15) signal at  $\delta_{\text{H}}$  5.79 as doublet of doublets ( $J = 17.4, 10.6$  Hz) and the olefinic proton (H-14) signal at  $\delta_{\text{H}}$  5.27 as singlet. The olefinic proton (H-16) was found at  $\delta_{\text{H}}$  5.04 – 4.73 as multiplet. The TMS group signal was detected at  $\delta_{\text{H}}$  0.18 as doublet ( $J = 0.5$  Hz).

### 2.18.3 Synthesis of (*R*)-1,1,1-Trichloro-4-(hex-5-yn-1-ylamino)-4-oxobutan-2-yl sulfamate

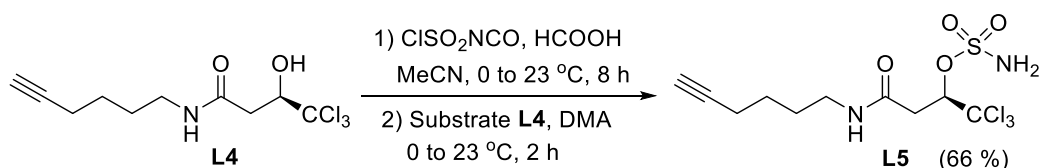
(*R*)-1,1,1-Trichloro-4-(hex-5-yn-1-ylamino)-4-oxobutan-2-yl sulfamate (**L5**) was prepared for C-H amination of sandaracopimaradiene-3 $\beta$ ,18-diol (**D1**) at allylic proton (H-7). (*R*)-(-)-3-Hydroxy-4,4,4-trichlorobutyric  $\beta$ -lactone was reacted with hex-5-yn-1-amine, which was synthesized according to the procedure described in the previous research [67], an (*i*-Pr) $_2$ NEt in  $\text{CH}_2\text{Cl}_2$  at 0 to 23 °C for 2 h to afford (*R*)-4,4,4-trichloro-*N*-(hex-5-yn-1-yl)-3-hydroxybutanamide (**L4**) in 32% yield (Scheme 2.61). The  $^1\text{H}$  NMR spectrum of compound **L4** (Figure A44) displayed NH proton at  $\delta_{\text{H}}$  6.01 as a broad singlet and hydroxyl proton at  $\delta_{\text{H}}$  5.02 as singlet. The terminal alkyne proton signal was found at  $\delta_{\text{H}}$  1.98 as a triplet ( $J = 2.6$  Hz). Two methylene protons revealed the signals at  $\delta_{\text{H}}$  1.65-1.56 as multiplet and methylene proton ( $\text{CH}_2\text{-NH}$ ) signal was found at  $\delta_{\text{H}}$  3.32 (dd,  $J = 12.9, 6.9$  Hz). Other methylene proton signals ( $\text{CH-CH}_2\text{-CO}$ ) were detected at  $\delta_{\text{H}}$  2.94 as doublet of doublets ( $J = 14.9, 2.4$  Hz) and 2.59 as doublet of doublets ( $J = 15.0, 9.3$  Hz). The CH proton signal ( $\text{OH-CH-CCl}_3$ ) was detected at  $\delta_{\text{H}}$  4.59 as a doublet ( $J = 9.2$  Hz). The methylene proton ( $\text{CH}_2\text{-C}\equiv\text{CH}$ ) signal was detected at  $\delta_{\text{H}}$  2.24 (td,  $J = 6.8, 2.6$  Hz). The  $^{13}\text{C}$  NMR spectrum of compound **L4** (Figure A45) exhibited the carbonyl of amide signal at  $\delta_{\text{C}}$  170.0 and two carbon signals of alkyne at  $\delta_{\text{C}}$  102.4 and 83.9. The carbon signal of  $\text{CCl}_3$  could be assigned at  $\delta_{\text{C}}$  79.7 and tertiary

carbon ( $\text{C}\text{C}\text{Cl}_3$ ) signal was found at  $\delta_{\text{C}}$  68.9. Five methylene carbon signals were observed at  $\delta_{\text{C}}$  39.2, 37.9, 28.4, 25.6 and 18.1 [67].



**Scheme 2.61** The preparation of (*R*)-4,4,4-trichloro-*N*-(hex-5-yn-1-yl)-3-hydroxybutanamide (**L4**)

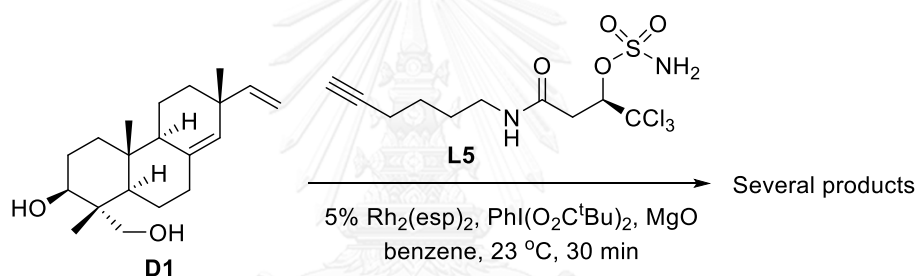
Chlorosulfonyl isocyanate ( $\text{ClSO}_2\text{NCO}$ ) was reacted with formic acid ( $\text{HCOOH}$ ) in MeCN at 0 to 23 °C for 8 h and then the solution of (*R*)-4,4,4-trichloro-*N*-(hex-5-yn-1-yl)-3-hydroxybutanamide (**L4**) in DMA was added at 0 to 23 °C for 2 h to give (*R*)-1,1,1-trichloro-4-(hex-5-yn-1-ylamino)-4-oxobutan-2-yl sulfamate (**L5**) in 66% yield (Scheme 2.62). The  $^1\text{H}$  NMR spectrum of compound **L5** (Figure A46) exhibited NH proton at  $\delta_{\text{H}}$  6.07 as a broad singlet. The terminal alkyne proton signal was found at  $\delta_{\text{H}}$  2.00 as a triplet ( $J = 2.4$  Hz). Two methylene protons revealed signals at  $\delta_{\text{H}}$  1.67 and 1.65 as multiplet and methylene proton ( $\text{CH}_2\text{-NH}$ ) signal was detected at  $\delta_{\text{H}}$  3.33 (dd,  $J = 6.2, 2.7$  Hz). Methylene proton signals ( $\text{CH-CH}_2\text{-CO}$ ) were observed at  $\delta_{\text{H}}$  3.19 as doublet of doublets ( $J = 16.5, 1.8$  Hz) and 2.95 as doublet of doublets ( $J = 16.5, 8.7$  Hz). The CH proton signal ( $\text{HO-CH-C}\text{Cl}_3$ ) was found at  $\delta_{\text{H}}$  5.52 as doublet of doublets ( $J = 6.8, 2.0$  Hz). The methylene proton ( $\text{CH}_2\text{-C}\equiv\text{CH}$ ) signal was visualized at  $\delta_{\text{H}}$  2.24 (dt,  $J = 6.8, 2.2$  Hz). The  $^{13}\text{C}$  NMR spectrum of compound **L5** (Figure A47) displayed the carbonyl of amide signal at  $\delta_{\text{C}}$  168.9 and two carbon signals of alkyne at  $\delta_{\text{C}}$  98.4 and 85.8. The carbon signal ( $\text{-C}\text{Cl}_3$ ) was presented at  $\delta_{\text{C}}$  83.9, whereas tertiary carbon ( $\text{-C}\text{C}\text{Cl}_3$ ) signal was detected at  $\delta_{\text{C}}$  69.1. Five methylene carbon signals were observed at  $\delta_{\text{C}}$  39.6, 38.0, 28.3, 25.5 and 18.0 [67].



**Scheme 2.62** The synthesis of (*R*)-1,1,1-trichloro-4-(hex-5-yn-1-ylamino)-4-oxobutan-2-yl sulfamate (**L5**)

#### 2.18.4 C-H Amination of Sandaracopimaradiene-3 $\beta$ ,18-diol (**D1**)

Sandaracopimaradiene-3 $\beta$ ,18-diol (**D1**) was reacted with (*R*)-1,1,1-trichloro-4-(hex-5-yn-1-ylamino)-4-oxobutan-2-yl sulfamate (**L5**) via C-H amination at allylic proton (H-7) in combination with  $\text{Rh}_2(\text{esp})_2$ ,  $\text{MgO}$  and  $\text{PhI}(\text{O}_2\text{C}^t\text{Bu})_2$  in benzene at 23 °C for 30 min (Scheme 2.63).



**Scheme 2.63** C-H Amination of sandaracopimaradiene-3 $\beta$ ,18-diol (**D1**) with compound **L5**

However, there were several products on TLC observed after the reaction was completed. With the aids of LCMS, the molecular ion of 666.2 (ACPI+) (Figure 2.27), the isotope pattern of chlorine atom at  $\text{CCl}_3$  group was detected. This molecular ion was confirmed that not only the reaction gave the desired C-H amination product **P1**, but also it provided undesired aziridinated product **P2**, with the same molecular ion (Figure 2.28). This might be derived from the low chemoselectivity of this reaction.



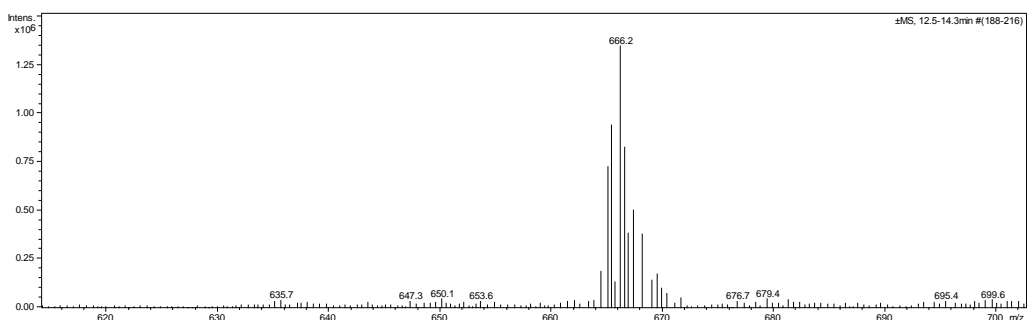


Figure 2.27 Mass spectrum of C-H amination reaction by LCMS

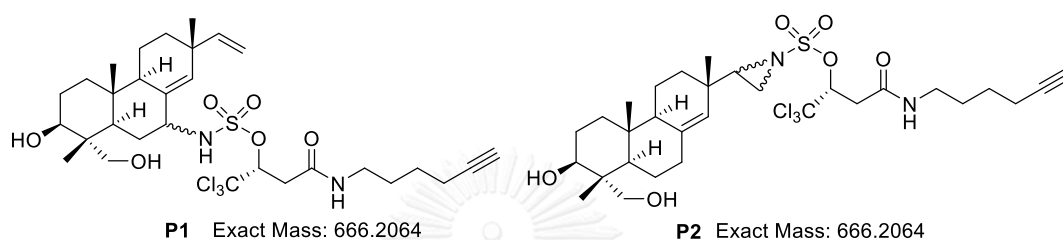
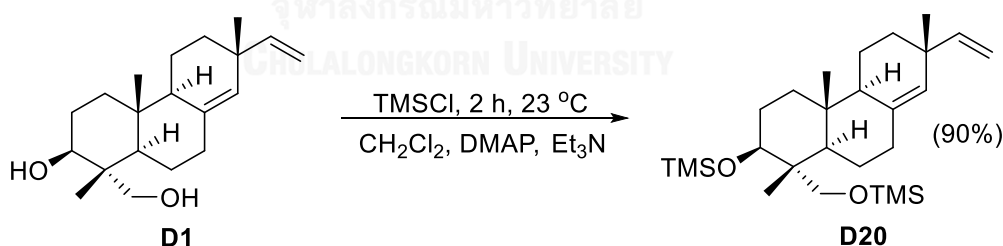


Figure 2.28 The exact mass of C-H amination product **P1** and aziridinated product **P2**

### 2.18.5 Cyclopropanation of Sandaracopimaradiene-3 $\beta$ ,18-diol (**D1**)

The hydroxyl groups at C-3 and C-18 of sandaracopimaradiene-3 $\beta$ ,18-diol (**D1**) was protected to prevent the O-H insertion [69] with alkynyl diazo acetate **L3** using TMSCl, DMAP and Et<sub>3</sub>N in CH<sub>2</sub>Cl<sub>2</sub> at 23 °C for 2 h to yield compound **D20** in 90% yield (Scheme 2.64).



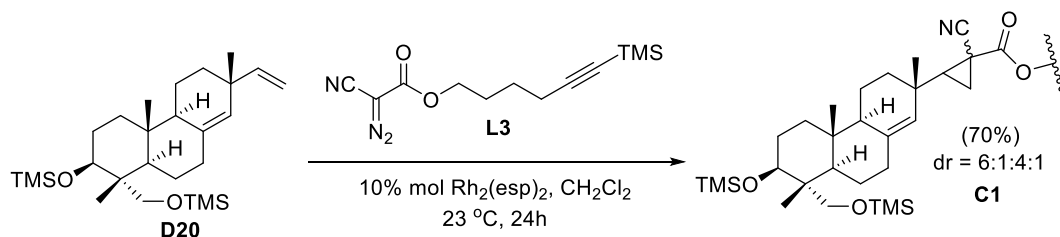
Scheme 2.64 The synthesis of di-OTMS-sandaracopimara-3 $\beta$ ,18-diene (**D20**)

The <sup>1</sup>H NMR spectrum of compound **D20** (Figure A48) displayed a doublet of doublets signal of vinyl proton (H-15) at  $\delta_{\text{H}}$  5.77 ( $J = 17.5, 10.6$  Hz) and a singlet signal of vinyl proton (H-14) at  $\delta_{\text{H}}$  5.22. Two signals of vinyl proton (H-16) was visualized at  $\delta_{\text{H}}$  4.92 ( $J = 12.4, 1.5$  Hz) as a doublet of doublets and  $\delta_{\text{H}}$  4.87 ( $J = 5.6, 1.5$  Hz) as a doublet of doublets. The doublet of doublets signal of proton (H-3) was found at  $\delta_{\text{H}}$  3.73 ( $J = 11.2, 4.8$  Hz), while the signal of methylene proton (H-18) at  $\delta_{\text{H}}$

3.19 as a doublet of doublets ( $J = 17.1, 9.9$  Hz) was observed. Two signals of methylene proton (H-7) were observed at  $\delta_{\text{H}}$  2.24 ( $J = 14.0, 4.3, 2.1$  Hz) as doublet of doublet of doublets and  $\delta_{\text{H}}$  2.03 ( $J = 13.3, 5.7$  Hz) as triplet of doublets. Three methyl groups displayed singlet signals at  $\delta_{\text{H}}$  1.01 (H-19), 0.82 (H-20) and 0.62 (H-17). Five methyl signals (H-1, 2, 6, 12 and 11) and two CH proton signals (H-5 and H-9) were observed in ranged  $\delta_{\text{H}}$  1.78-1.13. Two signals of TMS protons were observed at  $\delta_{\text{H}}$  0.09 and 0.08 as singlet.

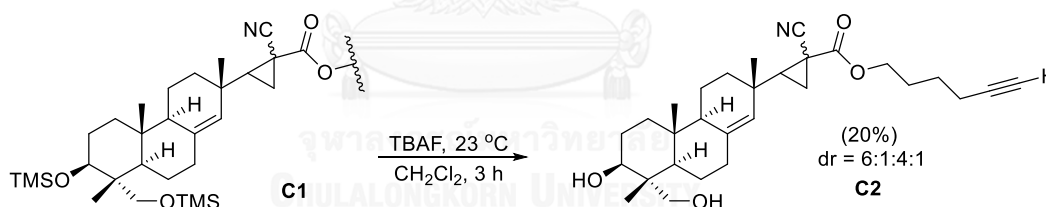
The  $^{13}\text{C}$  NMR spectrum (Figure A49) displayed resonances for all twenty carbons belonging to sandaracopimaradiene-3 $\beta$ ,18-diol (**D1**). Four olefinic carbons were observed at  $\delta_{\text{C}}$  149.0 (C-15), 137.1 (C-8), 128.6 (C-14) and 110.1 (C-16) and two oxygenated carbons were found at  $\delta_{\text{C}}$  71.9 (C-3) and 63.7 (C-18). Three methyl carbons were visualized at  $\delta_{\text{C}}$  26.0 (C-17), 15.6 (C-20) and 12.8 (C-19). Moreover, six methylene carbons were detected at  $\delta_{\text{C}}$  36.9 (C-1), 27.5 (C-2), 34.6 (C-7), 21.8 (C-6), 35.7 (C-12) and 18.8 (C-11). Two tertiary carbons at  $\delta_{\text{C}}$  50.3 (C-9), 44.9 (C-5) and three quaternary carbons at  $\delta_{\text{C}}$  43.1 (C-13), 37.7 (C-10) and 37.4 (C-4) were observed. Two signals of TMS protons were presented at  $\delta_{\text{C}}$  0.41 and -0.50.

This compound **D20** was reacted with alkynyl diazo acetate **L3** in combination with  $\text{Rh}_2(\text{esp})_2$  as a catalyst in  $\text{CH}_2\text{Cl}_2$  at 23 °C for 24 h to provide cyclopropanation derivative **C1** in 70% yield with exclusive chemoselectivity at C15-16 (Scheme 2.65). Four diastereomers with dr = 6:1:4:1 were determined by  $^1\text{H}$  NMR (Figure A50) at proton signals (H-14)  $\delta_{\text{H}} = 5.39 : 5.33 : 5.26 : 4.94$ .



**Scheme 2.65** Cyclopropanation reaction of di-OTMS-sandaracopimara-3 $\beta$ ,  
18-diene (**D20**)

Finally, two TMS groups in compound **C1** were removed using TBAF in  $\text{CH}_2\text{Cl}_2$  at 23 °C for 3 h (Scheme 2.66) to give cyclopropanation desired product **C2** in 20% yield (65% base on recovered starting material **C1**) and four diastereomers with diastereomeric ratio (dr) = 6:1:4:1, were determined by  $^1\text{H}$  NMR (Figure A52) at proton signals (H-14)  $\delta_{\text{H}} = 5.39 : 5.26 : 5.12 : 4.94$ . Its molecular ion of  $[\text{M}+\text{H}]^+$  468.3108 was in good agreement with the molecular formula  $\text{C}_{29}\text{H}_{41}\text{NO}_4$  (MW = 467.6500). The purity of compound **C2** was confirmed by LCMS (ACPI+) with 95% of purity and showed molecular ion of 468.26 (Figure 2.29).



**Scheme 2.66** Desilylation of compound **C1**

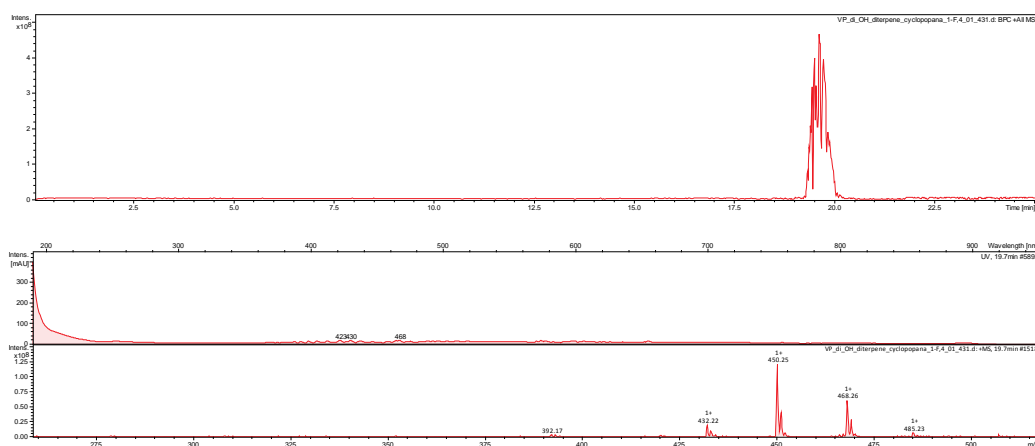


**Figure 2.29** LCMS Data of cyclopropanation derivative **C2** (Purity 95%)

## 2.19 Biological Activity of Diterpenoids and Their Derivatives

### 2.19.1 Antibacterial Activity

The preliminary result (Figure 2.30 and Table 2.4) of eight compounds: sandaracopimaradiene-3 $\beta$ ,18-diol (D1), sandaracopimaradien-3-one (D2), sandaracopimaradien-3 $\beta$ -ol (D3), sandaracopimaradiene-3 $\beta$ ,18-olal (D7), 3 $\beta$ -hydroxysandaracopimaric acid (D8), keto acid derivative D15, hydroxy acid derivative D18 and beta-lactone derivative D19 at 1,000  $\mu$ M by disc diffusion method showed moderate to good activity against five bacteria: *S. aureus*, *P. acnes*, *S. mutans*, *S. sobrinus* (Gram-positive) and *S. typhi* (Gram-negative). Moreover, compound D1, bearing two hydroxyl groups, showed better activity than compounds D2 and D3, which had one carbonyl and one hydroxy group, respectively. From this result, the hydroxy group in diterpenoids might be important for antibacterial activity. Compounds D7, D8 and D19 showed better activity than compound D1. In contrast, Compounds D15 and D18 with the lost tricyclic ring system, gave lower activity than compound D1.

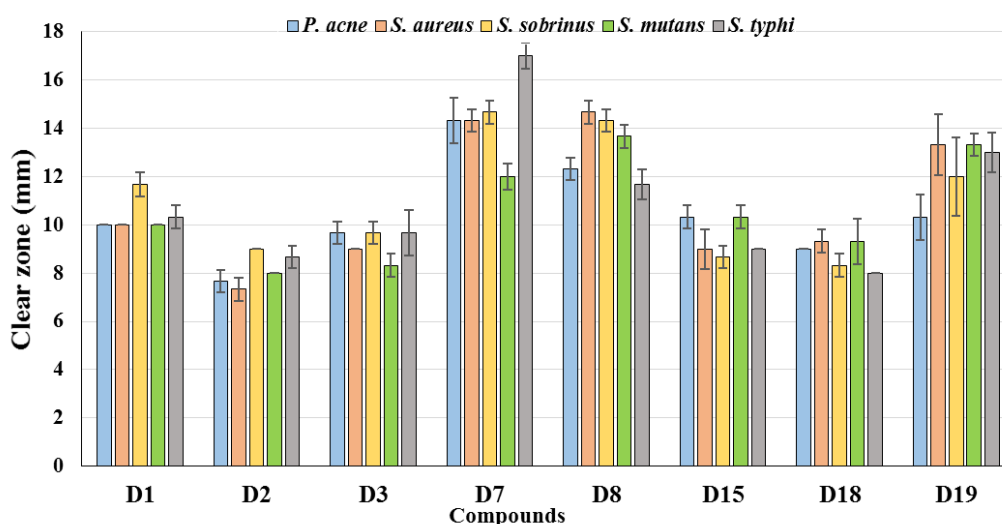
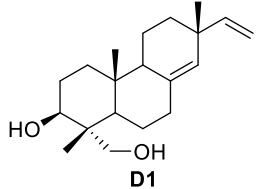
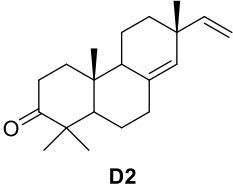
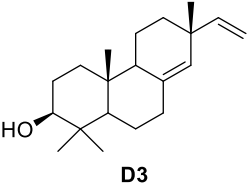
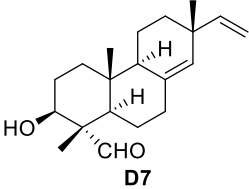
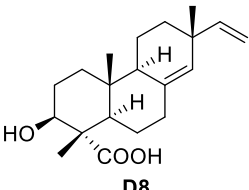
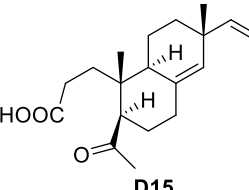
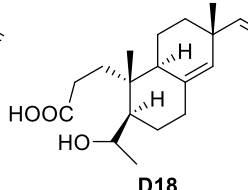
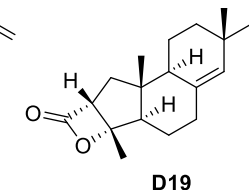


Figure 2.30 Preliminary antibacterial activity of compounds D1-D3, D7, D8, D15, D18 and D19 at 1.0 mM by disc diffusion method

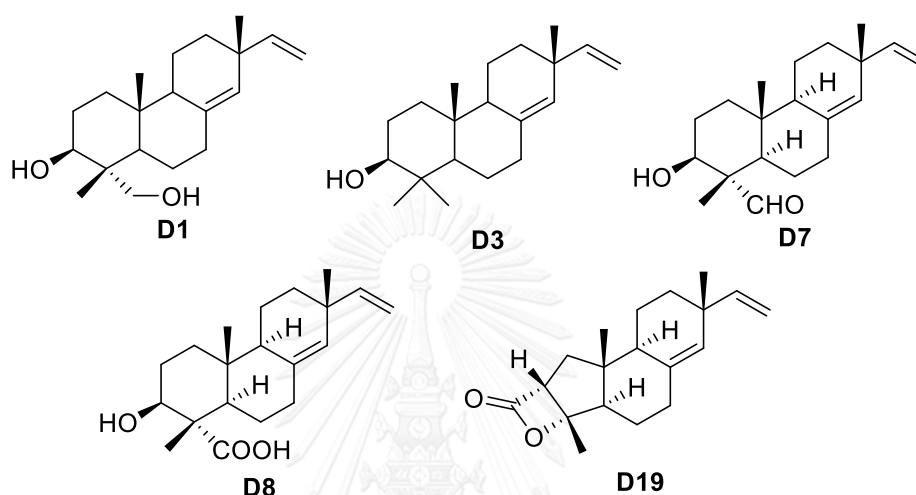
**Table 2.4** Preliminary antibacterial activity of compounds **D1-D3**, **D7**, **D8**, **D15**, **D18** and **D19** at 1,000  $\mu$ M by disc diffusion method

Compounds	Clear zone (mm)				
	Gram-positive			Gram-negative	
	<i>P. acne</i>	<i>S. aureus</i>	<i>S. sobrinus</i>	<i>S. mutans</i>	<i>S. typhi</i>
 <b>D1</b>	10.00 $\pm$ 0.00	10.00 $\pm$ 0.00	11.67 $\pm$ 1.25	10.00 $\pm$ 0.00	10.33 $\pm$ 0.47
 <b>D2</b>	7.67 $\pm$ 0.47	7.33 $\pm$ 0.47	9.00 $\pm$ 0.00	8.00 $\pm$ 0.00	8.67 $\pm$ 0.47
 <b>D3</b>	9.67 $\pm$ 0.47	9.00 $\pm$ 0.00	9.67 $\pm$ 0.47	8.33 $\pm$ 0.47	9.67 $\pm$ 0.94
 <b>D7</b>	14.33 $\pm$ 0.94	14.33 $\pm$ 0.47	14.67 $\pm$ 0.47	12.00 $\pm$ 0.82	17.00 $\pm$ 2.16
 <b>D8</b>	12.33 $\pm$ 0.47	14.67 $\pm$ 0.47	14.33 $\pm$ 0.47	13.67 $\pm$ 0.47	11.67 $\pm$ 1.70
 <b>D15</b>	10.33 $\pm$ 0.47	9.00 $\pm$ 0.82	8.67 $\pm$ 0.47	10.33 $\pm$ 0.47	9.00 $\pm$ 0.00
 <b>D18</b>	9.00 $\pm$ 0.00	9.33 $\pm$ 0.47	8.33 $\pm$ 0.47	9.33 $\pm$ 0.94	8.00 $\pm$ 0.00
 <b>D19</b>	10.33 $\pm$ 0.94	13.33 $\pm$ 1.25	12.00 $\pm$ 1.63	13.33 $\pm$ 0.47	13.00 $\pm$ 0.82
Control	0.00 $\pm$ 0.00	0.00 $\pm$ 0.00	0.00 $\pm$ 0.00	0.00 $\pm$ 0.00	0.00 $\pm$ 0.00

From the preliminary result, five compounds: **D1**, **D3**, **D7**, **D8**, and **D19** were selected to evaluate minimum inhibitory concentration (MIC) and minimum bactericidal concentration (MBC) using micro dilution method and chloramphenicol was used as a positive control (Table 2.5). Among the tested compounds, compound **D7** containing formyl at C-18 and hydroxy at C-3 and beta-lactone derivative **D19**

showed higher antibacterial activity than other compounds against *S. aureus*, *S. mutans*, *S. sobrinus*, and *S. typhi* with MIC values in range of 31.25 – 62.5  $\mu\text{M}$ . In addition, only compound **D7** could kill *S. mutans*, *S. sobrinus*, and *S. typhi* with MBC values of 62.6, 1,000, 1,000  $\mu\text{M}$ , respectively.

**Table 2.5** MIC and MBC of compounds **D1**, **D3**, **D7**, **D8**, and **D19**



Compounds	Minimum inhibitory concentration (MIC) ( $\mu\text{M}$ )				
	Gram-positive			Gram-negative	
	<i>P. acne</i>	<i>S. aureus</i>	<i>S. sobrinus</i>	<i>S. mutans</i>	<i>S. typhi</i>
<b>D1</b>	>1,000	>1,000	62.5 <sup>a</sup>	500.0 <sup>a</sup>	62.5 <sup>a</sup>
<b>D3</b>	>1,000	>1,000	>1,000	>1,000	>1,000
<b>D7</b>	>1,000	62.5 <sup>a</sup>	62.5 (62.5) <sup>b</sup>	62.5 (1,000) <sup>b</sup>	31.25 (1,000) <sup>b</sup>
<b>D8</b>	>1,000	500.0 <sup>a</sup>	500.0 <sup>a</sup>	1,000 <sup>a</sup>	500.0 <sup>a</sup>
<b>D19</b>	>1,000	62.5 <sup>a</sup>	31.25 <sup>a</sup>	62.5 <sup>a</sup>	31.25 <sup>a</sup>
Chloramphenicol	62.5 (>250) <sup>b</sup>	15.62 (>250) <sup>b</sup>	15.62 (>250) <sup>b</sup>	15.62 (>250) <sup>b</sup>	15.62 (>250) <sup>b</sup>

<sup>a</sup> MBC > 1,000  $\mu\text{M}$ , <sup>b</sup> Minimum bactericidal concentration MBC ( $\mu\text{M}$ )

According to these results, the hydroxyl group at C-3 was crucial for activity. The formyl group present in compound **D7** could enhance the inhibitory efficiency and kill bacteria better than those compounds containing carboxyl and

hydroxyl groups at C-18. The tricyclic ring system of diterpenoid also demonstrated an important role for antibacterial activity. Moreover, the beta-lactone ring in derivative **D19** could improve antibacterial activity.

### 2.19.2 Antifungal Activity

The preliminary screening of dichloromethane and ethyl acetate extracts against four phytopathogenic fungi: *A. porri*, *C. gloeosporioides*, *F. oxysporum*, and *P. parasitica* at the final concentration (10 mg/mL) with metalaxyl (10 mg/mL) as a positive control using the agar medium assay was conducted and % inhibition was calculated (Figure 2.31). Only dichloromethane and ethyl acetate extracts provided moderate inhibition against *A. porri* (53 and 49%, respectively) and *P. parasitica* (69 and 55%, respectively). The dichloromethane extract exhibited better activity than ethyl acetate extract against all four phytopathogenic fungi and showed good activity to inhibit *P. parasitica*. Thus, this extract was used for further study.

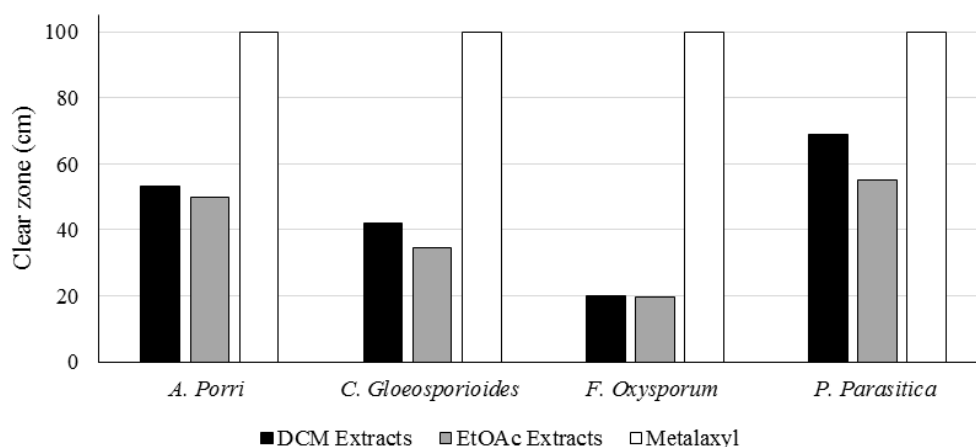


**Figure 2.31** Effects of  $\text{CH}_2\text{Cl}_2$  and EtOAc extracts on the mycelia growth of phytopathogenic fungi on PDA: concentration of testing sample at 10 mg/mL and metalaxyl at 10 mg/mL

Moreover, the isolated diterpenoids from the dichloromethane extract were further examined for antifungal activity against *P. parasitica*. Three diterpenoids,

sandaracopimaradiene-3 $\beta$ ,18-diol (**D1**), sandaracopimaradiene-3-one (**D2**), and sandaracopimaric acid (**D4**) were tested with antiphytopathogenic against *P. parasitica* at 1.0 mM and metalaxyl (10 ppm) as a positive control (Figure 2.32). Only compound **D1** displayed a moderate inhibition (53%). From these results, the hydroxy groups at C-3 and C-18 might be important for antifungal activity against *P. parasitica*.

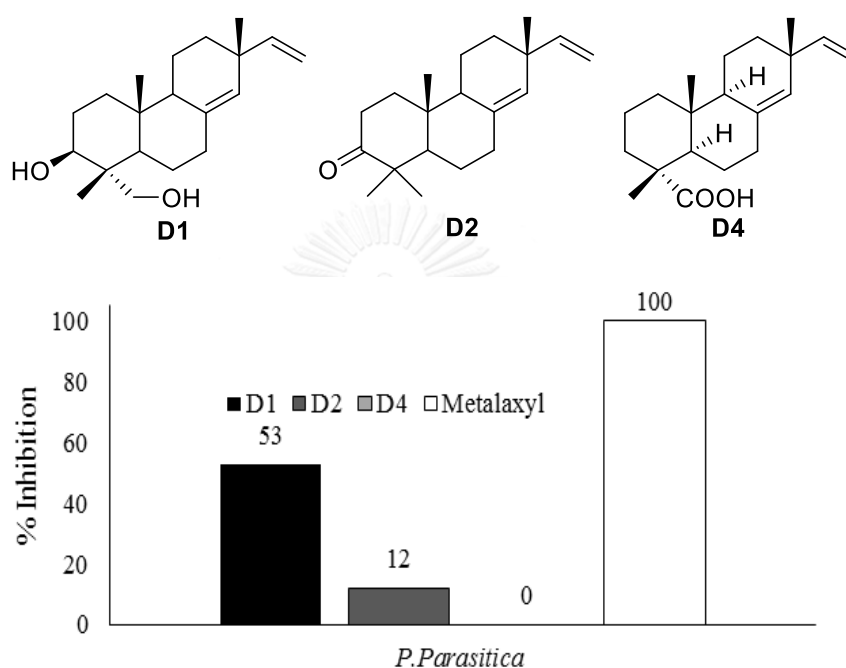


**Figure 2.32** Inhibitory effects of compounds **D1**, **D2** and **D4** on the mycelial growth of *P. Parasitica* on a solid culture medium (concentration of testing sample at 1.0 mM and metalaxyl at 10 ppm)

### 2.19.3 Cytotoxic Activity

The preliminary cytotoxicity by MTS assay of nine compounds: sandaracopimaradiene-3 $\beta$ ,18-diol (**D1**), sandaracopimaradiene-3-one (**D2**), sandaracopimaradiene-3 $\beta$ -ol (**D3**), sandaracopimaradiene-3 $\beta$ ,18-olal (**D7**), 3 $\beta$ -hydroxysandaracopimaric acid (**D8**), keto acid derivative **D15**, hydroxy acid derivative **D18**, beta-lactone derivative **D19** and cyclopropanation derivative **C2** against HepG2 cell line at 5  $\mu$ M (Figure 2.33) indicated that compounds **D7**, **D8**, **D15** and **D18** exhibited



good activity with cell proliferation (%) in range of 25–33% at 5.0  $\mu\text{M}$ . Compounds **D7**, **D15** and **D18** possessed  $\text{IC}_{50}$  values of  $3.45 \pm 0.47$ ,  $1.00 \pm 0.47$  and  $0.99 \pm 0.08 \mu\text{M}$ , respectively.

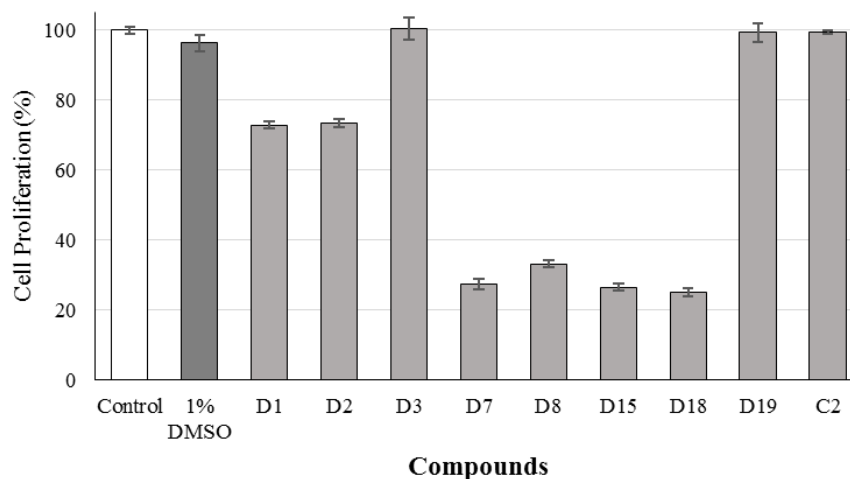
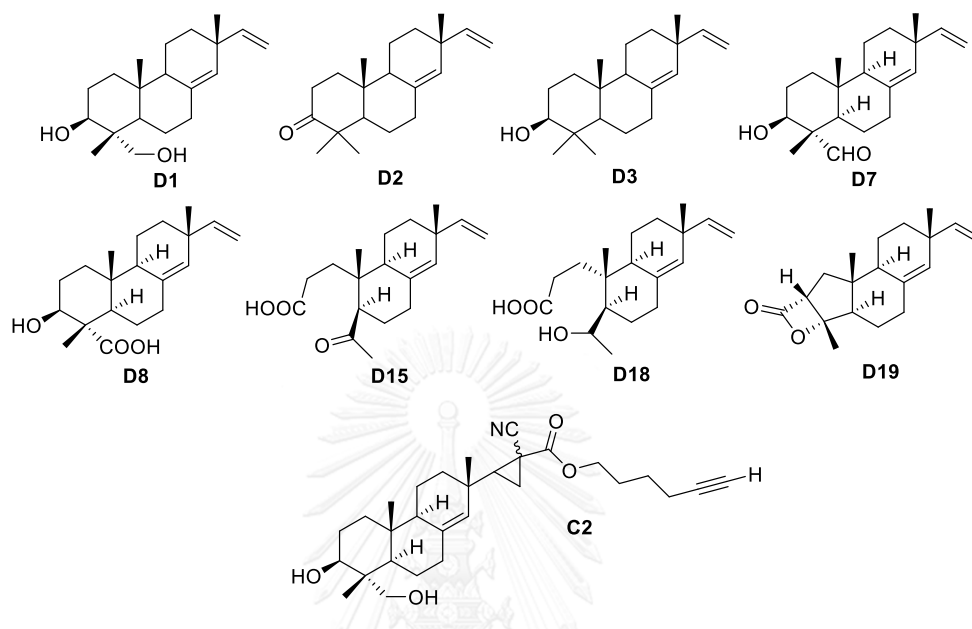


**Figure 2.33** Preliminary cytotoxicity of compounds **D1-3**, **7**, **8**, **15**, **18**, **19** and **C2** at 5.0  $\mu\text{M}$  against HepG2 by MTS assay (treated cells for 24 h)

From these results, the probe **C2** lost the activity, thus the olefinic group at C15-C16 in compound **D1** seemed to be important for activity. Moreover, the keto group in compound **D2** and hydroxyl group in compound **D3** at C-3 did not show significant role towards cytotoxicity. The formyl group containing compound **D7** could

enhance the cytotoxicity more than the carboxyl group in compound **D8** and hydroxyl group in compound **D1** at C-18. However, the tricyclic ring system of diterpenoid did not have an important role for cytotoxicity in compounds **D15** and **D18** because the activity increased when the ring system was removed. Moreover, the beta-lactone derivative compound **D19** might reveal good activity by increasing the covalent interaction from beta-lactone ring according to the results from previous research [50]. However, compound **D19** lost this cytotoxic activity against HepG2.



## CHAPTER III

### BERBERINE AND ITS DERIVATIVES FROM

#### *Coscinium fenestratum* (Goetgh.) Colebr. AND SAR STUDIES

## I. Introduction

### 3.1 Biological Activities of Berberine

#### 3.1.1 Antibacterial Activity

In 2001, Scazzocchio and co-workers isolated berberine,  $\beta$ -hydrastine, canadine and canadine (Figure 3.1) from *Hydrastis canadensis* L. (Ranunculaceae) extract. These compounds were tested for antibacterial activity against five bacterial strains including *Streptococcus aureus* (ATCC 25993 and ATCC 6538P), *Streptococcus sanguis* (ATCC10556), *Escherichia coli* (ATCC 25922), and *Pseudomonas aeruginosa* (ATCC 27853). The measuring “killing time” results found that berberine, canadine, and canadine (Figure 3.1) were active at 3.0 to 1.5 mg/mL from 4 to 30 min, while  $\beta$ -hydrastine was inactive against all tested bacteria. Canadine was more active than berberine on Gram-positive bacteria (MIC = 0.25 mg/mL); however, all tested compounds did not show activity against Gram-negative strains (MIC > 1.0 mg/mL) [87].

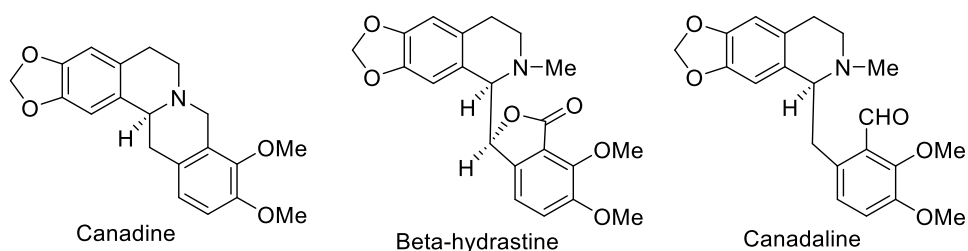


**Figure 3.1** The structures of canadine, beta-hydrastine and canadine

In 2009, Wang *et al.* observed that berberine showed bacteriostatic for *Staphylococcus epidermidis* and could block the formation of *S. epidermidis* biofilm at sub-minimal inhibitory concentration (30-45  $\mu$ g/mL) by tissue culture plate (TCP)

method, confocal laser scanning microscopy and scanning electron microscopy for both *S. epidermidis* ATCC 35984 and a clinical isolate strain SE243. Moreover, the bacterial metabolism was inhibited at 15-30  $\mu\text{g/mL}$  by berberine [88].

### 3.1.2 Antifungal Activity

In 2003, Volleková and co-workers isolated berberine, palmatine and jatrorrhizine (Figure 3.2) from the stem barks of *Mahonia aquifolium* (Berberidaceae) and tested for inhibitory activity against various fungal species. Jatrorrhizine showed the most effective against all fungi (MIC ranged from 62.5 to 125  $\mu\text{g/mL}$ ) compared with fluconazole and bifonazole (MIC ranges were 12.5 to  $>100$   $\mu\text{g/mL}$ ). Berberine and palmatine exhibited only minimal activity (MIC 500 to  $\geq 1000$   $\mu\text{g/mL}$ ) [89].

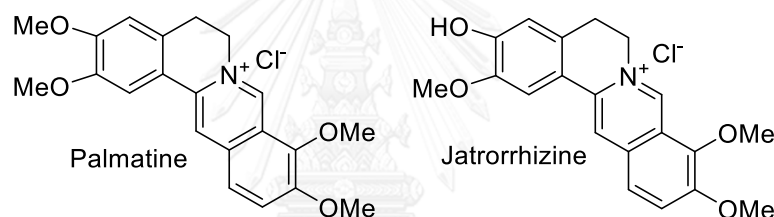


Figure 3.2 The structures of palmatine and jatrorrhizine

### 3.1.3 Anti-Inflammatory

In 2004, Kuo and co-workers illustrated that the anti-inflammatory mechanism of berberine was mediated through cyclooxygenase-2 (COX-2) regulation, promoted in prostaglandins (PGs) synthesis for inflammation. Berberine inhibited basal and TPA mediated PGE<sub>2</sub> level and COX-2 expression by inhibiting AP-1 binding in oral cancer cell line OC2 and KB cells. This anti-inflammatory effect was also obvious *in vivo* that berberine pretreatment of Wistar rat inhibited the production of PGE<sub>2</sub> and exudated in carrageenan influenced air pouch. The anti-inflammatory and anticancer potential of berberine could be explained because both AP-1 and COX-2 had been linked to carcinogenesis and inflammation [18].

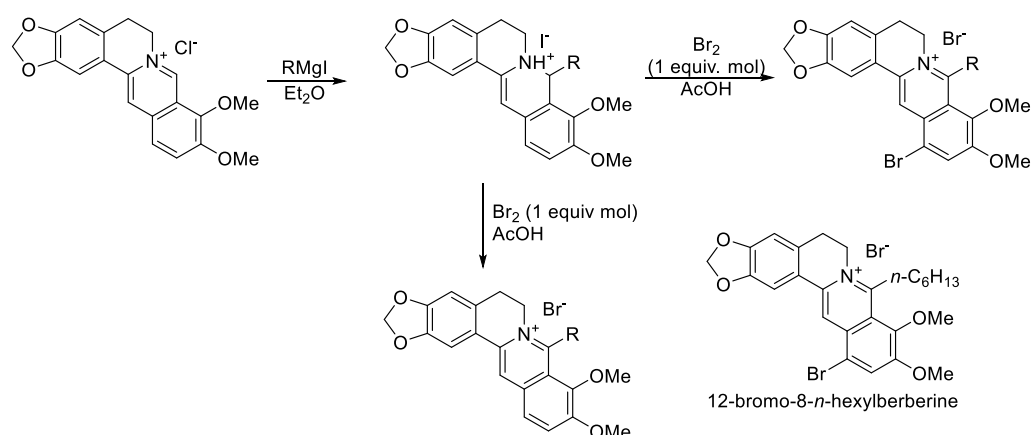
### 3.1.4 Anticancer Activity

In 2006, Letasiova *et al.* found the cytotoxicity of berberine on both the human tumour U937 and murine melanoma B16 cell lines. The melanoma B16 cells were much more sensitive to berberine treatment ( $IC_{100}$  was  $< 1$  mg/mL) than the U937 cells ( $IC_{100}$  was  $< 100$  mg/mL). The values of  $IC_{50}$  were found to be less than 4 mg/mL for both cell lines under the long-term influence. Berberine did not affect on the cell cycle profile of the U937 and B16 cells. However, berberine induced apoptosis of the U937 cells. In contrast, the berberine-treated B16 was observed cell lysis or necrosis as the result of the integrity damage of the cytoplasmic membrane [90].

## 3.2 Literature Review of Berberine and its Derivatives for SAR Study

### 3.2.1 Antimicrobial Activity

In 1998, Iwasa *et al.* synthesized 8-alkyl-, 8-phenyl-substituted and 12-bromo-derivatives from berberine (Scheme 3.1) to test antimicrobial activity *in vitro* and evaluate structure activity relationships. The results displayed that the alkyl or phenyl and bromo groups at C-8 and C-12 positions could increase the antimicrobial activity. The increased length of the aliphatic chain also improved the activity except for *Candida albicans* and *E. coli*. 12-Bromo-8-*n*-hexylberberine exhibited a better activity than berberine in 64, 256, 128, 16, and 32 times more active against *S. aureus*, *Bacillus subtilis*, *Salmonella enteritidis*, *E. coli*, and *C. albicans*, respectively [91].



**Scheme 3.1** The synthesis of 8-alkyl-, 8-phenyl-substituted and 12-bromo-derivatives from berberine

In 2009, Samosorn and co-workers synthesized berberine derivatives *via* conjugation of NorA substrate berberine and the NorA inhibitor 5-nitro-2-phenyl-1*H*-indole (INF55 as synthetic NorA inhibitor) with methylene ether linking group to give 13-substituted berberine-NorA inhibitor hybrid (**H1**). Several general arylmethyl ether hybrid derivatives were prepared (Figure 3.3). Compound **H1** displayed an excellent antibacterial activity against *S. aureus* (MIC = 1.7  $\mu\text{M}$ ), which was over 382-fold more active than berberine, and also blocked the NorA efflux pump in *S. aureus* [26].

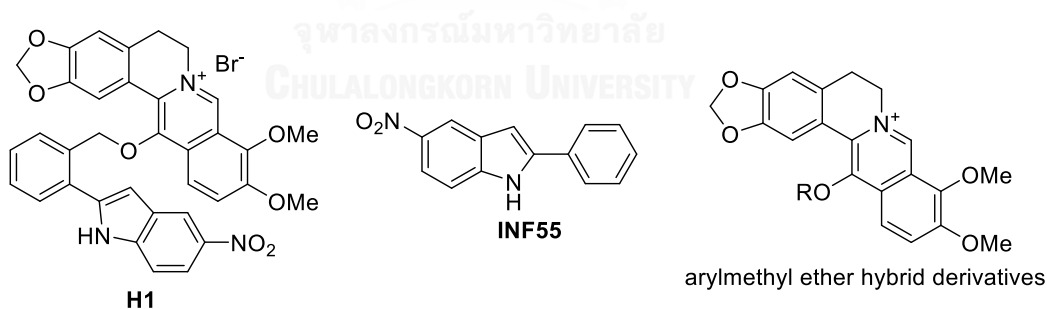


**Figure 3.3** The structures of compounds **H1**, **INF55** and arylmethyl ether hybrid derivatives

In 2012, Zuo *et al.* reported antibacterial activity of berberine (**B1**) and 8-acetyl-dihydroberberine (**B2**) on ten clinical isolates of SCCmec III type methicillin-resistant *Staphylococcus aureus* (MRSA). Moreover, these two compounds were studied for combination with antibacterial agents including ampicillin (AMP),

azithromycin (AZM), cefazolin (CFZ) and levofloxacin (LEV). A broth micro-dilution method and the checkerboard were used for testing. These results showed that compounds **B1** and **B2** enhanced the *in vitro* inhibitory efficacy of AZM and LEV to the same extent, which had potential for further examination in combinatory therapeutic applications of patients infected with MRSA [92].

In 2013, Zhang and co-workers synthesized a series of novel berberine triazoles (Figure 3.4), and screened for antimicrobial activities against Gram-positive and Gram-negative bacteria and fungal strains. These berberine derivatives exhibited good antibacterial and antifungal activities (MIC values = 2 to 64  $\mu\text{g/mL}$ ) and were comparable to better activity than the reference: berberine, chloromycin, norfloxacin and fluconazole. The competitive interactions between metal ions to human serum albumin (HSA) and compound **H2** disclosed that the participation of  $\text{Mg}^{2+}$  and  $\text{Fe}^{3+}$  ions in compound **H2**–HSA association could result in the concentration increase of free compound **H2**, shorten the storage time and half-life of compound **H2** in the blood, thus improving its antimicrobial efficacy [93].

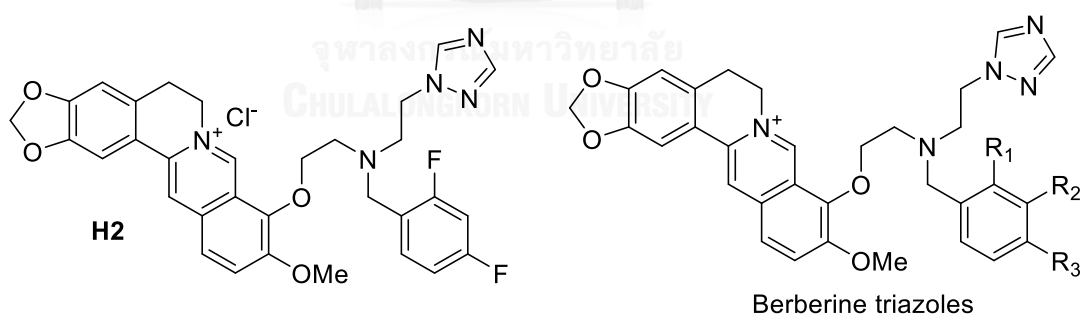
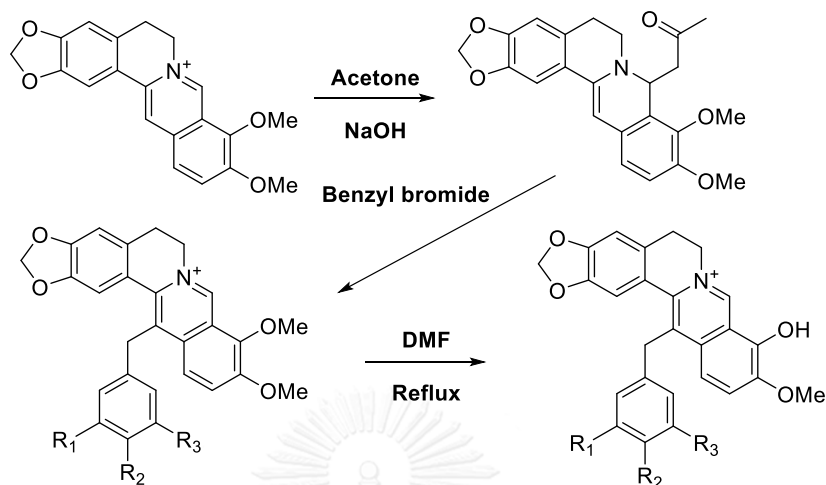


**Figure 3.4** The structures of compound **H2** and berberine triazoles

### 3.2.2 Antifungal Activity

In 2006, Park *et al.* synthesized 13-(substituted benzyl) berberine and berberrubine derivatives through acetyl-berberine (Scheme 3.2) and these derivatives were examined for antifungal activity against human pathogenic fungi. The synthesized compounds illustrated more potent inhibition than berberine and

berberrubine. Moreover, all berberine derivatives showed higher activity than all berberrubine derivatives [21].

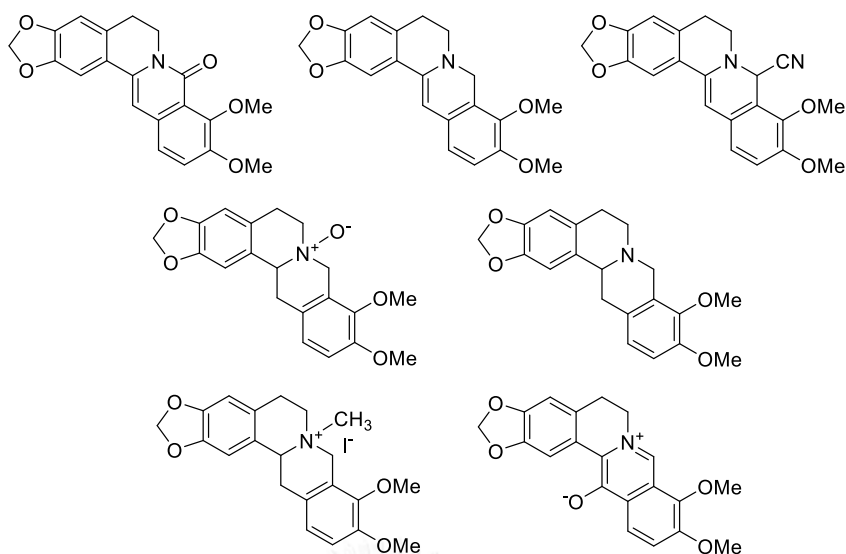


**Scheme 3.2** The preparation of 13-(substituted benzyl) of berberine and berberrubine derivatives

### 3.2.3 Antiprotozoal Activity

In 1988, Vennerstrom and co-workers tested berberine, palmatine, jatrorrhizine and several synthesized derivatives (Scheme 3.3) for antimalarial activity *in vitro* against *Plasmodium falciparum* and *in vivo* against *Plasmodium berghei*. Palmatine and jatrorrhizine as their chlorides were isolated from *Enantia chlorantha*. All protoberberine alkaloids were inactive *in vivo*, though some derivatives showed a potency *in vitro* [94].





**Scheme 3.3** The structures of synthesized berberine derivatives

In 2011, Bahar and co-workers synthesized 5,6-didehydro-8,8-diethyl-13-oxodihydroberberine chloride (Figure 3.5) from berberine. This compound showed antiprotozoal activity at *nM* level potency against *in vitro* models of malaria, leishmaniasis, and trypanosomiasis and also *in vivo* visceral leishmaniasis model [95].

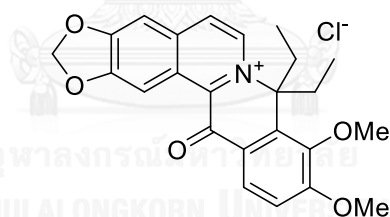


**Figure 3.5** The structure of 5,6-didehydro-8,8-diethyl-13-oxodihydroberberine chloride

### 3.2.4 Anticancer Activity

In 2000, Orfila *et al.* evaluated the cytotoxicity of berberine, lincangene, thaicanine and their 8-hydroxy-7,8-dihydro-derivatives (Figure 3.6) at 10-1,000 mg/mL against Hela (uterus carcinoma), SVKO<sub>3</sub> (ovary carcinoma), Hep-2 (larynx carcinoma), primary culture from mouse embryon, and human fibroblast cells. Lincangene and thaicanine were isolated from the leaves of *Guatteria schomburgkiana* Mart. Berberine showed the highest cytotoxicity with LC<sub>50</sub> 10 µg/mL

for all cell lines. These results indicated that the cytotoxicity was notably reduced by structural changes including the changing planarity. The hydroxyl group at C-8 caused and was concomitant saturation of double bond between N and C-8 in molecules [96].

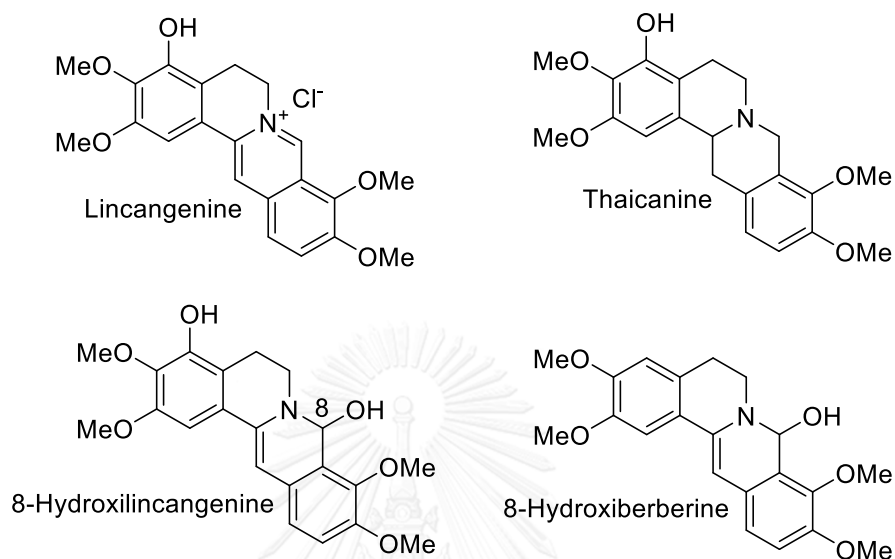


**Figure 3.6** The structures of lincanganine, thaicanine and their 8-hydroxy-7,8-dihydro-derivatives

In 2012, Zhang and co-workers synthesized 13-*n*-hexyl and 13-*n*-octyl derivatives of berberine and palmatine (Figure 3.7) to examine cytotoxic activity in seven human cancer cell lines including 7701QGY, SMMC7721, HepG2, CEM, CEM/VCR, K562 and Lewis. 13-*n*-Octyl palmatine provided an excellent inhibitory activity with  $IC_{50}$  of  $0.02 \pm 0.01 \mu\text{M}$  for SMMC7721. The 13-*n*-alkyl berberine and palmatine derivatives showed more cytotoxicity than berberine and palmatine for all cell lines. Moreover, these derivatives exhibited more potent cytotoxicity in mice with S180 sarcoma xenografted *in vivo* [97].

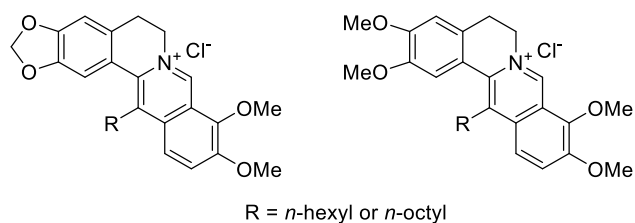
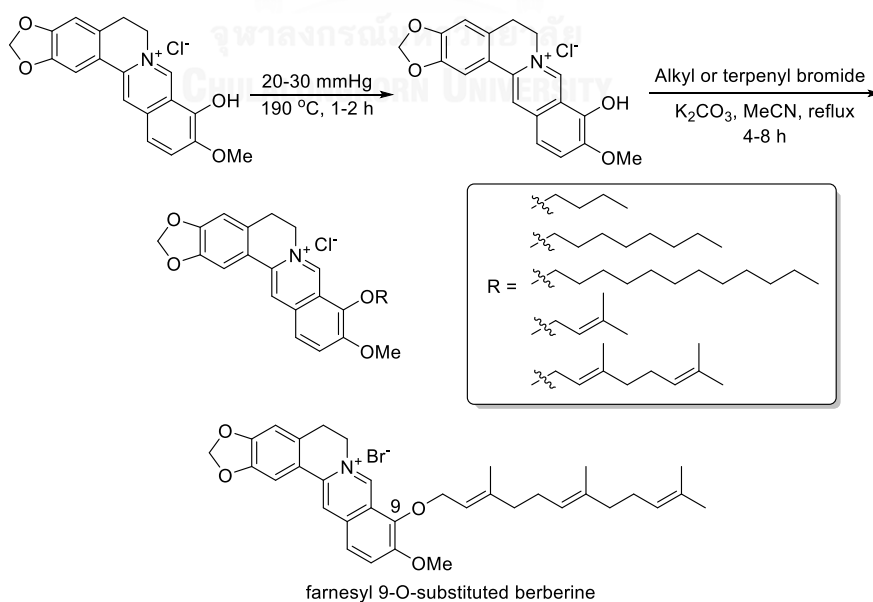


**Figure 3.7** The structures of 13-*n*-hexyl and 13-*n*-octyl derivatives of berberine and palmatine

In 2013, Lo and co-workers synthesized a series of analogues bearing 9-*O*-alkyl- or 9-*O*-terpenyl- substituted berberine (Scheme 3.4) to increase its hydrophobicity for anticancer activity against human cancer HepG2 and HT29 cell lines. The results exhibited that the lipophilic substitute had an important role to inhibit the human cancer cell growth and the activity could be maximized with the optimized chain length and substituent type. Interestingly, a farnesyl 9-*O*-substituted berberine showed better cytotoxic activity against HepG2 cell line than berberine to 104-fold for anti-proliferation activity after 48 h. In addition, this compound induced apoptosis in HepG2 cells at lower concentration than berberine for 24 h in Hoechst 33258 and annexin V-FITC/PI staining analyses [28].



**Scheme 3.4** The synthesis of 9-*O*-alkyl- and 9-*O*-terpenyl- substituted berberine

### 3.3 Reactive Oxygen Species and Enzymatic Antioxidants

Reactive oxygen species (ROS) are oxygen-centered free radicals produced in mitochondria *via* aerobic metabolism or received from the external sources including infections, dietary intake, pollution, and cigarette smoking [98]. A low level of ROS affects several cellular processes, including cell proliferation, signal transduction, development of cells, and necrotic or apoptotic cell death [99]. A moderate to high level of ROS in oxidative stress can interfere the intracellular antioxidant system and damage cytoplasmic biomolecules such as protein, lipid, DNA, and RNA [100]. Cells can normally maintain an optimal level of ROS by reducing oxidative stress *via* enzymatic and non-enzymatic systems. Major enzymatic antioxidants frequently mentioned are superoxide dismutase (SOD), catalase (CAT), glutathione peroxidases (GPx), and glutathione reductase (GR) [101]. ROS are key molecules causing several diseases including Alzheimer, cancer, inflammation, rheumatoid arthritis, diabetes, *etc* [102]. In cancer, ROS influence mutations and alter gene functions resulting in carcinogenesis through oxidative process [103].

The role of antioxidant enzymes (Figure 3.8) displayed that SOD catalyzed the dismutation of  $\bullet\text{O}_2$  into  $\text{H}_2\text{O}_2$  and  $\text{O}_2$ . Glutathione peroxidase (GPx) reduced  $\text{H}_2\text{O}_2$  and lipid peroxides (LOOH) to water and lipid alcohols (LOH), respectively. Glutathione (GSH) was oxidized to glutathione disulfide (GSSG), could be recycled by glutathione reductase (GR) to reduced GSH utilizing NADPH as a substrate. Catalase (CAT) is an intracellular antioxidant enzyme that is mainly located in cellular peroxisomes and catalyzes the reaction of  $\text{H}_2\text{O}_2$  to  $\text{H}_2\text{O}$  and  $\text{O}_2$ . Catalase is very effective in high level oxidative stress and protects cells from  $\text{H}_2\text{O}_2$  produced within the cell. Thioredoxin (TR) participates in thiol-dependent cellular reductive processes [101, 104].

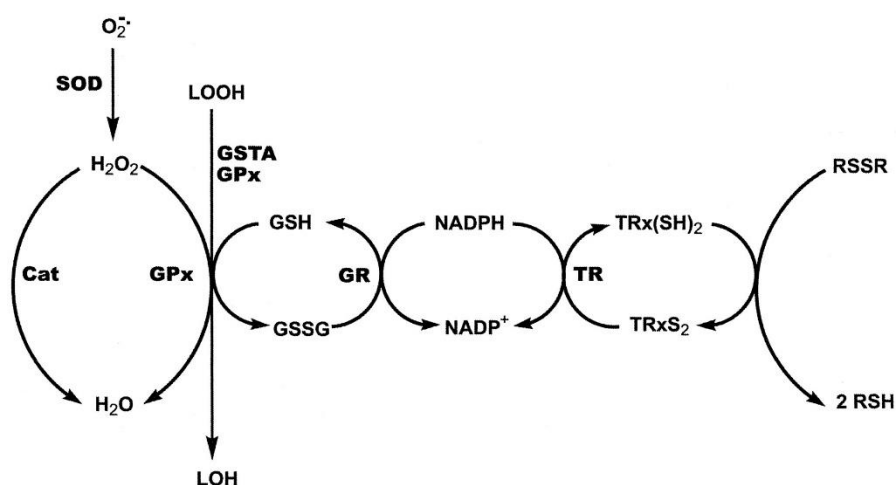


**Figure 3.8** The role of antioxidant enzymes in the combat of oxidative stress

Healthy individuals have higher plasma levels of antioxidant enzymes (SOD, CAT, and GPx) than patients with oral cancer. In contrast, up-regulation or enhancement of antioxidant enzyme activities including SOD, CAT, and GPx has been proposed as an effective strategy for both cancer prevention and therapy [105]. For example, progestin induction for catalase activity has been proven to be effective against breast cancer [106]. Taurine, an abundant free amino acid, was reported to decrease ROS levels and increase the expression of antioxidant enzymes: SOD, GPx, and CAT in the B16F10 melanoma cell line [107].

Recently, numerous scientific research have shown new antioxidants from natural products for chemoprevention and cancer therapy. Many secondary metabolites from plants, such as alkaloids, are interesting for its potential use in a variety of diseases especially cancer. Berberine, an isoquinoline alkaloid, has been used for traditional medical systems in eastern countries. It possesses several biological activities including anti-inflammatory [108], anticancer [109, 110], anti-diabetic [111], antibacterial [112], and antifungal functions [113]. The antioxidant capacity of berberine has demonstrated both direct [114, 115] and indirect activities [98, 116]. Recently, berberine has been structurally modified to yield new derivatives which are able to

improve their biological functions: antibacterial [92, 93], antifungal [30], antiprotozoal [95], and anticancer activities [28, 97].

### 3.4 The Literature Reviews of Berberine for Antioxidant Activity

In 2002, Hwang and co-workers studied the inhibitory effect of berberine on *tert*-butyl hydroperoxide (*t*-BHP)-induced lipid peroxidation and cytotoxicity in rat liver. In the preliminary study, DPPH scavenging result of berberine showed a moderate activity. Furthermore, berberine (0.01-1.0 mM) could decrease the leakage of alanine aminotransferase (ALT), lactate dehydrogenase (LDH), and the formation of malondialdehyde (MDA) after treatment of *t*-BHP (1.5 mM). Berberine could attenuate the level of *t*-BHP which decreased GSH and also increased the level of the DNA repair synthesis. In *in vivo* study, the intraperitoneal pretreatment with berberine (0.5 and 5 mg/kg) for 5 days before a single dose of *t*-BHP (0.1 mmol/kg) showed significantly reduced the serum levels of hepatic enzyme markers (ALT and aspartate aminotransferase) and decreased oxidative stress in the liver [98].

In 2007, Tan and co-workers examined the antioxidant activity of berberine on corpus cavernosum smooth muscle cells (CCSMC) in penile erectile dysfunction, damaged by H<sub>2</sub>O<sub>2</sub>. The results disclosed that the treatment of H<sub>2</sub>O<sub>2</sub> (1 mmol/L) significantly decreased the cell viability, NO (nitric oxide) products, and SOD activity of CCSMC. Moreover, it increased LDH release and MDA content. However, the treatment of berberine at 10-1,000 μmol/L could inhibit the damaging effects of H<sub>2</sub>O<sub>2</sub>, with increased cell viability, NO production and SOD activity, and also decreased LDH release and MDA content [116].

In 2009, Jang *et al.* isolated four isoquinoline alkaloids: berberine, berberrubine, coptisine and palmatine (Figure 3.9) from *Coptis chinensis* Franch to study their structural characteristics to scavenge •OH via Fe(II)-catalyzed Fenton reaction. The scavenging activity of all compounds at 1 mM concentration using ESR spectrometry

method displayed that berberrubine showed the strongest  $\bullet\text{OH}$  scavenging activity (85%) and the decreasing order of coptisine (79%), berberine (23%), and palmatine (22%) were observed. The ferrous ion chelating effects of these compounds displayed similar pattern with their  $\bullet\text{OH}$  scavenging effects. Moreover, metal chelating functional groups including hydroxyl group at C-9 of berberubine and methylenedioxy group at C-9 and C-10 of coptisine were thought to contribute to the  $\bullet\text{OH}$  scavenging activities [114].

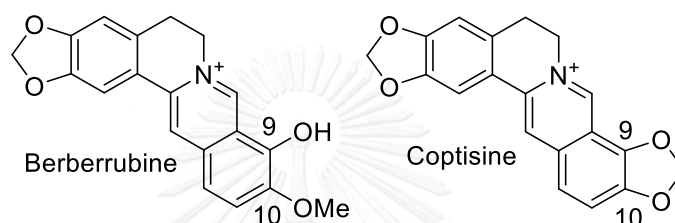


**Figure 3.9** The structures of berberrubine and coptisine

In 2011, Bashir and Gilani reported that berberine inhibited *in vitro* ferrous-ascorbate induced lipid peroxidation of rat kidney homogenate similar to the 3,5-di-*tert*-butyl-4-hydroxytoluene (BHT) standard. In addition, berberine displayed inhibitory of calcium oxalate crystal retention in renal tubules thus could have been caused by its antioxidant activity [115].

### 3.5 The Human Fibrosarcoma Cells (HT1080)

Fibrosarcoma (Figure 3.10) is a malignant tumor that derives from fibrous connective tissue generally found in male of age 30-40 years. It is characterized by the presence of immature proliferating fibroblasts or undifferentiated anaplastic spindle cells. It originates in fibrous tissues of the bone and invades long or flat bones, for instant femur, tibia or mandible and also involves periosteum and the overlying muscle. HT 1080 is a fibrosarcoma cell line and has been used widely in preclinical research. The cell lines are created from biopsy of fibrosarcoma tissue present in a 35

year old male [117]. Moreover, this cell line has a number of antioxidant gene including SOD, GPx, GR, and CAT to study gene expression [118].

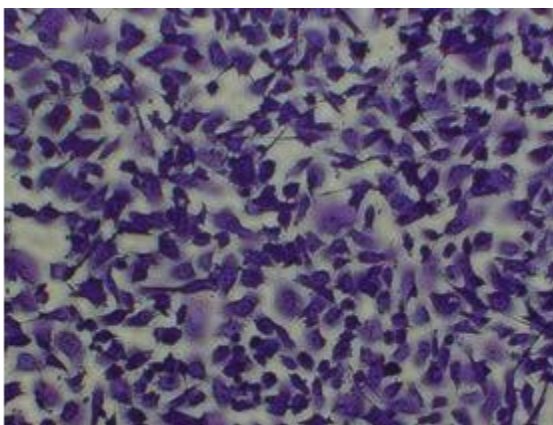


**Figure 3.10** The Human Fibrosarcoma Cells (HT1080)

### 3.6 Objective of This Research

Aforementioned, berberine showed a wide variety of biological activities and their derivatives sometime displayed better activities. The SAR study provided the informative data for an important role of activity. However, a few SAR studies of berberine derivatives have been reported for direct and indirect antioxidant activity. Thus, the SAR study of berberine and its derivatives for antibacterial activity and the effect on antioxidant gene in cancer cell lines should be investigated. The objectives of this work could be summarized as follows:

1. The isolation of berberine from the vines of *C. fenestratum*
2. The synthesis of berberine derivatives
3. The SAR study for antibacterial, antioxidant, cytotoxic activity of berberine and its derivatives



## II. Experimental

### 3.7 General Information

Reactions were completed under a nitrogen atmosphere. Tetrahydrofuran was freshly distilled over sodium and benzophenone. Acetonitrile and methanol were distilled from calcium hydride. Commercially available reagents were used as received from Sigma-Aldrich.  $^1\text{H}$  NMR spectra were measured at 400 MHz and chemical shifts are reported as  $\delta$  values in ppm relative to  $\text{CDCl}_3$  (7.26 ppm), DMSO (2.50 ppm) or  $\text{CD}_3\text{OD}$  (4.78 and 3.31 ppm), coupling constants ( $J$ ) are reported in Hertz (Hz), and multiplicity follows normal convention: s, singlet; d, doublet; t, triplet; q, quartet; dd, doublet of doublets; ddd, doublet of doublet of doublets; dt, doublet of triplets; m, multiplet; bs, broad singlet.  $^{13}\text{C}$  NMR spectra were measured at 125, 100 or 75 MHz with  $\text{CDCl}_3$  (77.2 ppm), DMSO (39.5 ppm) or  $\text{CD}_3\text{OD}$  (49.2 ppm) as the internal standard. Column chromatography was performed using 60 Å silica gel (Silicycle, 230-400 mesh). Thin layer chromatography was performed using 60 Å silica gel F-254. Developed plates were visualized by potassium permanganate stain followed by heating.

### 3.8 Extraction of Berberine (B1) from *C. fenestratum*

The vines of *Coscinium fenestratum* (Goetgh.) Colebr (Figure 3.11) were purchased from Chaokrompoe store in Bangkok during March 2011. Then they were ground and soaked in MeOH for 5 days (3 times). The concentrated methanolic extract was acidified, adjusted to pH = 2 by conc. HCl, filtered to collect a yellow precipitate, and finally recrystallized in MeOH to obtain berberine chloride (Figure 3.12) as a yellow powder with 4.8% yield [17].



Figure 3.11 The vines of *Coscinium fenestratum*

**Berberine chloride (B1):** Yellow powder. TLC (MeOH:CH<sub>2</sub>Cl<sub>2</sub>, 1:10 v/v):  $R_f = 0.34$ ; <sup>1</sup>H NMR (400 MHz, CD<sub>3</sub>OD):  $\delta$  9.65 (s, 1H), 8.54 (s, 1H), 7.99 (d,  $J = 9.0$  Hz, 1H), 7.88 (d,  $J = 9.0$  Hz, 1H), 7.50 (s, 1H), 6.84 (s, 1H), 5.99 (s, 2H), 4.83 (t,  $J = 6.4$  Hz, 2H), 4.09 (s, 3H), 3.99 (s, 3H), 3.13 (t,  $J = 6.2$  Hz, 2H); <sup>13</sup>C NMR (100 MHz, CD<sub>3</sub>OD):  $\delta$  152.2, 152.0, 149.9, 146.3, 145.8, 139.6, 135.2, 131.9, 128.1, 124.6, 123.3, 121.8, 121.5, 109.4, 106.5, 103.7, 62.6, 57.7, 57.2, 28.2 [17].

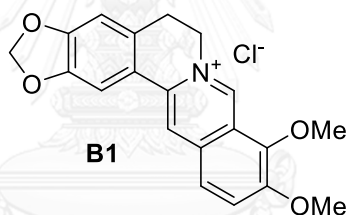
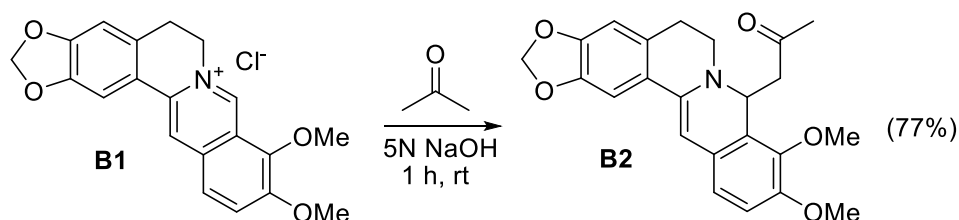


Figure 3.12 The structure of berberine chloride (B1)

### 3.9 Synthesis of Berberine Derivatives B2-B9

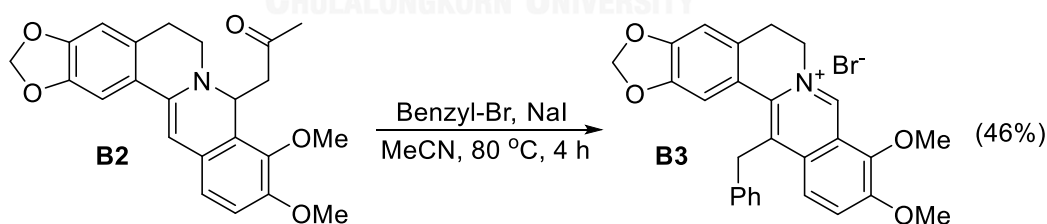
**Acetonyl-berberine (B2):** Berberine chloride (B1) (1.0 g, 2.730 mmol) was dissolved in acetone (1.2 mL) and water (2 mL) and then stirred at 0 °C. While stirring, 5N NaOH (5 mL) was added dropwise and then warmed up to rt (30 °C). After stirring for 1 h, the reaction mixture was filtered and washed with 80% MeOH to give the desired product (827.0 mg, 77% yield) as bright yellow powder (Scheme 3.5). TLC (MeOH:CH<sub>2</sub>Cl<sub>2</sub>, 1:20 v/v):  $R_f = 0.27$ ; <sup>1</sup>H NMR (400 MHz, CDCl<sub>3</sub>):  $\delta$  7.15 (s, 1H), 6.78 (m, 2H), 6.60 (s, 1H), 5.97 (d,  $J = 2.4$  Hz, 2H), 5.91 (s, 1H), 5.35 (dd,  $J = 7.0, 4.1$  Hz, 1H), 3.92 (s, 3H), 3.86 (s, 3H), 3.37 (m, 2H), 3.09 (dd,  $J = 15.4, 7.0$  Hz, 1H), 2.85 (m, 2H), 2.43 (dd,  $J = 15.5, 4.0$  Hz, 1H), 2.07 (s, 3H); <sup>13</sup>C NMR (100 MHz, CDCl<sub>3</sub>):  $\delta$  207.3, 150.1, 147.3, 146.6,

143.7, 138.5, 129.0, 127.8, 125.6, 123.6, 118.6, 112.1, 107.9, 104.2, 101.0, 95.1, 60.7, 56.1, 54.3, 47.7, 46.2, 30.8, 30.4 [21].



**Scheme 3.5** The synthesis of acetonil-berberine (**B2**)

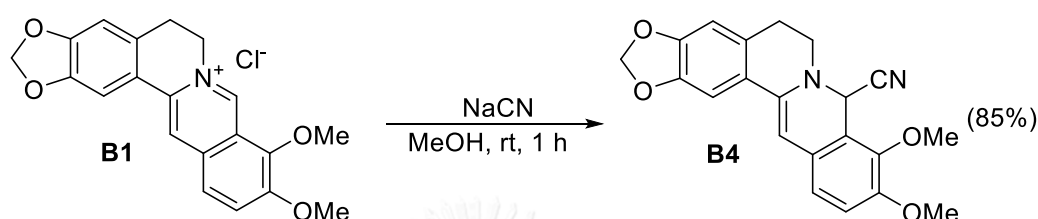
**13-Benzyl-berberine (B3):** Acetonil-berberine (**B2**) (500 mg, 1.271 mmol) was dissolved in MeCN (8 mL) and added NaI (248 mg, 1.652 mmol) and benzyl bromide (230  $\mu$ L, 1.966 mmol). The mixture was stirred at 80 °C for 4 h. The reaction mixture was filtered and washed with  $\text{CH}_2\text{Cl}_2$  to receive the desired product (296.0 mg, 46% yield) as dark yellow solid (Scheme 3.6). TLC (MeOH: $\text{CH}_2\text{Cl}_2$ , 1:10 v/v):  $R_f = 0.56$ ;  $^1\text{H}$  NMR (400 MHz,  $\text{CDCl}_3$ ):  $\delta$  10.60 (s, 1H), 7.68 (d,  $J = 9.4$  Hz, 1H), 7.60 (d,  $J = 9.3$  Hz, 1H), 7.37 (t,  $J = 7.3$  Hz, 3H), 7.31 (d,  $J = 6.9$  Hz, 2H), 6.94 (s, 1H), 6.87 (s, 1H), 5.99 (s, 2H), 5.28 (m, 2H), 4.67 (s, 2H), 4.40 (s, 3H), 4.01 (s, 3H), 3.28 (m, 2H);  $^{13}\text{C}$  NMR (100 MHz,  $\text{CDCl}_3$ ):  $\delta$  150.5, 149.9, 147.1, 147.0, 146.4, 138.2, 137.4, 133.8, 133.7, 129.9, 129.5, 127.9, 127.3, 125.6, 121.9, 120.8, 120.0, 108.8, 108.5, 101.9, 63.3, 57.8, 56.8, 36.5, 28.5 [21].



**Scheme 3.6** The synthesis of 13-benzyl-berberine (**B3**)

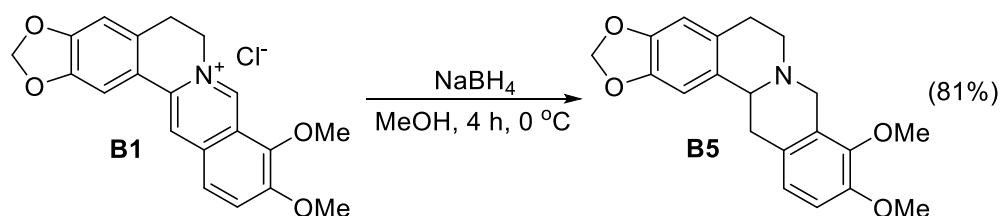
**8-Cyano-13,14-dehydrocanadiene (B4):** Berberine chloride (**B1**) (1.0 g, 2.730 mmol) was dissolved in MeOH (25 mL) and added dropwise with a solution of NaCN (1.338 g, 27.300 mmol, in water 5 mL). The reaction mixture was stirred for 1 h at rt (30 °C). After reaction complete, the mixture was filtered to yield the desired product (841 mg, 85% yield) as pale yellow solid (Scheme 3.7). TLC (MeOH: $\text{CH}_2\text{Cl}_2$ , 3:100 v/v):

$R_f = 0.53$ ;  $^1\text{H NMR}$  (400 MHz,  $\text{CDCl}_3$ ):  $\delta$  7.19 (s, 1H), 6.89 (dd,  $J = 19.5, 8.4$  Hz, 2H), 6.62 (s, 1H), 6.17 (s, 1H), 5.99 (dd,  $J = 6.4, 1.2$  Hz, 2H), 5.78 (s, 1H), 4.00 (s, 3H), 3.90 (s, 3H), 3.45 (m, 1H), 3.29 (m, 1H), 3.05 (dt,  $J = 10.9, 4.3$  Hz, 1H), 2.86 (dt,  $J = 15.3, 2.8$  Hz, 1H);  $^{13}\text{C NMR}$  (100 MHz,  $\text{CDCl}_3$ )  $\delta$  150.7, 147.8, 147.0, 144.5, 138.4, 128.5, 127.0, 124.2, 119.8, 117.1, 116.6, 113.9, 107.8, 104.2, 101.2, 98.2, 60.9, 56.1, 50.0, 48.0, 29.6 [119].



**Scheme 3.7** The synthesis of 8-cyano-13,14-dehydrocanadine (**B4**)

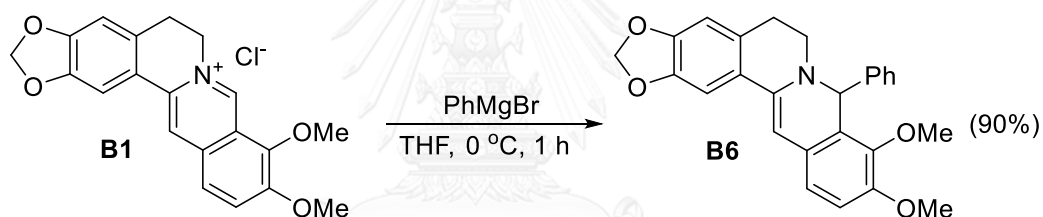
**Canadine (B5):** Berberine chloride (**B1**) (1.0 g, 2.730 mmol) was dissolved in MeOH 25 mL, and then stirred at 0 °C.  $\text{NaBH}_4$  (25 mg, 0.661 mmol) was slowly added and further stirred for 4 h. The reaction mixture was filtered and washed with water (20 mL) to give the desired product (746 mg, 81% yield) as pale yellow solid (Scheme 3.8). TLC ( $\text{MeOH}:\text{CH}_2\text{Cl}_2$ , 1:20 v/v):  $R_f = 0.55$ ;  $^1\text{H NMR}$  (400 MHz,  $\text{CDCl}_3$ ):  $\delta$  6.89 (d,  $J = 8.4$  Hz, 1H), 6.81 (d,  $J = 8.4$  Hz, 1H), 6.76 (s, 1H), 6.61 (d, 1H), 5.94 (s, 1H), 4.26 (s, 1H), 3.87 (2s, 6H), 3.54 (m, 2H), 3.30 – 3.09 (m, 4H), 2.90 (t,  $J = 5.8$  Hz, 1H), 2.73 – 2.59 (m, 2H);  $^{13}\text{C NMR}$  (100 MHz,  $\text{CDCl}_3$ )  $\delta$  150.4, 147.2, 146.8, 145.0, 130.9, 128.6, 127.8, 127.7, 123.8, 111.1, 108.4, 105.5, 100.7, 60.7, 59.5, 55.9, 53.9, 51.4, 36.4, 29.1 [120].



**Scheme 3.8** The synthesis of canadine (**B5**)

**8-Phenyl-13,14-dehydrocanadine (B6):** Berberine chloride (**B1**) (468 mg, 1.391 mmol) was dissolved in dried THF (50 mL) and kept cool to 0 °C under nitrogen atmosphere. The solution of  $\text{PhMgBr}$  (1.0 M in THF, 3 mL, 3.000 mmol) was added

dropwise to mixture, and then further stirred for 1 h at 0 °C. The reaction was quenched with saturated NH<sub>4</sub>Cl (20 mL) and extracted with Et<sub>2</sub>O (2 x 50 mL). The organic layer was washed with brine, dried over anhydrous Na<sub>2</sub>SO<sub>4</sub> and concentrated *in vacuo*. The residue was recrystallized from Et<sub>2</sub>O to afford the desired product (517.8 mg, 90% yield) as pale yellow solid (Scheme 3.9). TLC (MeOH:CH<sub>2</sub>Cl<sub>2</sub>, 3:100 v/v): R<sub>f</sub> = 0.55; <sup>1</sup>H NMR (400 MHz, CDCl<sub>3</sub>): δ 7.44 (d, *J* = 6.9 Hz, 2H), 7.26 – 7.13 (m, 4H), 6.81 (dd, *J* = 18.5, 8.4 Hz, 2H), 6.56 (s, 1H), 5.95 (s, 2H), 5.88 (s, 1H), 5.78 (s, 1H), 3.83 (s, 3H), 3.58 (s, 3H), 3.35 – 3.24 (m, 1H), 3.11 (td, *J* = 11.6, 3.1 Hz, 1H), 3.02 – 2.89 (m, 1H), 2.70 (dt, *J* = 15.0, 3.0 Hz, 1H); <sup>13</sup>C NMR (100 MHz, CDCl<sub>3</sub>) δ 150.3, 147.2, 146.6, 144.8, 142.0, 139.0, 128.9, 128.2, 127.7, 127.4, 127.4, 125.7, 124.7, 119.0, 112.2, 107.7, 104.4, 101.0, 94.3, 62.1, 60.1, 55.9, 46.3, 30.3 [121].

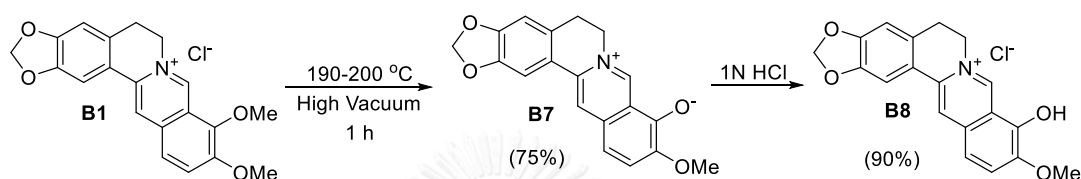


**Scheme 3.9** The synthesis of 8-phenyl-13, 14-dehydrocanadiene (**B6**)

**Berberrubine (B7):** Berberine chloride (**B1**) (1.0 g, 2.730 mmol) was stirred and heated to 190-200 °C under high vacuum atmosphere for 1 h. The reaction was cooled down to rt and obtained the desired product (658 mg, 75% yield) as red solid (Scheme 3.10). TLC (MeOH:CH<sub>2</sub>Cl<sub>2</sub>, 1:10 v/v): R<sub>f</sub> = 0.20 <sup>1</sup>H NMR (400 MHz, CDCl<sub>3</sub>): δ 9.18 (s, 1H), 7.56 (s, 1H), 7.23 (d, *J* = 7.3 Hz, 2H), 6.74 (s, 1H), 6.48 (d, *J* = 7.9 Hz, 1H), 6.05 (s, 2H), 4.40 (s, 2H), 3.89 (s, 3H), 3.08 (s, 2H); <sup>13</sup>C NMR (100 MHz, CDCl<sub>3</sub>) δ 167.8, 150.8, 149.0, 148.1, 145.6, 132.9, 131.3, 128.1, 122.2, 120.5, 120.1, 117.4, 108.3, 104.5, 102.9, 101.7, 56.1, 53.2, 28.6 [122].

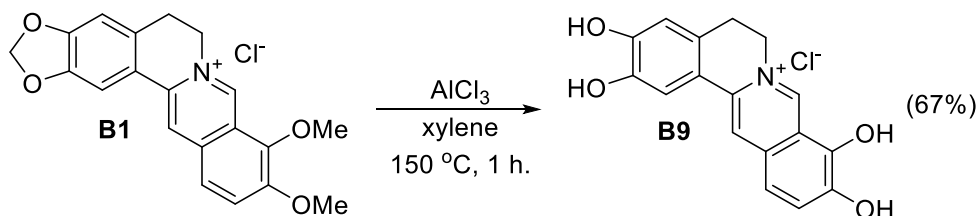
**Berberrubine chloride (B8):** Berberrubine (**B7**) (300 mg, 0.8385 mmol) was dissolved in water (1 mL) before 1 N HCl (1 mL) was added. The yellow precipitate was soon filtered and dried under high vacuum to receive the desired product (270 mg,

90% yield) as yellow solid (Scheme 3.10). TLC (MeOH:CH<sub>2</sub>Cl<sub>2</sub>, 1:10 v/v): R<sub>f</sub> = 0.25. <sup>1</sup>H NMR (400 MHz, DMSO-*d*<sub>6</sub>) δ 9.83 (s, 1H), 8.77 (s, 1H), 8.05 (d, *J* = 9.0 Hz, 1H), 7.79 – 7.65 (m, 2H), 7.05 (s, 1H), 6.14 (s, 2H), 4.87 (t, *J* = 6.1 Hz, 2H), 4.02 (s, 3H), 3.29 – 3.04 (m, 2H); <sup>13</sup>C NMR (100 MHz, DMSO-*d*<sub>6</sub>) δ 149.57, 147.59, 145.59, 145.33, 143.67, 136.53, 132.36, 130.41, 125.45, 120.55, 119.75, 118.13, 117.54, 108.36, 105.28, 101.95, 57.01, 54.97, 26.43 [122].



**Scheme 3.10** The synthesis of berberrubine (B7) and berberrubine chloride (B8)

**2,3,9,10-tetra-Hydroxyberberine chloride (B9):** Berberine chloride (B1) (2.50 g, 6.723 mmol) was dissolved in xylene (100 mL), added anhydrous AlCl<sub>3</sub> (12.5 g, 9.375 mmol) and stirred at 150 °C for 1 h. The solution of 5% HCl (250 mL) was added and heated to dissolve for 15 min. The reaction mixture was stirred at 0 °C, filtered to collect precipitate and purified by recrystallization in MeOH to afford the desired product (1.494 g, 67% yield) as pale yellow solid (Scheme 3.11). TLC (MeOH:CH<sub>2</sub>Cl<sub>2</sub>, 1:10 v/v): R<sub>f</sub> = 0.11; <sup>1</sup>H NMR (400 MHz, CD<sub>3</sub>OD): δ 9.50 (s, 1H), 8.28 (s, 1H), 7.58 (d, *J* = 8.7 Hz, 1H), 7.47 (d, *J* = 8.7 Hz, 1H), 7.33 (s, 1H), 6.68 (s, 1H), 3.21 (dt, *J* = 3.2, 1.6 Hz, 2H), 3.04 (t, *J* = 6.2 Hz, 2H). <sup>13</sup>C NMR (100 MHz, CD<sub>3</sub>OD) δ 150.4, 147.0, 145.3, 144.8, 143.1, 138.7, 134.3, 130.2, 128.4, 120.4, 119.8, 119.8, 119.5, 115.7, 113.2, 57.3, 27.8 [123].



**Scheme 3.11** The synthesis of 2,3,9,10-tetra-hydroxyberberine chloride (B9)

### 3.10 Preliminary Screening Test of Antibacterial Activity by Diffusion Method (B1-B9)

Two bacteria: *Xanthomonas oryzae* pv. *oryzae* (TB0006) and pv. *oryzicola* (TS8203) were purchased from the plant pathology research group, plant protection research and development office, Bangkok, Thailand. All compounds **B1-B9** at the concentration of 1,000  $\mu\text{M}$  in DMSO were tested for antibacterial activity against pathogens. Agar diffusion method was carried out with some modifications [124]. Firstly, these bacteria were cultivated in nutrient agar and incubated at 37 °C for 18 to 24 h. The testing used a freshly cell suspension which were standardized to cell density  $1.5 \times 10^8$  CFU/mL obtained from a McFarland turbidity standard No. 0.5 and adjusted by 0.5% sterile NaCl. The nutrient agar (19 mL) was mixed with bacterial suspension (1 mL), poured into the petri plates, and was allowed to set and harden. The required number of wells is cut using a 6 mm sterile cork borer ensuring proper distribution of wells. The tested compound solution 40  $\mu\text{L}$  was put into the well and DMSO 40  $\mu\text{L}$  was used as a negative control. The plates were incubated at 37 °C overnight. Antimicrobial activity was evaluated by measuring the diameter of the inhibition zone around the disc in duplicate.

### 3.11 Antioxidant Activity (DPPH assay)

Berberine and derivatives **B2-B9** were dissolved with 1% DMSO in EtOH and serial dilutions of all compounds were carried out to give a suitable concentration ( $\mu\text{M}$ ). A serial dilution of 3,5-di-*tert*-4-butylhydroxytoluene (BHT) was used as a positive control. All diluted compounds, 250  $\mu\text{L}$ , were added to 250  $\mu\text{L}$  of DPPH in EtOH solution (33  $\mu\text{M}$  in EtOH;  $\text{ABS} \cong 1.600$ ) in micro centrifuge tube. After incubation at rt for 20 min, the absorbance was detected at 520 nm by UV-spectrophotometer (Biotex-synergy-HT). The percentage of scavenged DPPH was measured as % inhibition from the following equation [103].

$$\% \text{ inhibition} = [(A_{\text{blank}} - A_{\text{compound}}) / A_{\text{blank}}] \times 100$$

$A_{\text{blank}}$  = absorbance of blank and  $A_{\text{compound}}$  = absorbance of compound

The concentration of compound exhibited 50% inhibition ( $IC_{50}$ ) from dose response curve was calculated and used to compare the scavenging ability of each compound. All assays were done in triplicate.

### 3.12 General Procedure of Cytotoxicity on HT1080 Cell Lines

#### 3.12.1 Dulbecco's Modified Eagle Medium (DMEM)

DMEM powder (1 pack) was brought from Gibco, Gibthai, Thailand. All of the powder in each 1 L pack was transferred in to 1 L beaker and then DI water (1.0 L),  $\text{NaHCO}_3$  (2.00 g), penicillin G sodium ( $10^5$  unit), streptomycin (100 mg) were added and well mixed with magnetic stirrer, adjusted final volume to 1 L. 1.0 N of NaOH or HCl was used to adjust final pH to 7.2. The solution was then filtered through 0.22 micron polyvinylidene fluoride membrane in laminar air flow hood, sealed and kept at  $4^\circ\text{C}$  in the refrigerator. Fetalbovine serum was inactivated in the  $56^\circ\text{C}$  water bath for 30 min.

#### 3.12.2 Phosphate Buffered Saline (PBS Buffer)

Sodium chloride (NaCl, 8.00 g), potassium chloride (KCl, 0.20 g), disodium hydrogenphosphate ( $\text{Na}_2\text{HPO}_4$ , 1.15 g), potassium dihydrogenphosphate ( $\text{KH}_2\text{PO}_4$ , 0.20 g) were dissolved in DI water (1.0 L) and stirred with magnetic stirrer. 1.0 N NaOH or HCl was used to adjust the final pH to 7.4. Final volume was adjusted to 1 L and then the solution was autoclaved.

#### 3.12.3 0.02% EDTA solution

Ethylenediaminetetraacetic acid (EDTA, 0.02 g) was added into phosphate buffer saline (100 mL), well mixed and filtered through 0.22 micron polyvinylidene fluoride membrane and kept at rt.



#### 3.12.4 0.1% Trypsin

Trypsin (0.10 g) was added into phosphate buffer saline (100 mL), well mixed and filtered through 0.22 micron polyvinylidene fluoride membrane and kept at 4°C in the refrigerator. The working solution was obtained by mixing the same volume of 0.1% trypsin solution and 0.02% EDTA solution for using in cell harvest.

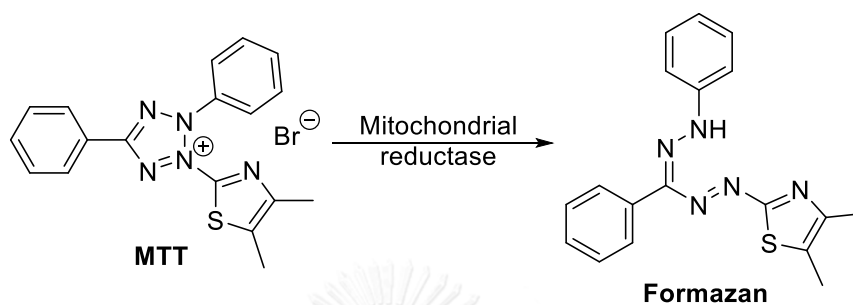
#### 3.13 Cell Cultures

The human fibrosarcoma cells (HT1080), received from Professor Thompson EW, Department of Surgery, St. Vincent's Hospital, the University of Melbourne, Australia, were treated in Dulbecco's Modified Eagle Medium (DMEM) (Gibco BRL) supplemented with 10% fetal bovine serum (FBS) (Gibco BRL), 100 U/mL penicillin (Gibco BRL), and 100  $\mu\text{g}/\text{mL}$  streptomycin (Gibco BRL). The cells were kept in a CO<sub>2</sub> incubator at 37 °C with humidified air containing 5% CO<sub>2</sub> until 80% confluence and then subcultured twice a week [125].

#### 3.14 Cytotoxic Assay

The cytotoxic effect to the human fibrosarcoma cell (HT1080) of berberine and its derivatives was explored *via* the proliferation assay using 3-(4,5- dimethylthiazol-2-yl)-2, 5-diphenyltetrazolium bromide (MTT) reagent as reported previously with some modification [125, 126]. Briefly, the cells were seeded in 48-well tissue culture plates at a density of 60,000, 30,000 and 20,000 cells/well for 1-, 4-, and 7-day treatments, respectively and grown to 80% confluency. Briefly, the cells were seeded in 48-well tissue culture plates at a density of 60,000, 30,000, and 20,000 cells/well for 1-, 4-, and 7-day treatments, respectively and grown to 80% confluency. After that, they were treated with several concentrations of berberine, 0.05 to 1.0  $\mu\text{M}$ , and its derivatives, 1 to 12  $\mu\text{M}$ , for 1, 4, and 7 days. After incubation, the cells were washed twice with phosphate-buffered saline and 300  $\mu\text{L}$  of free-serum culture medium containing 1 mg/mL of MTT was added into each well and incubated further for 1 h. The medium

containing MTT was then replaced with 200  $\mu\text{L}$  of DMSO. The blue crystals of the oxidized MTT (formazan) (Scheme 3.12) were quantified by spectrophotometry at 570 nm using ELISA microplate reader (Biotex-synergy-HT). Percentage of proliferation was plotted against control (untreated) group. All assays were done in triplicate.



**Scheme 3.12** Reduction of MTT to formazan

### 3.15 RNA Extraction and Reverse Transcriptase PCR

Cells were treated with berberine chloride (**B1**) and its derivatives **B7-B9** at 0.1 and 1.0  $\mu\text{M}$  for 7 days. Then, total RNA from treated and non-treated fibrosarcoma cells were isolated using Trizol reagent (Invitrogen, USA). RNA purification and concentration were checked by measuring the absorbance at 260 and 280 nm. Same amount of RNA from each sample were taken for reverse transcription into cDNA using SuperScript RT kit (Invitrogen, USA) according to the manufacturer's instructions.

The primers (Table 3.1) were designed based on the sequences in the GenBank and used to amplify the target genes, SOD, CAT and GAPDH using i-Taq kit (iNtRON Biotechnology). The PCR products from Bio-Rad C1000 were electrophoretically analyzed on a 2% agarose gel, stained by 2% ethidium bromide and photographed. Each sample was assayed in triplicate [127, 128].

**Table 3.1** List of primers used for PCR amplification

Gene	Nucleotide sequence (5' – 3')	Size (bp)
SOD	GAGACTTGGGCAATGTGACTG	201
	TTACACCACAAGCCAAACGA	
CAT	CCTGGAGCACAGCATCCAAT	85
	GAATGCCCGCACCTGAGTAA	
GAPDH	AGTCCACTGGCGTCTTCACC	119
	GTTCACACCCATGACGAACATG	

### 3.16 Statistical Analysis

SPSS (IBM Singapore Pte Ltd; Registration No.1975-01566-C) was used for statistical analyses. Data are expressed as the means of at least three individual experiments  $\pm$  standard deviation of control. Statistical significance was determined when  $p < 0.05$ . The Student's t-test was used for statistical comparisons between groups.

## III. Results and Discussion

### 3.17 Extraction of Berberine Chloride (B1) from *C. fenestratum*

The vines of *C. fenestratum* were ground to small pieces and soaked in MeOH for 5 days (3 times). The solution was acidified with conc. HCl to adjust pH = 2 and

was filtered to collect yellow precipitate which was recrystallized in MeOH to obtain berberine chloride (**B1**) as a yellow solid in 4.8 %yield (Figure 3.13). It was confirmed by  $^1\text{H}$  and  $^{13}\text{C}$  NMR [17].

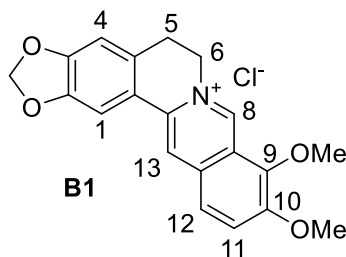


**Figure 3.13** The structure of berberine chloride (**B1**)

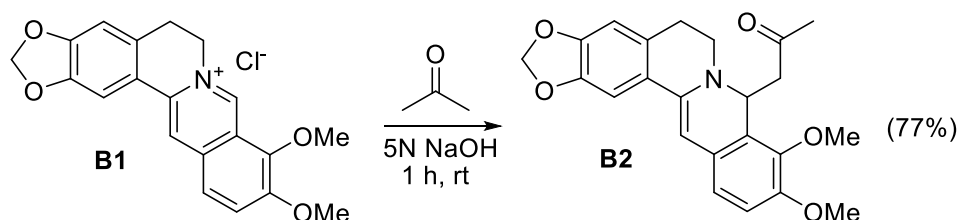
The  $^1\text{H}$  NMR spectrum of berberine chloride (**B1**) (Figure A54) exhibited aromatic proton signals of H-8 at  $\delta_{\text{H}}$  9.65 as singlet, H-13 at  $\delta_{\text{H}}$  8.54 as singlet, H-11 at  $\delta_{\text{H}}$  7.99 as doublet ( $J = 9.0$  Hz), H-12 at  $\delta_{\text{H}}$  7.88 as doublet ( $J = 9.0$  Hz), H-1 at  $\delta_{\text{H}}$  7.50 as singlet and H-4 at  $\delta_{\text{H}}$  6.84 as singlet. Methylene proton signal ( $\text{OCH}_2\text{O}$ ) was found at  $\delta_{\text{H}}$  5.99 as singlet and two methylene proton signals were detected at  $\delta_{\text{H}}$  4.83 (H-6) as triplet ( $J = 6.4$  Hz) and 3.13 (H-5) as triplet ( $J = 6.2$  Hz). Two methoxy proton signals were observed at  $\delta_{\text{H}}$  4.09 (H-9) and 3.99 (H-10) as singlet [129].

The  $^{13}\text{C}$  NMR spectrum (Figure A55) showed aromatic carbon signals at  $\delta_{\text{C}}$  152.2 (C-3), 152.0 (C-10), 149.9 (C-2), 146.3 (C-8), 145.8 (C-9), 139.6 (C-13a), 135.2 (C-12a), 131.9 (C-4a), 128.1 (C-11), 124.6 (C-12), 123.3 (C-8a), 121.8 (C-13), 121.5 (C-13b), 109.4 (C-4) and 106.5 (C-1). The methylene carbon signal ( $\text{OCH}_2\text{O}$ ) was visualized at  $\delta_{\text{C}}$  103.7 and two methoxy carbon signals were found at  $\delta_{\text{C}}$  62.6 (C-9) and 57.7 (C-10). Two methylene carbon signals were observed at  $\delta_{\text{C}}$  57.2 (C-6) and 28.2 (C-5) [129].

### 3.18 Synthesis of Berberine Derivative B2-B9

Berberine chloride (**B1**) was used as a lead structure to synthesize several derivatives for SAR study of antibacterial, antioxidant and cytotoxic activities. Acetylberberine (**B2**) was synthesized from berberine chloride (**B1**) (Scheme 3.13) by reacting

with acetone in 5N NaOH for 1 h at rt to give the desired product in 77% yield as bright yellow powder [21].

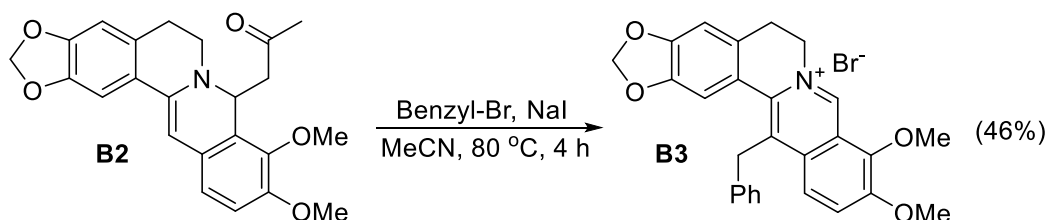


**Scheme 3.13** The synthesis of acetyl-berberine (**B2**)

The <sup>1</sup>H NMR spectrum of acetyl-berberine (**B2**) (Figure A56) revealed aromatic proton signals of H-1 at  $\delta_{\text{H}}$  7.15 as singlet, H-11 and H-12 at  $\delta_{\text{H}}$  6.78 as multiplet, H-4 at  $\delta_{\text{H}}$  6.60 as singlet, H-8 at  $\delta_{\text{H}}$  5.35 as doublet of doublets ( $J = 7.0, 4.1$  Hz). Methylene proton signal (OCH<sub>2</sub>O) was found at  $\delta_{\text{H}}$  5.97 as doublet ( $J = 2.4$  Hz) and methylene proton signals were detected at  $\delta_{\text{H}}$  3.37 (H-6) as multiplet and 2.85 (H-5) as multiplet. The methylene proton signal (CH<sub>2</sub>CO) was visualized at  $\delta_{\text{H}}$  3.09 as doublet of doublets ( $J = 15.4, 7.0$  Hz) and 2.43 as doublet of doublets ( $J = 15.5, 4.0$  Hz). Two methoxy proton signals were observed at  $\delta_{\text{H}}$  3.92 and 3.86 as singlet. The methyl proton signal (COCH<sub>3</sub>) was observed at  $\delta_{\text{H}}$  2.07 as singlet [21].

The <sup>13</sup>C NMR spectrum (Figure A57) showed the carbonyl carbon signal at  $\delta_{\text{C}}$  207.3 and aromatic carbon signals at  $\delta_{\text{C}}$  150.1 (C-10), 147.3 (C-9), 146.6 (C-3), 143.7 (C-2), 138.5 (C-13a), 129.0 (C-4a), 127.8 (C-12a), 125.6 (C-13b), 123.6 (C-8a), 118.6 (C-12), 112.1 (C-11), 107.9 (C-4), 104.2 (C-1) and 95.1 (C-13). The methylene carbon signal (OCH<sub>2</sub>O) was assigned for  $\delta_{\text{C}}$  101.0 and two methoxy carbon signals were found at  $\delta_{\text{C}}$  60.7 (C-9) and 56.1 (C-10). Three methylene carbon signals were detected at  $\delta_{\text{C}}$  47.7 (C-6), 30.8 (C-5) and 46.2 (CH<sub>2</sub>CO). The tertiary carbon signal (C-8) was observed at  $\delta_{\text{C}}$  54.3, while methyl carbon signal was found at  $\delta_{\text{C}}$  30.4 [21].

Acetylonyl-berberine (**B2**) was reacted with benzyl bromide and NaI undergo electrophilic aromatic substitution at C-13 in MeCN at 80 °C for 4 h to furnish 13-benzyl-berberine (**B3**) (Scheme 3.14) in 46% yield as dark yellow solid [21].

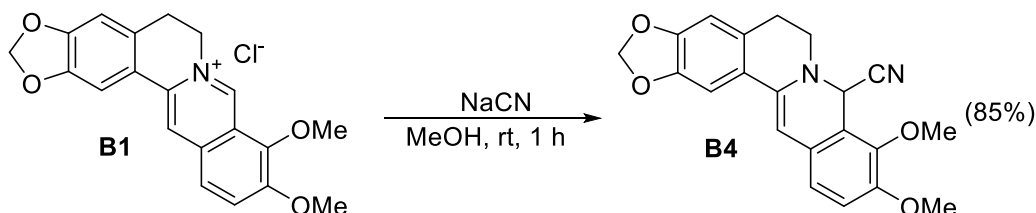


**Scheme 3.14** The synthesis of 13-benzyl-berberine (**B3**)

The  $^1\text{H}$  NMR spectrum of 13-benzyl-berberine (**B3**) (Figure A58) exhibited aromatic proton signals of H-8 at  $\delta_{\text{H}}$  10.60 as singlet, H-11 at  $\delta_{\text{H}}$  7.68 as doublet ( $J = 9.4$  Hz), H-12 at 7.60 as doublet ( $J = 9.3$  Hz), H-1 at  $\delta_{\text{H}}$  6.94 as singlet, H-4 at  $\delta_{\text{H}}$  6.87 as singlet. Benzyl proton signals were observed at  $\delta_{\text{H}}$  7.37 as triplet ( $J = 7.3$  Hz, 3H), 7.31 as doublet ( $J = 6.9$  Hz, 2H) and methylene proton signal ( $\text{CH}_2\text{Ph}$ ) at  $\delta_{\text{H}}$  4.67 as singlet. Methylene proton signal ( $\text{OCH}_2\text{O}$ ) was found at  $\delta_{\text{H}}$  5.99 as singlet whereas methylene proton signals were presented at  $\delta_{\text{H}}$  5.28 (H-6) as multiplet and 3.28 (H-5) as multiplet. The methylene proton signal ( $\text{CH}_2\text{CO}$ ) was found at  $\delta_{\text{H}}$  3.09 as doublet of doublets ( $J = 15.4, 7.0$  Hz) and 2.43 as doublet of doublets ( $J = 15.5, 4.0$  Hz). Two methoxy proton signals were observed at  $\delta_{\text{H}}$  4.40 (H-9) and 4.01 (H-10) as singlet [21].

The  $^{13}\text{C}$  NMR spectrum (Figure A59) displayed aromatic carbon signals at  $\delta_{\text{C}}$  150.5 (C-10), 147.0 (C-9), 149.9 (C-3), 146.4 (C-9), 147.1 (C-2), 133.8 (C-13), 137.4 (C-13a), 129.9 (C-13b), 120.0 (C-4a), 120.8 (C-12), 133.7 (C-12a), 121.9 (C-8a), 125.6 (C-11), 108.5 (C-4), 108.8 (C-1). Benzyl carbon signals were observed at  $\delta_{\text{C}}$  138.2, 129.5, 127.9, 127.3 and methylene carbon signal ( $\text{CH}_2\text{Ph}$ ) at  $\delta_{\text{C}}$  36.5. The methylene carbon signal ( $\text{OCH}_2\text{O}$ ) was detected at  $\delta_{\text{C}}$  101.9 and two methoxy carbon signals were found at  $\delta_{\text{C}}$  63.3 (C-9) and 56.7 (C-10). Two methylene carbon signals were observed at  $\delta_{\text{C}}$  56.8 (C-6) and 28.5 (C-5) [21].

Berberine chloride (**B1**) was reacted with NaCN *via* nucleophilic addition at C-8 (Scheme 3.15) in MeOH at rt for 1 h to give 8-cyano-13,14-dehydrocanadiene (**B4**) in 85% yield as pale yellow solid [119].

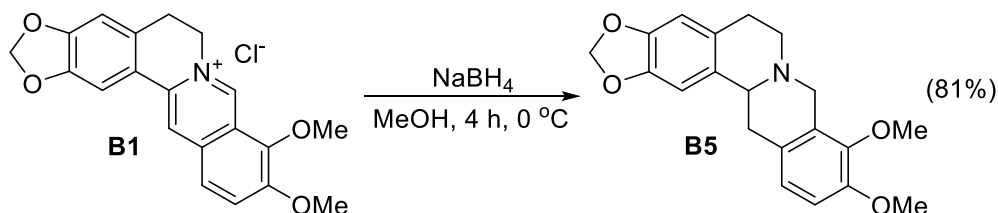


**Scheme 3.15** The preparation of 8-cyano-13,14-dehydrocanadiene (**B4**)

The <sup>1</sup>H NMR spectrum of 8-cyano-13,14-dehydrocanadiene (**B4**) (Figure A60) showed aromatic proton signals of H-1 at  $\delta_{\text{H}}$  7.19 as singlet, H-11 and H-12 at  $\delta_{\text{H}}$  6.89 as doublet of doublets ( $J = 19.5, 8.4$  Hz), H-4 at  $\delta_{\text{H}}$  6.62 as singlet, H-13 at  $\delta_{\text{H}}$  6.17 as singlet. The proton signal of H-8 was detected at  $\delta_{\text{H}}$  5.78 as singlet. Methylene proton signal (OCH<sub>2</sub>O) was found at  $\delta_{\text{H}}$  5.99 as doublet of doublets ( $J = 6.4, 1.2$  Hz). Two methylene proton signals of H-6 were assigned at  $\delta_{\text{H}}$  3.45 as multiplet and 3.05 as doublet of triplets ( $J = 10.9, 4.3$  Hz) and those of H-5 were observed at  $\delta_{\text{H}}$  3.29 as multiplet and 2.86 as doublet of triplets ( $J = 15.3, 2.8$  Hz). Two methoxy proton signals were observed at  $\delta_{\text{H}}$  4.00 (H-9) and 3.90 (H-10) as singlet [119].

The <sup>13</sup>C NMR spectrum (Figure A61) displayed aromatic carbon signals at  $\delta_{\text{C}}$  150.7 (C-2), 147.8 (C-3), 147.0 (C-9), 144.5 (C-10), 138.4 (C-4a), 128.5 (C-8a), 127.0 (C-12a), 124.2 (C-13b), 119.8 (C-1), 117.1 (C-13a), 113.9 (C-4), 107.8 (C-11), 104.2 (C-12) and 98.2 (C-13). The cyano carbon signal was found at  $\delta_{\text{C}}$  116.6, while the carbon signal of C-8 was appeared at  $\delta_{\text{C}}$  50.0. The methylene carbon signal (OCH<sub>2</sub>O) was detected at  $\delta_{\text{C}}$  101.2 and two methoxy carbon signals were found at  $\delta_{\text{C}}$  60.9 (C-9) and 56.1 (C-10). Two methylene carbon signals were observed at  $\delta_{\text{C}}$  48.0 (C-6) and 29.6 (C-5) [119].

The reduction of berberine chloride (**B1**) (Scheme 3.16) could be accomplished using  $\text{NaBH}_4$  at  $0\text{ }^\circ\text{C}$  for 4 h in MeOH to provide canadine (**B5**) in 81% as pale yellow solid [120].



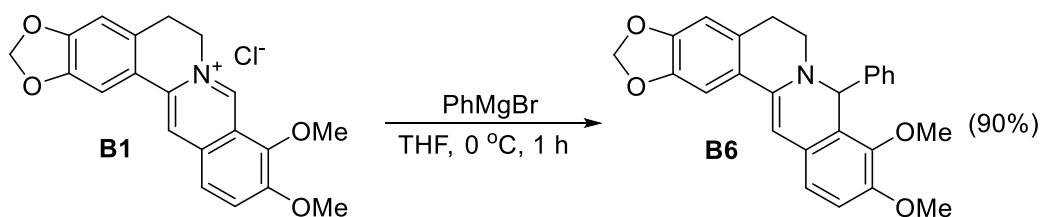
**Scheme 3.16** The preparation of canadine (**B5**)

The  $^1\text{H}$  NMR spectrum of canadine (**B5**) (Figure A62) exhibited aromatic proton signals of H-11 at  $\delta_{\text{H}}$  6.89 as doublet ( $J = 8.4$  Hz), H-12 at  $\delta_{\text{H}}$  6.81 as doublet ( $J = 8.4$  Hz), H-1 at  $\delta_{\text{H}}$  6.76 as singlet and H-4 at  $\delta_{\text{H}}$  6.61 as singlet. Methylene proton signal ( $\text{OCH}_2\text{O}$ ) was found at  $\delta_{\text{H}}$  5.94 as singlet. Four methylene proton signals were detected at  $\delta_{\text{H}}$  3.30 – 3.09 (H-6 and H-13) as multiplet, 2.73 – 2.59 (H-5) as multiplet and 4.26 (H-8) as singlet and H-13a at  $\delta_{\text{H}}$  3.54 as multiplet. Two methoxy proton signals were observed at  $\delta_{\text{H}}$  3.87 as singlet (6H) [120].

The  $^{13}\text{C}$  NMR spectrum (Figure A63) showed aromatic carbon signals at  $\delta_{\text{C}}$  150.4 (C-10), 147.2 (C-2), 146.8 (C-3), 145.0 (C-9), 130.9 (C-13b), 128.6 (C-8a), 127.8 (C-4a), 127.7 (C-12a), 123.8 (C-12), 111.1 (C-11), 108.4 (C-4) and 105.5 (C-1). The methylene carbon signal ( $\text{OCH}_2\text{O}$ ) was visualized at  $\delta_{\text{C}}$  100.7 and two methoxy carbon signals were detected at  $\delta_{\text{C}}$  59.5 (C-9) and 55.9 (C-10). Tertiary carbon signal (C-13a) was found at  $\delta_{\text{C}}$  60.7. Four methylene carbon signals were observed at  $\delta_{\text{C}}$  53.9 (C-8), 51.4 (C-6), and 36.4 (C-5) and 29.1 (C-13) [120].

8-Phenyl-13,14-dehydrocanadiene (**B6**) could be prepared from reacting berberine chloride (**B1**) with 1.0 M  $\text{PhMgBr}$  solution in dried THF at  $0\text{ }^\circ\text{C}$  for 1 h to give the desired product in 90% yield as pale yellow solid (Scheme 3.17) [121].





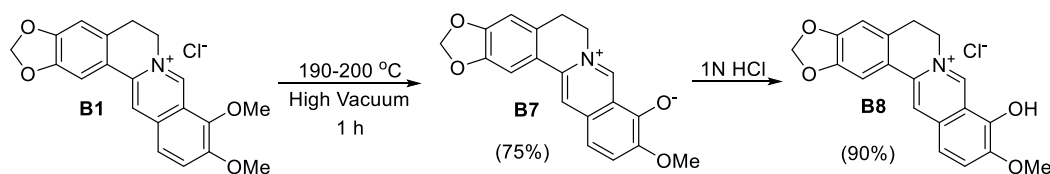
**Scheme 3.17** The preparation of 8-phenyl-13,14-dehydrocanadiene (**B6**)

The  $^1\text{H}$  NMR spectrum of 8-cyano-13,14-dehydrocanadiene (**B4**) (Figure A64) showed aromatic proton signals of H-1 at  $\delta_{\text{H}}$  7.13 as singlet, H-11 and H-12 at  $\delta_{\text{H}}$  6.81 as doublet of doublets ( $J = 18.5, 8.4$  Hz), H-4 at  $\delta_{\text{H}}$  6.56 as singlet, H-13 at  $\delta_{\text{H}}$  5.88 as singlet. Phenyl proton signals were observed at  $\delta_{\text{H}}$  7.44 as doublet ( $J = 6.9$  Hz, 2H) and 7.26 – 7.20 as multiplet (3H). The proton signal of H-8 was assigned at  $\delta_{\text{H}}$  5.78 as singlet. Methylene proton signal ( $\text{OCH}_2\text{O}$ ) was found at  $\delta_{\text{H}}$  5.95 as singlet. Two methylene proton signals of H-6 were detected at  $\delta_{\text{H}}$  3.35 – 3.24 as multiplet and 3.11 as triplet of doublets ( $J = 11.6, 3.1$  Hz) and H-5 were observed at  $\delta_{\text{H}}$  3.02 – 2.89 as multiplet and 2.70 as doublet of triplets ( $J = 15.0, 3.0$  Hz). Two methoxy proton signals were observed at  $\delta_{\text{H}}$  3.83 (H-9) and 3.58 (H-10) as singlet [121].

The  $^{13}\text{C}$  NMR spectrum (Figure A65) exhibited aromatic carbon signals at  $\delta_{\text{C}}$  150.3 (C-2), 147.2 (C-3), 146.6 (C-9), 144.8 (C-10), 139.0 (C-4a), 128.9 (C-8a), 127.3 (C-12a), 124.7 (C-13b), 119.0 (C-1), 127.5 (C-13a), 112.2 (C-4), 107.7 (C-11), 104.4 (C-12) and 94.3 (C-13). The phenyl carbon signals were observed at  $\delta_{\text{C}}$  142.0, 128.2, 127.7 and 125.7. The carbon signal of C-8 was detected at  $\delta_{\text{C}}$  62.1. The methylene carbon signal ( $\text{OCH}_2\text{O}$ ) was appeared at  $\delta_{\text{C}}$  101.0, while two methoxy carbon signals were found at  $\delta_{\text{C}}$  60.1 (C-9) and 55.9 (C-10). Two methylene carbon signals were observed at  $\delta_{\text{C}}$  46.3 (C-6) and 30.3 (C-5) [121].

Berberubine (**B7**) could be synthesized from berberine chloride (**B1**) *via* heating at 190-200 °C under high vacuum atmosphere for 1 h to furnish demethylation at C-9 (Scheme 3.18) and gave the desired product in 75% yield as dark red solid. Moreover,

berberrubine (**B7**) was acidified with 1N HCl to afford berberrubine chloride (**B8**) (Scheme 3.18) in 90% as yellow solid [122].



**Scheme 3.18** The synthesis of berberrubine (**B7**) and berberrubine chloride (**B8**)

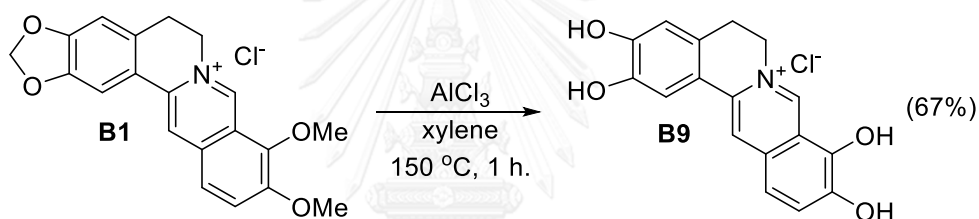
The  $^1\text{H}$  NMR spectrum of berberrubine (**B7**) (Figure A66) showed aromatic proton signals of H-8 at  $\delta_{\text{H}}$  9.18 as singlet, H-13 at  $\delta_{\text{H}}$  7.56 as singlet, H-11 and H-12 at  $\delta_{\text{H}}$  7.23 as doublet ( $J = 7.3$  Hz), H-1 at  $\delta_{\text{H}}$  6.74 as singlet and H-4 at  $\delta_{\text{H}}$  6.48 as singlet. Methylene proton signal ( $\text{OCH}_2\text{O}$ ) was found at  $\delta_{\text{H}}$  6.05 as singlet and two methylene proton signals were detected at  $\delta_{\text{H}}$  4.40 (H-6) as multiplet and 3.08 (H-5) as multiplet. The methoxy proton signals were observed at  $\delta_{\text{H}}$  3.89 (H-10) as singlet [122].

The  $^{13}\text{C}$  NMR spectrum (Figure A67) showed carbonyl aromatic carbon signals at  $\delta_{\text{C}}$  167.8 (C-8), 150.8 (C-3), 149.0 (C-10), 148.1 (C-2), 145.6 (C-9), 132.9 (C-13a), 131.3 (C-12a), 128.1 (C-4a), 122.2 (C-11), 120.5 (C-12), 120.1 (C-8a), 117.4 (C-13), 108.3 (C-13b), 104.5 (C-4) and 102.9 (C-1). The methylene carbon signal ( $\text{OCH}_2\text{O}$ ) was detected at  $\delta_{\text{C}}$  101.7 and the methoxy proton signals were found at  $\delta_{\text{C}}$  56.1 (C-10). Two methylene carbon signals were observed at  $\delta_{\text{C}}$  53.2 (C-6) and 28.6 (C-5) [122].

The  $^1\text{H}$  NMR spectrum of berberrubine chloride (**B8**) (Figure A68) revealed aromatic proton signals of H-8 at  $\delta_{\text{H}}$  9.83 as singlet, H-13 at  $\delta_{\text{H}}$  8.77 as singlet, H-11 8.05 as doublet ( $J = 9.0$  Hz), H-12 and H-1 at  $\delta_{\text{H}}$  7.79 – 7.65 as multiplet and H-4 at  $\delta_{\text{H}}$  7.05 as singlet. Methylene proton signal ( $\text{OCH}_2\text{O}$ ) was visualized at  $\delta_{\text{H}}$  6.14 as singlet, while the methylene proton signals were detected at  $\delta_{\text{H}}$  4.87 (H-6) as triplet ( $J = 6.1$  Hz) and 3.29 – 3.04 (H-5) as multiplet. The methoxy proton signals were observed at  $\delta_{\text{H}}$  4.02 (H-10) as singlet.

The  $^{13}\text{C}$  NMR spectrum (Figure A69) showed carbonyl aromatic carbon signals at  $\delta_{\text{C}}$  149.6 (C-3), 147.6 (C-10), 145.6 (C-2), 145.3 (C-8), 143.7 (C-9), 136.5 (C-13a), 132.4 (C-12a), 130.4 (C-4a), 125.4 (C-11), 120.5 (C-12), 119.8 (C-8a), 118.1 (C-13), 117.5 (C-13b), 108.4 (C-4) and 105.3 (C-1). The methylene carbon signal ( $\text{OCH}_2\text{O}$ ) could be assigned at  $\delta_{\text{C}}$  101.9, while the methoxy proton signals was found at  $\delta_{\text{C}}$  57.0 (C-10). Two methylene carbon signals were observed at  $\delta_{\text{C}}$  55.0 (C-6) and 26.4 (C-5).

2,3,9,10-*tetra*-Hydroxyberberine chloride (**B9**) could be synthesized from the reaction of berberine chloride (**B1**) with  $\text{AlCl}_3$  in xylene at  $150\text{ }^\circ\text{C}$  for 1 h (Scheme 3.19) to remove two methyl groups (C-9 and C-10) and methylene group yielding the desired product in 67% yield as pale yellow solid [123].



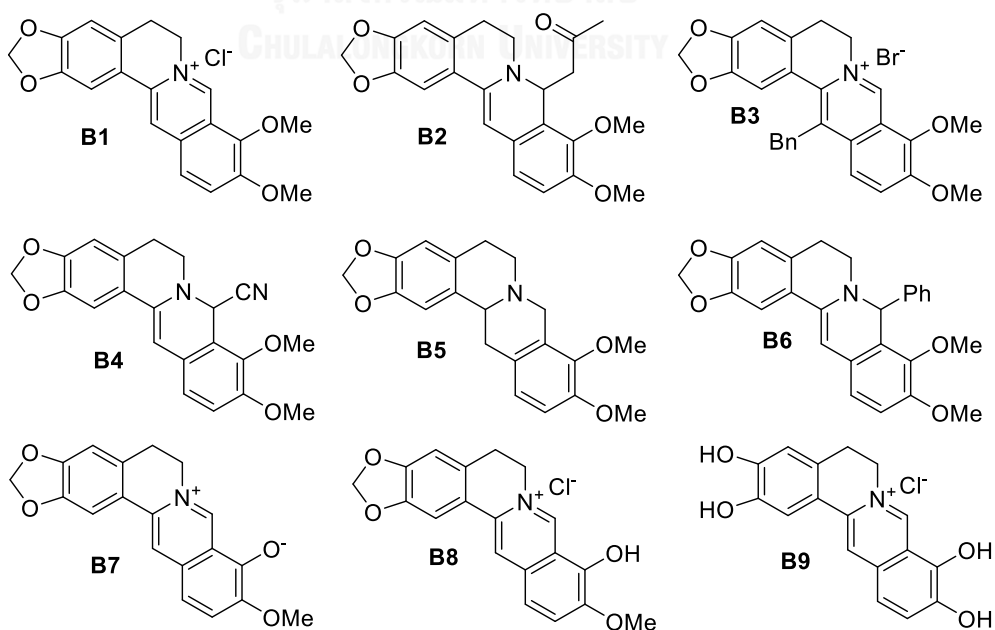
**Scheme 3.19** The synthesis of 2,3,9,10-*tetra*-hydroxyberberine chloride (**B9**)

The  $^1\text{H}$  NMR spectrum of 2,3,9,10-*tetra*-Hydroxyberberine chloride (**B9**) (Figure A70) displayed aromatic proton signals of H-8 at  $\delta_{\text{H}}$  9.50 as singlet, H-13 at  $\delta_{\text{H}}$  8.28 as singlet, H-11 at  $\delta_{\text{H}}$  7.58 as doublet ( $J = 8.7\text{ Hz}$ ), H-12 at  $\delta_{\text{H}}$  7.47 as doublet ( $J = 8.7\text{ Hz}$ ), H-1 at  $\delta_{\text{H}}$  7.33 as singlet and H-4 at  $\delta_{\text{H}}$  6.68 as singlet. Two methylene proton signals were detected at  $\delta_{\text{H}}$  3.21 (H-6) as doublet of triplets ( $J = 3.2, 1.6\text{ Hz}$ ) and 3.04 (H-5) as triplet ( $J = 6.2\text{ Hz}$ ). The  $^{13}\text{C}$  NMR spectrum (Figure A71) exhibited aromatic carbon signals at  $\delta_{\text{C}}$  150.4 (C-3), 147.0 (C-10), 145.3 (C-2), 143.8 (C-8), 143.1 (C-9), 138.7 (C-13a), 134.3 (C-12a), 130.2 (C-4a), 128.4 (C-11), 120.4 (C-12), 119.8 (C-8a), 119.6 (C-13), 119.5 (C-13b), 115.7 (C-4) and 113.2 (C-1). Two methylene carbon signals were observed at  $\delta_{\text{C}}$  57.3 (C-6) and 27.8 (C-5) [123].

### 3.19 The Preliminary Results of Antibacterial Activity of Berberine and Its Derivatives B2-B9

Berberine chloride (**B1**) and its derivatives **B2-B9** were tested for antibacterial activity against *X. oryzae* pv. *oryzae* and *X. oryzae* pv. *oryzicola* at 1.0 mM in triplicate. The preliminary result (Table 3.2) showed that compound **B1** gave a moderate inhibition against these two bacteria. The phenolic-OH at C-9 of compounds **B7** and **B8** demonstrated a moderate activity to inhibit only *X. oryzae* pv. *oryzae*. The nucleophilic addition of acetyl, cyano and phenyl groups to C-8 yielding compounds **B2**, **B4**, and **B6**, respectively was conducted. Compound **B5**, derived from the hydrogenation of two double bonds at C-8 and C-13, was inactive. Moreover the full demethylation at C-9 and 10 and demethylenation at methylene group (-OCH<sub>2</sub>O-) was carried on providing compound **B9**. Those synthesized compounds (**B2**, **B4**, **B5**, **B6** and **B9**) were inactive. Only compound **B3** with a benzyl group at C-13, displayed better activity than berberine chloride (**B1**) against *X. oryzae* pv. *oryzae* and *X. oryzae* pv. *oryzicola*.

**Table 3.2** Antibacterial activity of berberine chloride (**B1**) and its derivatives **B2-B9**



Compounds	Clear zone (mm)	
	<i>X. oryzae</i> pv. <i>oryzae</i>	<i>X. oryzae</i> pv. <i>oryzicola</i>
Berberine chloride ( <b>B1</b> )	5.00 ± 0.70	5.00 ± 0.70
Acetonylberberine ( <b>B2</b> )	0.00 ± 0.00	0.00 ± 0.00
13-Benzylberberine ( <b>B3</b> )	10.0 ± 0.00	8.30 ± 1.00
8-Cyano-7,8-dihydroberberine ( <b>B4</b> )	0.00 ± 0.00	0.20 ± 0.00
Canadiene ( <b>B5</b> )	0.00 ± 0.00	0.00 ± 0.00
8-Phenyl-7,8-dihydroberberine ( <b>B6</b> )	1.50 ± 0.70	3.00 ± 0.00
Berberubine ( <b>B7</b> )	4.80 ± 0.30	0.00 ± 0.00
Berberubine chloride ( <b>B8</b> )	4.10 ± 2.00	0.00 ± 0.00
2,3,9,10- <i>tetra</i> -Hydroxyberberine chloride ( <b>B9</b> )	0.00 ± 0.00	0.00 ± 0.00
Control (DMSO)	0.00 ± 0.00	0.00 ± 0.00

<sup>a</sup> concentration of compounds: 1.0 mM

The SAR study of compounds **B1-B9** against *X. oryzae* pv. *oryzae* and *X. oryzae* pv. *oryzicola* indicated that the methylenedioxy (-OCH<sub>2</sub>O-) and two methoxy groups at C-9 and 10 seemed to be important for antibacterial activity. In addition, the aromaticity of isoquinoline ring demonstrated an important role for this activity. Only the benzyl group at C-13 in compound **B3** influenced the antibacterial activity against these two bacteria.

### 3.20 The Antioxidant Activity of Berberine (B1) and Its Derivatives B2-B9

Berberine chloride (**B1**) and its derivative **B2-B9** were selected to determine IC<sub>50</sub> using DPPH assay (33 μM in EtOH). The results (Figure 3.14) displayed that compounds **B1-B4** and **B6** did not show the antioxidant activity with an IC<sub>50</sub> > 500 μM.

Compounds **B5** and **B7** showed a moderate antioxidant activity with an  $IC_{50}$   $97.15 \pm 4.52$  and  $87.35 \pm 6.65 \mu\text{M}$ , respectively. Nonetheless, compounds **B8** and **B9** gave better activity ( $IC_{50}$   $55.24 \pm 2.24$  and  $10.72 \pm 1.76 \mu\text{M}$ , respectively) than standard BHT ( $IC_{50} = 72.74 \pm 7.22 \mu\text{M}$ ).

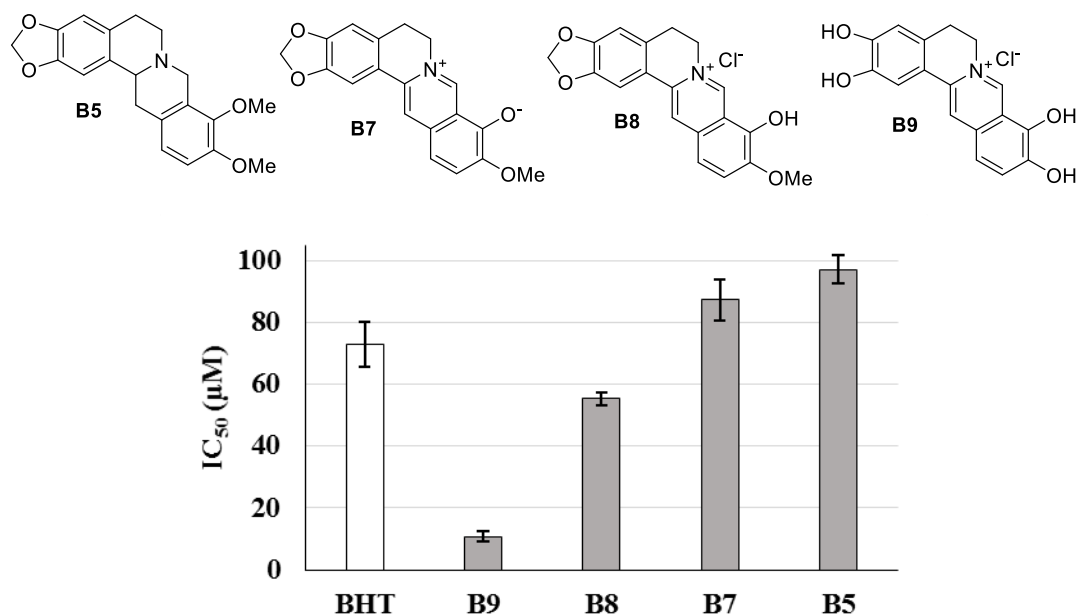


**Figure 3.14** The  $IC_{50}$  of compounds **B5**, **B7**, **B8**, **B9** and BHT

Most of the active antioxidants contain more than one active functional group such as  $\text{NH}_2$  or  $\text{OH}$  in *ortho* position. That is the reason why catechol, containing two hydroxyl groups in *ortho* position, is classified as the most active antioxidant compounds due to the ability to trap two peroxy radicals [130]. The more phenolic groups were believed to produce more antioxidant activity as found in the previous report [131].

These phenolic derivatives were synthesized including compound **B7** with single phenolate, compound **B8** with single phenolic-OH and a chloride, and compound **B9** with four phenolic OH (two catechol-like structures). All compounds were characterized by  $^1\text{H}$  and  $^{13}\text{C}$  NMR and well matched with reference structures in previous work [17, 122, 123]

From DPPH assay, compounds **B7-B9** exhibited good antioxidant activity with  $IC_{50}$  lower than  $100 \mu M$ , whereas berberine (**B1**) was higher than  $500 \mu M$ . Compounds **B8** and **B9** exhibited better DPPH scavenging activity than the standard antioxidant, BHT. Compound **B9** exhibited the best antioxidant activity probably due to the presence of 1,2 hydroxyl groups in its molecule as mentioned in the previous report [132]. The better free radical scavenging activity of two hydroxyl groups in *ortho* position should be firstly functioned through the abstraction of first hydrogen atom to generate the stable phenoxy radical *via* an intramolecular hydrogen bonding and followed by second abstraction [132]. For compounds **B7** and **B9** containing single phenolic-OH, the addition of chloride into the molecule could significantly increase the scavenging activity.

### 3.21 The Results of Cytotoxicity of Compounds B1 and B7-B9

The human fibrosarcoma cells (HT1080) were treated with berberine chloride (**B1**) and its phenolic derivatives **B7-B9** for 1, 4 and 7 days. MTT assay was used to determine the viable and dead cells. The % proliferation was calculated compared to control (untreated cells) and was expressed as mean  $\pm$  standard deviation. The results of cytotoxicity (Figure 3.15) showed that compounds **B1**, **B7** and **B9** significantly decreased viability of HT1080 at all concentrations with both dose- and time-dependent fashion ( $p < 0.05$ ). Compounds **B1**, **B7** and **B9** showed the  $IC_{50}$  at  $0.44 \pm 0.03$ ,  $6.05 \pm 0.64$  and  $2.88 \pm 0.23 \mu M$ , respectively, for 7 days. The  $IC_{50}$  for compound **B8** was not able to determine due to the higher value more than  $12 \mu M$ .

Compounds **B7-B9** with good scavenging activity were further investigated with the human fibrosarcoma cell due to the relationship between antioxidant activity and chemoprevention previously reported [103, 128]. For cytotoxicity assay,  $IC_{50}$  at 1- and 4-day treatments could not be calculated because the survival cells were higher than 50%. The values at 7-day treatment of compound **B8** could not be estimated either.

The sequence of  $IC_{50}$  at 7-day treatment was **B1** < **B9** < **B7** ( $0.44 \pm 0.03$ ,  $2.88 \pm 0.23$ , and  $6.05 \pm 0.64 \mu\text{M}$ , respectively).

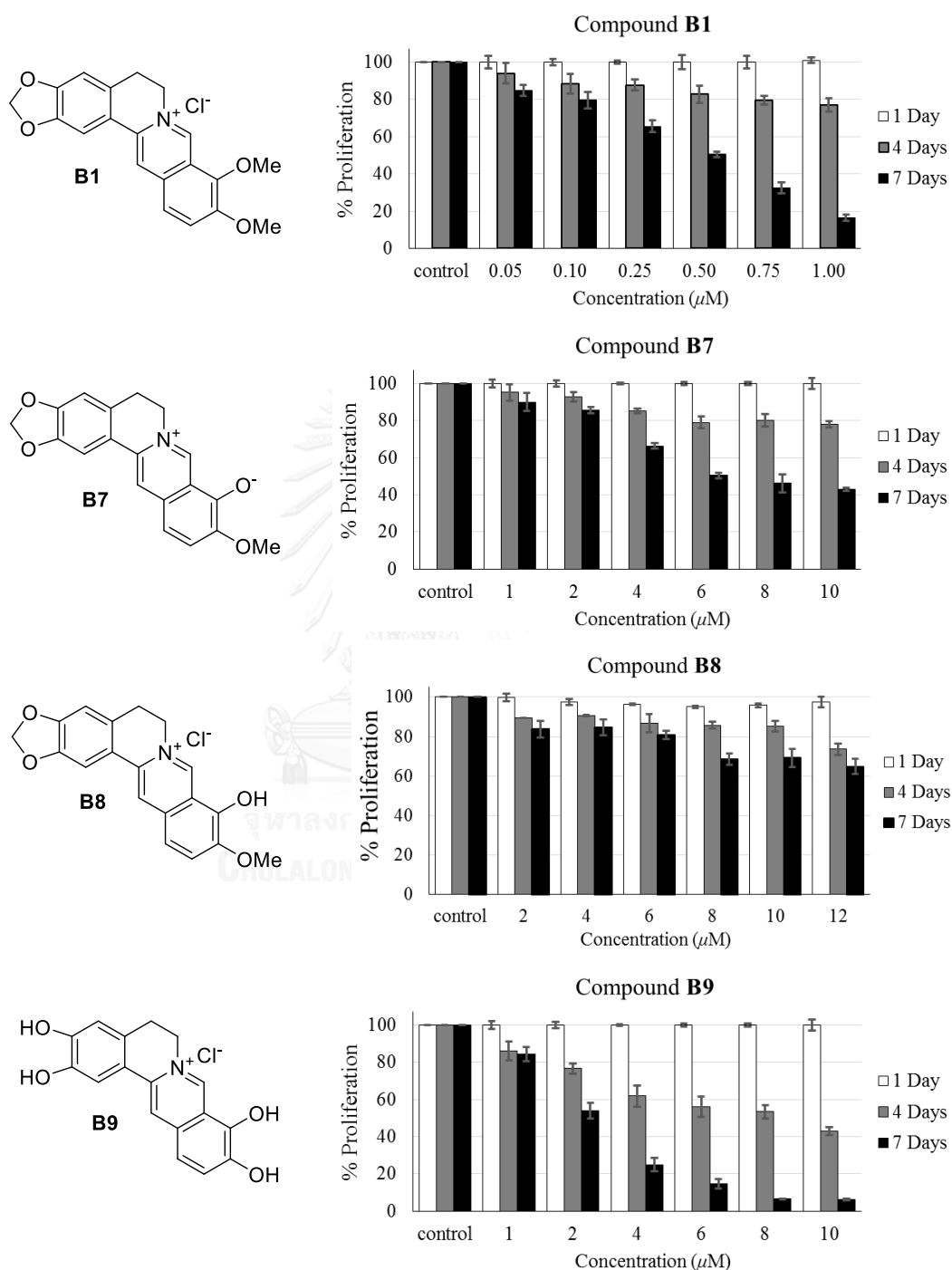


**Figure 3.15** The effect of compounds **B1** and **B7-B9** on % proliferation of HT1080 for 1, 4 and 7 days



The compound with chloride ion (**B7**) might not improve cytotoxicity. In contrast, the compound without phenolic-OH (**B1**) and with four phenolic-OH (**B9**) gave better cytotoxic effect than those with one phenolate ion and phenolic-OH (**B7** and **B8**).

### 3.22 Antioxidant Gene Expression of Compounds **B1** and **B7-B9** on HT1080

The human fibrosarcoma cells (HT1080) were treated with compounds **B1** and **B7-B9** at 0.1 and 1.0  $\mu\text{M}$  for 7 days and gene expression of SOD and CAT was examined *via* RT-PCR (Figure 3.16). Primers of SOD, CAT and GAPDH are shown in Table 5.1. HT1080 could not survive for 7 days with berberine chloride (**B1**) at 1.0  $\mu\text{M}$ . **B1** and **B7-B9** showed significant down regulation of CAT expression compared to the untreated cells ( $p < 0.05$ ). In contrast, **B7-B9** did not show the significant difference in CAT expression compared to **B1**. Interestingly, **B1** and **B7-B9** exhibited a significant up-regulation for SOD expression in a dose dependent fashion ( $p < 0.05$ ) compared to the untreated cells. **B7** and **B9** also showed the better SOD up-regulation than **B1**.

Further studies were performed to investigate the indirect effect of these compounds to antioxidant enzymes, SOD and CAT in human fibrosarcoma cell (Figure 3.16). Berberine chloride (**B1**) and its derivatives **B7-B9** showed the down-regulation on CAT expression and up-regulation on SOD expression compared to the untreated cells. If the control (untreated cells) was excluded, CAT expression among **B1** and **B7-B9** were approximately the same level. SOD expression was found to be up-regulated in dose-dependent fashion compared to the untreated cells especially for compounds containing single phenolate ion (**B7**) and four phenolic-OH (**B9**). If the control was excluded, SOD expression of **B2** and **B4** were still higher than **B1**.

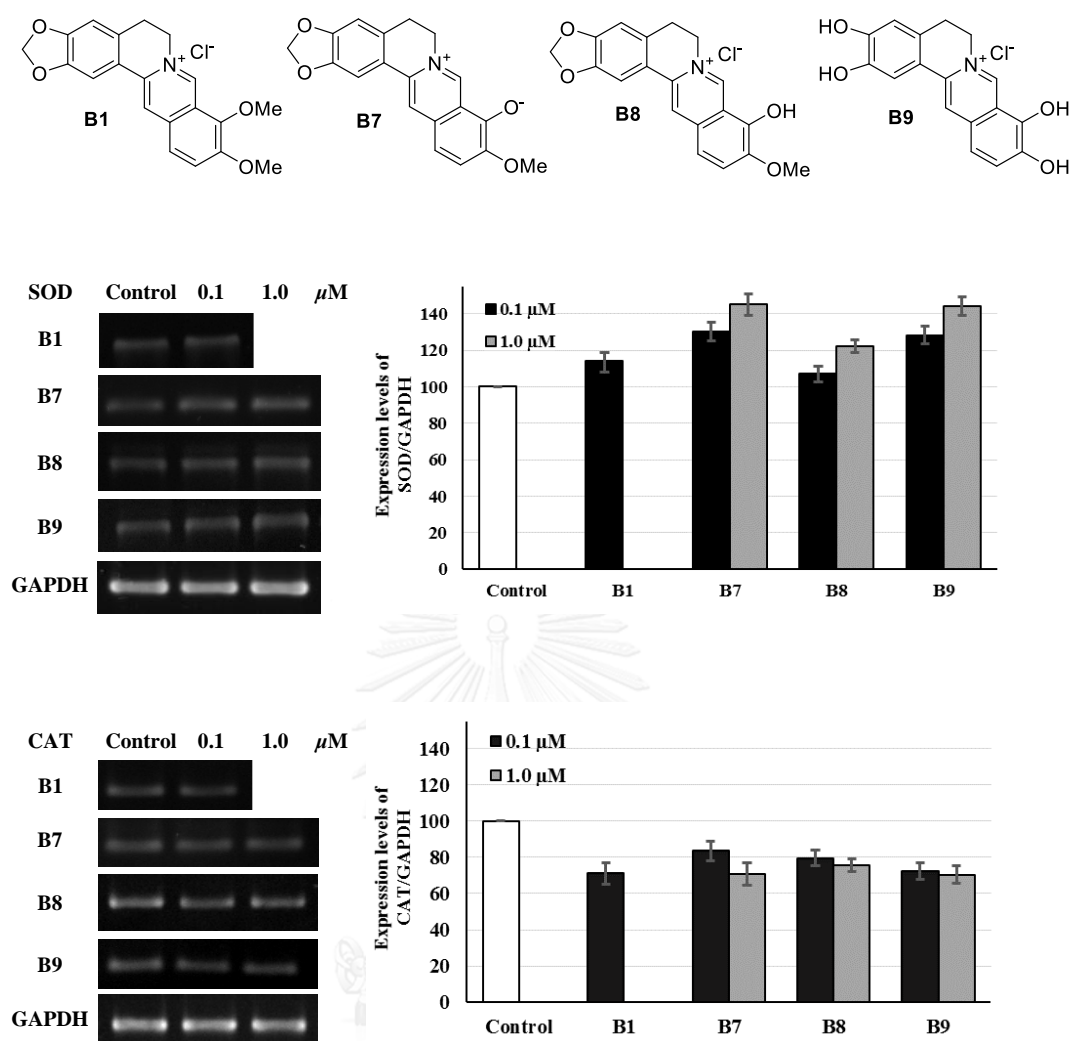


**Figure 3.16** The effect of compounds **B1** and **B7-B9**

on the expression levels of SOD and CAT.

The relationship of SOD-CAT function and mechanistic pathway could be suggested that the increasing of SOD expression should elevate the  $\text{H}_2\text{O}_2$  concentration from  $\bullet\text{O}_2^-$  [105]. In addition, the decreasing of CAT expression made the redox imbalance because of the less decomposition of  $\text{H}_2\text{O}_2$  [133]. The low CAT expression could also be found in redox imbalance of endothelial cells exposed to nicotine [134]. Consequently, the increasing concentration of  $\text{H}_2\text{O}_2$  that accumulated intracellularly might damage target biomolecules including protein, lipid, DNA, and RNA [100]. This might cause of the cell death *via* apoptotic or non-apoptotic mechanism [135].

## CHAPTER IV

### CONCLUSION

Four known diterpenoids: sandaracopimaradiene-3 $\beta$ ,18-diol (**D1**), sandaracopimaradien-3-one (**D2**), sandaracopimaradien-3 $\beta$ -ol (**D3**), and sandaracopimaric acid (**D4**) were isolated from the dichloromethane extract of *X. xylocarpa*. The structure of compound (**D1**) was confirmed *via* single-crystal X-ray diffraction analysis using Cu K $\alpha$  radiation and was used as a model for structure-activity relationship study. Two known derivatives including sandaracopimaradiene-3 $\beta$ ,18-olal (**D7**) and 3 $\beta$ -hydroxysandaracopimaric acid (**D8**), and four new compounds: keto acid **D15** and keto derivative **D16**, hydroxy acid derivative **D18**, and beta-lactone derivative **D19** were synthesized. Moreover, the probe **C2** was synthesized *via* cyclopropanation of compound **D1** with alkynyl diazoacetate (**L5**) for simultaneous arming and SAR studies (Figure 4.1).

The antifungal activity of compounds **D1**, **D2** and **D4** against *A. porri*, *C. gloeosporioides*, *F. oxysporum*, and *P. parasitica* exhibited that only compound **D1** displayed a moderate activity to *inhibit* *P. parasitica* because the hydroxy groups at C-3 and C-18 might be important for antifungal activity.

The antibacterial results of eight compounds: **D1-D3**, **D7**, **D8**, **D15**, **D18** and **D19** against five bacteria: *S. aureus*, *P. acnes*, *S. mutans*, *S. sobrinus* (Gram-positive) and *S. typhi* (Gram-negative), exhibited that only compounds **D7** and **D19** displayed MIC in range of 31.2–62.5  $\mu$ M against *S. aureus*, *S. mutans*, *S. sobrinus*, and *S. typhi* and only compound **D7** showed MBC at 62.5  $\mu$ M to kill *S. sobrinus*. From the SAR results, the hydroxyl group at C-3 was necessary for activity. Furthermore, the formyl group present in compound **D7** could enhance the inhibitory efficiency and kill bacteria better than those compounds containing carboxyl (**D8**) and hydroxyl groups at C-18

(D1). The tricyclic ring system of diterpenoid also demonstrated an important role for antibacterial activity. Moreover, the beta-lactone ring in derivative **D19** could improve antibacterial activity.

In addition, only compounds **D7**, **D15** and **D18** demonstrated good cytotoxicity against HepG2 cell line with  $IC_{50}$  of 3.73, 2.32 and 2.83  $\mu M$ , respectively. According to SAR study, it has been shown that the keto group in compound **D2** and hydroxyl group in compound **D3** at C-3 did not show a significant role towards cytotoxicity. Moreover, the hydroxyl group at C-3, formyl group at C-18 displayed the significant role for cytotoxicity. However, the probe **C2** lost the activity, thus the olefinic group at C15-C16 in compound **D1** seemed to be important for activity. The tricyclic ring system of diterpenoid did not have an important role for cytotoxicity in compounds **D15** and **D18** because the activity increased when the ring system was removed.

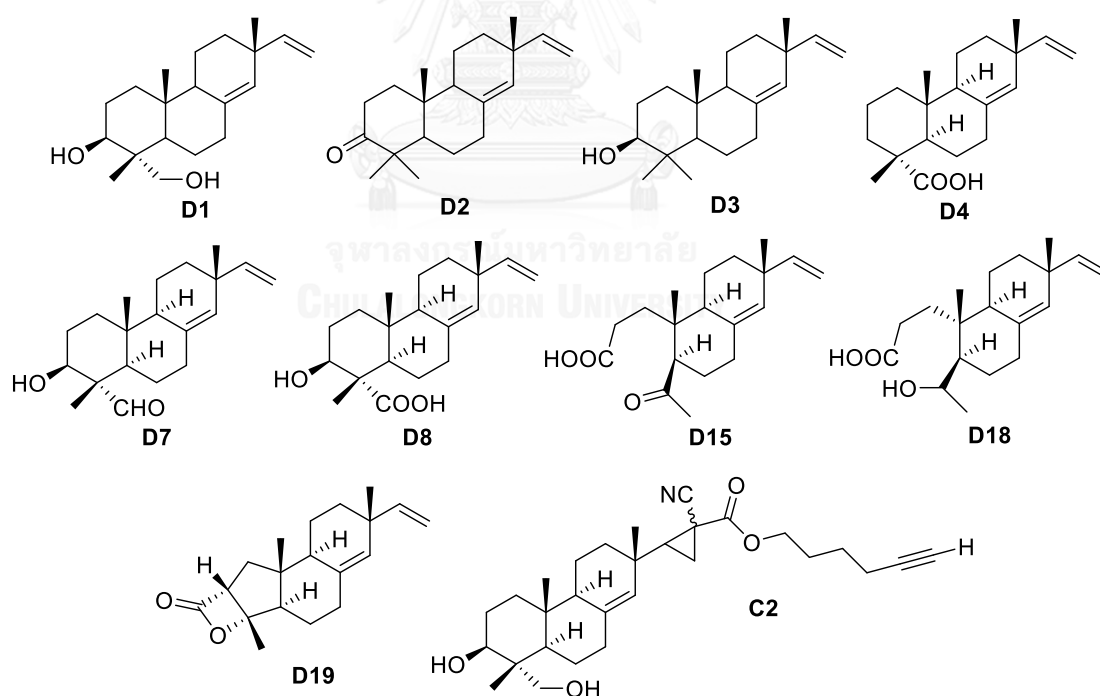


**Figure 4.1** The structures of four known diterpenoids (**D1-D4**) and six derivatives (**D7**, **D8**, **D15**, **D18**, **D19** and **C2**)

Berberine chloride (**B1**) was isolated from vines of *Coscinium fenestratum* (Goetgh.) Colebr and was used as a lead structure to synthesize eight derivatives for SAR studies including acetonil-berberine (**B2**), 13-benzyl-berberine (**B3**), 8-cyano-13,14-dehydrocanadiene (**B4**), canadine (**B5**), 8-phenyl-13,14-dehydrocanadiene (**B6**), berberrubine (**B7**), berberrubine chloride (**B8**) and 2,3,9,10-*tetra*-hydroxyberberine chloride (**B9**) (Figure 4.2).

The antibacterial activity of berberine chloride and their derivatives against *Xanthomonas oryzae* pv. *oryzae* and pv. *oryzicola* disclosed that only compound **B3**, which had benzyl group at C-13, showed better activity than berberine chloride (**B1**) and other derivatives. The SAR study exhibited that the methylene (-OCH<sub>2</sub>O-) and two methoxy groups at C-9 and 10 seemed to be important for antibacterial activity. Furthermore, the aromaticity of isoquinoline ring demonstrated an important role for this activity. Only benzyl group at C-13 in compound **B3** influenced the antibacterial activity against these two bacteria.

For antioxidant activity *via* DPPH assay, only compounds **B7-B9** exhibited good antioxidant activity with IC<sub>50</sub> lower than 100 μM, whereas that of berberine (**B1**) was higher than 500 μM. Compounds **B8** and **B9** exhibited better DPPH scavenging activity than the antioxidant standard, BHT. The SAR study found that berberine derivatives containing phenolic groups could improve direct-antioxidant activity in cell-free system especially compound **B9**, because of *ortho* position of hydroxyl groups and the intramolecular hydrogen bonding. However, berberine possessed a better cytotoxic activity against HT1080 than its derivatives (**B7-B9**). Berberine derivatives containing a single phenolate (**B7**) and four phenolic-OH (**B9**) exhibited a better up-regulation of SOD gene expression. Berberine derivatives with a phenolic-OH showed the antioxidant potential both extracellular fluid in a cell-free system and intracellular fluid in a cell-based system through the up-regulation of SOD gene expression. The cytotoxic action

might not be the main target of berberine derivatives. Moreover, a chloride counter ion might not be important for an indirect antioxidant action.

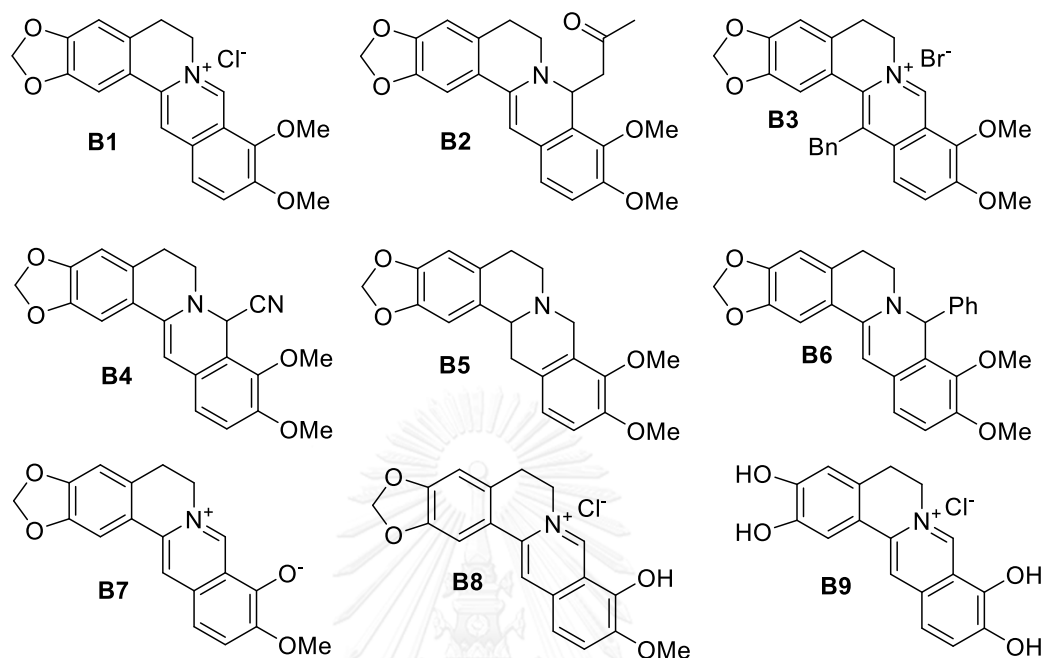


Figure 4.2 The structures of berberine chloride (B1) and eight derivatives (B2-B9)

## REFERENCES

- [1] Li, W.H., Chang, S.T., Chang, S.C., and Chang, H.T. Isolation of antibacterial diterpenoids from *Cryptomeria japonica* bark. Nat. Prod. Res. 22(12) (2008): 1085-1093.
- [2] Porto, T.S., *et al.* Pimarane-type diterpenes: antimicrobial activity against oral pathogens. Molecules 14(1) (2009): 191-199.
- [3] Zhao, J.X., *et al.* Eurifoloids A-R, structurally diverse diterpenoids from *Euphorbia nerifolia*. J. Nat. Prod. 77(10) (2014): 2224-2233.
- [4] Asili, J., *et al.* Labdanes and isopimaranes from *Platyclusus orientalis* and their effects on erythrocyte membrane and on *Plasmodium falciparum* growth in the erythrocyte host cells. J. Nat. Prod. 67(4) (2004): 631-637.
- [5] Wu, X.D., *et al.* Diterpenoids from the twigs and leaves of *Fokienia hodginsii*. J. Nat. Prod. 76(6) (2013): 1032-1038.
- [6] Liu, N., *et al.* Highly oxygenated *ent*-pimarane-type diterpenoids from the Chinese liverwort *Pedinophyllum interruptum* and their allelopathic activities. J. Nat. Prod. 76(9) (2013): 1647-1653.
- [7] Laidlaw, R.A. and Morgan, J.W.W. Diterpenes of *Xylia dolabriformis*. J. Chem. Soc. 85 (1963): 644-650.
- [8] Porto, T.S., *et al.* Pimarane-type diterpenes obtained by biotransformation: antimicrobial properties against clinically isolated gram-positive multidrug-resistant bacteria. Phytother. Res. 27(10) (2013): 1502-1507.
- [9] Porto, T.S., *et al.* Antimicrobial *ent*-pimarane diterpenes from *Viguiera arenaria* against Gram-positive bacteria. Fitoterapia 80(7) (2009): 432-436.
- [10] Aoyagi, Y., *et al.* Cytotoxicity of abietane diterpenoids from *Perovskia abrotanoides* and of their semisynthetic analogues. Bioorg. Med. Chem. 14(15) (2006): 5285-5291.

- [11] Sittiwong, W. Insect control agents from heartwood of *Xylia Xylocarpa* Taub. Ph.D. Dissertation, Department of Chemistry, Chulalongkorn University, Bangkok, 2003.
- [12] Chen, S., Zhang, Y., Niu, S., Liu, X., and Che, Y. Cytotoxic cleistanthane and cassane diterpenoids from the entomogenous fungus *Paraconiothyrium hawaiiense*. J. Nat. Prod. 77(6) (2014): 1513-1518.
- [13] Urzúa, A., Rezende, M., Mascayano, C., and Vásquez, L. A structure-activity study of antibacterial diterpenoids. Molecules 13(4) (2008): 882-891.
- [14] Suh, Y.G., *et al.* Pimarane cyclooxygenase 2 (COX-2) inhibitor and its structure-activity relationship. Bioorg. Med. Chem. Lett. 11(4) (2001): 559-562.
- [15] Zhao, J., *et al.* Diterpenoids from the feces of *Trogopterus xanthipes*. J. Nat. Prod. 73(5) (2010): 865-869.
- [16] Chen, J.D., Yi, R.Z., Sun, C.L., Feng, D.Q., and Lin, Y.M. Antifouling activity of simple synthetic diterpenoids against larvae of the barnacle *Balanus albicostatus* Pilsbry. Molecules 15 (2010): 8072-8081.
- [17] Nair, J.A., Sudhakaran, P.R., Rao, M.J., and Ramakrishna, S.V. Berberine synthesis by callus and cell suspension cultures of *Cosciniium fenestratum*. Plant Cell Tiss. Org. 29(1) (1992): 7-10.
- [18] Kuo, C.L., Chi, C.W., and Liu, T.Y. The anti-inflammatory potential of berberine *in vitro* and *in vivo*. Cancer Lett. 203(2) (2004): 127-137.
- [19] Nair, G.M., Narasimhan, S., Shiburaj, S., and Abraham, T.K. Antibacterial effects of *Cosciniium fenestratum*. Fitoterapia 76(6) (2005): 585-587.
- [20] Jayasinghe, U.L., Kumarihamy, B.M., Bandara, A.G., Waiblinger, J., and Kraus, W. Antifeedant activity of some Sri Lankan plants. Nat. Prod. Res. 17(1) (2003): 5-8.
- [21] Park, K.D., Lee, J.H., Kim, S.H., Kang, T.H., Moon, J.S., and Kim, S.U. Synthesis of 13-(substituted benzyl) berberine and berberrubine derivatives as antifungal agents. Bioorg. Med. Chem. Lett. 16(15) (2006): 3913-3916.



- [22] Inoue, K., *et al.* Tumor-specific cytotoxicity and apoptosis-inducing activity of berberines. *Anticancer Res.* 25(6b) (2005): 4053-4059.
- [23] Leng, S.H., Lu, F.E., and Xu, L.J. Therapeutic effects of berberine in impaired glucose tolerance rats and its influence on insulin secretion. *Acta Pharmacol. Sin.* 25(4) (2004): 496-502.
- [24] Marek, R., Seckarova, P., Hulova, D., Marek, J., Dostal, J., and Sklenar, V. Palmatine and berberine isolation artifacts. *J. Nat. Prod.* 66(4) (2003): 481-486.
- [25] Das, B. and Srinivas, K.V.N.S. Treatment of berberine with indium. *Synth. Commun.* 31(12) (2001): 1815-1817.
- [26] Samosorn, S., *et al.* Antibacterial activity of berberine-NorA pump inhibitor hybrids with a methylene ether linking group. *Bioorg. Med. Chem.* 17(11) (2009): 3866-3872.
- [27] Liu, H., *et al.* Structural optimization of berberine as a synergist to restore antifungal activity of fluconazole against drug-resistant *Candida albicans*. *Chem. Med. Chem.* 9(1) (2014): 207-216.
- [28] Lo, C.Y., *et al.* Synthesis and anticancer activity of a novel series of 9-O-substituted berberine derivatives: a lipophilic substitute role. *Bioorg. Med. Chem. Lett.* 23(1) (2013): 305-309.
- [29] Germoush, M.O. and Mahmoud, A.M. Berberine mitigates cyclophosphamide-induced hepatotoxicity by modulating antioxidant status and inflammatory cytokines. *J. Cancer Res. Clin. Oncol.* 140(7) (2014): 1103-1109.
- [30] Liu, X., *et al.* Berberine attenuates axonal transport impairment and axonopathy induced by Calyculin A in N2a cells. *PLoS One.* 9(4) (2014): 93974.
- [31] Bang, S., Kwon, H., Hwang, H.S., Park, K.D., Kim, S.U., and Bahn, Y.S. 9-O-butyl-13-(4-isopropylbenzyl)berberine, KR-72, is a potent antifungal agent that inhibits the growth of *Cryptococcus neoformans* by regulating gene expression. *PLoS One.* 9(10) (2014): 109863.

- [32] Smitinand, T. and Larsen-Aarhus, K. Flora of Thailand. Vol. 4 part. 2: Bangkok: TISTR Press, 1985.
- [33] บุญยะประกัศร, น. and โชคชัยเจริญพร, อ. สมุนไพร ไม้พุ่มบ้าน (2). Vol. 1: ประชาชน: กรุงเทพมหานคร, 2541.
- [34] KuMar, K.A., Srimannarayana, G., Subba Rao, N. V. A. A new trimeric proanthocyanidin from *Xylia dalabriformis*. Indian J. Chem. 14 (1976): 654-656.
- [35] Mester, L., Szabados, L., Mester, M., and Yadav, N. Identification by carbon-<sup>13</sup>NMR spectroscopy of *trans*-5-hydroxypipelic acid a new inhibitor of platelet aggregation induced by serotonin in the leaves of *Xylia xylocarpa*. Planta Med. 35(4) (1979): 339-341.
- [36] Li, C., *et al.* Bioactive briarane diterpenoids from the South China Sea gorgonian *Dichotella gemmacea*. Bioorg. Med. Chem. Lett. 22(13) (2012): 4368-4372.
- [37] Barrero, A.F., *et al.* Oxygenated diterpenes and other constituents from Moroccan *Juniperus phoenicea* and *Juniperus thurifera* var. *africana*. Phytochemistry 65(17) (2004): 2507-2515.
- [38] Carvalho, T.C., *et al.* Antimicrobial activity of diterpenes from *Viguiera arenaria* against endodontic bacteria. Molecules 16(1) (2011): 543-551.
- [39] Suh, Y.G., *et al.* Synthesis and anti-inflammatory effects of novel pimarane diterpenoid analogs. Bioorg. Med. Chem. Lett. 14(13) (2004): 3487-3490.
- [40] Lallemand, B., *et al.* Evaluation of *in vitro* anticancer activity of sphaeropsidins A-C, fungal rearranged pimarane diterpenes, and semisynthetic derivatives. Phytochem. Lett. 5(4) (2012): 770-775.
- [41] Murali Krishna, U. and Trivedi, G.K. Studies towards the synthesis of FCRR toxin: an expeditious entry into 7-5-6 ring systems via [5+2] oxidopyrylium-alkene cycloaddition. Tetrahedron Lett. 45(2) (2004): 257-259.

- [42] O'Neill, M.J., *et al.* Isolation of translactone-containing triterpenes with thrombin inhibitory activities from the leaves of *Lantana camara*. J. Nat. Prod. 61(11) (1998): 1328-1331.
- [43] Eto, K., Yoshino, M., Takahashi, K., Ishihara, J., and Hatakeyama, S. Total Synthesis of Oxazolomycin A. Org. Lett. 13(19) (2011): 5398-5401.
- [44] NTP 12th report on carcinogens. Rep. Carcinog. 12 (2011): 3-499.
- [45] Asai, A., Hasegawa, A., Ochiai, K., Yamashita, Y., and Mizukami, T. Belactosin A, a novel antitumor antibiotic acting on cyclin/CDK mediated cell cycle regulation, produced by *Streptomyces* sp. J. Antibiot. 53(1) (2000): 81-83.
- [46] Umezawa, H., Aoyagi, T., Uotani, K., Hamada, M., Takeuchi, T., and Takahashi, S. Ebelactone, an inhibitor of esterase, produced by actinomycetes. J. Antibiot. 33(12) (1980): 1594-1596.
- [47] Mutoh, M., *et al.* Panclitics, novel pancreatic lipase inhibitors. I. Taxonomy, fermentation, isolation and biological activity. J. Antibiot. 47(12) (1994): 1369-1375.
- [48] Weibel, E.K., Hadvary, P., Hochuli, E., Kupfer, E., and Lengsfeld, H. Lipstatin, an inhibitor of pancreatic lipase, produced by *Streptomyces toxytricini*. I. Producing organism, fermentation, isolation and biological activity. J. Antibiot. 40(8) (1987): 1081-1085.
- [49] Birari, R.B. and Bhutani, K.K. Pancreatic lipase inhibitors from natural sources: unexplored potential. Drug Discov. Today 12(19-20) (2007): 879-889.
- [50] Kumaraswamy, G., Padmaja, M., Markondaiah, B., Jena, N., Sridhar, B., and Kiran, M.U. Oppolzer sultam directed aldol as a key step for the stereoselective syntheses of antitumor antibiotic belactosin C and its synthetic congeners. J. Org. Chem. 71(1) (2006): 337-340.

- [51] Bottcher, T. and Sieber, S.A. Beta-lactones as privileged structures for the active-site labeling of versatile bacterial enzyme classes. Angew. Chem. Int. Ed. 47(24) (2008): 4600-4603.
- [52] Hochuli, E., Kupfer, E., Maurer, R., Meister, W., Mercadal, Y., and Schmidt, K. Lipstatin, an inhibitor of pancreatic lipase, produced by *Streptomyces toxytricini*. II. Chemistry and structure elucidation. J. Antibiot. 40(8) (1987): 1086-1091.
- [53] Kumaraswamy, G. and Markondaiah, B. Stereoselective synthesis of belactosin C and its derivatives using a catalytic proline catalyzed crossed-aldol reaction. Tetrahedron Lett. 48(10) (2007): 1707-1709.
- [54] Liu, G., Shirley, M.E., and Romo, D. A diastereoselective, nucleophile-promoted aldol-lactonization of ketoacids leading to bicyclic- $\beta$ -lactones. J. Org. Chem. 77(5) (2012): 2496-2500.
- [55] Tidwell, T.T. Ketene chemistry after 100 years: Ready for a new century. Eur. J. Org. Chem. 2006(3) (2006): 563-576.
- [56] Wynberg, H. and Staring, E.G.J. Asymmetric synthesis of (*S*)- and (*R*)-malic acid from ketene and chloral. J. Am. Chem. Soc. 104(1) (1982): 166-168.
- [57] Pommier, A.P., J. M. Recent advances in  $\beta$ -lactone chemistry. Synthesis 1993(5) (1993): 441-459.
- [58] Arnold, L.D., May, R.G., and Vederas, J.C. Synthesis of optically pure alpha-amino acids *via* salts of alpha-amino-beta-propiolactone. J. Am. Chem. Soc. 110(7) (1988): 2237-2241.
- [59] Schmidt, Y., Lehr, K., Breuninger, U., Brand, G., Reiss, T., and Breit, B. Enantioselective total synthesis of the unnatural and the natural stereoisomers of vittatalactone. J. Org. Chem. 75(13) (2010): 4424-4433.
- [60] Leverett, C.A., Purohit, V.C., Johnson, A.G., Davis, R.L., Tantillo, D.J., and Romo, D. Dyotropic rearrangements of fused tricyclic  $\beta$ -lactones: Application to the

- synthesis of (–)-curcumanolide A and (–)-curcumalactone. J. Am. Chem. Soc. 134(32) (2012): 13348-13356.
- [61] Harvey, N.L., Krysiak, J., Chamni, S., Cho, S.W., Sieber, S.A., and Romo, D. Synthesis of (±)-spongiolactone enabling discovery of a more potent derivative. Eur. J. Chem. 21(4) (2015): 1425-1428.
- [62] Romo, D., *et al.* Synthesis and inhibitory action on HMG-CoA synthase of racemic and optically active oxetan-2-ones ( $\beta$ -Lactones). Bioorg. Med. Chem. 6(8) (1998): 1255-1272.
- [63] Orr, R.K. and Calter, M.A. Asymmetric synthesis using ketenes. Tetrahedron 59(20) (2003): 3545-3565.
- [64] Wynberg, H. and Staring, E.G.J. The absolute configuration of 4-(trichloromethyl)oxetan-2-one; a case of double anchimeric assistance with inversion. J. Chem. Soc. Chem. Commun. (17) (1984): 1181-1182.
- [65] Peddibhotla, S., Dang, Y., Liu, J.O., and Romo, D. Simultaneous arming and structure/activity studies of natural products employing O-H insertions: an expedient and versatile strategy for natural products-based chemical genetics. J. Am. Chem. Soc. 129(40) (2007): 12222-12231.
- [66] Zhou, C.-Y., Li, J., Peddibhotla, S., and Romo, D. Mild arming and derivatization of natural products *via* an In(OTf)<sub>3</sub>-catalyzed arene iodination. Org. Lett. 12(9) (2010): 2104-2107.
- [67] Li, J., *et al.* Simultaneous structure–activity studies and arming of natural products by C–H amination reveal cellular targets of eupalmerin acetate. Nature Chem. 5(6) (2013): 510-517.
- [68] Robles, O., Serna-Saldivar, S.O., Gutiérrez-Urbe, J.A., and Romo, D. Cyclopropanations of olefin-containing natural products for simultaneous arming and structure activity studies. Org. Lett. 14(6) (2012): 1394-1397.

- [69] Chamni, S., He, Q.L., Dang, Y., Bhat, S., Liu, J.O., and Romo, D. Diazo reagents with small steric footprints for simultaneous arming/SAR studies of alcohol-containing natural products *via* O–H insertion. ACS Chem. Biol. 6(11) (2011): 1175-1181.
- [70] Huigens Iij, R.W., Morrison, K.C., Hicklin, R.W., Flood Jr, T.A., Richter, M.F., and Hergenrother, P.J. A ring-distortion strategy to construct stereochemically complex and structurally diverse compounds from natural products. Nature Chem. 5(3) (2013): 195-202.
- [71] Borthakur, M. and Boruah, R.C. A microwave promoted and Lewis acid catalysed solventless approach to 4-azasteroids. Steroids 73(6) (2008): 637-641.
- [72] Harding, K.E., May, L.M., and Dick, K.F. Selective oxidation of allylic alcohols with chromic acid. J. Org. Chem. 40 (1975): 1664-1665.
- [73] Eisenbraun, E.J. Cyclooctanone. Org. Synth. 45 (1965): 28.
- [74] Einhorn, J., Einhorn, C., Ratajczak, F., and Pierre, J.L. Efficient and highly selective oxidation of primary alcohols to aldehydes by *N*-chlorosuccinimide mediated by oxoammonium salts. J. Org. Chem. 61(21) (1996): 7452-7454.
- [75] Chen, D., Song, Y., Lu, Y., and Xue, X. Synthesis and *in vitro* cytotoxicity of andrographolide-19-oic acid analogues as anti-cancer agents. Bioorg. Med. Chem. Lett. 23(11) (2013): 3166-3169.
- [76] Alqasoumi, S.I., Farraj, A.I., and Abdel-Kader, M.S. Study of the hepatoprotective effect of *Juniperus phoenicea* constituents. J. Pharm. Sci. 26(5) (2013): 999-1008.
- [77] Doi, K. and Kawamura, T. New diterpene from *Juniperus rigida*. Phytochemistry 11(2) (1972): 841-842.
- [78] But, T.Y.S. and Toy, P.H. Organocatalytic Mitsunobu reactions. J. Am. Chem. Soc. 128(30) (2006): 9636-9637.

- [79] Kvasnica, M., *et al.* Study of stereoselectivity of reduction of 18-oxo des-E triterpenoids by sodium borohydride in the presence of cerium chloride. Tetrahedron: Asymmetry 22(9) (2011): 1011-1020.
- [80] Goddard-Borger, E.D. and Stick, R.V. An efficient, inexpensive, and shelf-stable diazotransfer reagent: Imidazole-1-sulfonyl azide hydrochloride. Org. Lett. 9(19) (2007): 3797-3800.
- [81] Rahman, A., Choudhary, M.I., and Thomsen, W.J. Bioassay techniques for drug development Bioassay techniques for drug development (2001): 1-3.
- [82] Sarker, S.D., Nahar, L., and Kumarasamy, Y. Microtitre plate-based antibacterial assay incorporating resazurin as an indicator of cell growth, and its application in the *in vitro* antibacterial screening of phytochemicals. Methods 42(4) (2007): 321-324.
- [83] Bautista-Baños, S., *et al.* Chitosan as a potential natural compound to control pre and postharvest diseases of horticultural commodities. Crop Protection 25(2) (2006): 108-118.
- [84] Cory, A.H., Owen, T.C., Bartrop, J.A., and Cory, J.G. Use of an aqueous soluble tetrazolium/formazan assay for cell growth assays in culture. Cancer Commun. 3(7) (1991): 207-12.
- [85] Jacobsen, J., Pedersen, M., and Rassing, M.R. TR146 cells as a model for human buccal epithelium: II. Optimisation and use of a cellular sensitivity MTS/PMS assay. Int. J. Pharm. 141(1-2) (1996): 217-225.
- [86] Zaugg, J., Khom, S., Eigenmann, D., Baburin, I., Hamburger, M., and Hering, S. Identification and characterization of GABAA receptor modulatory diterpenes from *Biota orientalis* that decrease locomotor activity in mice. J. Nat. Prod. 74(8) (2011): 1764-1772.

- [87] Scazzocchio, F., Cometa, M.F., Tomassini, L., and Palmery, M. Antibacterial activity of *Hydrastis canadensis* extract and its major isolated alkaloids. Planta Med. 67(6) (2001): 561-564.
- [88] Wang, X., *et al.* Effect of berberine on *Staphylococcus epidermidis* biofilm formation. Int. J. Antimicrob. Agents 34(1) (2009): 60-66.
- [89] Vollekova, A., Kost'alova, D., Kettmann, V., and Toth, J. Antifungal activity of *Mahonia aquifolium* extract and its major protoberberine alkaloids. Phytother. Res. 17(7) (2003): 834-837.
- [90] Letasiova, S., Jantova, S., Cipak, L., and Muckova, M. Berberine-antiproliferative activity *in vitro* and induction of apoptosis/necrosis of the U937 and B16 cells. Cancer Lett. 239(2) (2006): 254-262.
- [91] Iwasa, K., Lee, D.U., Kang, S.I., and Wiegrebe, W. Antimicrobial activity of 8-alkyl- and 8-phenyl-substituted berberines and their 12-bromo derivatives. J. Nat. Prod. 61(9) (1998): 1150-1153.
- [92] Zuo, G.Y., Li, Y., Han, J., Wang, G.C., Zhang, Y.L., and Bian, Z.Q. Antibacterial and synergy of berberines with antibacterial agents against clinical multi-drug resistant isolates of methicillin-resistant *Staphylococcus aureus* (MRSA). Molecules 17 (2012): 10322-10330.
- [93] Zhang, S.L., *et al.* Novel berberine triazoles: synthesis, antimicrobial evaluation and competitive interactions with metal ions to human serum albumin. Bioorg. Med. Chem. Lett. 23(4) (2013): 1008-1012.
- [94] Vennerstrom, J.L. and Klayman, D.L. Protoberberine alkaloids as antimalarials. J. Med. Chem. 31(6) (1988): 1084-1087.
- [95] Bahar, M., *et al.* Potent antiprotozoal activity of a novel semi-synthetic berberine derivative. Bioorg. Med. Chem. Lett. 21(9) (2011): 2606-2610.



- [96] Orfila, L., Rodriguez, M., Colman, T., Hasegawa, M., Merentes, E., and Arvelo, F. Structural modification of berberine alkaloids in relation to cytotoxic activity *in vitro*. J. Ethnopharmacol. 71(3) (2000): 449-456.
- [97] Zhang, L., *et al.* Synthesis and cytotoxicity evaluation of 13-*n*-alkyl berberine and palmatine analogues as anticancer agents. Molecules 17 (2012): 11294-11302.
- [98] Hwang, J.M., *et al.* Inhibitory effect of berberine on *tert*-butyl hydroperoxide-induced oxidative damage in rat liver. Arch. Toxicol. 76(11) (2002): 664-670.
- [99] Finkel, T. and Holbrook, N.J. Oxidants, oxidative stress and the biology of ageing. Nature 408(6809) (2000): 239-247.
- [100] Park, S.M., *et al.* Oxidant-induced cell death in renal epithelial cells: differential effects of inorganic and organic hydroperoxides. Pharmacol. Toxicol. 92(1) (2003): 43-50.
- [101] 't Hoen, P.A., Van der Lans, C.A., Van Eck, M., Bijsterbosch, M.K., Van Berkel, T.J., and Twisk, J. Aorta of ApoE-deficient mice responds to atherogenic stimuli by a prelesional increase and subsequent decrease in the expression of antioxidant enzymes. Circ. Res. 93(3) (2003): 262-269.
- [102] Pohanka, M. Role of oxidative stress in infectious diseases. A review. Folia Microbiol. 58(6) (2013): 503-513.
- [103] Tangjitjaroenkun, J., Supabphol, R., and Chavasiri, W. Antioxidant effect of *Zanthoxylum limonella* Alston. J. Med. Plants Res. 6(8) (2012): 1407-1414.
- [104] Valko, M., Leibfritz, D., Moncol, J., Cronin, M.T., Mazur, M., and Telser, J. Free radicals and antioxidants in normal physiological functions and human disease. Int. J. Biochem. Cell Biol. 39(1) (2007): 44-84.
- [105] Khan, M.A., *et al.* Regulatory effects of resveratrol on antioxidant enzymes: a mechanism of growth inhibition and apoptosis induction in cancer cells. Mol. Cells 35(3) (2013): 219-225.

- [106] Petit, E., Courtin, A., Kloosterboer, H.J., Rostene, W., Forgez, P., and Gompel, A. Progesterins induce catalase activities in breast cancer cells through PRB isoform: correlation with cell growth inhibition. J. Steroid Biochem. Mol. Biol. 115(3-5) (2009): 153-160.
- [107] Yu, J. and Kim, A.K. Effect of taurine on antioxidant enzyme system in B16F10 melanoma cells. Adv. Exp. Med. Biol. 643 (2009): 491-499.
- [108] Chu, S.C., Yu, C.C., Hsu, L.S., Chen, K.S., Su, M.Y., and Chen, P.N. Berberine reverses epithelial-to-mesenchymal transition and inhibits metastasis and tumor-induced angiogenesis in human cervical cancer cells. Mol. Pharmacol. 86(6) (2014): 609-623.
- [109] Yip, N.K.Y. and Ho, W.S. Berberine induces apoptosis via the mitochondrial pathway in liver cancer cells. Oncol. Rep. 30(3) (2013): 1107-12.
- [110] Cai, Y., *et al.* Berberine inhibits the growth of human colorectal adenocarcinoma *in vitro* and *in vivo*. J. Nat. Med. 68(1) (2014): 53-62.
- [111] Rajendran, J., Jyothi, A., Jacob, L., Vinod, S., and Kochupappy, R.T. Simultaneous determination of berberine and  $\beta$ -sitosterol in the leaf extracts of *Naravelia zeylanica* by analytical methods and their *in vitro* anti diabetic activity. J. Adv. Pharm. Educ. Res. 4(3) (2014): 365-371.
- [112] Wojtyczka, R.D., *et al.* Berberine enhances the antibacterial activity of selected antibiotics against coagulase-negative *Staphylococcus* strains *in vitro*. Molecules 19(5) (2014): 6583-6596.
- [113] Zhu, S.l., *et al.* Berberine inhibits fluphenazine-induced up-regulation of CDR1 in *Candida albicans*. Biol. Pharm. Bull. 37(2) (2014): 268-273.
- [114] Jang, M.H., Kim, H.Y., Kang, K.S., Yokozawa, T., and Park, J.H. Hydroxyl radical scavenging activities of isoquinoline alkaloids isolated from *Coptis chinensis*. Arch. Pharm. Res. 32(3) (2009): 341-345.

- [115] Bashir, S. and Gilani, A.H. Antiurolithic effect of berberine is mediated through multiple pathways. Eur. J. Pharmacol. 651(1-3) (2011): 168-175.
- [116] Tan, Y., Tang, Q., Hu, B.R., and Xiang, J.Z. Antioxidant properties of berberine on cultured rabbit corpus cavernosum smooth muscle cells injured by hydrogen peroxide. Acta Pharmacol. Sin. 28(12) (2007): 1914-1918.
- [117] Rasheed, S., Nelson-Rees, W.A., Toth, E.M., Arnstein, P., and Gardner, M.B. Characterization of a newly derived human sarcoma cell line (HT-1080). Cancer. 33(4) (1974): 1027-1033.
- [118] Zwellig, L.A., *et al.* HT1080/DR4: a P-glycoprotein-negative human fibrosarcoma cell line exhibiting resistance to topoisomerase II-reactive drugs despite the presence of a drug-sensitive topoisomerase II. J. Natl. Cancer Inst. 82(19) (1990): 1553-1561.
- [119] Suau, R., Nájera, F., and Rico, R. The Polonovski–Potier reaction of berberine *N*-Oxides. Synthesis of 8-hydroxymethyl and 8-methylberberines. Tetrahedron 56(49) (2000): 9713-9723.
- [120] Qin, Y., Pang, J.Y., Chen, W.H., Cai, Z., and Jiang, Z.H. Synthesis, DNA-binding affinities, and binding mode of berberine dimers. Bioorg. Med. Chem. 14(1) (2006): 25-32.
- [121] Chen, L., Feng, L., Li, Y., and Wu, G. Novel isoquinoline derivatives. 2010, F. Hoffmann-La Roche AG, Switz. . 55 pages.
- [122] Kim, S.H., Lee, S.J., Lee, J.H., Sun, W.S., and Kim, J.H. Antimicrobial activity of 9-*O*-acyl- and 9-*O*-alkylberberubine derivatives. Planta Med. 68(3) (2002): 277-281.
- [123] Kim, J.H., *et al.* Preparation of protoberberine and 13,13 $\alpha$ -didehydroberberine derivatives as cholesterol biosynthesis inhibitor for treating hypercholesterolemia and hyperlipidemia. 2001, Hanwha Chemical Corporation, S. Korea . 21 pages.

- [124] National Committee for Clinical Laboratory Standards. Performance standards for antimicrobial susceptibility testing 6 th ed. Approved standard M2-A6 ed. Wayne, Pa:1997.
- [125] Yahayo, W., Supabphol, A., and Supabphol, R. Suppression of human fibrosarcoma cell metastasis by *Phyllanthus emblica* extract *in vitro*. Asian Pac. J. Cancer Prev. 14(11) (2013): 6863-6867.
- [126] Lobner, D. Comparison of the LDH and MTT assays for quantifying cell death: validity for neuronal apoptosis? J. Neurosci. Methods 96(2) (2000): 147-152.
- [127] Supabphol, R., Wattanachaiyingcharoen, R., Kamkaen, N., and Supabphol, A. Cytoprotective effect of *Vernonia cinerea* Less. extract on human umbilical vein endothelial cells against nicotine toxicity. J. Med. Plants Res. 7(15) (2013): 980-987.
- [128] Klongpityapong, P., Supabphol, R., and Supabphol, A. Antioxidant effects of gamma-oryzanol on human prostate cancer cells. Asian Pac. J. Cancer Prev. 14(9) (2013): 5421-5425.
- [129] Li, C.Y., Tsai, S.I., Damu, A.G., and Wu, T.S. A rapid and simple determination of protoberberine alkaloids in *Rhizoma Coptidis* by <sup>1</sup>H NMR and its application for quality control of commercial prescriptions. J. Pharm. Biomed. Anal. 49(5) (2009): 1272-1276.
- [130] Valgimigli, L., *et al.* The unusual reaction of semiquinone radicals with molecular oxygen. J. Org. Chem. 73(5) (2008): 1830-1841.
- [131] Bors, W., Heller, W., Michel, C., and Stettmaier, K. Flavonoids and polyphenols: Chemistry and biology. Handbook of Antioxidants. Eds Cadenas E and Packer L: Marcel Dekker, New York,, 1996, 409-466
- [132] Bendary, E., Francis, R.R., Ali, H.M.G., Sarwat, M.I., and El Hady, S. Antioxidant and structure–activity relationships (SARs) of some phenolic and anilines compounds. Annals of Agricultural Sciences 58(2) (2013): 173-181.

- [133] Khan, M.A., Tania, M., Zhang, D.Z., and Chen, H.C. Antioxidant enzymes and cancer. Chin. J. Cancer Res. 22(2) (2010): 87-92.
- [134] Supabphol, R. and Supabphol, A. Cytoprotective potential of royal jelly on human umbilical vein endothelial cells against nicotine toxicity *via* catalase. Eur. J. Med. Plants 3(1) (2013): 88-98.
- [135] Giorgio, M., *et al.* Electron transfer between cytochrome c and p66Shc generates reactive oxygen species that trigger mitochondrial apoptosis. Cell 122(2) (2005): 221-233.





APPENDIX

จุฬาลงกรณ์มหาวิทยาลัย  
CHULALONGKORN UNIVERSITY

**Table A1** Crystal data and structure refinement for sandaracopimaradiene-3 $\beta$ ,18-diol (D1).

Identification code	dioh	
Empirical formula	C <sub>20</sub> H <sub>32</sub> O <sub>2</sub>	
Formula weight	304.45	
Temperature	110.15 K	
Wavelength	1.54178 Å	
Crystal system	Monoclinic	
Space group	P 1 21 1	
Unit cell dimensions	a = 10.7594(4) Å	$\alpha = 90^\circ$ .
	b = 7.4389(3) Å	$\beta = 90.473(2)^\circ$ .
	c = 22.1725(8) Å	$\gamma = 90^\circ$ .
Volume	1774.58(12) Å <sup>3</sup>	
Z	4	
Density (calculated)	1.140 Mg/m <sup>3</sup>	
Absorption coefficient	0.547 mm <sup>-1</sup>	
F(000)	672	
Crystal size	0.4 x 0.085 x 0.042 mm <sup>3</sup>	
Theta range for data collection	3.987 to 60.876°.	
Index ranges	-12 ≤ h ≤ 12, -8 ≤ k ≤ 7, -25 ≤ l ≤ 25	
Reflections collected	40082	
Independent reflections	5179 [R(int) = 0.0673]	
Completeness to theta = 67.679°	83.5 %	
Absorption correction	Semi-empirical from equivalents	
Max. and min. transmission	0.6629 and 0.5376	
Refinement method	Full-matrix least-squares on F <sup>2</sup>	
Data / restraints / parameters	5179 / 1 / 404	
Goodness-of-fit on F <sup>2</sup>	1.168	
Final R indices [I > 2σ(I)]	R1 = 0.0466, wR2 = 0.1206	
R indices (all data)	R1 = 0.0506, wR2 = 0.1267	
Absolute structure parameter: Flack [Hooft]	-0.02(9) [0.03(9)]	
Extinction coefficient	0.038(2)	
Largest diff. peak and hole	0.380 and -0.470 e.Å <sup>-3</sup>	

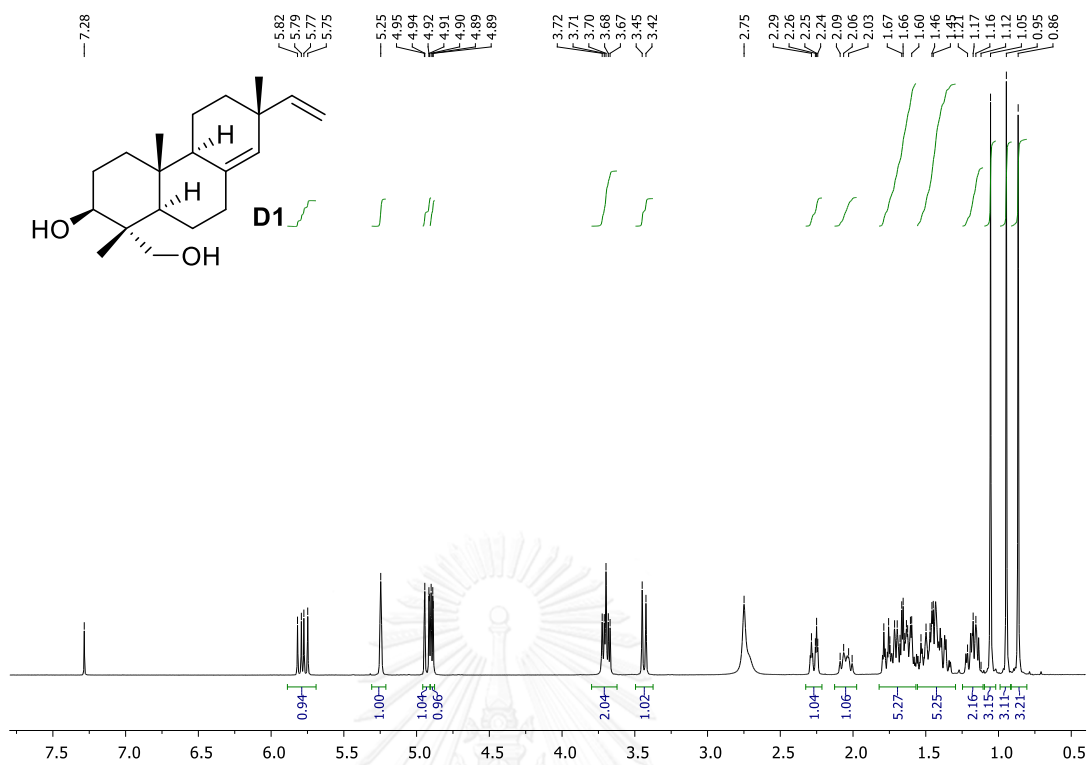


Figure A1 The  $^1\text{H}$  NMR spectrum of sandaracopimaradiene-3 $\beta$ ,18-diol (D1) (CDCl<sub>3</sub>)

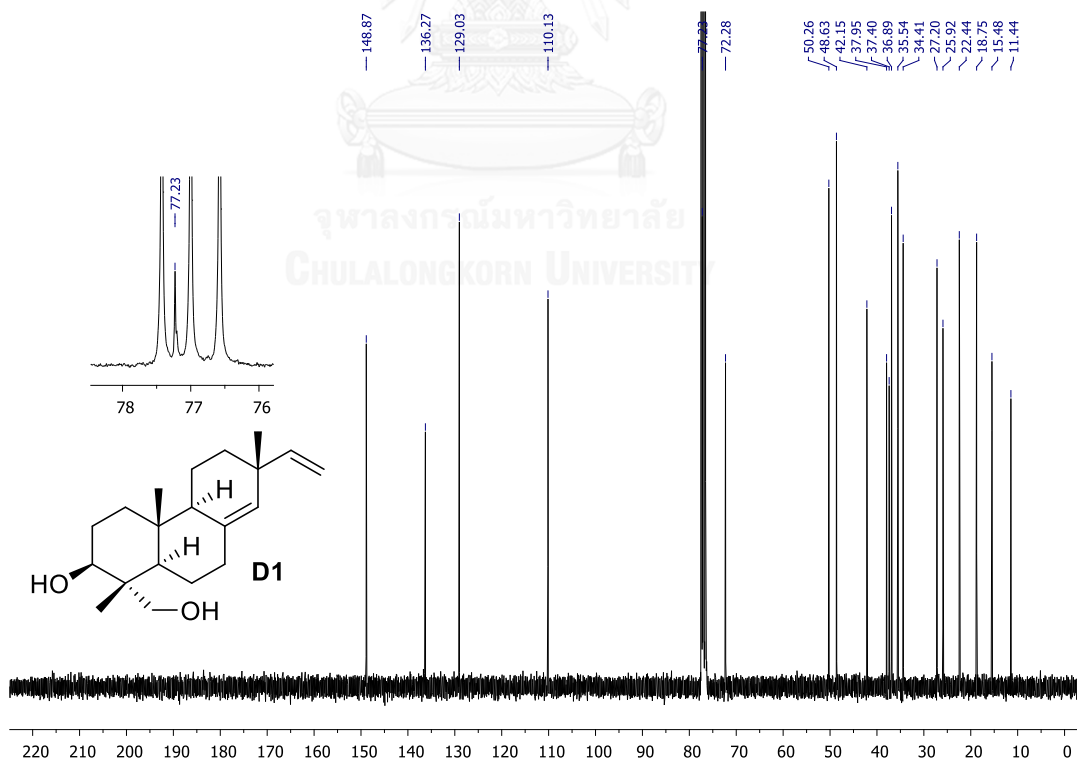


Figure A2 The  $^{13}\text{C}$  NMR spectrum of sandaracopimaradiene-3 $\beta$ ,18-diol (D1) (CDCl<sub>3</sub>)



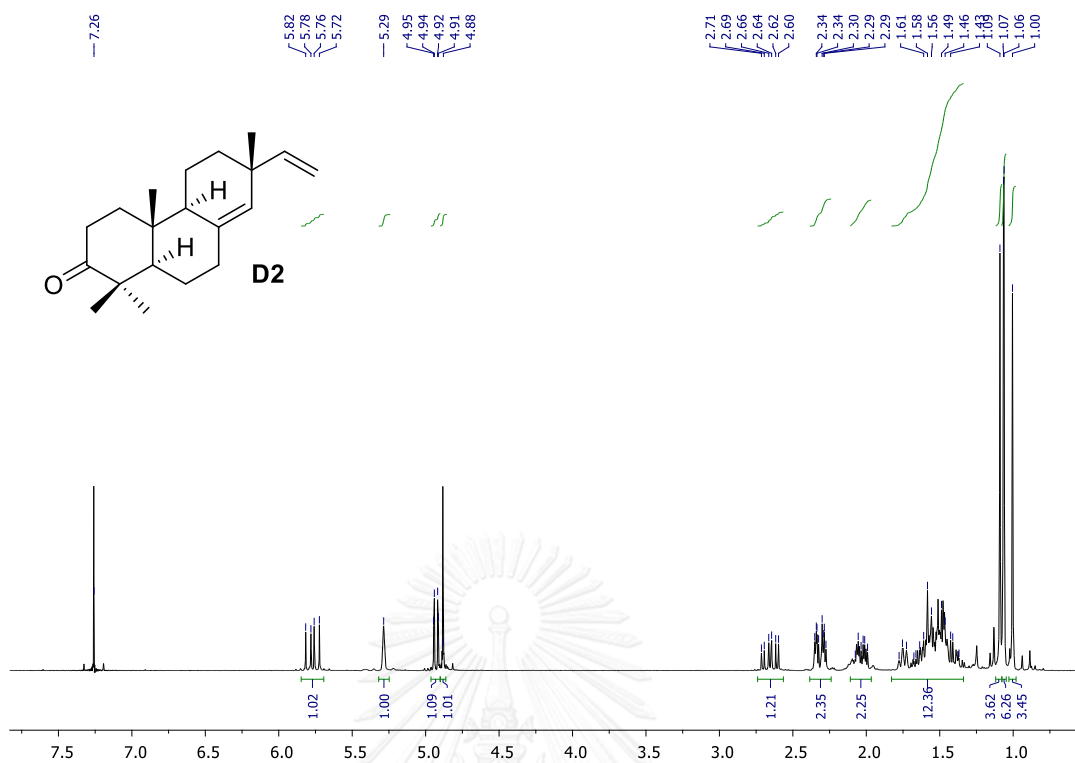


Figure A3 The <sup>1</sup>H NMR spectrum of sandaracopimaradien-3-one (D2) (CDCl<sub>3</sub>)

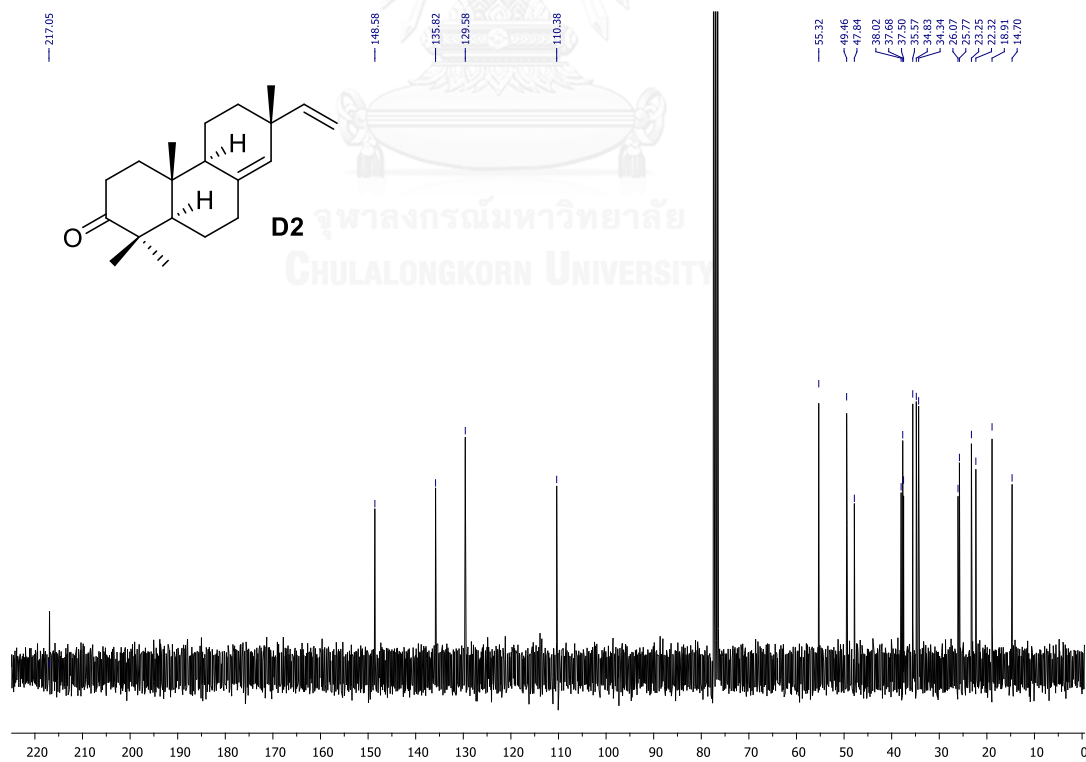


Figure A4 The <sup>13</sup>C NMR spectrum of sandaracopimaradien-3-one (D2) (CDCl<sub>3</sub>)

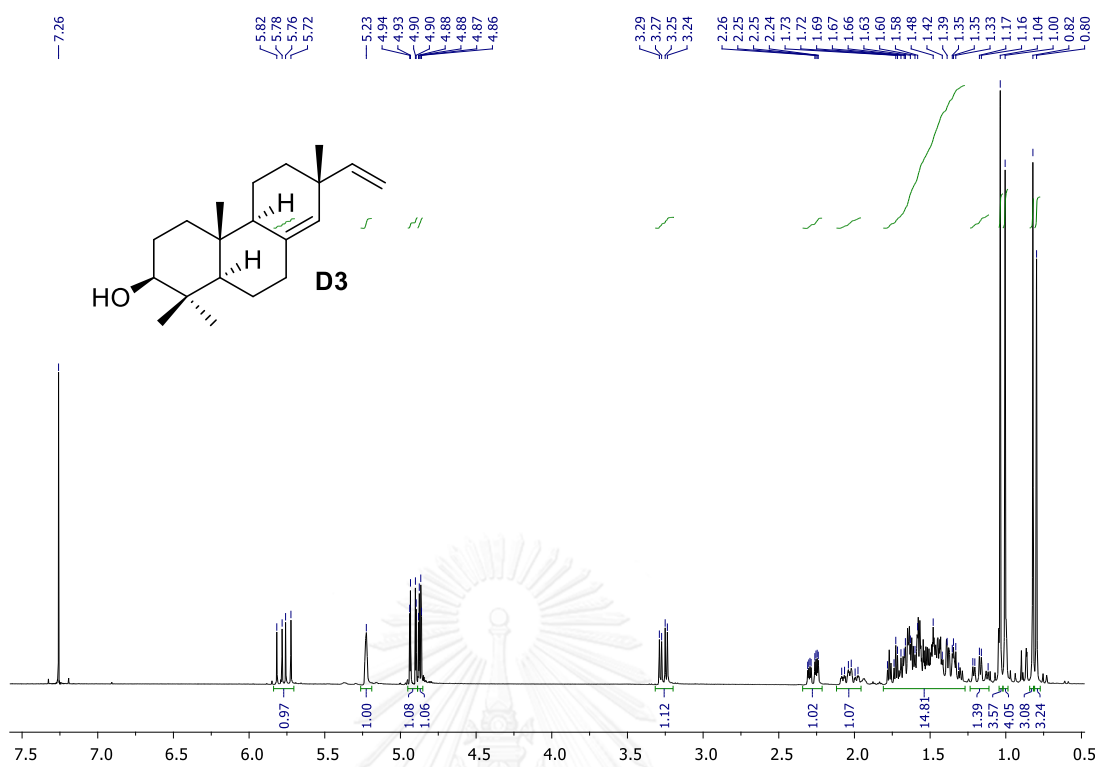


Figure A5 The  $^1\text{H}$  NMR spectrum of sandaracopimaradien-3 $\beta$ -ol (D3) (CDCl $_3$ )

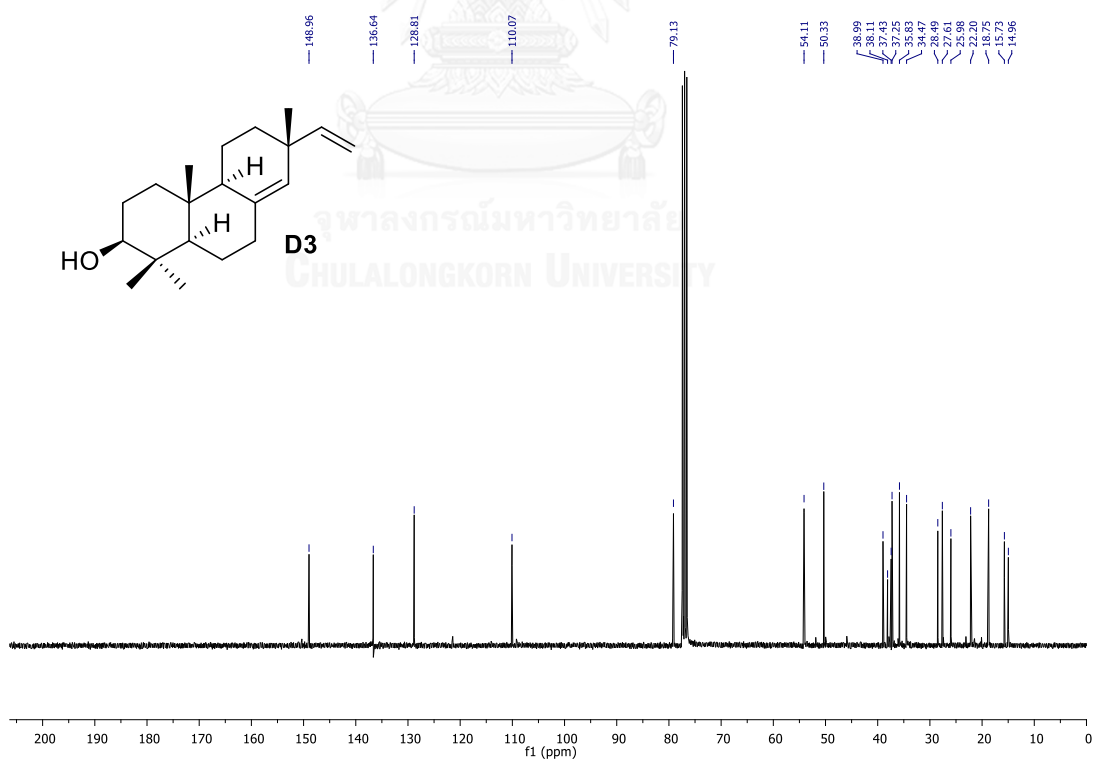


Figure A6 The  $^{13}\text{C}$  NMR spectrum of sandaracopimaradien-3 $\beta$ -ol (D3) (CDCl $_3$ )

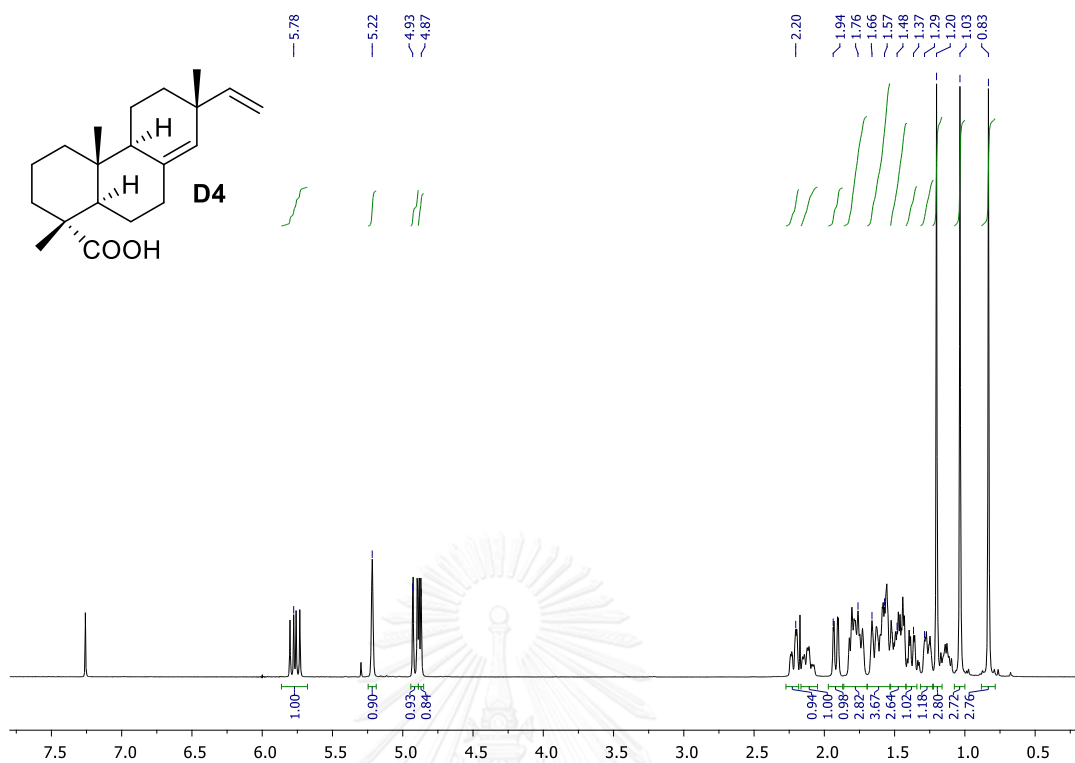


Figure A7 The  $^1\text{H}$  NMR spectrum of sandaracopimaric acid (D4) (CDCl<sub>3</sub>)

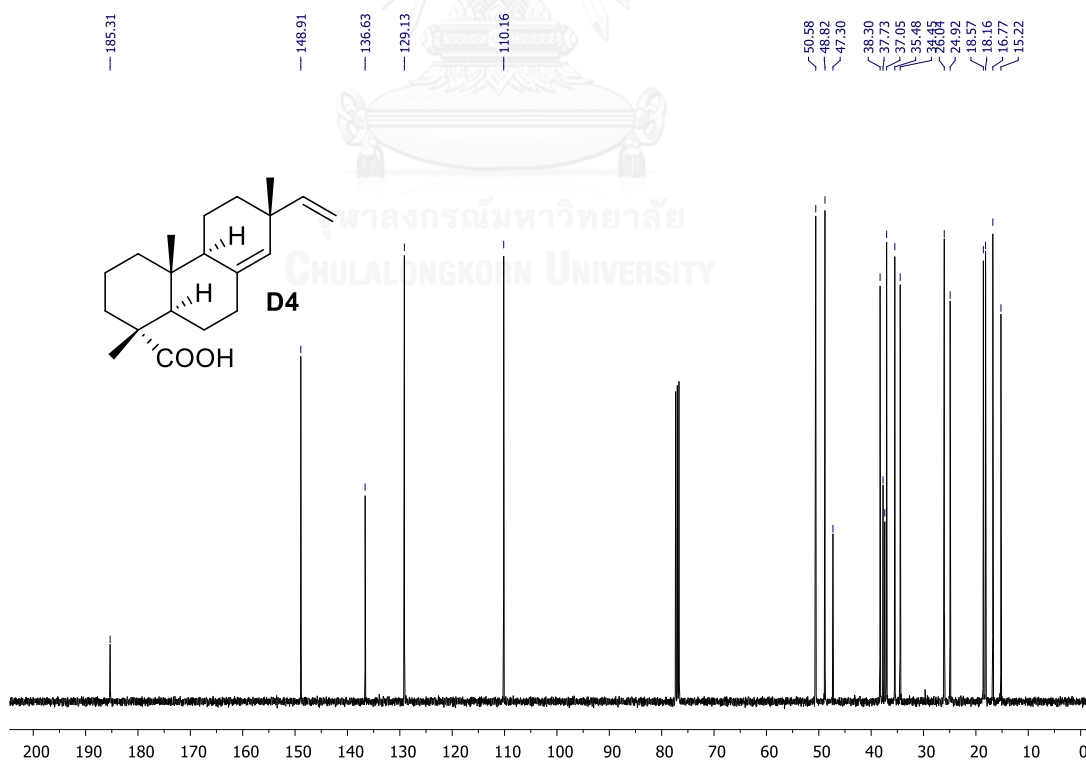


Figure A8 The  $^{13}\text{C}$  NMR spectrum of sandaracopimaric acid (D4) (CDCl<sub>3</sub>)

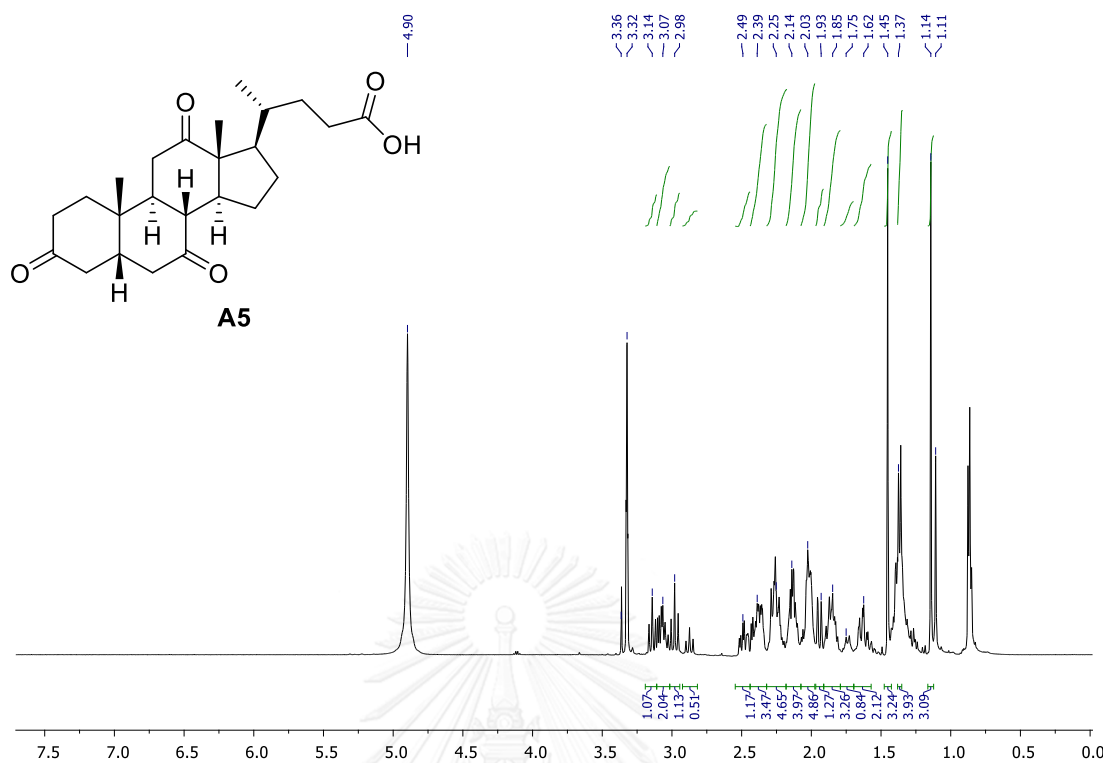


Figure A9 The  $^1\text{H}$  NMR spectrum of triketocholanic acid (A5) ( $\text{CD}_3\text{OD}$ )

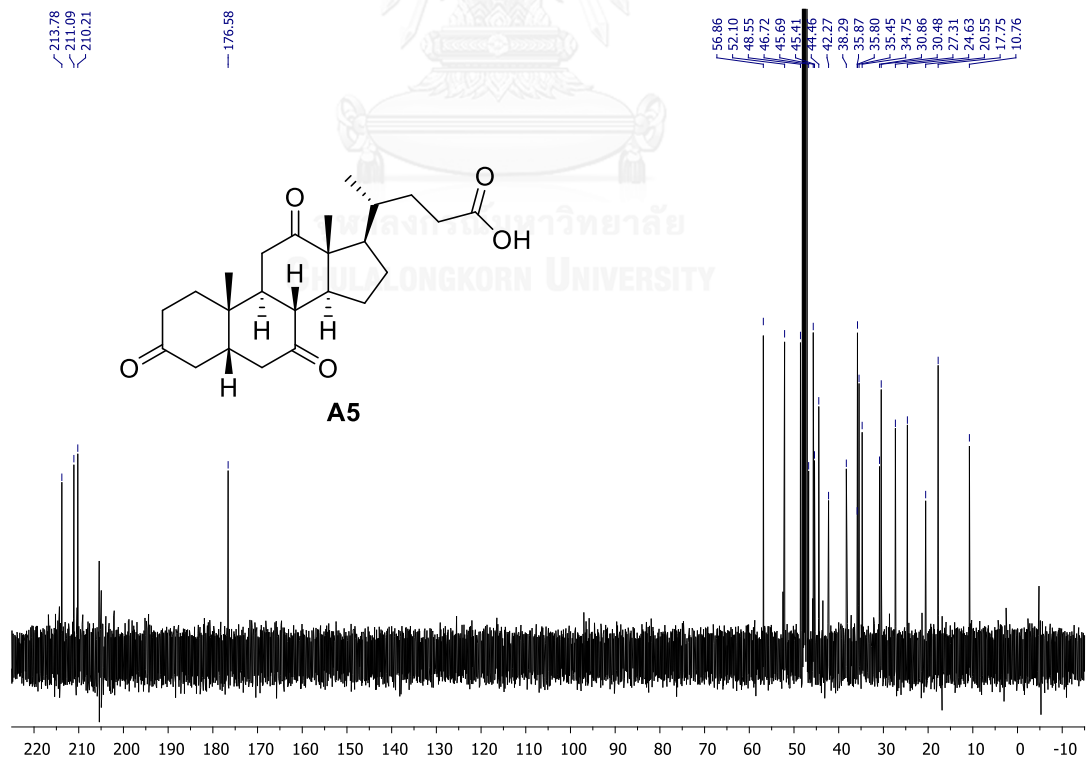


Figure A10 The  $^{13}\text{C}$  NMR spectrum of triketocholanic acid (A5) ( $\text{CD}_3\text{OD}$ )

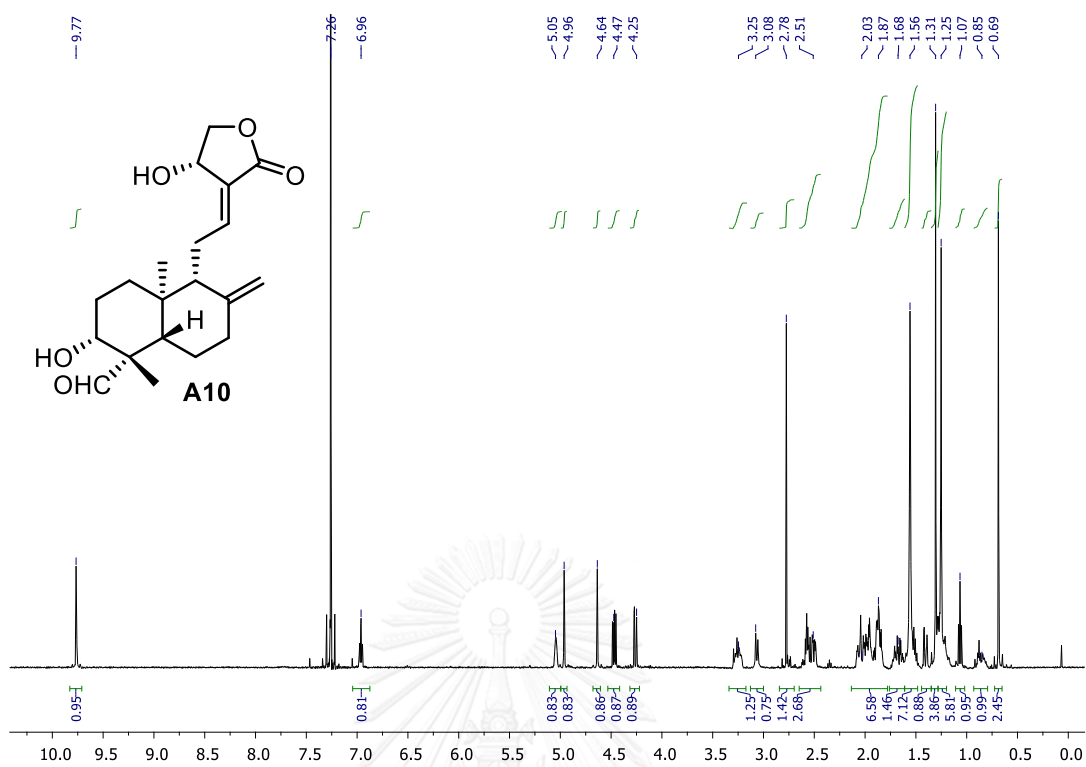


Figure A11 The  $^1\text{H}$  NMR spectrum of 19-dehydroandrographolide (A10) (CDCl<sub>3</sub>)

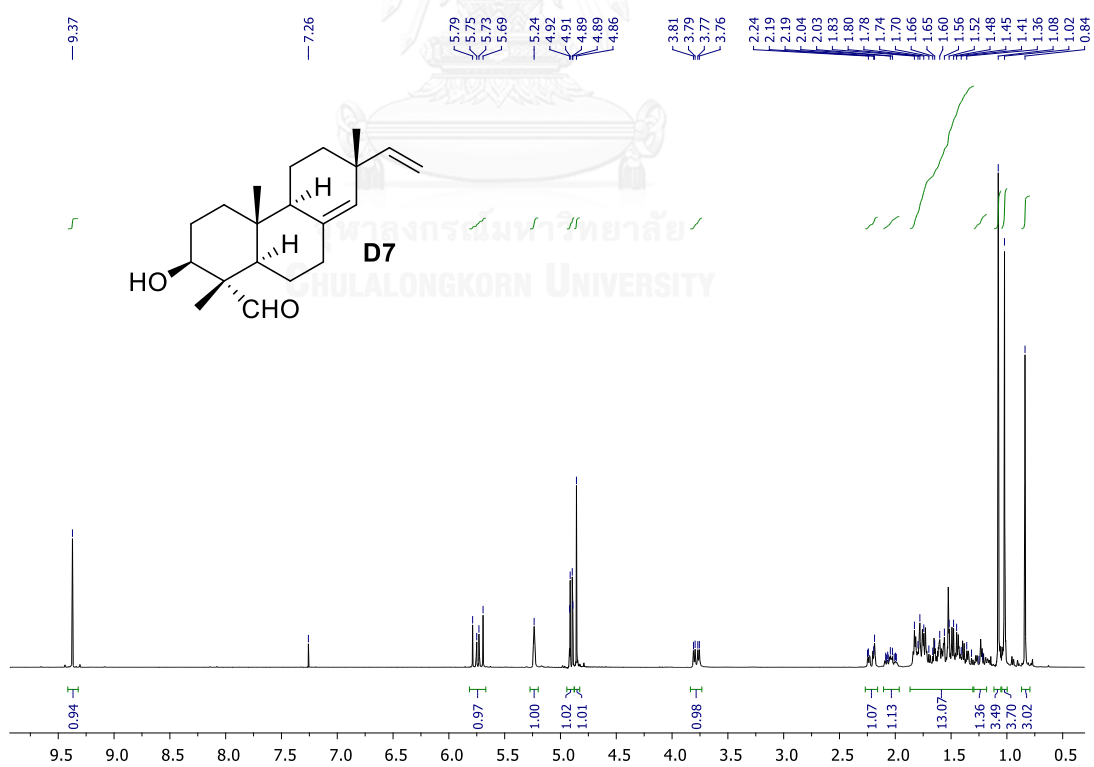


Figure A12 The  $^1\text{H}$  NMR spectrum of sandaracopimaradien-3 $\beta$ ,18-olal (D7) (CDCl<sub>3</sub>)

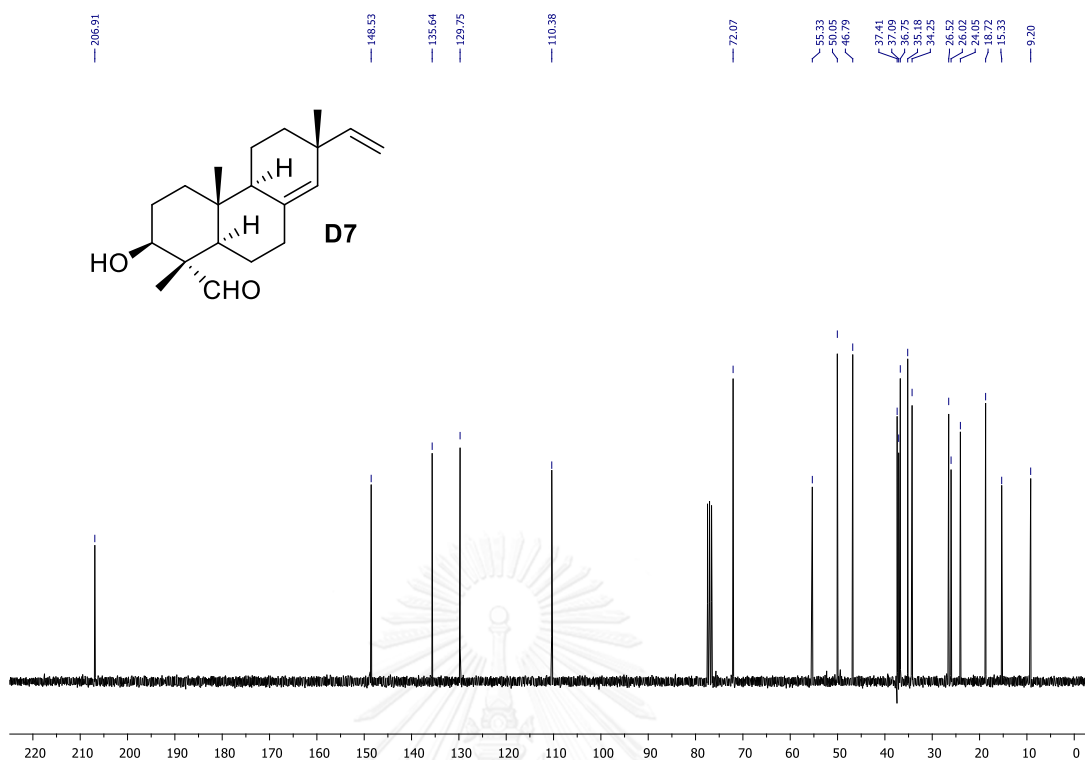


Figure A13 The <sup>13</sup>C NMR spectrum of sandaracopimaradien-3β,18-olal (D7) (CDCl<sub>3</sub>)

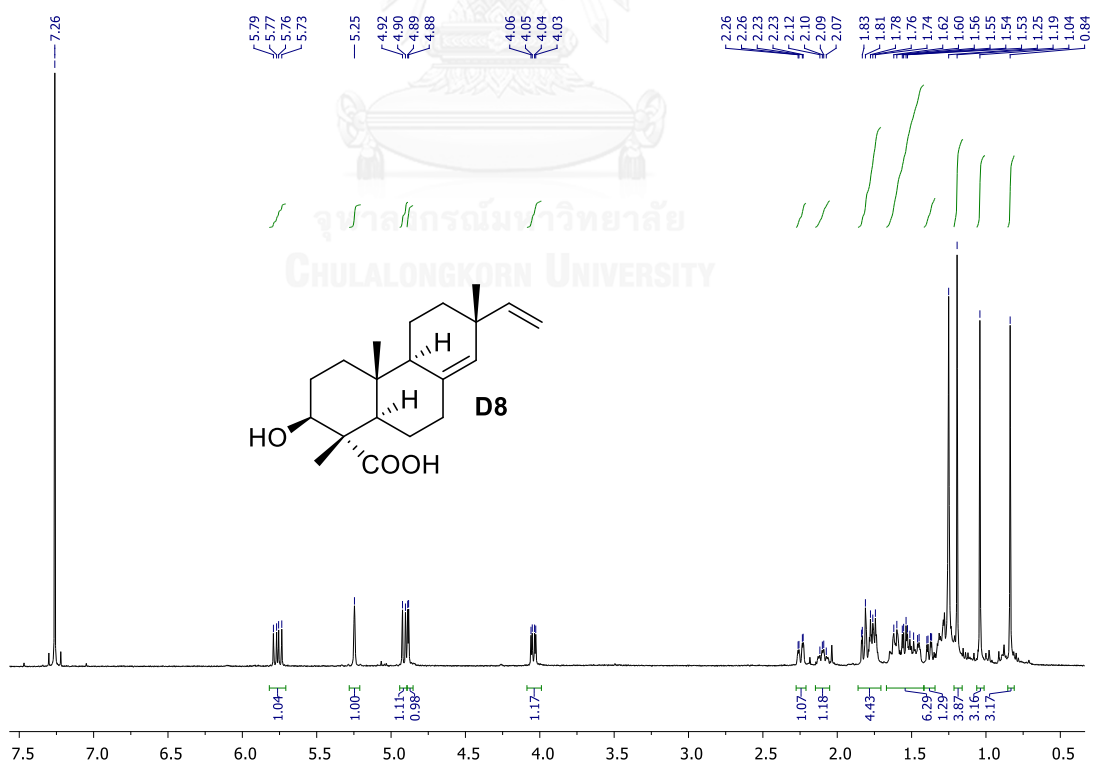


Figure A14 The <sup>1</sup>H NMR spectrum of 3β-hydroxysandaracopimaric acid (D8) (CDCl<sub>3</sub>)

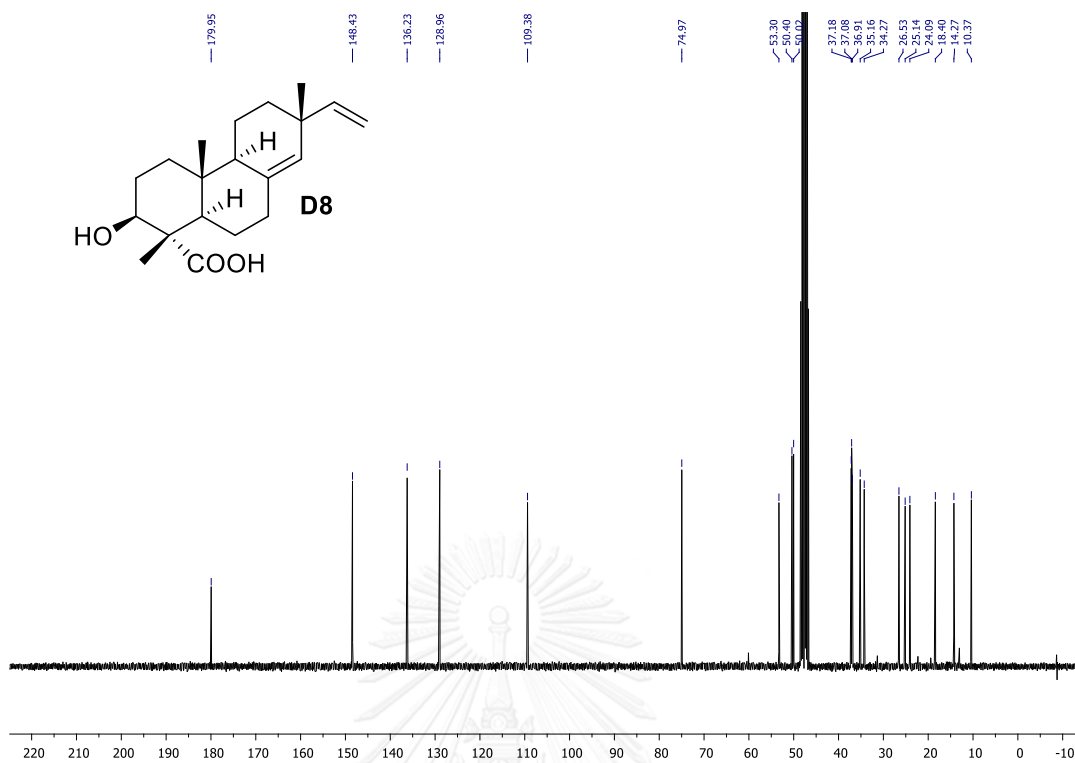


Figure A15 The  $^{13}\text{C}$  NMR spectrum of  $3\beta$ -hydroxysandaracopimaric acid (**D8**) ( $\text{CD}_3\text{OD}$ )

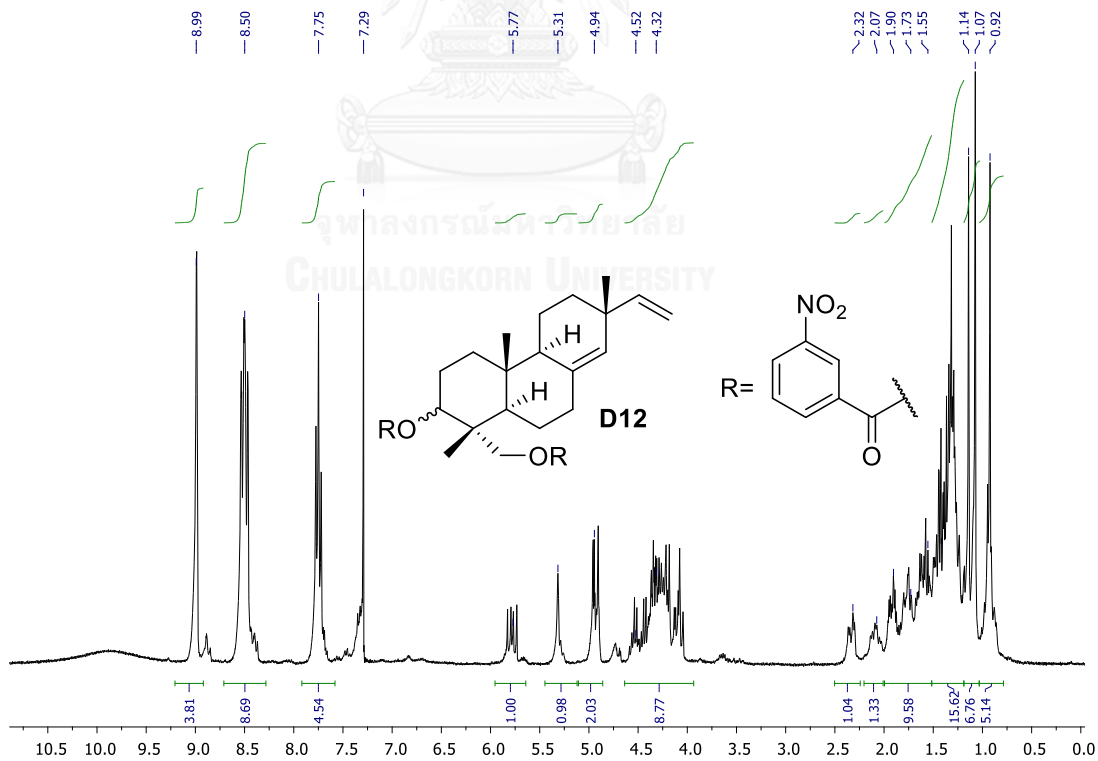
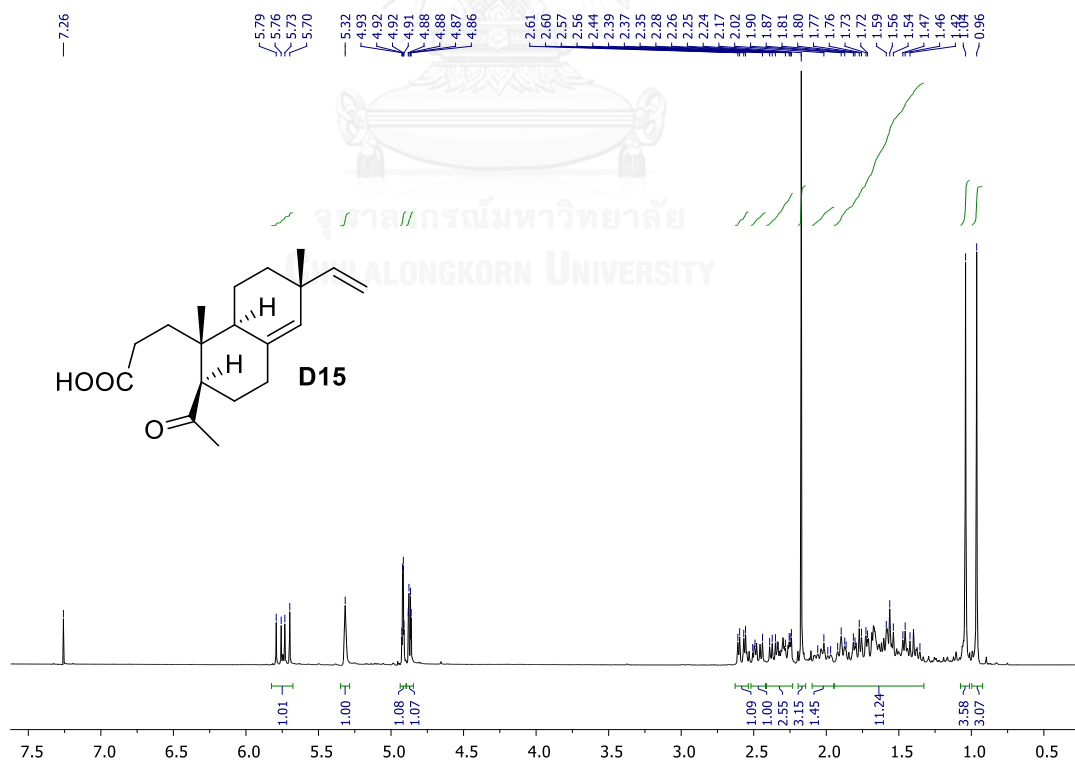
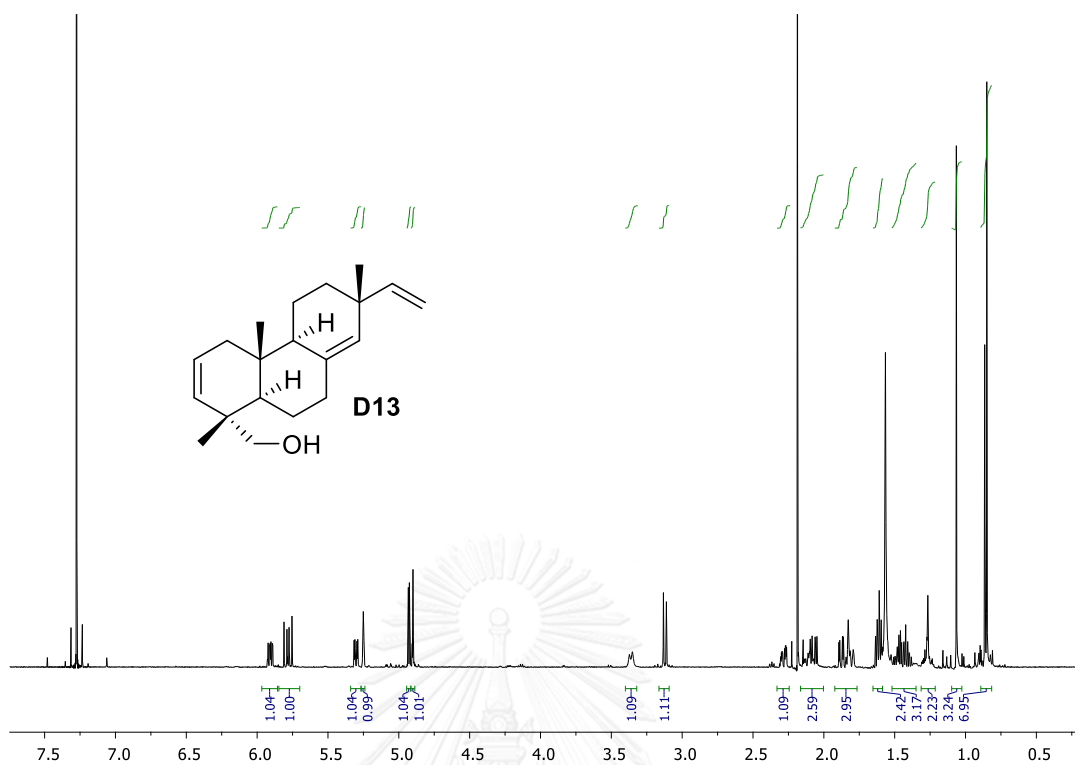


Figure A16 The  $^1\text{H}$  NMR spectrum of ester derivative **D12** ( $\text{CDCl}_3$ )





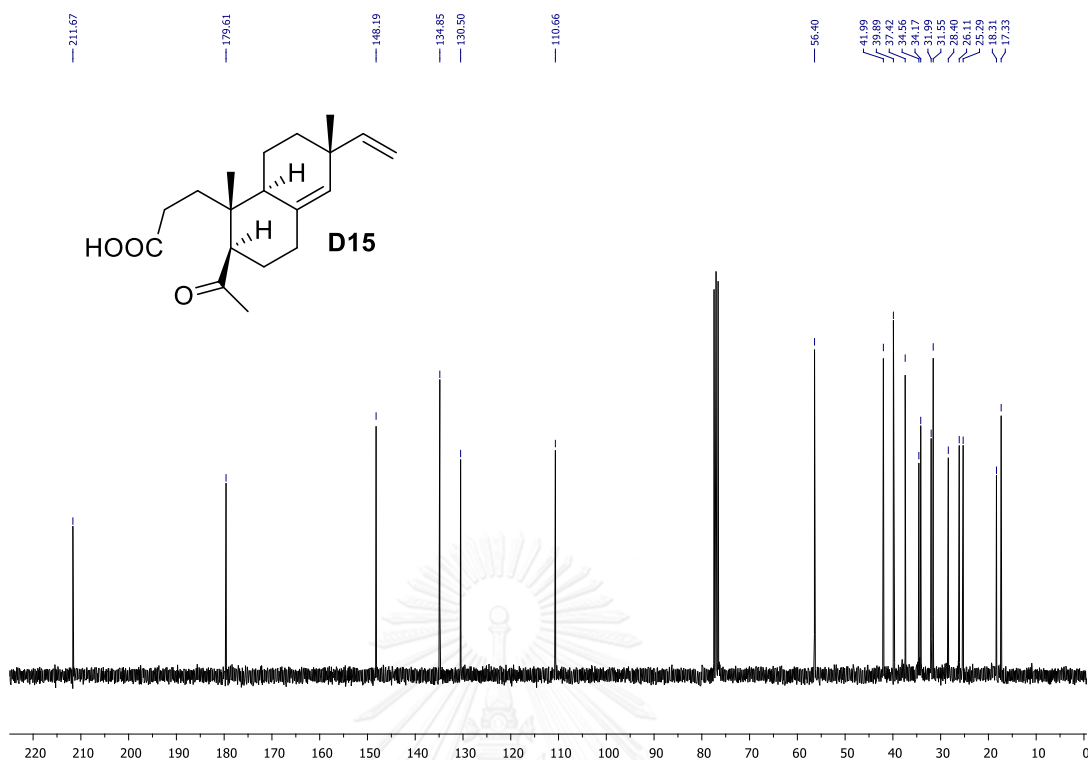


Figure A19 The  $^{13}\text{C}$  NMR spectrum of keto acid derivative **D15** (CDCl<sub>3</sub>)

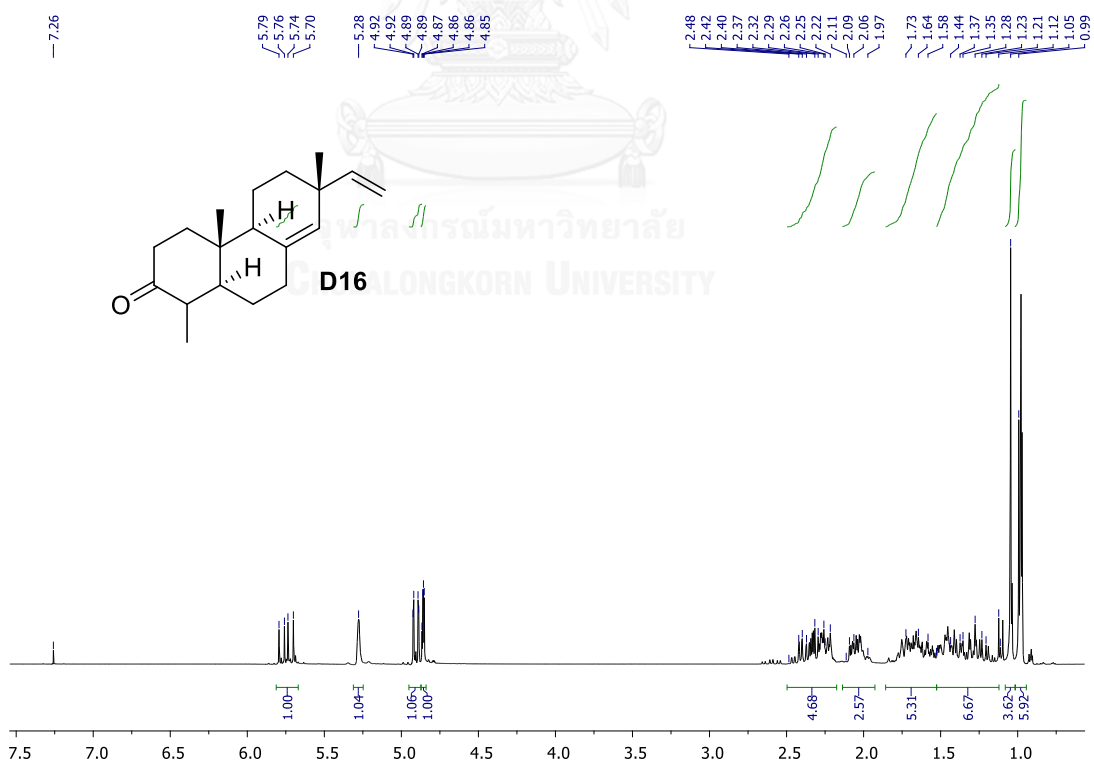


Figure A20 The  $^1\text{H}$  NMR spectrum of keto derivative **D16** (CDCl<sub>3</sub>)

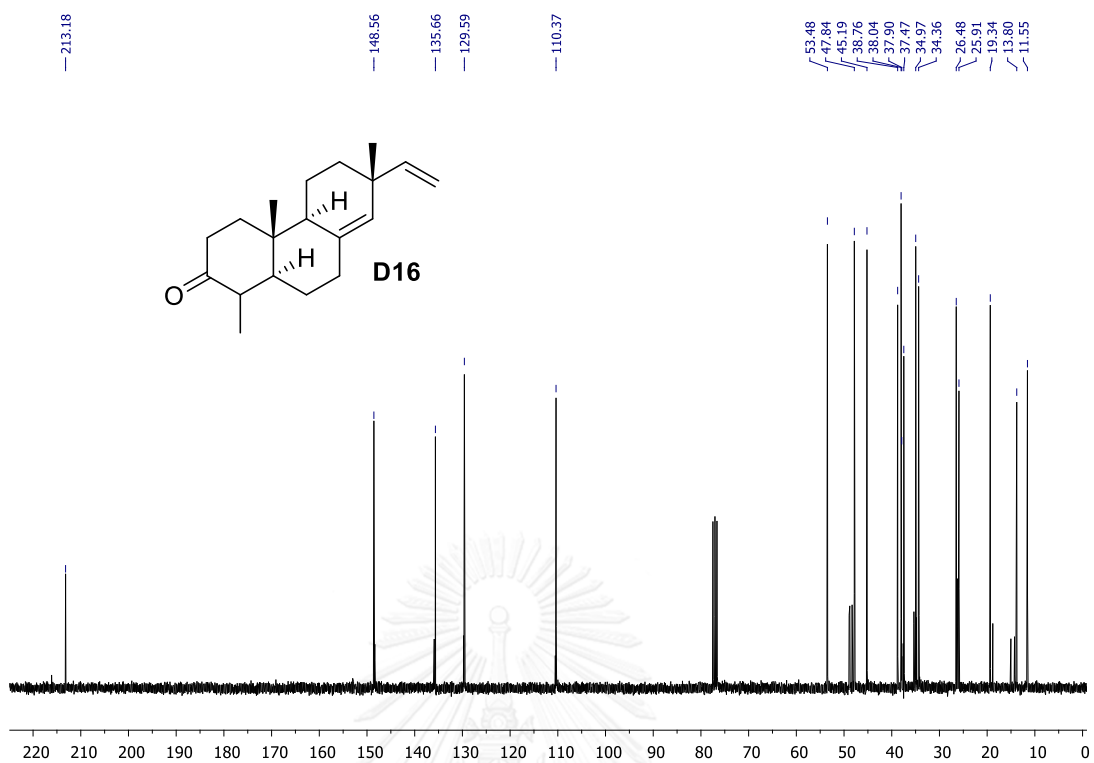


Figure A21 The  $^{13}\text{C}$  NMR spectrum of keto derivative **D16** (CDCl<sub>3</sub>)

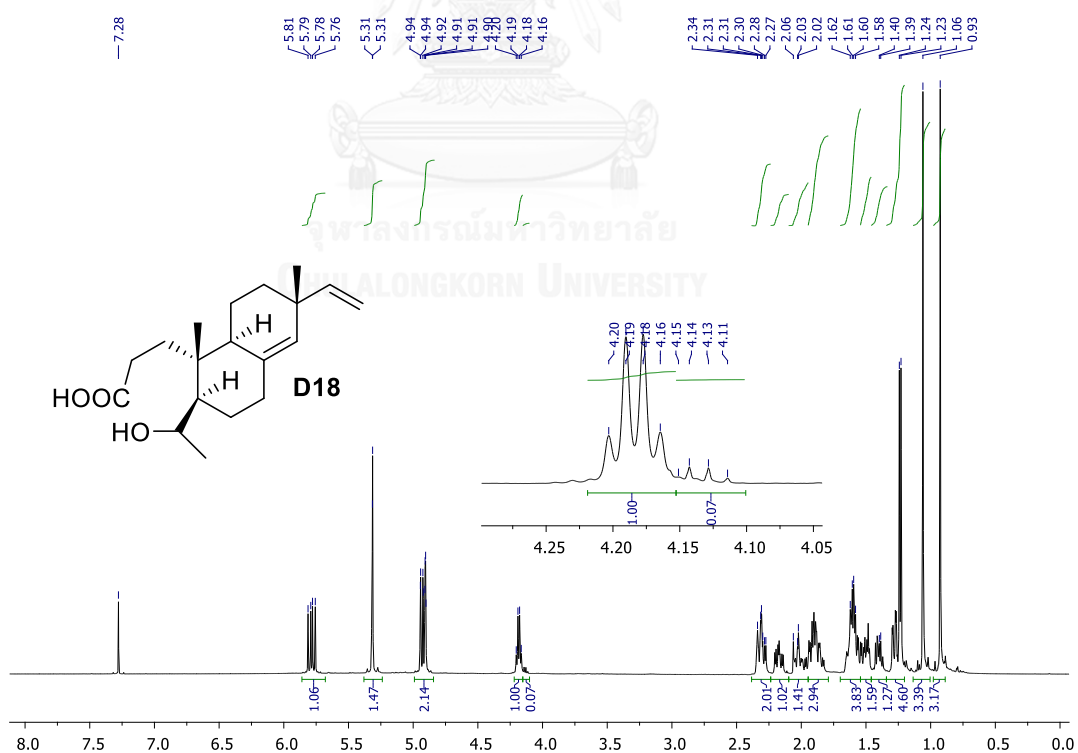


Figure A22 The  $^1\text{H}$  NMR spectrum of hydroxy acid derivative **D18** (CDCl<sub>3</sub>)

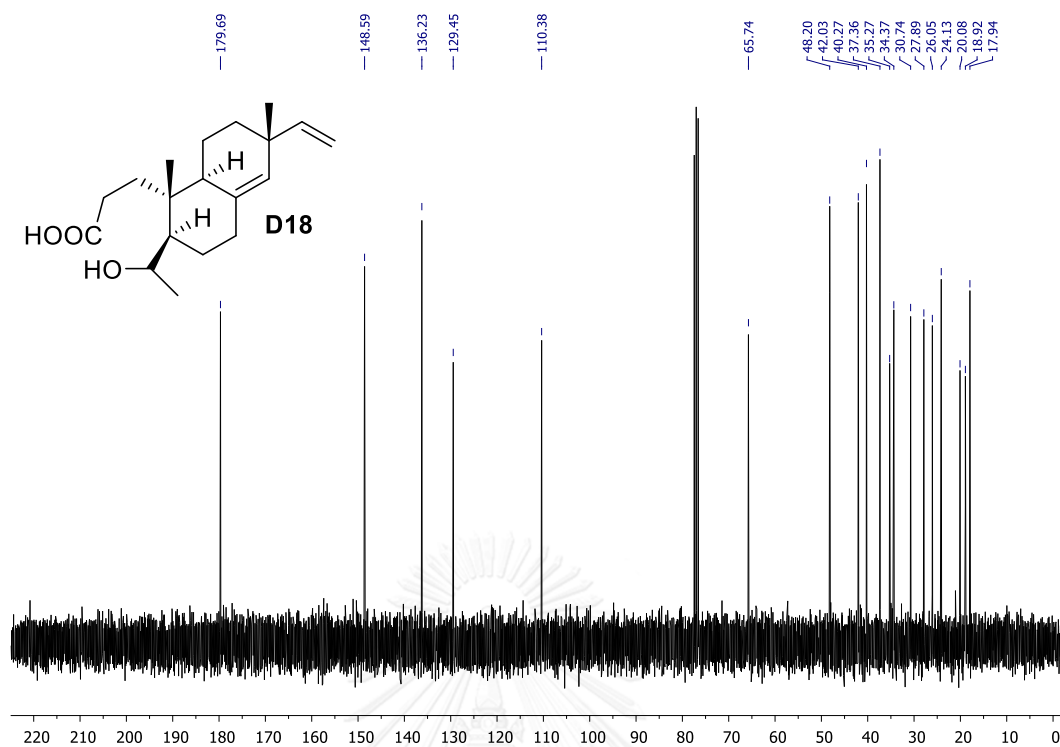


Figure A23 The  $^{13}\text{C}$  NMR spectrum of hydroxy acid derivative **D18** (CDCl<sub>3</sub>)

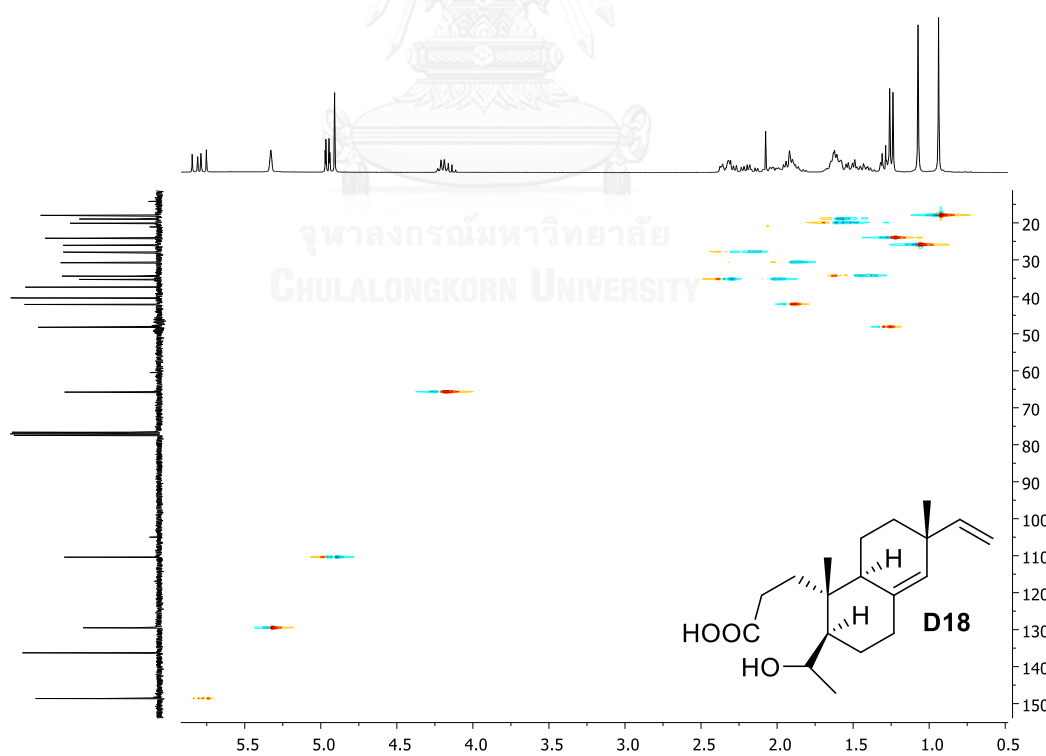


Figure A24 The HSQC spectrum of hydroxy acid derivative **D18** (CDCl<sub>3</sub>)

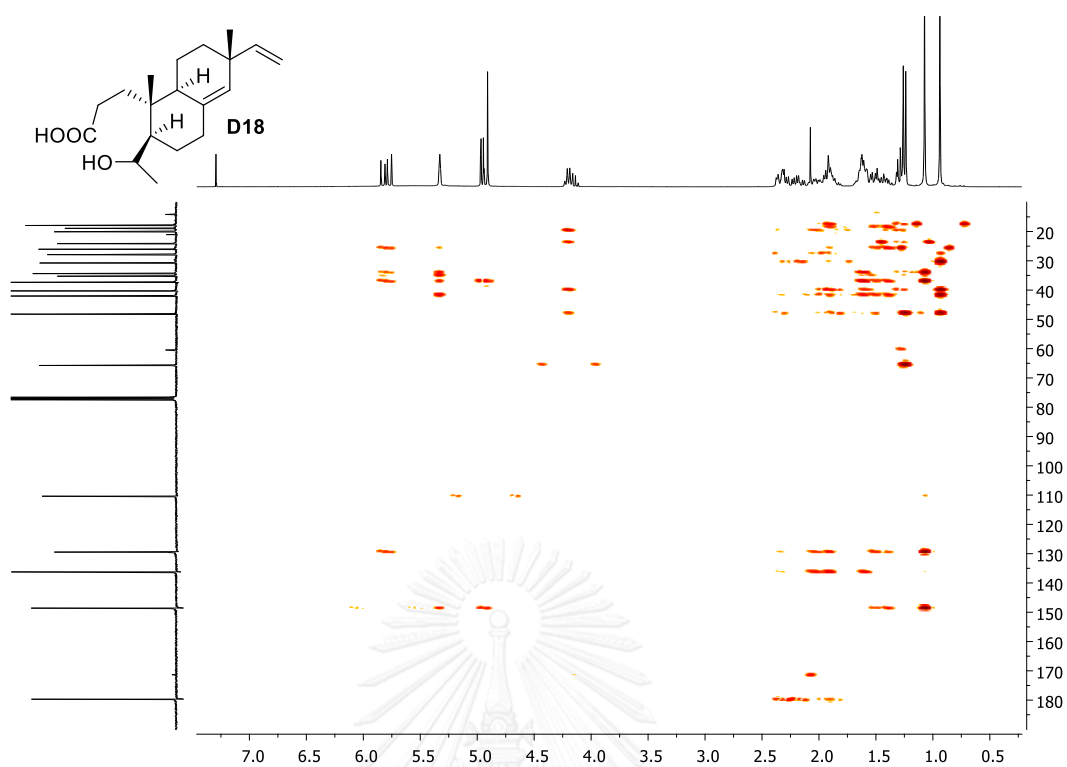


Figure A25 The HMBC spectrum of hydroxy acid derivative **D18** ( $\text{CDCl}_3$ )

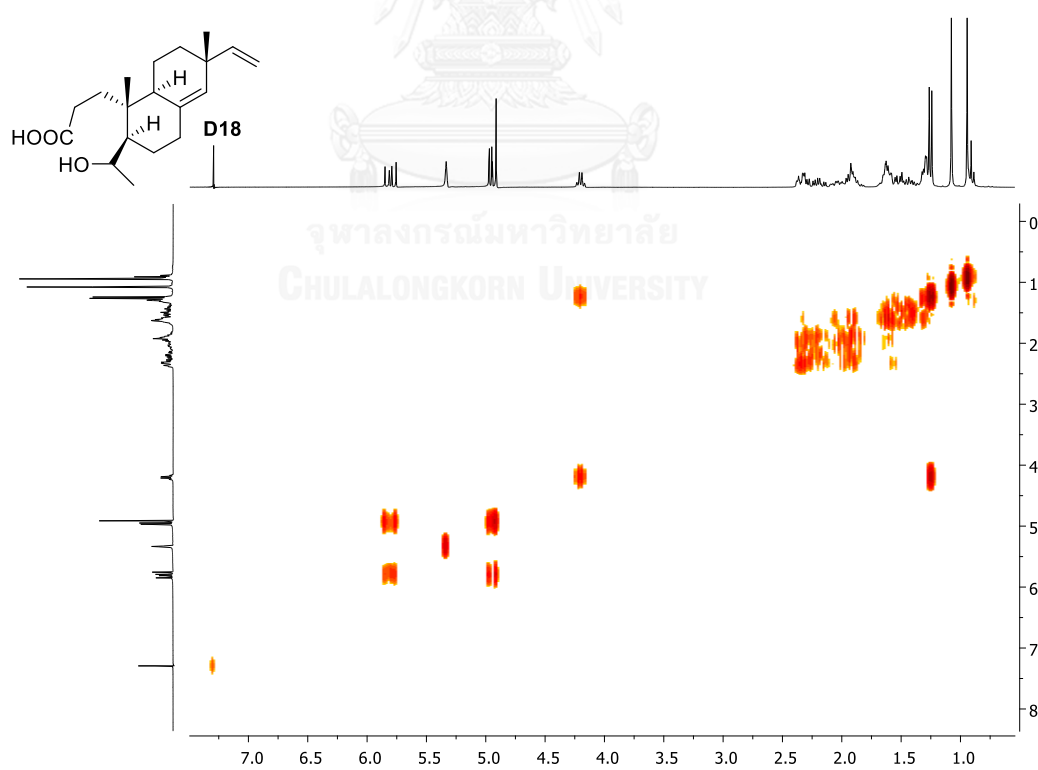
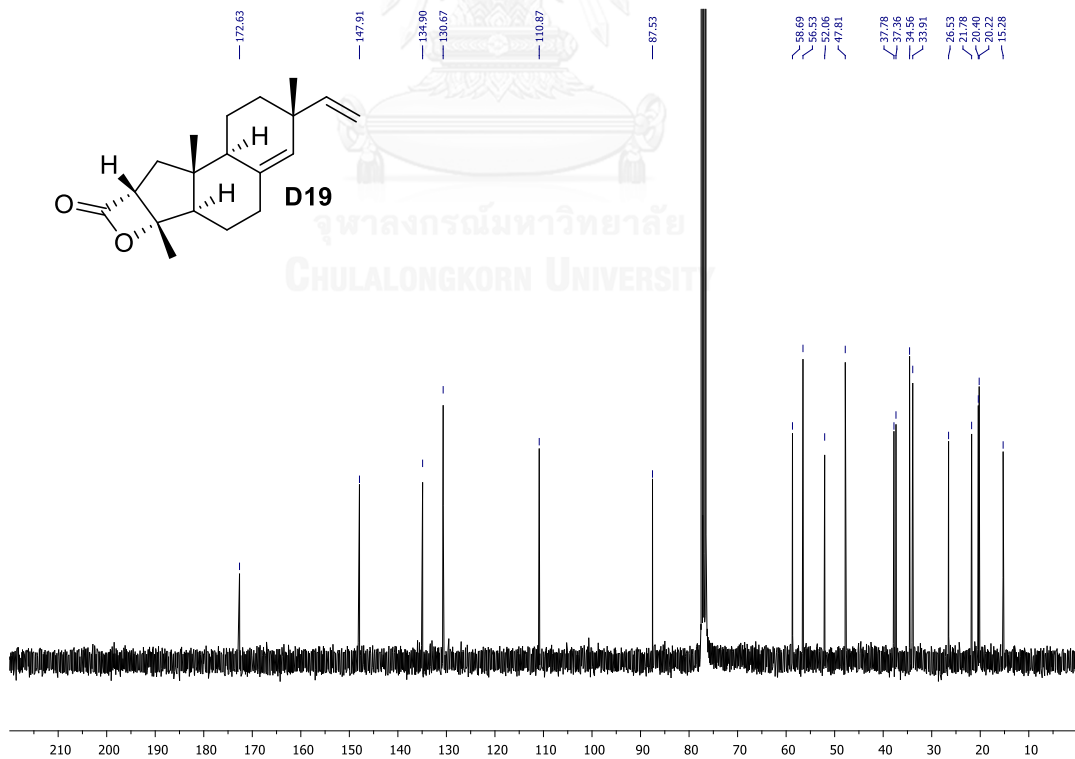
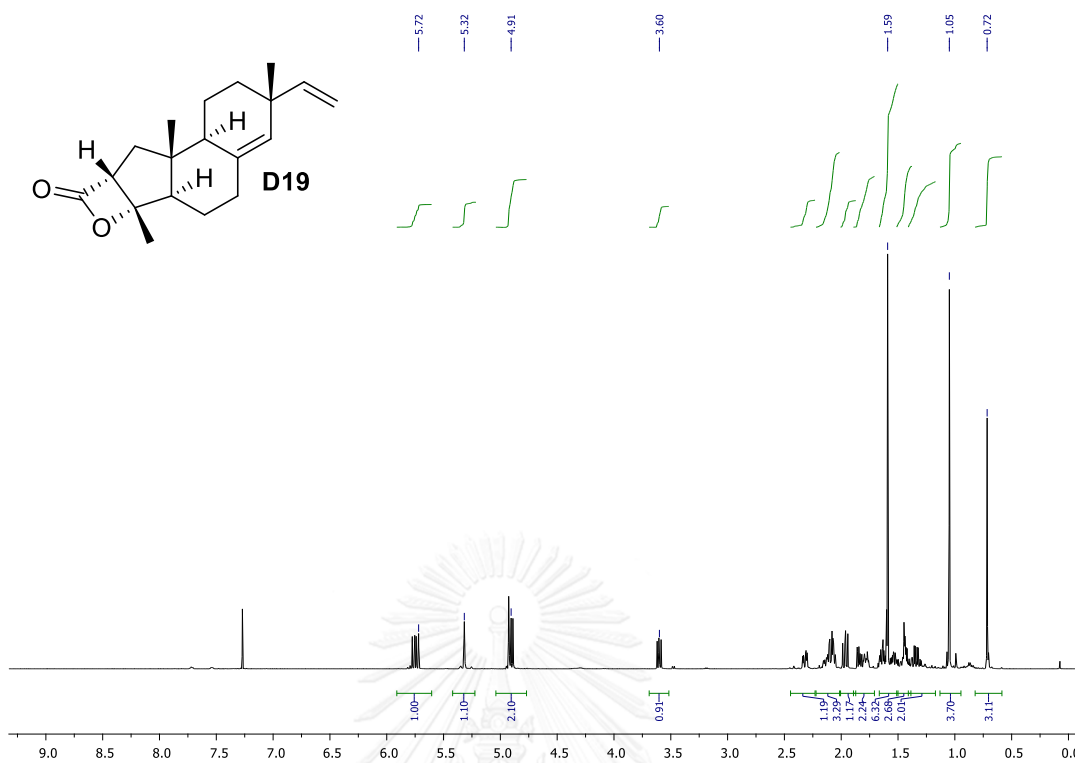


Figure A26 The COSY spectrum of hydroxy acid derivative **D18** ( $\text{CDCl}_3$ )



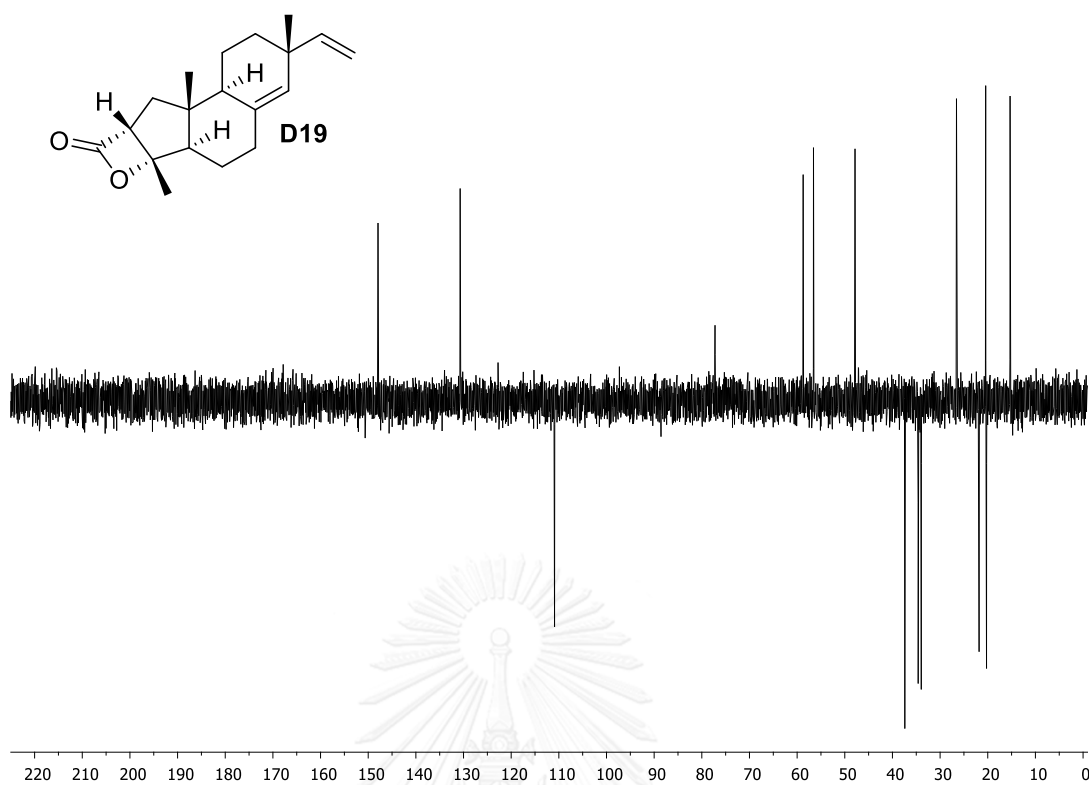


Figure A29 The  $^{13}\text{C}$  NMR (DEPT 135°) spectrum of beta-lactone derivative **D19** ( $\text{CDCl}_3$ )

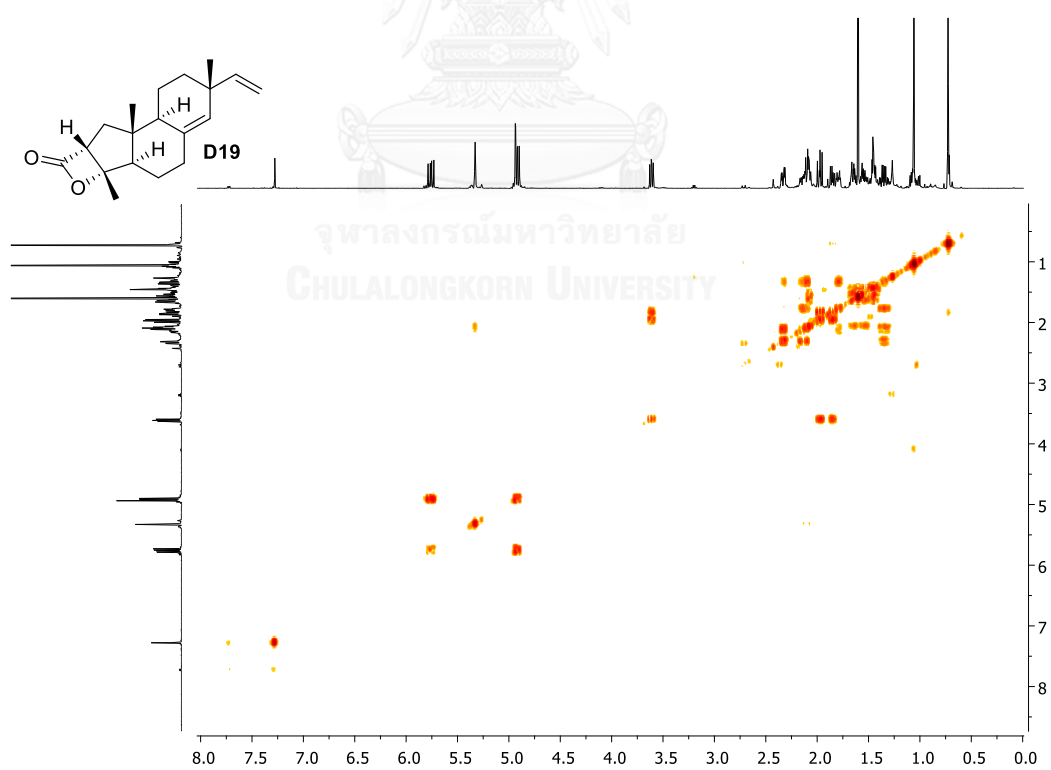


Figure A30 The COSY spectrum of beta-lactone derivative **D19** ( $\text{CDCl}_3$ )

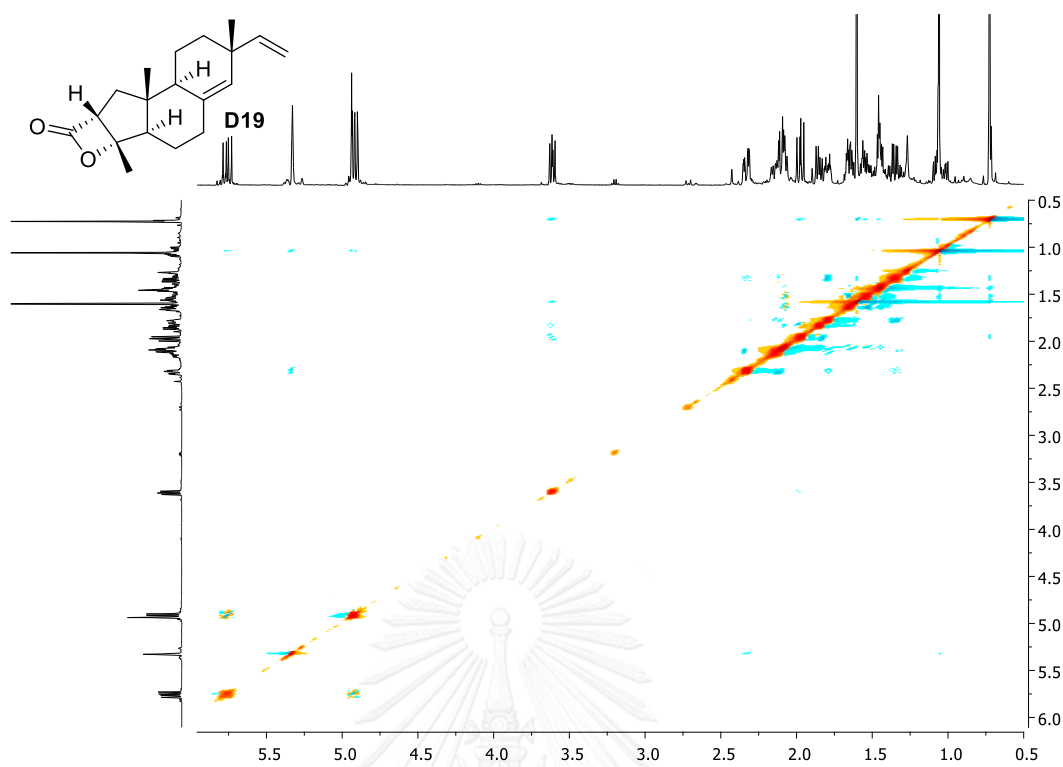


Figure A31 The NOSEY spectrum of beta-lactone derivative **D19** (CDCl<sub>3</sub>)

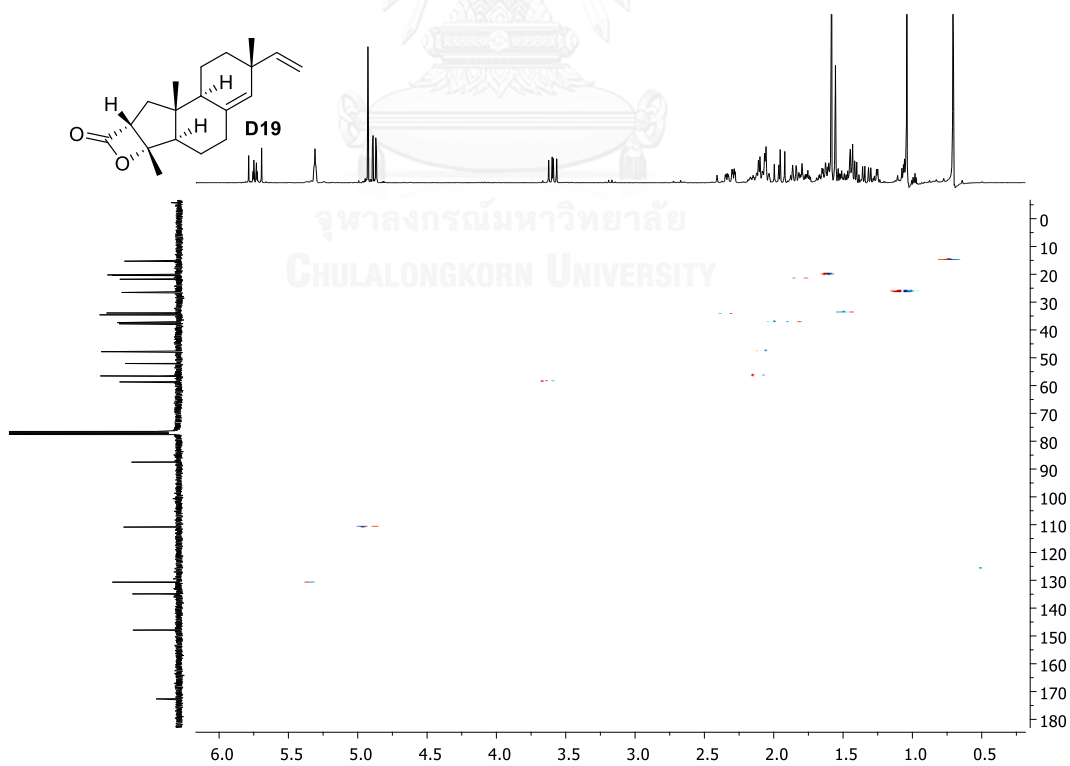


Figure A32 The HSQC spectrum of beta-lactone derivative **D19** (CDCl<sub>3</sub>)

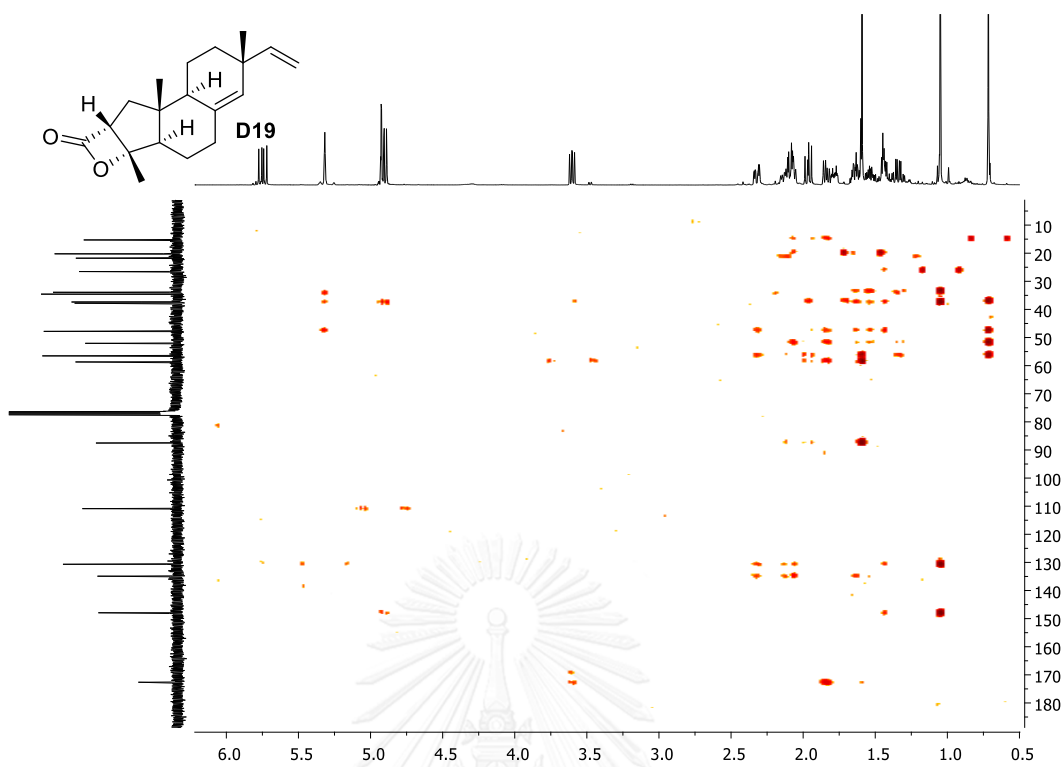


Figure A33 The HMBC spectrum of beta-lactone derivative **D19** ( $\text{CDCl}_3$ )

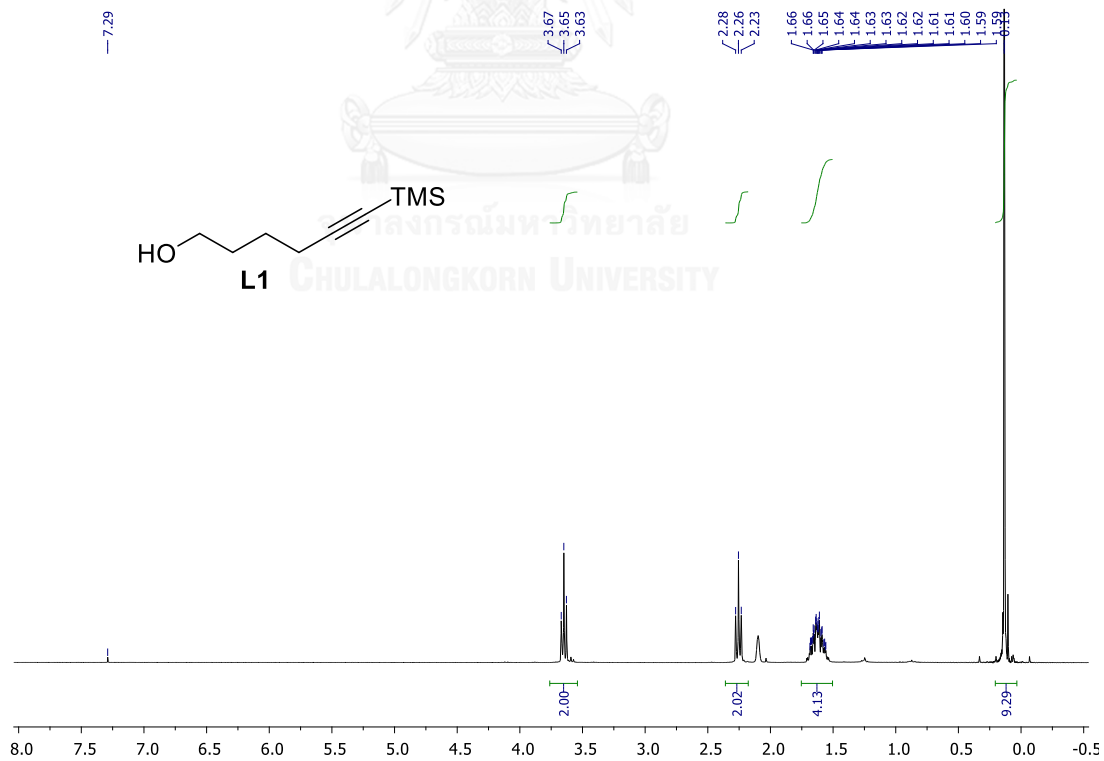


Figure A34 The  $^1\text{H}$  NMR spectrum of 6-(trimethylsilyl)hex-5-yn-1-ol (**L1**) ( $\text{CDCl}_3$ )



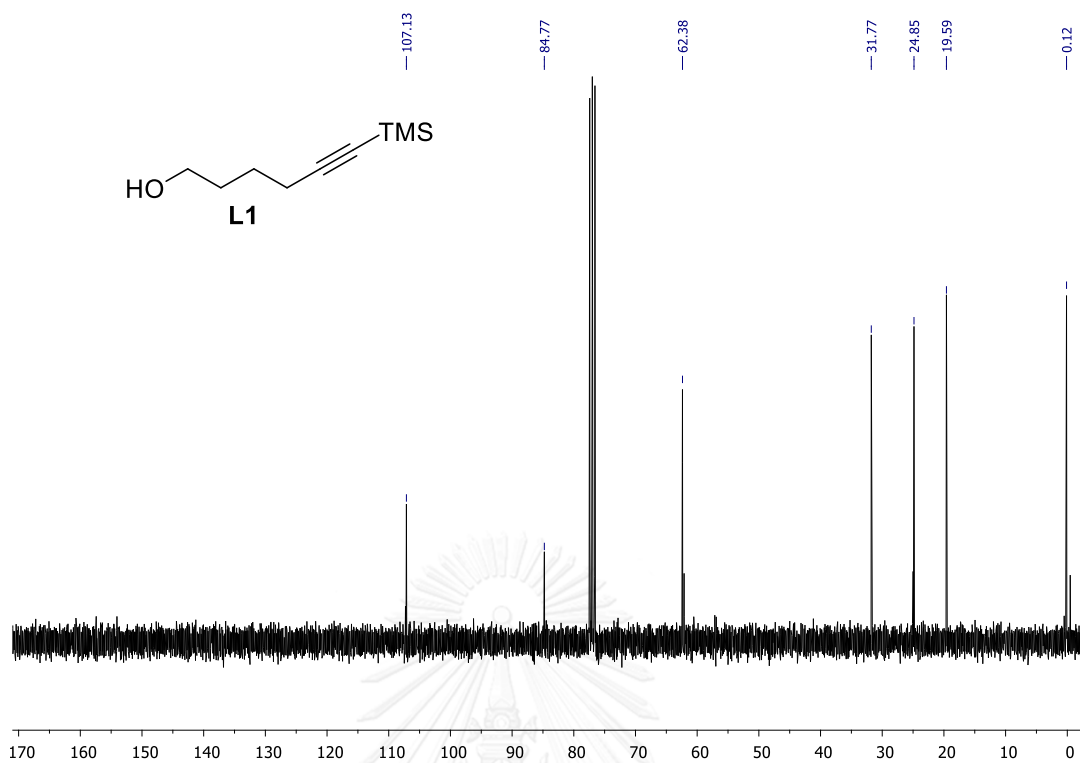


Figure A35 The  $^{13}\text{C}$  NMR spectrum of 6-(trimethylsilyl)hex-5-yn-1-ol (L1) ( $\text{CDCl}_3$ )

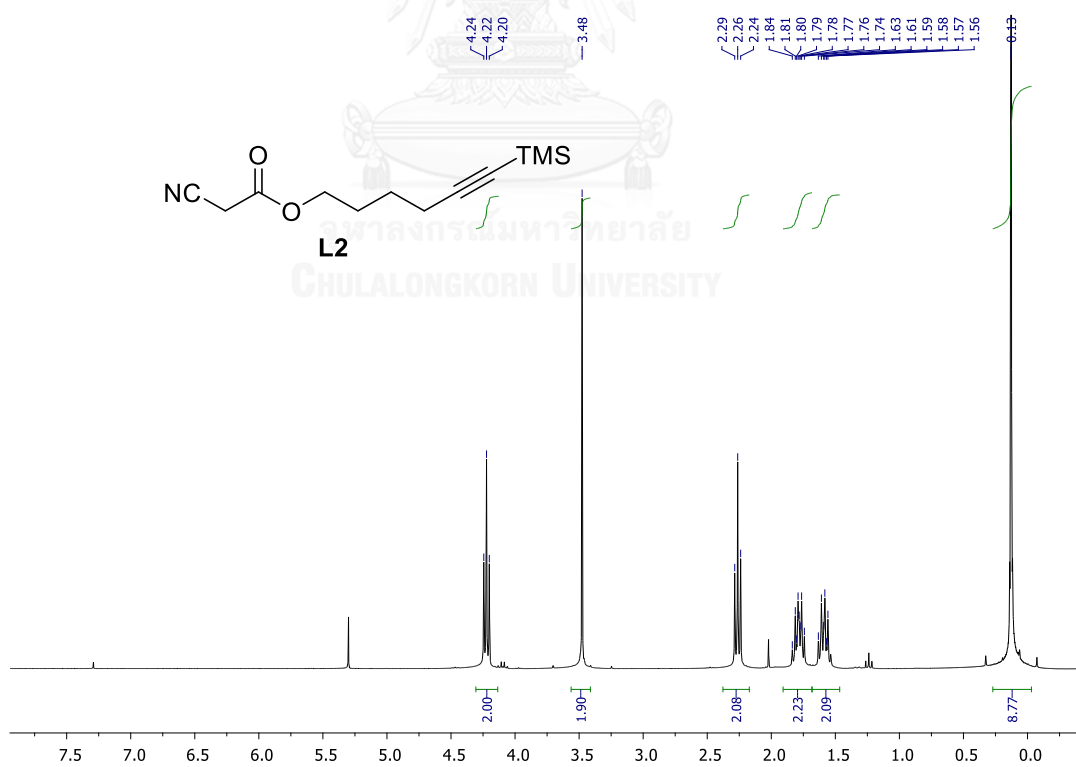


Figure A36 The  $^1\text{H}$  NMR spectrum of 6-(trimethylsilyl)hex-5-yn-1-yl 2-cyanoacetate (L2) ( $\text{CDCl}_3$ )

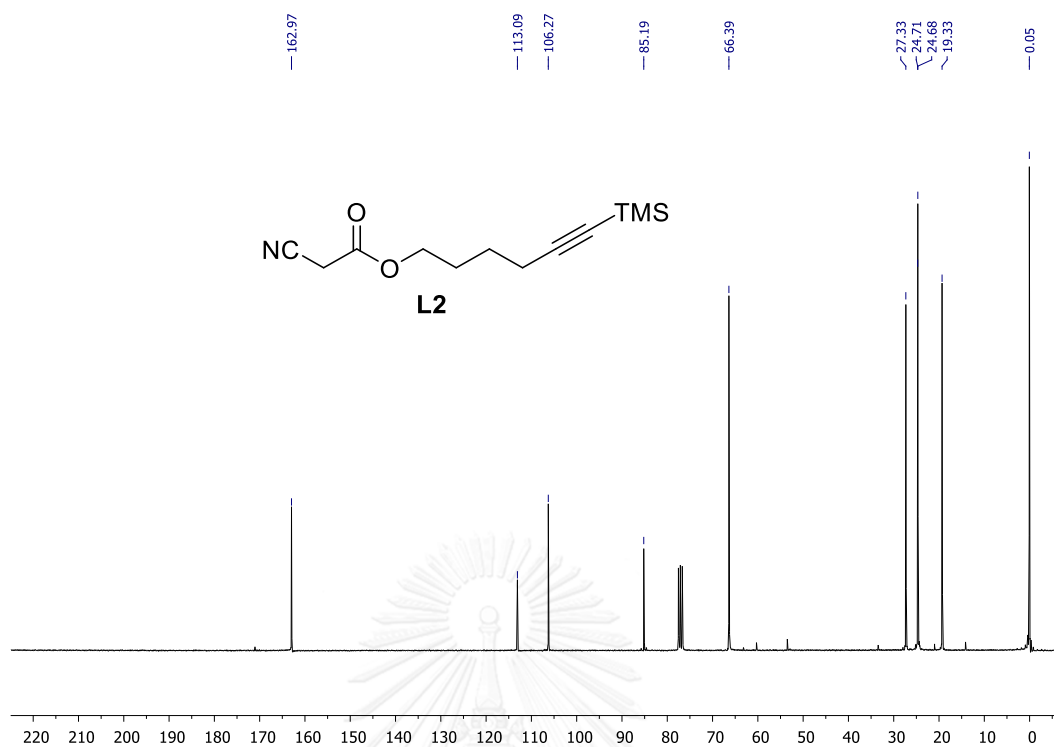


Figure A37 The  $^{13}\text{C}$  NMR spectrum of 6-(trimethylsilyl)hex-5-yn-1-yl 2-cyanoacetate (L2) ( $\text{CDCl}_3$ )

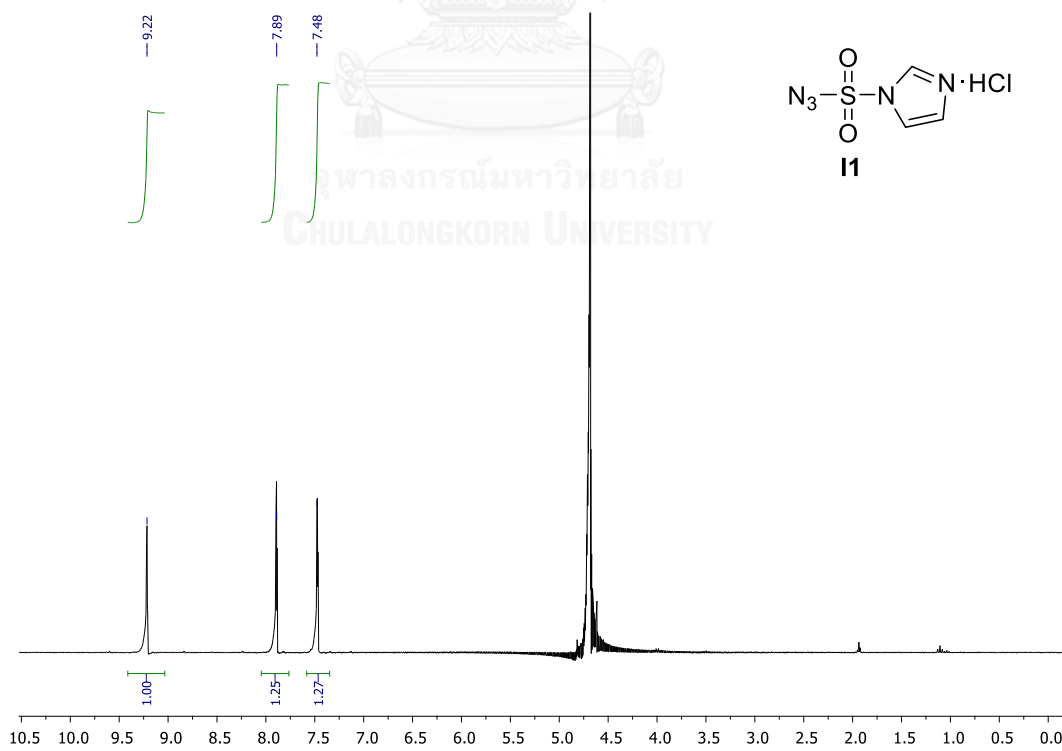


Figure A38 The  $^1\text{H}$  NMR spectrum of imidazole-1-sulfonyl azide hydrochloride (I1) ( $\text{D}_2\text{O}$ )

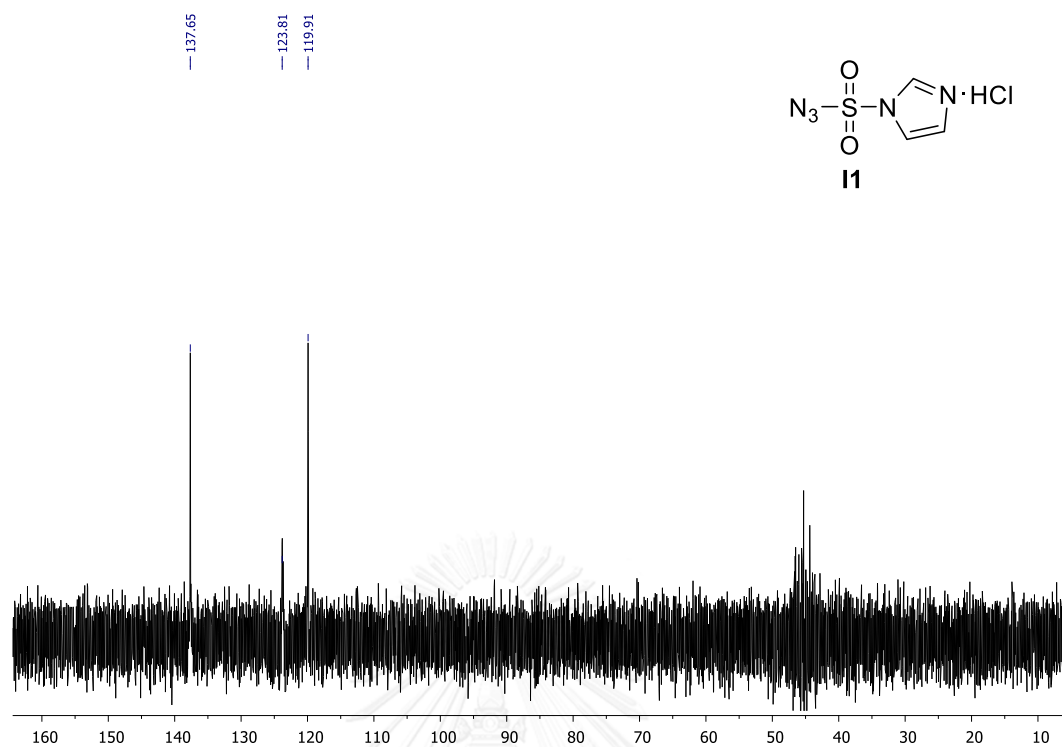


Figure A39 The  $^{13}\text{C}$  NMR spectrum of imidazole-1-sulfonyl azide hydrochloride (**11**) ( $\text{D}_2\text{O}$ )

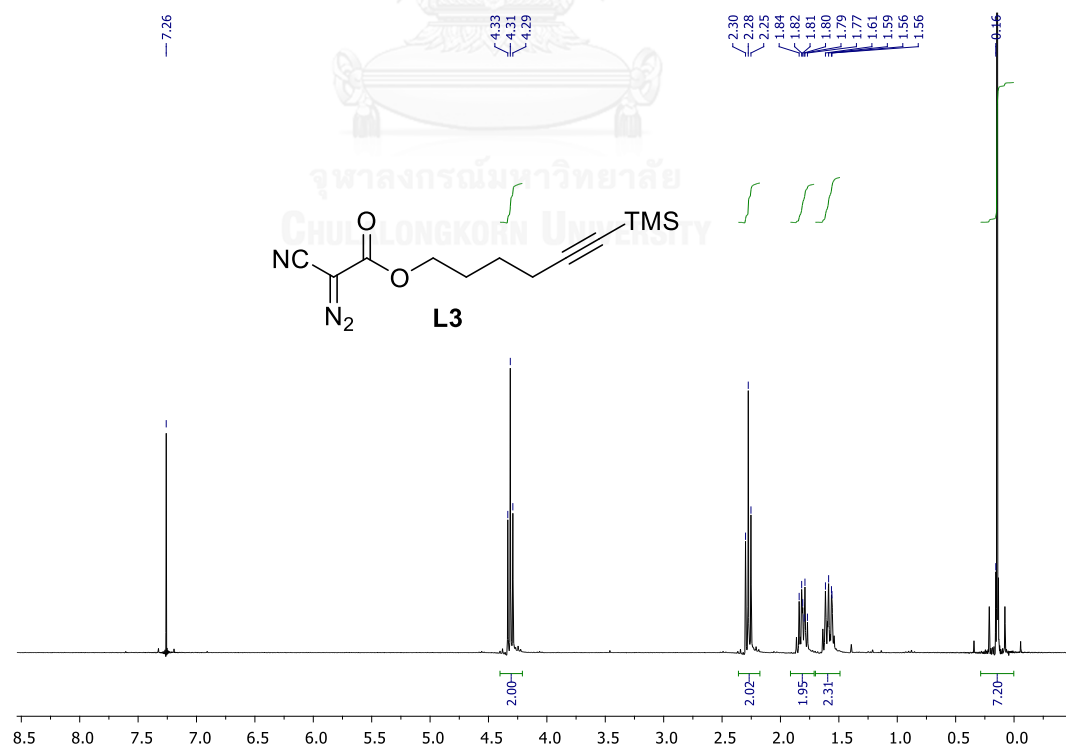


Figure A40 The  $^1\text{H}$  NMR spectrum of 6-(trimethylsilyl)hex-5-yn-1-yl 2-cyano-2-diazoacetate (**L3**) ( $\text{CDCl}_3$ )

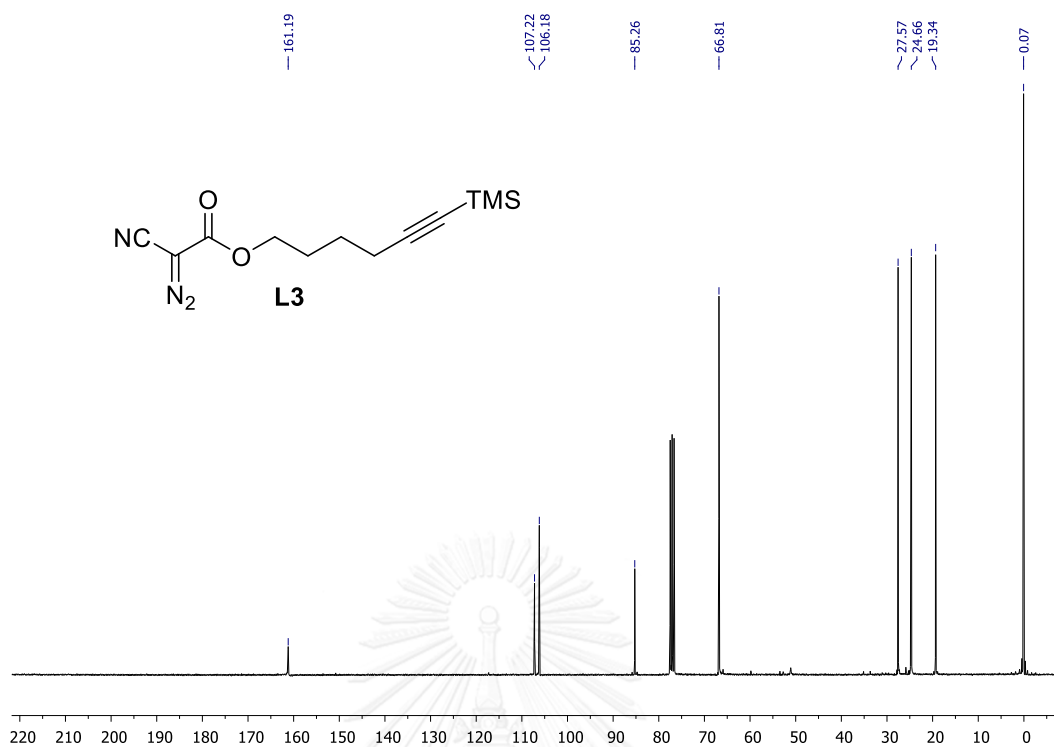


Figure A41 The  $^{13}\text{C}$  NMR spectrum of 6-(trimethylsilyl)hex-5-yn-1-yl 2-cyano-2-diazoacetate (**L3**) ( $\text{CDCl}_3$ )

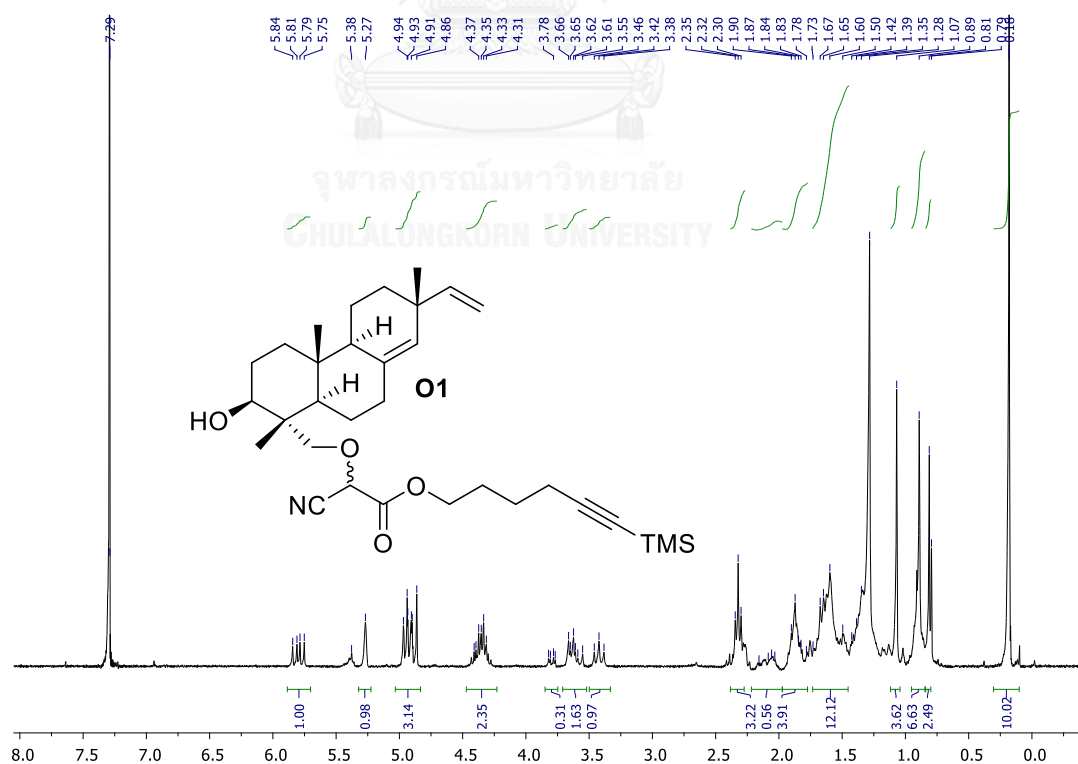


Figure A42 The  $^1\text{H}$  NMR spectrum of mixture diastereomer **1 (O1)** ( $\text{CDCl}_3$ )

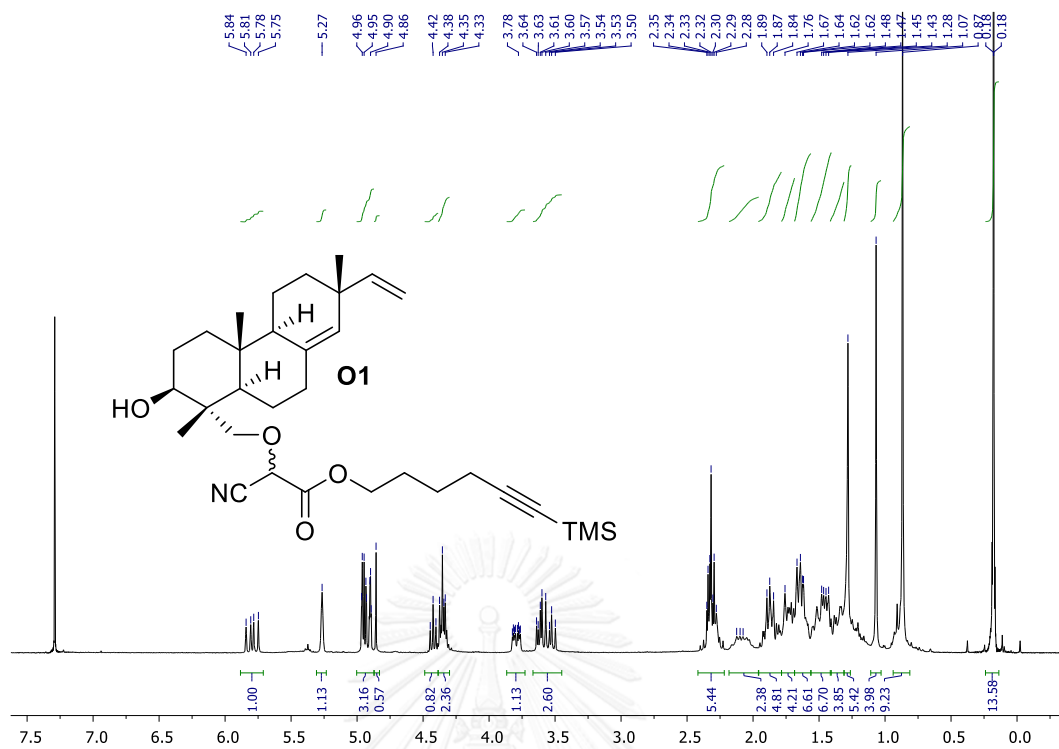


Figure A43 The <sup>1</sup>H NMR spectrum of mixture diastereomer **2 (O1)** (CDCl<sub>3</sub>)

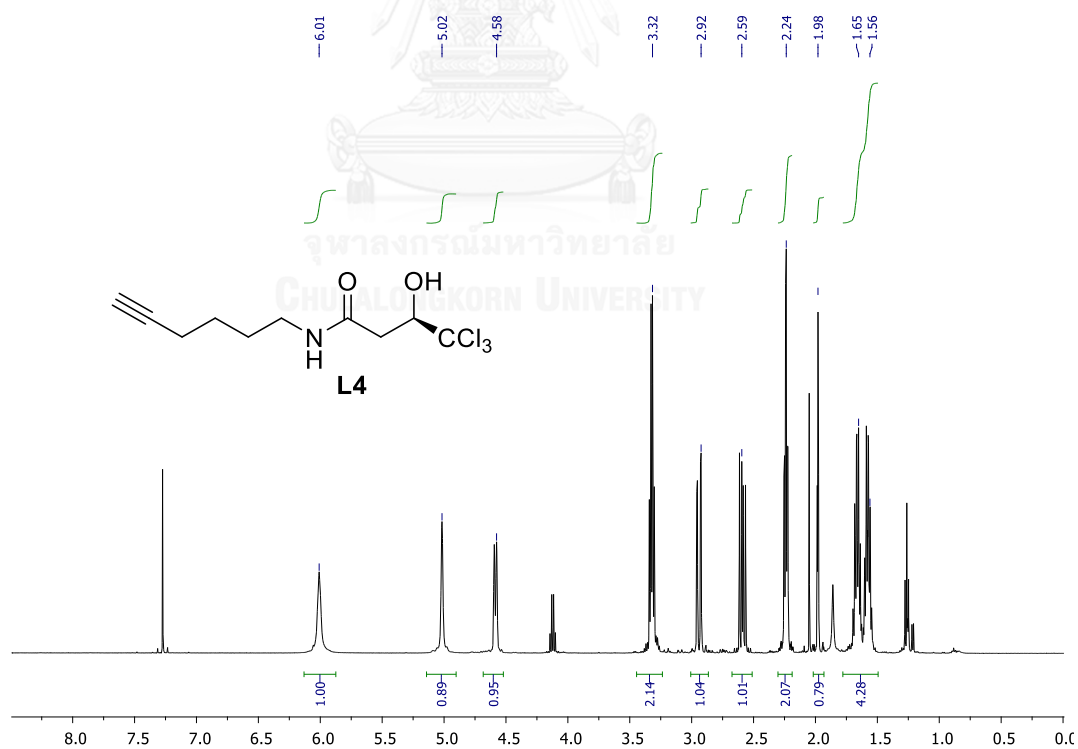


Figure A44 The <sup>1</sup>H NMR spectrum of (*R*)-4,4,4-trichloro-*N*-(hex-5-yn-1-yl)-3-hydroxybutanamide (**L4**) (CDCl<sub>3</sub>)

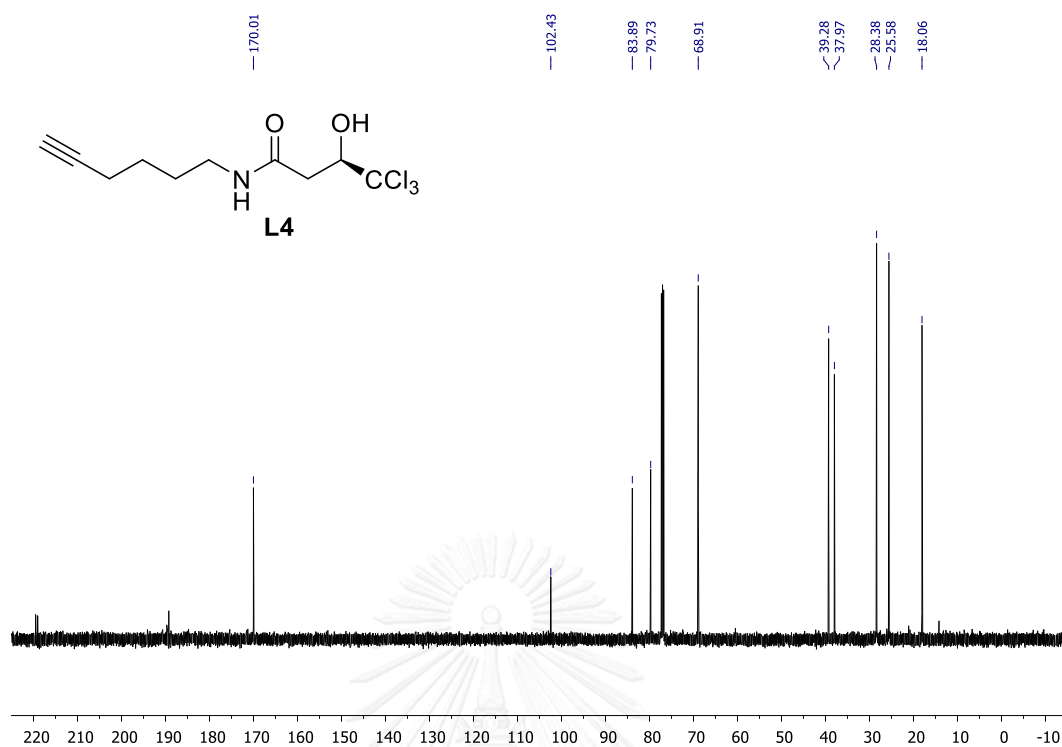


Figure A45 The  $^{13}\text{C}$  NMR spectrum of (*R*)-4,4,4-trichloro-*N*-(hex-5-yn-1-yl)-3-hydroxybutanamide (**L4**) ( $\text{CDCl}_3$ )

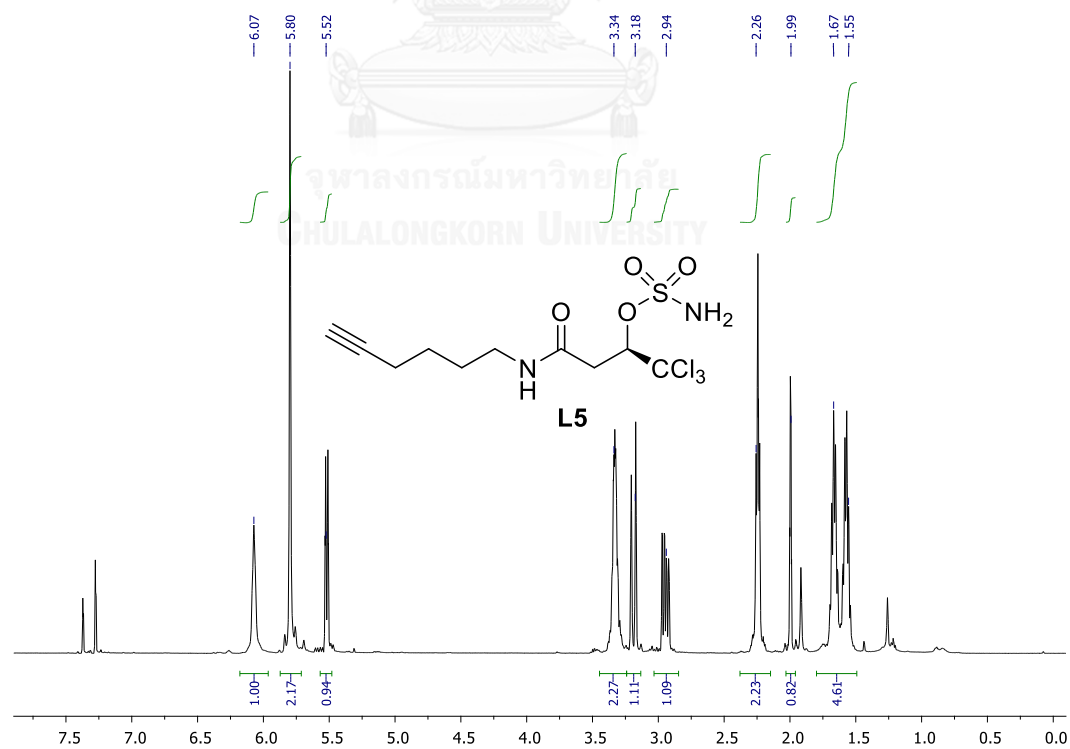


Figure A46 The  $^1\text{H}$  NMR spectrum of (*R*)-1,1,1-trichloro-4-(hex-5-yn-1-ylamino)-4-oxobutan-2-yl sulfamate (**L5**) ( $\text{CDCl}_3$ )

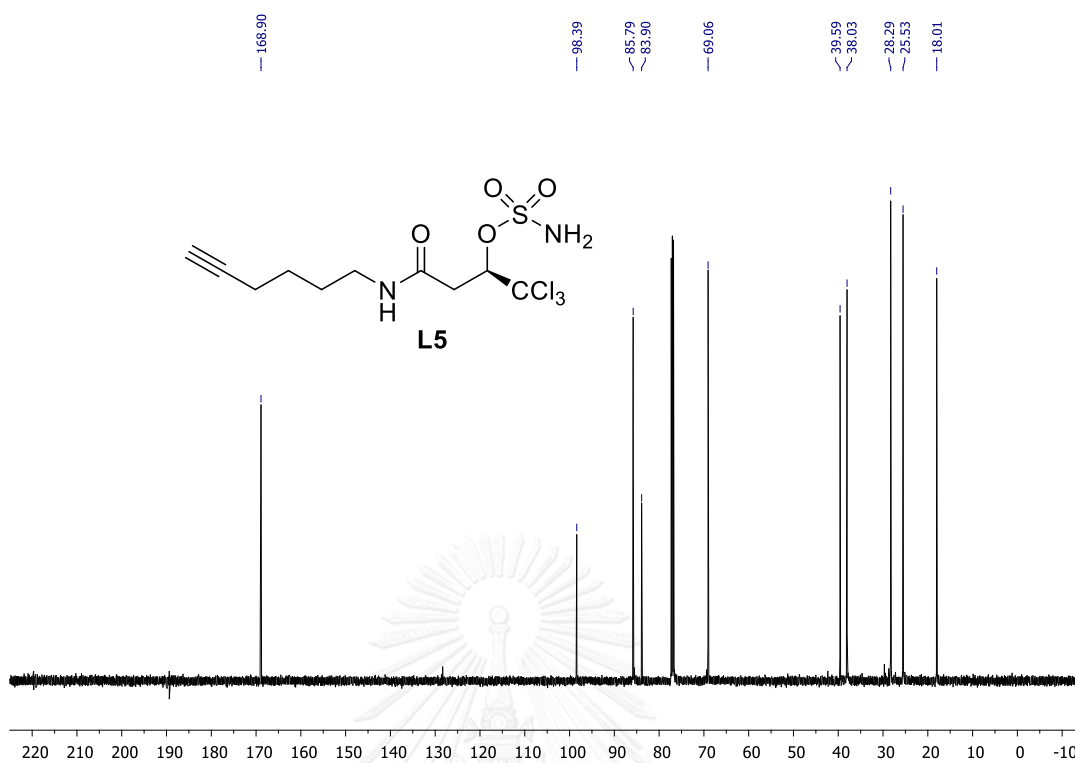


Figure A47 The  $^{13}\text{C}$  NMR spectrum of (*R*)-1,1,1-trichloro-4-(hex-5-yn-1-ylamino)-4-oxobutan-2-yl sulfamate (**L5**) ( $\text{CDCl}_3$ )

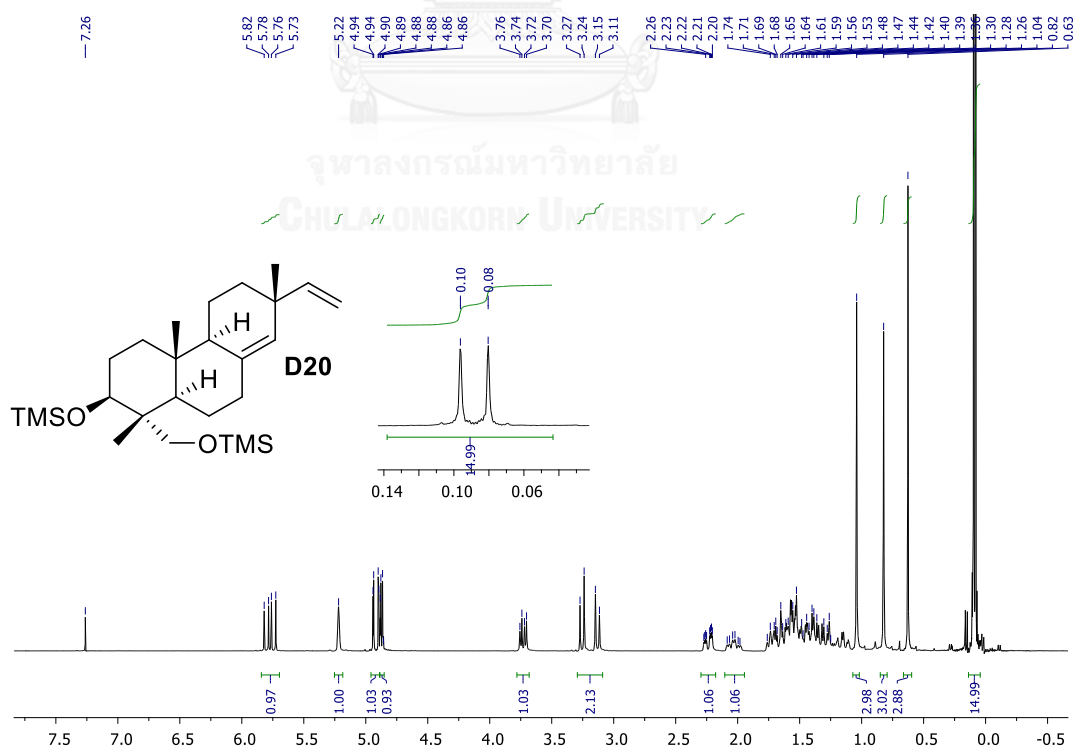


Figure A48 The  $^1\text{H}$  NMR spectrum of Di-OTMS-sandaracopimaradiene (**D20**) ( $\text{CDCl}_3$ )

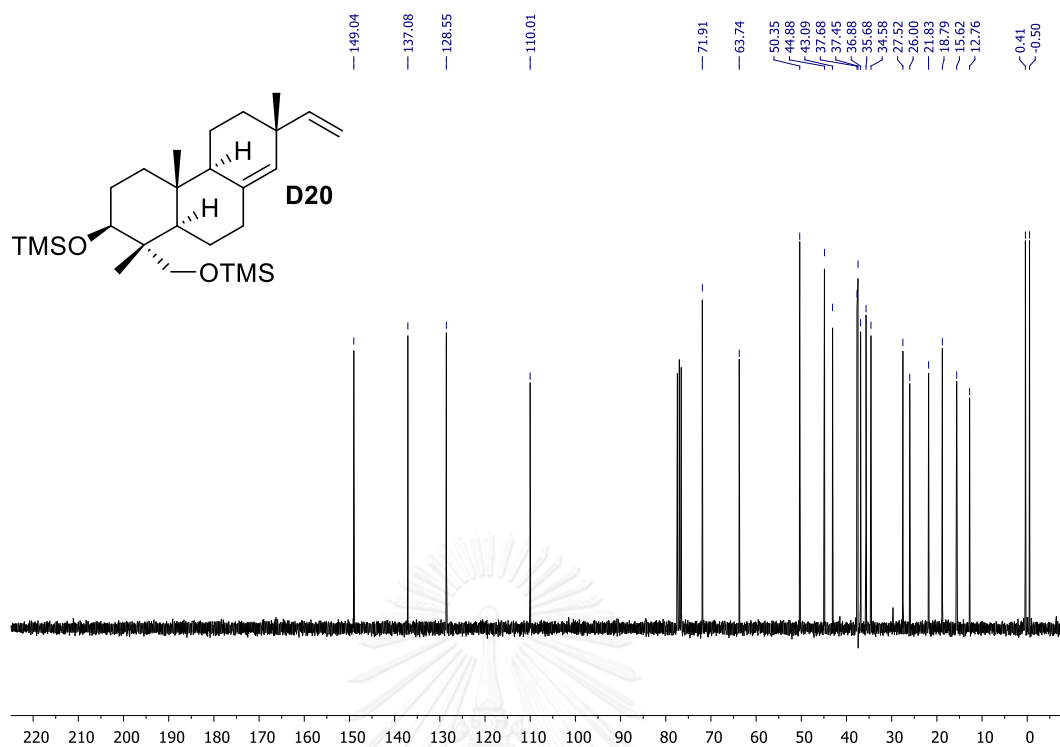


Figure A49 The  $^{13}\text{C}$  NMR spectrum of Di-OTMS-sandaracopimaradiene (**D20**) ( $\text{CDCl}_3$ )

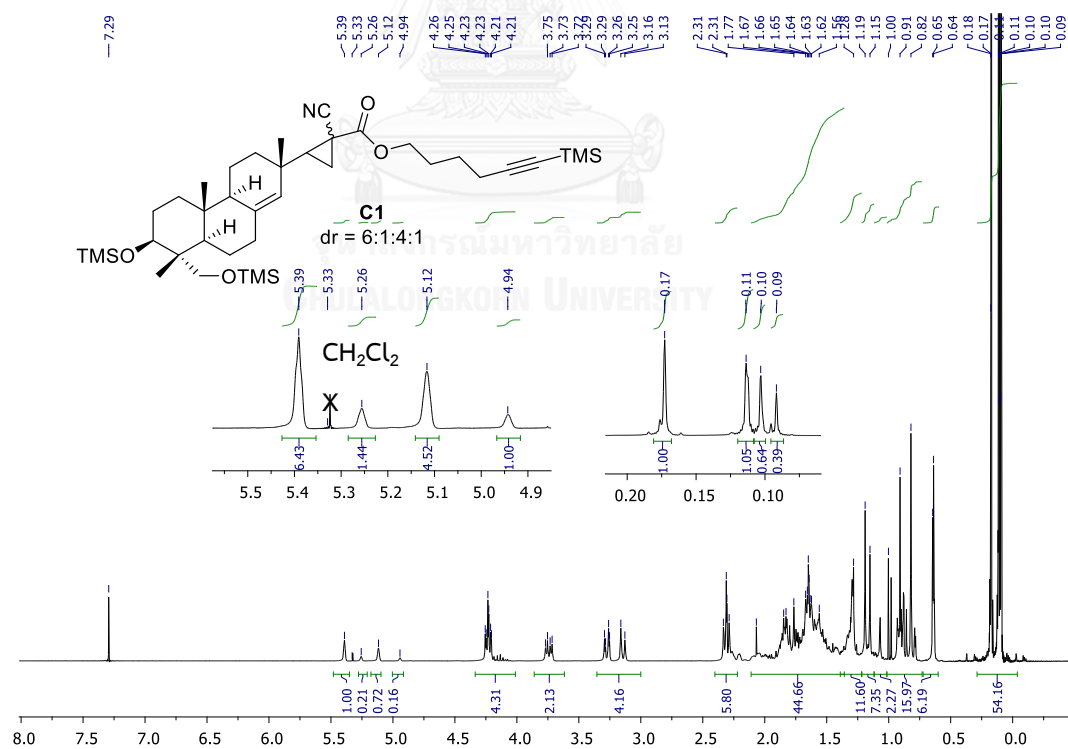


Figure A50 The  $^1\text{H}$  NMR spectrum of Di-OTMS-sandaracopimaradiene **C1** with dr = 6:1:4:1 ( $\text{CDCl}_3$ )



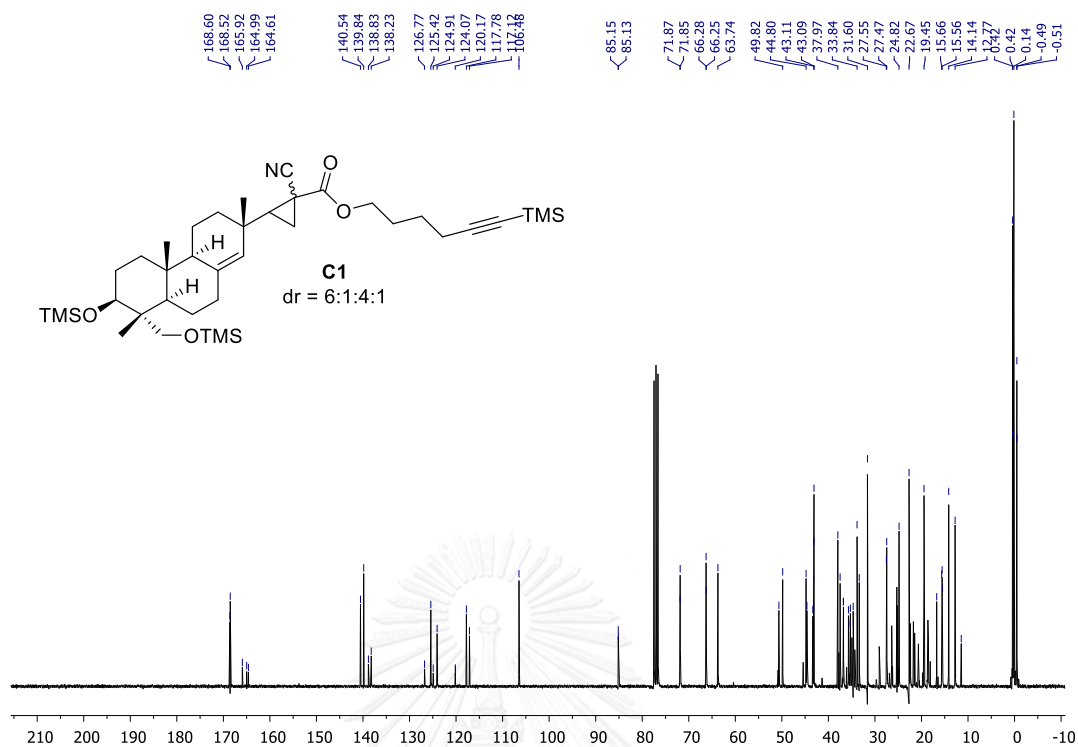


Figure A51 The  $^{13}\text{C}$  NMR spectrum of Di-OTMS-sandaracopimaradiene **C1** with **dr = 6:1:4:1** (CDCl<sub>3</sub>)

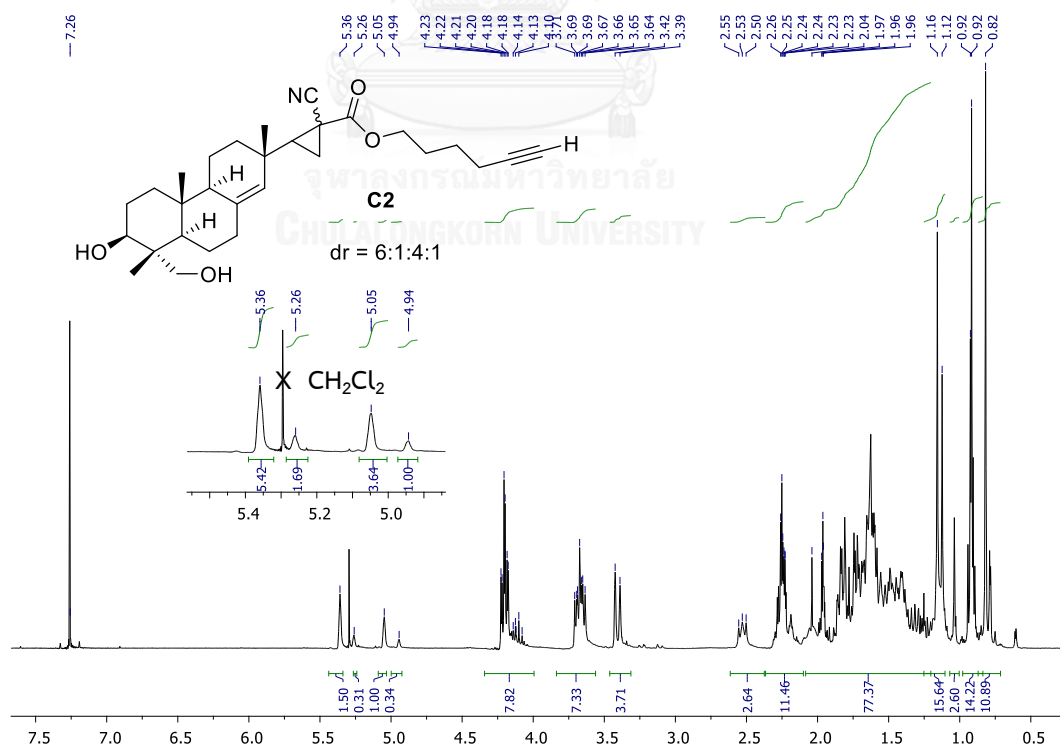


Figure A52 The  $^1\text{H}$  NMR spectrum of cyclopropanation derivative **C2** with **dr = 6:1:4:1** (CDCl<sub>3</sub>)

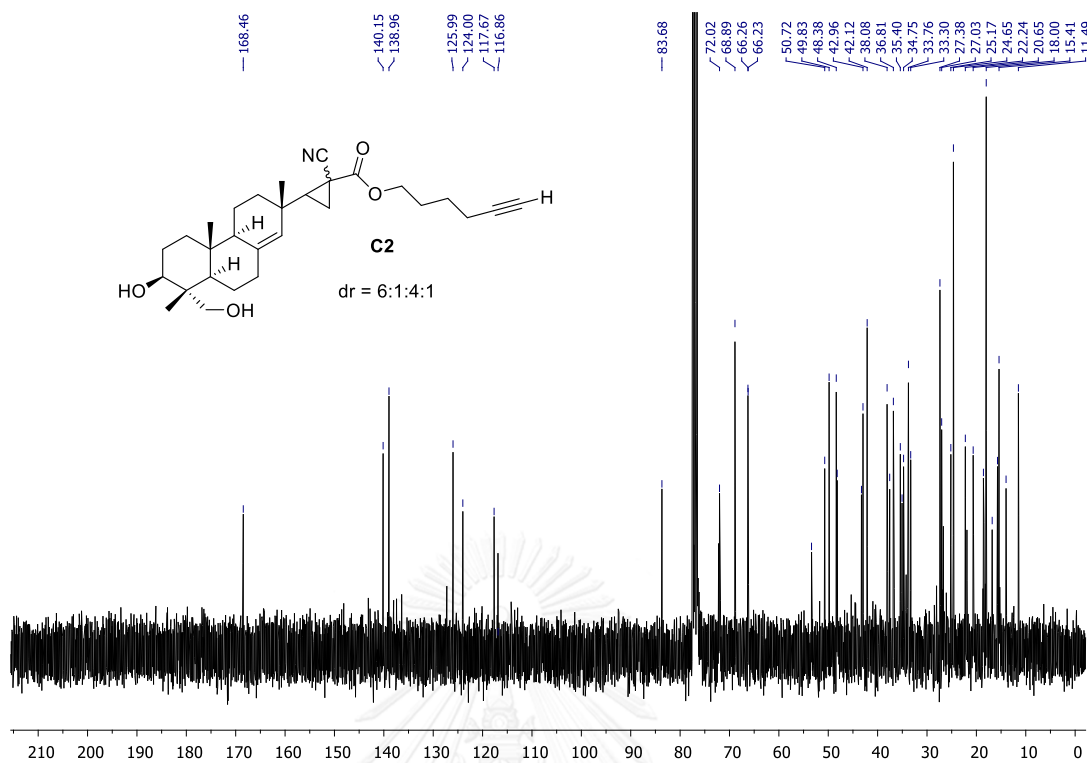


Figure A53 The  $^{13}\text{C}$  NMR spectrum of cyclopoponan derivative **C2** with dr = 6:1:4:1 ( $\text{CDCl}_3$ )

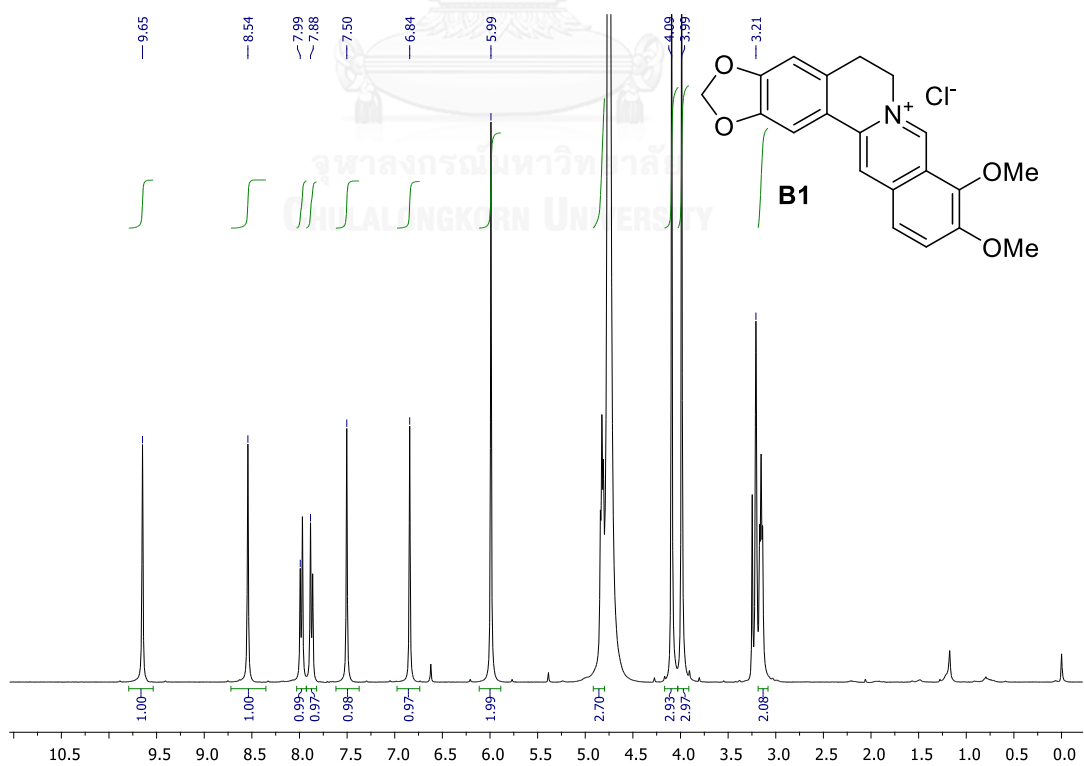


Figure A54 The  $^1\text{H}$  NMR spectrum of berberine chloride (**B1**) ( $\text{CD}_3\text{OD}$ )

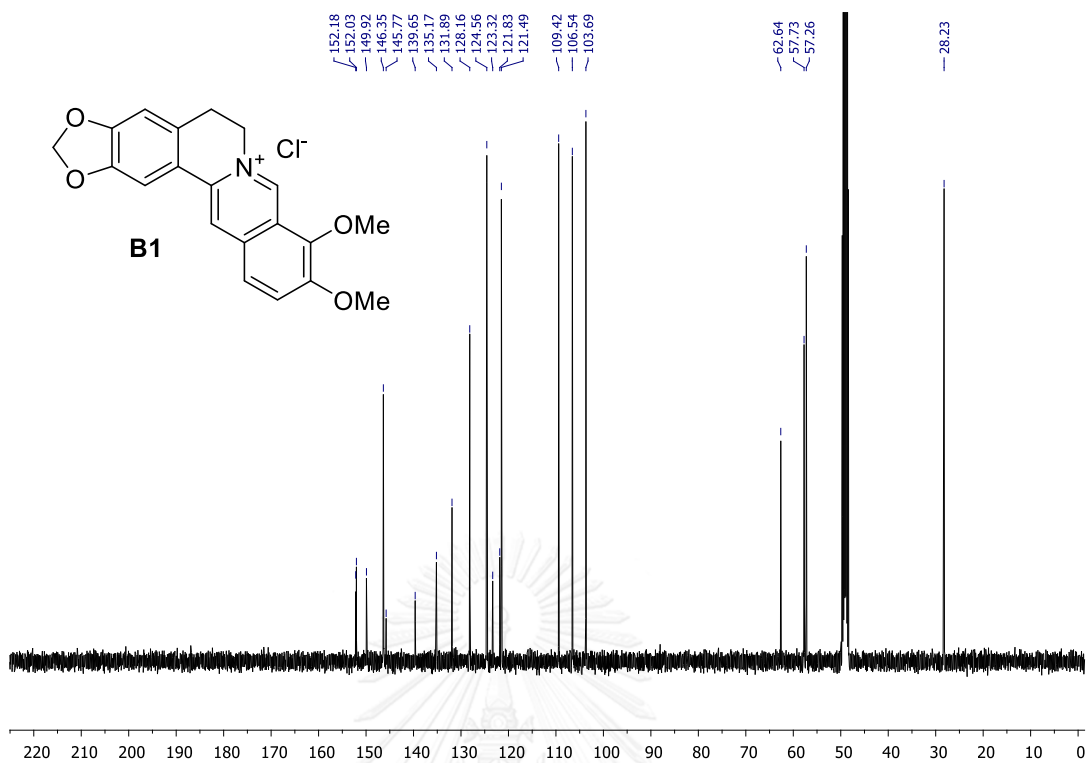


Figure A55 The  $^{13}\text{C}$  NMR spectrum of berberine chloride (B1) ( $\text{CD}_3\text{OD}$ )

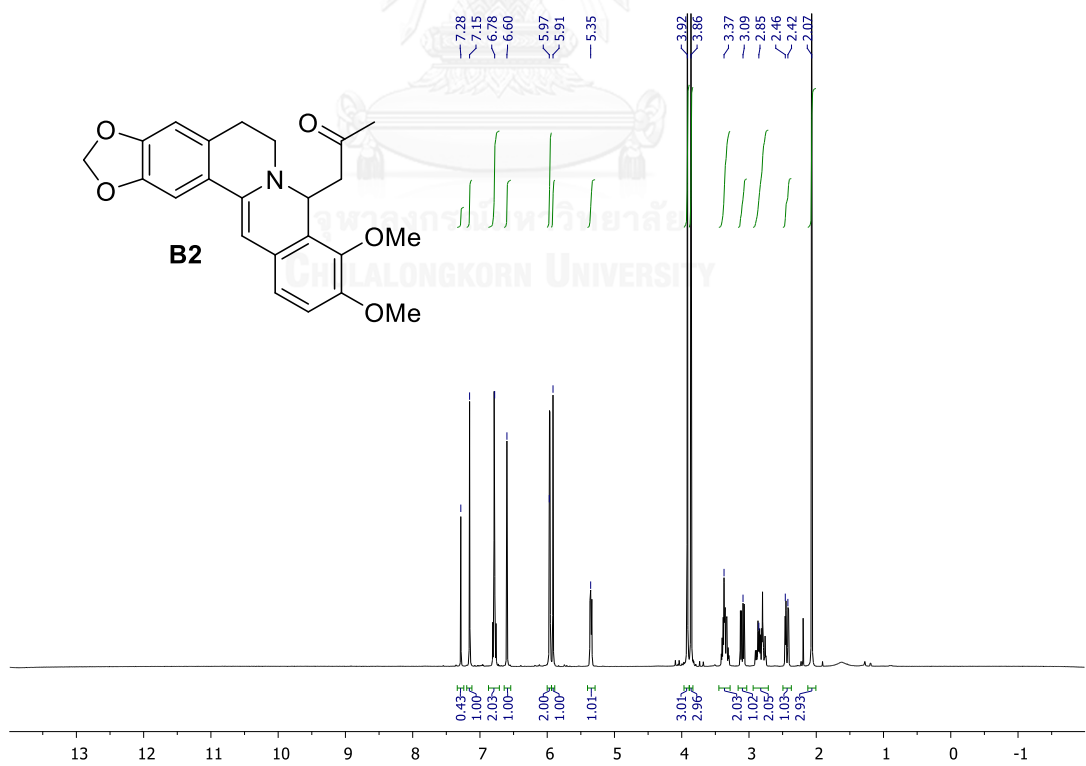


Figure A56 The  $^1\text{H}$  NMR spectrum of acetyl-berberine (B2) ( $\text{CDCl}_3$ )

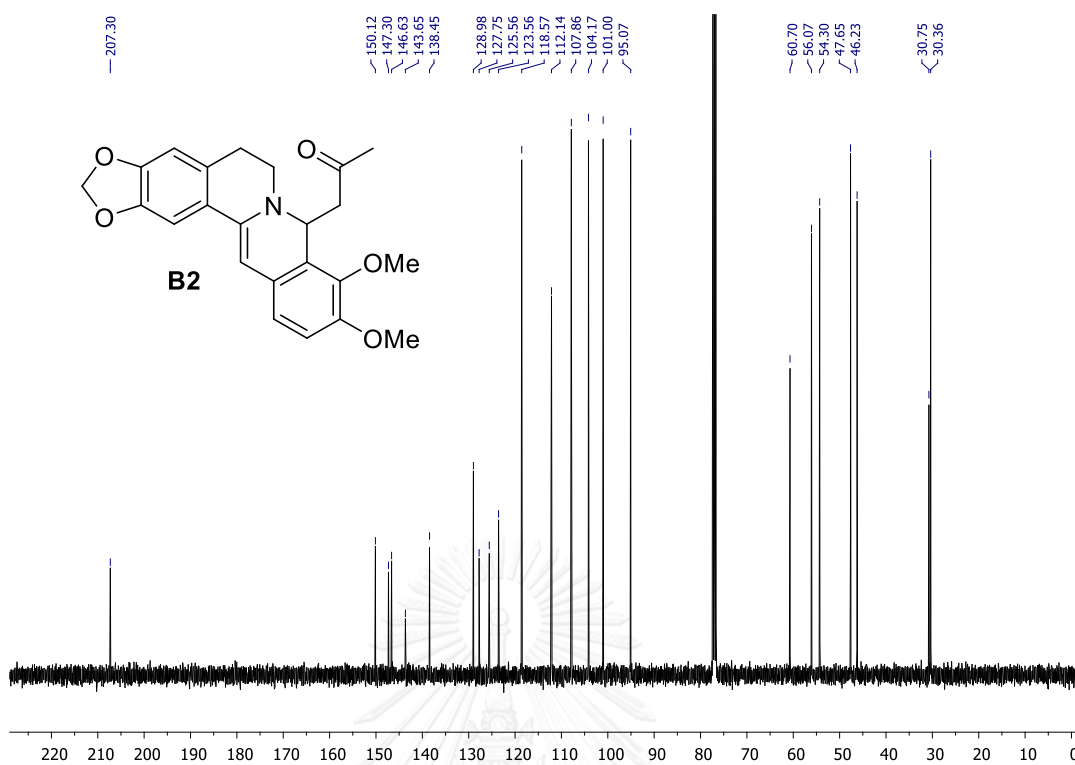


Figure A57 The  $^{13}\text{C}$  NMR spectrum of acetyl-berberine (**B2**) ( $\text{CDCl}_3$ )

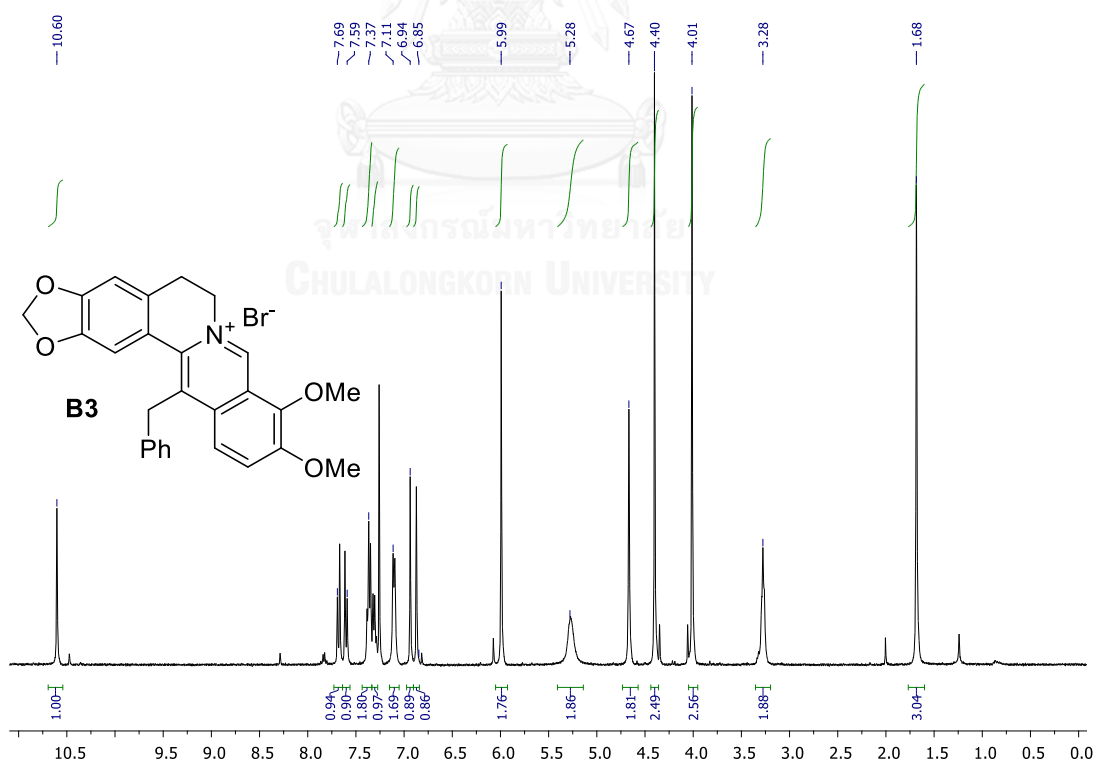


Figure A58 The  $^1\text{H}$  NMR spectrum of 13-benzyl-berberine (**B3**) ( $\text{CDCl}_3$ )

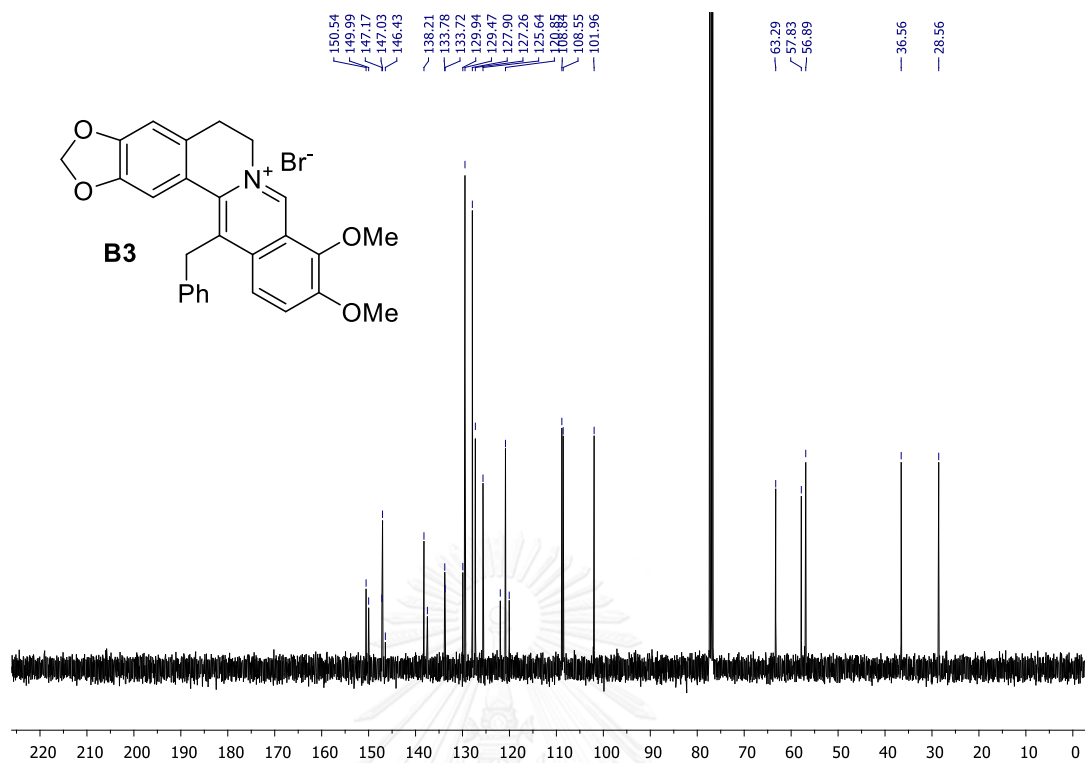


Figure A59 The  $^{13}\text{C}$  NMR spectrum of 13-benzyl-berberine (**B3**) ( $\text{CDCl}_3$ )

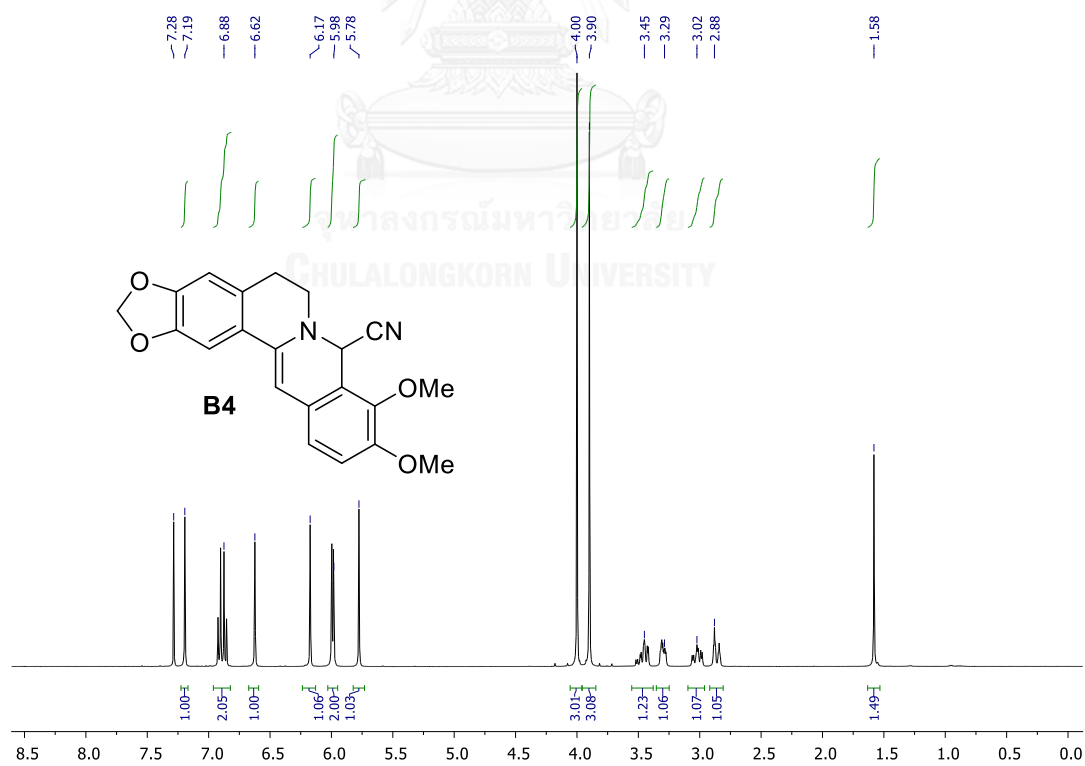


Figure A60 The  $^1\text{H}$  NMR spectrum of 8-cyano-13, 14-dehydrocanadiene (**B4**) ( $\text{CDCl}_3$ )

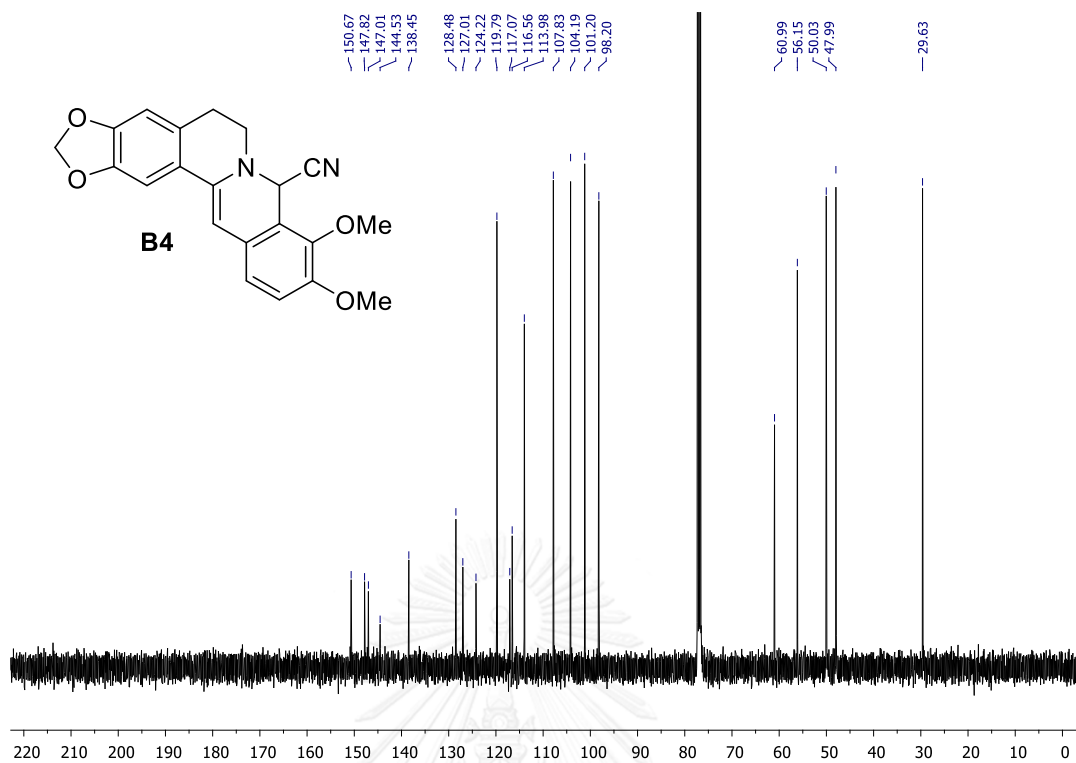


Figure A61 The  $^{13}\text{C}$  NMR spectrum of 8-cyano-13,14-dehydrocanadiene (**B4**) ( $\text{CDCl}_3$ )

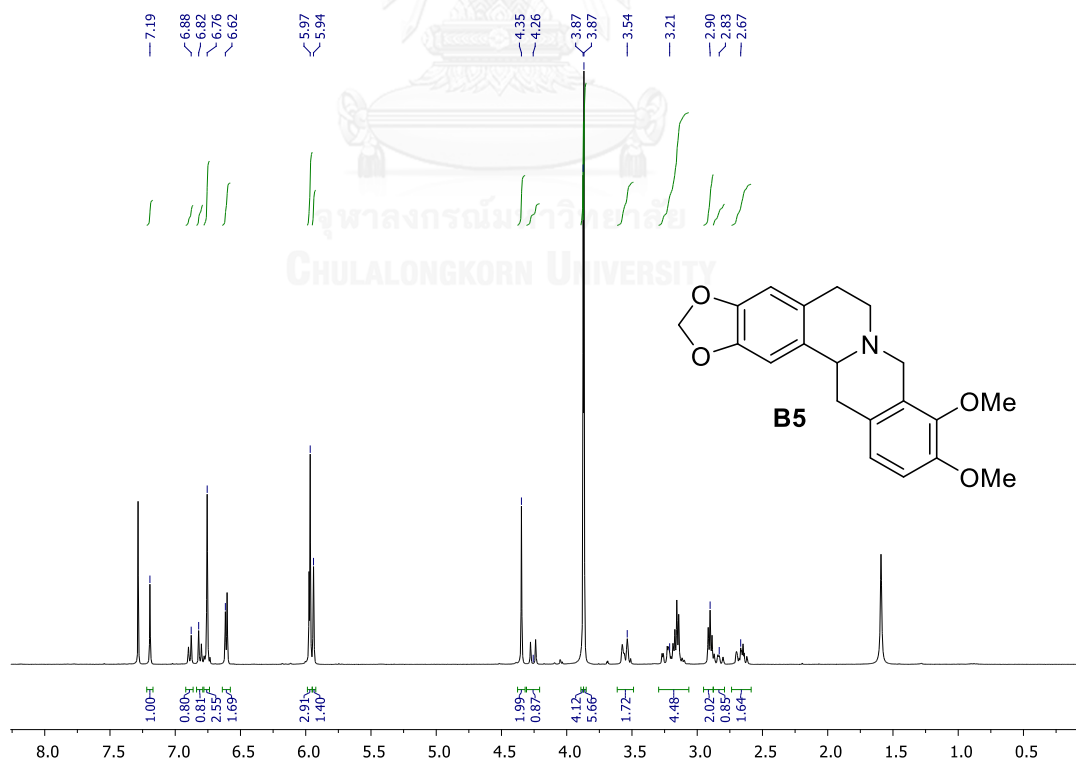


Figure A62 The  $^1\text{H}$  NMR spectrum of canadine (**B5**) ( $\text{CDCl}_3$ )

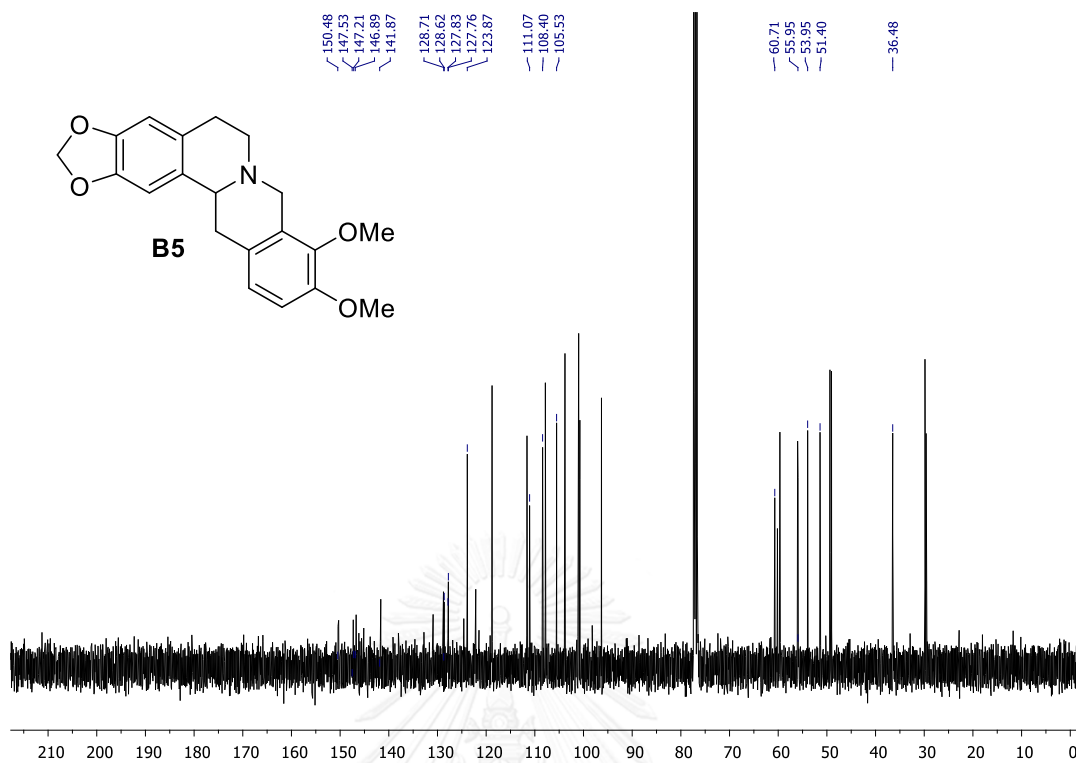


Figure A63 The  $^{13}\text{C}$  NMR spectrum of canadine (**B5**) ( $\text{CDCl}_3$ )

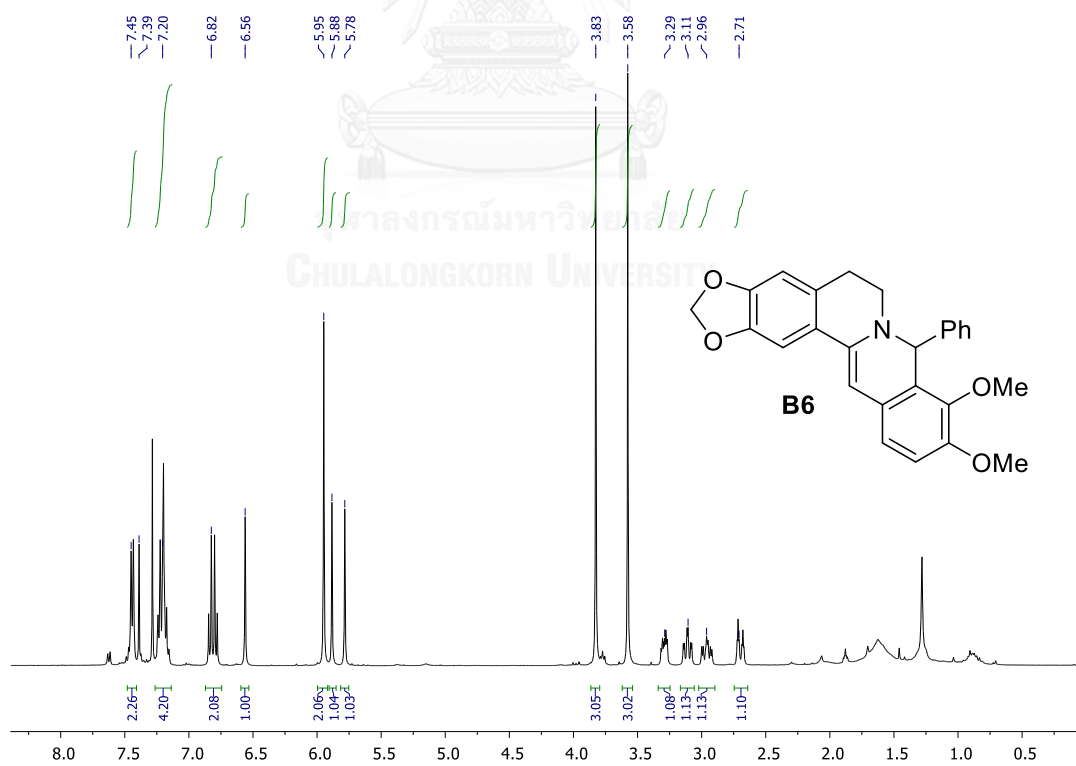


Figure A64 The  $^1\text{H}$  NMR spectrum of 8-phenyl-13, 14-dehydrocanadiene (**B6**) ( $\text{CDCl}_3$ )

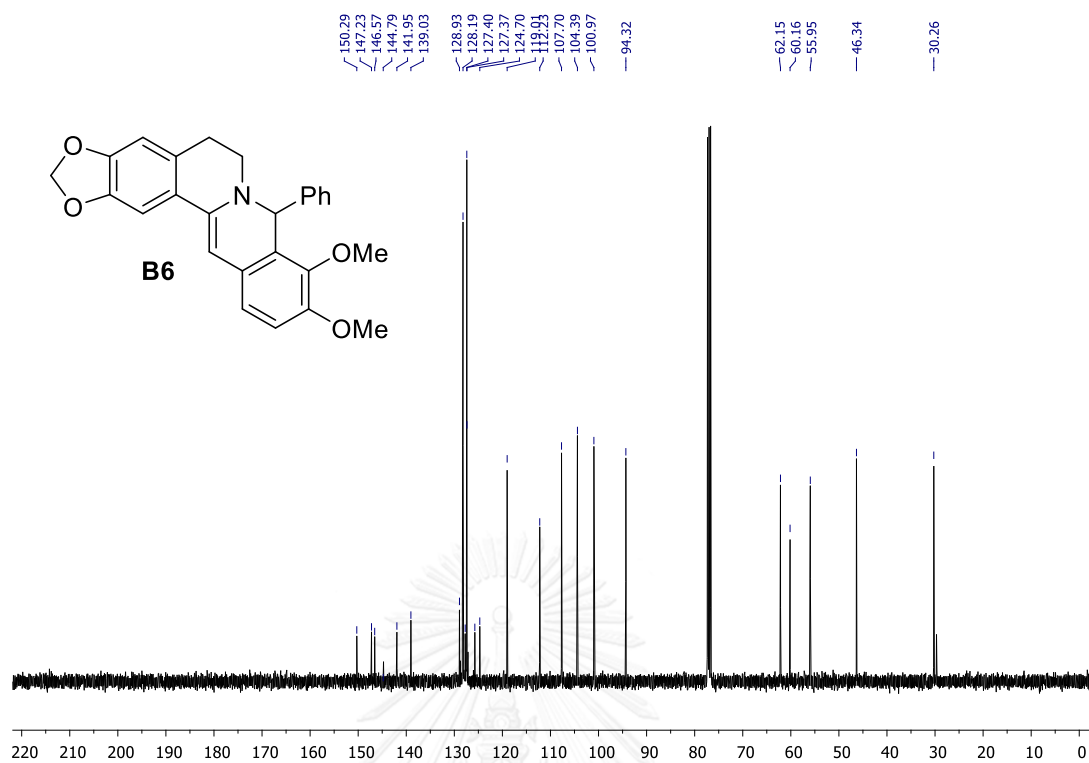


Figure A65 The  $^{13}\text{C}$  NMR spectrum of 8-phenyl-13, 14-dehydrocanadiene (**B6**) ( $\text{CDCl}_3$ )

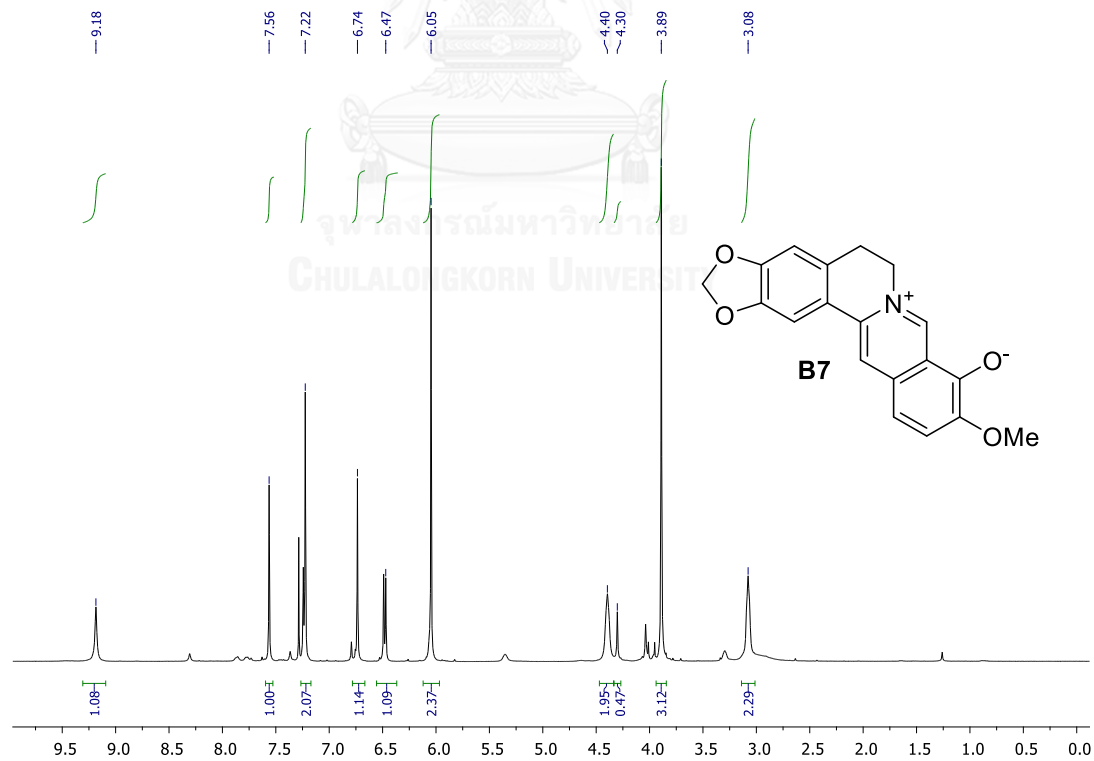


Figure A66 The  $^1\text{H}$  NMR spectrum of berberrubine (**B7**) ( $\text{CDCl}_3$ )



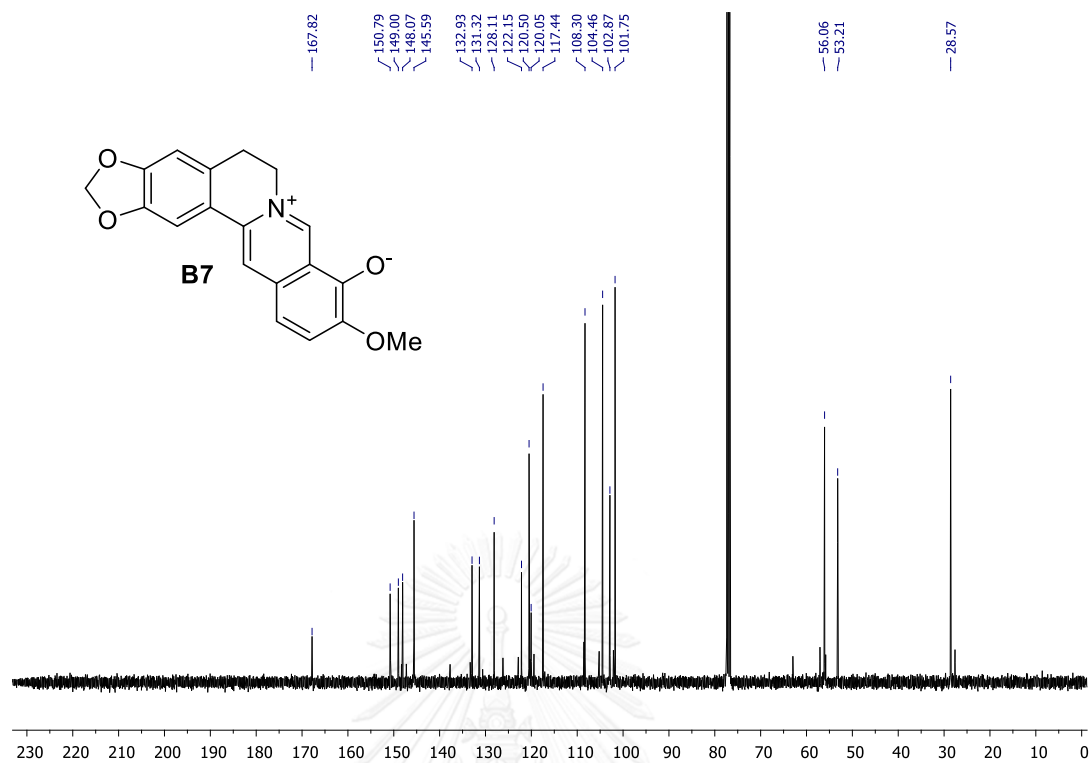


Figure A67 The  $^{13}\text{C}$  NMR spectrum of berberrubine (B7) ( $\text{CDCl}_3$ )

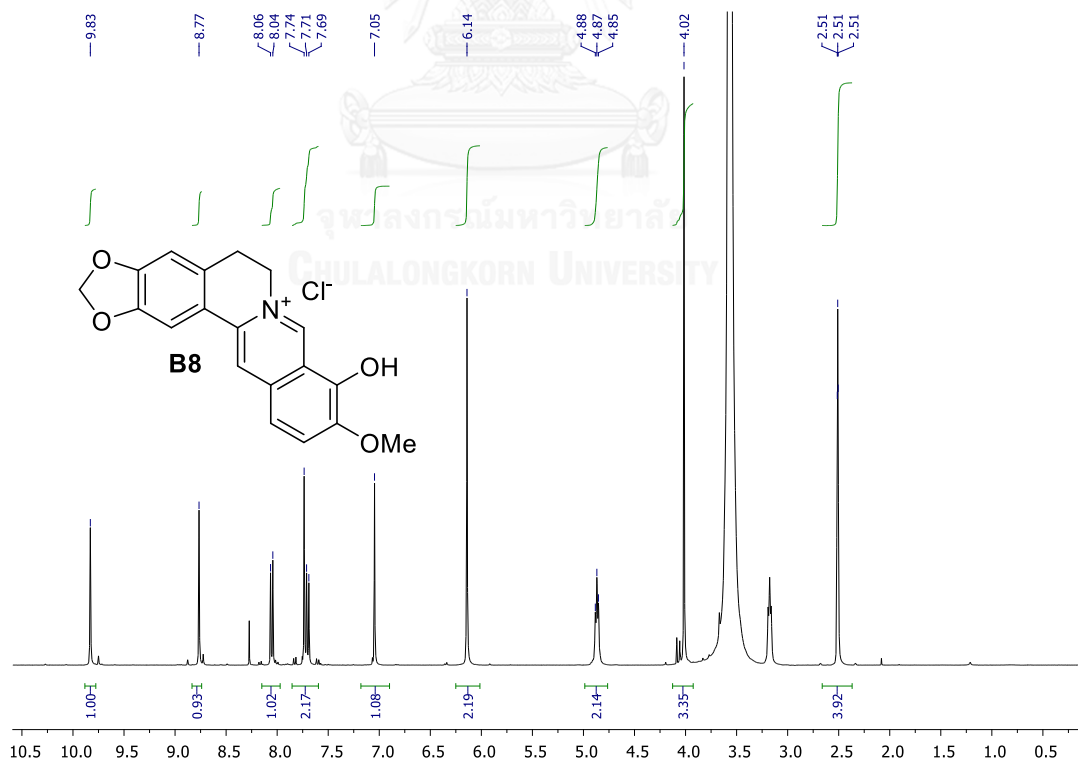


Figure A68 The  $^1\text{H}$  NMR spectrum of berberrubine HCl (B8) ( $\text{DMSO}-d_6$ )

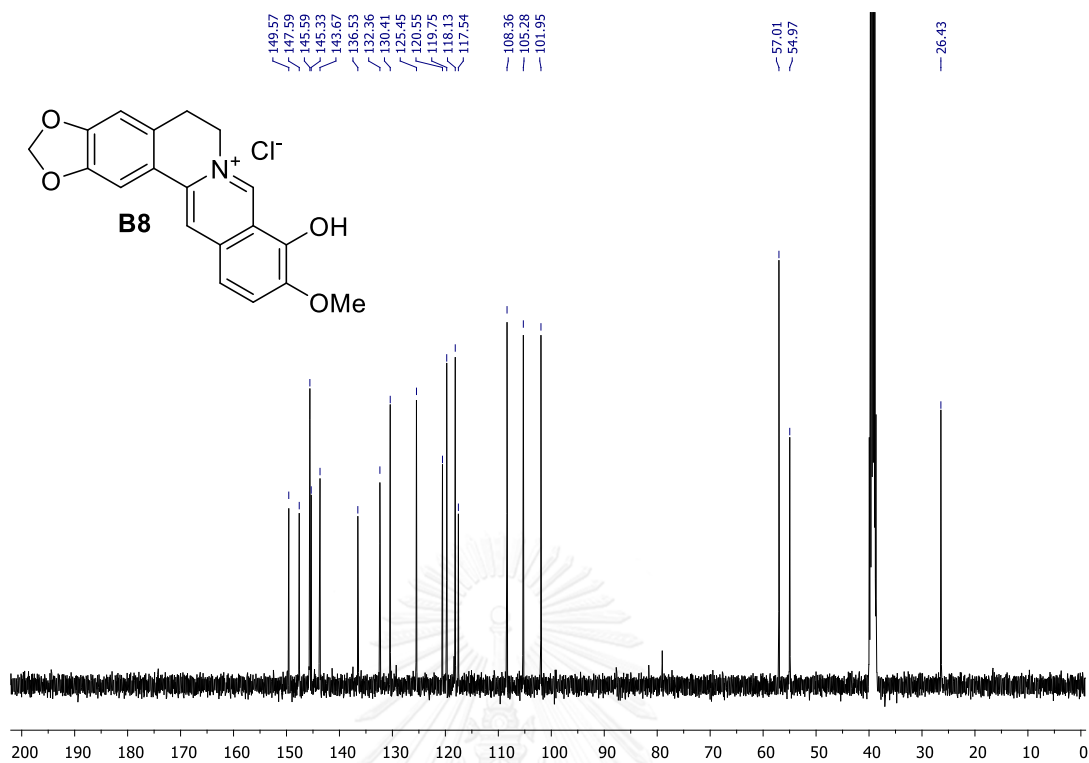


Figure A69 The <sup>13</sup>C NMR spectrum of berberrubine HCl (**B8**) (DMSO-d<sub>6</sub>)

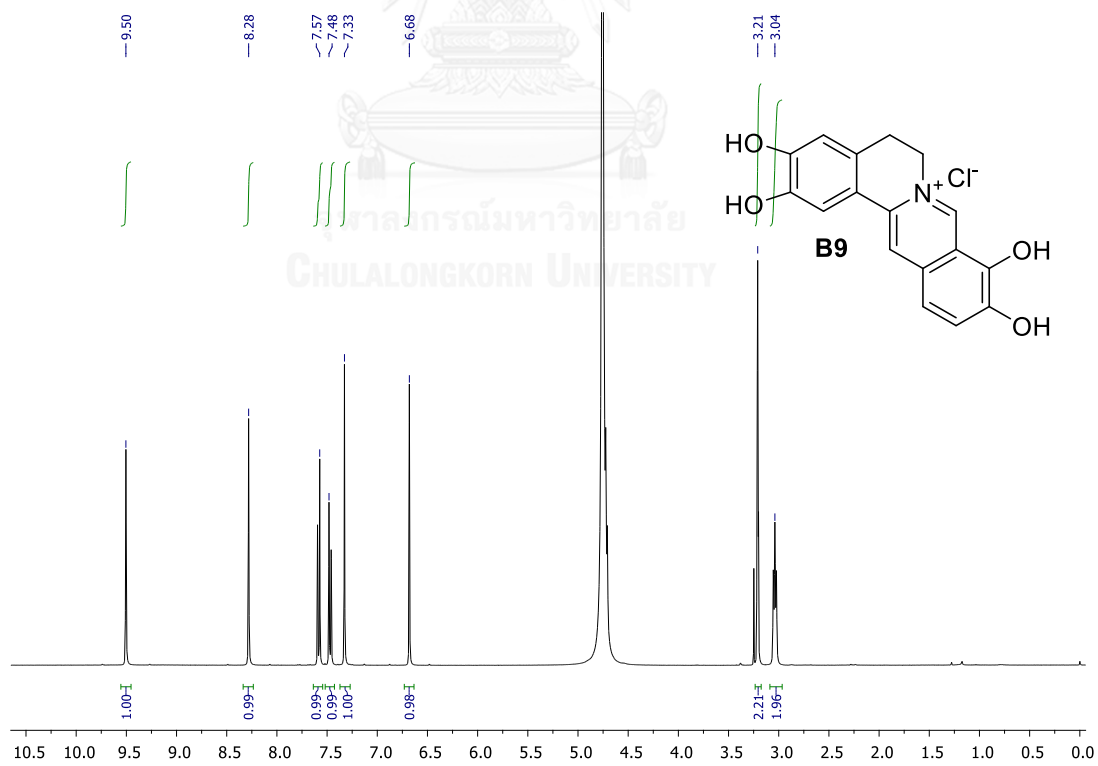
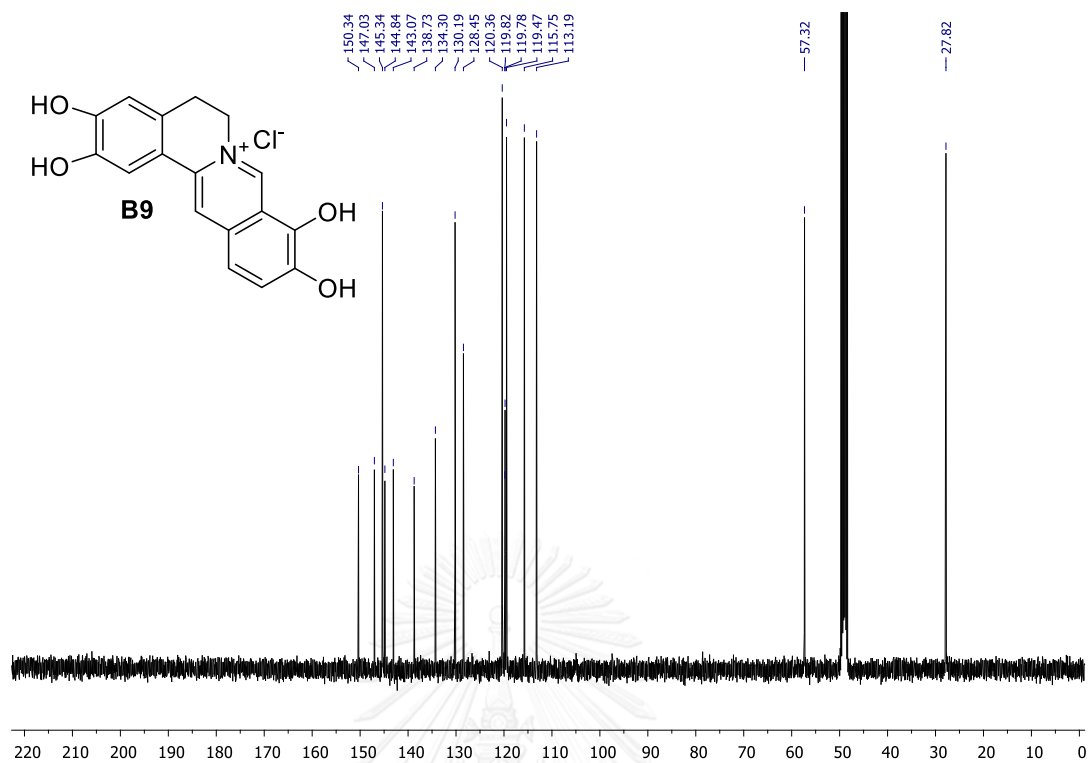


Figure A70 The <sup>1</sup>H NMR spectrum of 2,3,9,10-tetra-hydroxyberberine chloride (**B9**)

(CD<sub>3</sub>OD)



**Figure A71** The  $^{13}\text{C}$  NMR spectrum of 2,3,9,10-tetra-hydroxyberberine chloride (**B9**) ( $\text{CD}_3\text{OD}$ )

## VITA

Mr. Veerachai Pongkittiphan was born on February 9, 1985 in Bangkok, Thailand. He graduated with Bachelor Degree and Master Degree of Science in Chemistry from Chulalongkorn University in 2006 and 2008, respectively. Since then, he has been a Doctor of Philosophy student studying Organic Chemistry at Chulalongkorn University. In 2013, he has been a visiting scholar research for 1 year at Department of Chemistry, Texas A&M University, College Station, Texas, USA under the supervisor of Prof. Dr. Danial Romo. He was supported by research grant for this Doctor of Philosophy Degree's thesis from Chulalongkorn University Dutsadi Phiphat Scholarship.

His present address is 26 Maitri Chit Road, Pomprap, Pomprap Sattruphai, Bangkok, 10100, Thailand.

